LOAN DOCUMENT

AD-A247 350

DTIC ACCESSION NUMBER

LEVEL

INVENTORY

①

RL-TR-91-80

DOCUMENT IDENTIFICATION

Jun 91
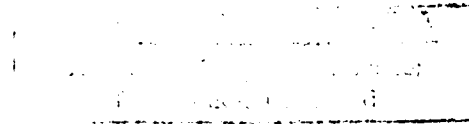
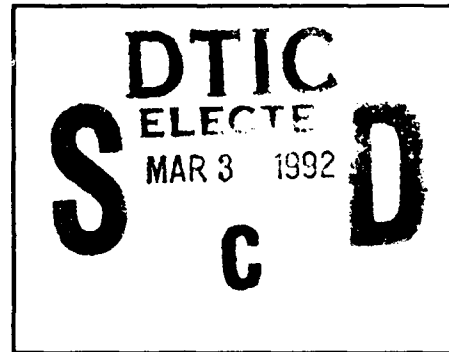DISTRIBUTION STATEMENT

H
A
N
D
L
E

W
I
T
H

C
A
R
E

ACCESSION FOR

NTIS	GRA&I	☑
DTIC	TRAC	☐
UNANNOUNCED		☐
JUSTIFICATION		

BY

DISTRIBUTION/

AVAILABILITY CODES

DISTRIBUTION	AVAILABILITY AND/OR SPECIAL

A-1

DISTRIBUTION STAMP

DTIC
S **ELECTE**
C MAR 3 1992 **D**

DATE ACCESSIONED

DATE RETURNED

92 1 13 091

DATE RECEIVED IN DTIC

92-01188

REGISTERED OR CERTIFIED NUMBER

DTIC FORM 70A
JUN 90

DOCUMENT PROCESSING SHEET

PREVIOUS EDITIONS MAY BE USED UNTIL
STOCK IS EXHAUSTED

LOAN DOCUMENT

AD-A247 350
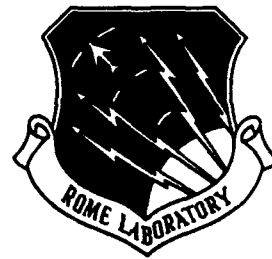
RL-TR-91-80
In-House Report
June 1991

IMPROVEMENT IN RADAR DETECTION UNDER SCAN TO SCAN PROCESSING AND SCAN RATE REDUCTION

Dr. Donald D. Weiner, RL/OCTS

Dr. Joon Song, Syracuse University

APPROVED FOR PUBLIC RELEASE; DISTRIBUTION UNLIMITED.

**Rome Laboratory
Air Force Systems Command
Griffiss Air Force Base, NY 13441-5700**

This report has been reviewed by the Rome Laboratory Public Affairs Office (PA) and is releasable to the National Technical Information Service (NTIS). At NTIS it will be releasable to the general public, including foreign nations.

RL-TR-91-80 has been reviewed and is approved for publication.

APPROVED:

FRED J. DEMMA
Chief, Surveillance Technology Division
Directorate of Surveillance

APPROVED:

JAMES W. YOUNGBERG, Lt Col, USAF
Deputy Director of Surveillance

FOR THE COMMANDER:

JAMES W. HYDE III
Directorate of Plans & Programs

REPORT DOCUMENTATION PAGE

Form Approved
OMB No. 0704-0188

1. AGENCY USE ONLY (Leave Blank)	2. REPORT DATE	3. REPORT TYPE AND DATES COVERED
	June 1991	In-House Jan 90 – Dec 90

4. TITLE AND SUBTITLE

IMPROVEMENT IN RADAR DETECTION UNDER SCAN TO SCAN
PROCESSING AND SCAN RATE REDUCTION

5. FUNDING NUMBERS

PE - 62702F
PR - 4506
TA - PROJ

6. AUTHOR(S)
Dr. Donald D. Weiner - Rome Laboratory (OCTS) *
Dr. Joon Song   - Syracuse University

7. PERFORMING ORGANIZATION NAME(S) AND ADDRESS(ES)

Rome Laboratory (OCTS)
Griffiss AFB NY 13441-5700

8. PERFORMING ORGANIZATION REPORT NUMBER

RL-TR-91-80

9. SPONSORING/MONITORING AGENCY NAME(S) AND ADDRESS(ES)

AFOSR/XOT
Bolling AFB DC 20332-6448

10. SPONSORING/MONITORING AGENCY REPORT NUMBER

N/A

11. SUPPLEMENTARY NOTES   (see reverse)

Rome Laboratory Project Engineer: Michael C. Wicks/OCTS/(315) 330-4437
*This PhD dissertation research was performed by Dr. Joon Song of Syracuse

12a. DISTRIBUTION/AVAILABILITY STATEMENT

Approved for public release; distribution unlimited.

12b. DISTRIBUTION CODE

13. ABSTRACT (Maximum 200 words)

Recent advances in signal processing technology have resulted in a significantly greater computational capability at lower cost. As a result, many investigations are currently under way to determine how increased signal processing can be used to improve the detection performance of existing radars without requiring major equipment modifications. Two approaches towards this goal are examined: The first is a scan-to-scan processing (SSP) also known as track-before-detect (TBD). The second involves scan rate reduction along with efficient post detection integration. Detailed analyses are carried out for the two methods.

14. SUBJECT TERMS

Signal Processing, radar, tracking

15. NUMBER OF PAGES
328

16. PRICE CODE

17. SECURITY CLASSIFICATION OF REPORT	18. SECURITY CLASSIFICATION OF THIS PAGE	19. SECURITY CLASSIFICATION OF ABSTRACT	20. LIMITATION OF ABSTRACT
UNCLASSIFIED	UNCLASSIFIED	UNCLASSIFIED	UL

Block 11 (Cont'd)

and his advisor, Dr. Donald D. Weiner of Rome Laboratory. Dr. Weiner is a
visiting scientist at the Rome Laboratory under AFOSR sponsorship.
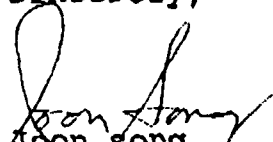
March 7, 1991

Rome Laboratory/OCTS (M. Wicks)
FAX No. (315) 336-7352

    I hereby grant permission to Rome Laboratory to publish my dissertation as a government technical report coauthored by Dr. D. Weiner and myself.

    I also agree to the copyright clause, "This material may be reproduced by or for the US government."

Sincerely,

Joon Song

6551 24th Ave. N.E.
Seattle, WA 98115

CONTENTS

Page

LIST OF TABLES

LIST OF FIGURES

Figure   Page

CHAPTER 1

INTRODUCTION

1.1 Problem Definition

It takes enormous technical and financial resources and commitment to successfully develop a long range surveillance radar. Two successful examples are the US Navy E-2C Hawkeye and US Air Force E-3B AWACS Surveillance Radars. These airborne surveillance radar systems are pictured in Figure 1.1-1. It is said that the success rate of a major radar development program from conception to deployment is on the order of 1% [1]. Therefore, when a new threat emerges, it is preferable with respect to cost and risk to seek improvements in detection performance of an existing and proven radar system rather than embarking on a totally new radar development program.

This report presents for the first time a detailed analysis of the Scan-to-Scan Processing (SSP) concept which has been pursued over the past ten or more years through several independent industrial research and development programs as a means for improving radar detection performance.

The past efforts to evaluate performance have primarily relied on the manipulation of raw radar data at the output of the analog-to-digital converter with a computer simulation package. Although significant improvement has been claimed, the careful analysis and interpretation of the results presented in this report reveals that only a marginal improvement can be attributed to the Scan-to-Scan Processing. Consequently, an alternate approach which relies on scan rate reduction and noncoherent integration (NCI), in lieu of the M of N binary post detection integration widely used today, is proposed and investigated. It is shown that slowing down the scan rate coupled with noncoherent integration, can potentially deliver higher performance improvement with less risk.

1
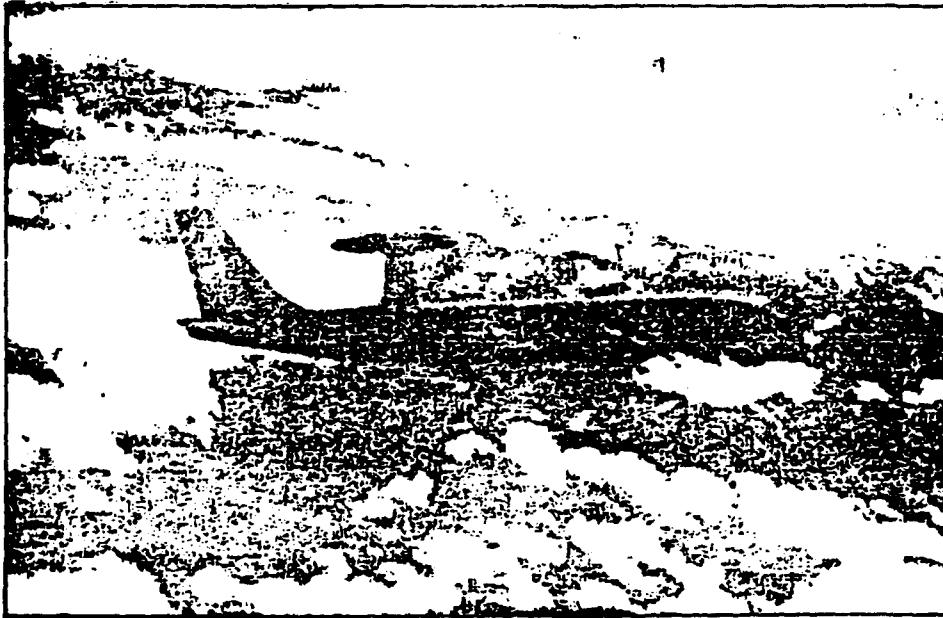
(a) USAF E-3 AWACS AEW Aircraft with Rotodome Antenna
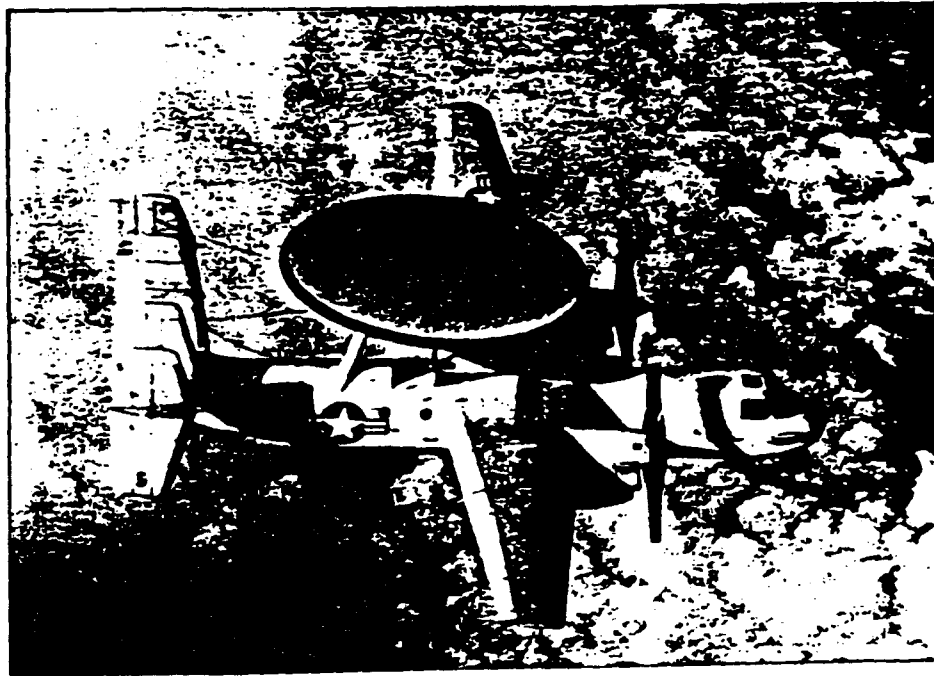
(b) USN E-2C Hawkeye AEW Aircraft with Rotodome Antenna

Figure 1.1-1

Examples of Airborne Surveillance Radar Systems

In this section a description of the radar under consideration in its baseline configuration is presented first. The constraints under which improvement is sought are then specified. Finally, the criterion by which the improvement is measured is discussed.

1.1.1 Description of the Airborne Long Range Surveillance Radar under Consideration

A brief description of the receiver/processor portion of the radar system under consideration in its baseline configuration is given here. Performance of this receiver/processor will provide a basis for determining any performance improvement in the modified configuration. The radar for which a detection improvement is sought is a high PRF, pulse doppler radar with a superheterodyne receiver followed by an analog-to-digital converter (ADC) and digital signal processor section. A basic receiver and processor block diagram, common to all pulse doppler radars, is shown in Figure 1.1-2.

A superheterodyne receiver typically has two frequency down conversion stages to reach the final intermediate frequency (IF). Not only is amplification at IF less costly and more stable than at a microwave frequency, but the wider percentage bandwidth occupied by the desired signal simplifies the filtering operation. In addition, the superheterodyne receiver allows variation of the local oscillator frequency to follow any desired or unintentional tuning variation of the transmitter without disturbing the filtering at IF. The reference signal applied to the first mixer is provided by the STALO (stable local oscillator) while the reference signal applied to the second mixer is provided by the COHO (coherent local oscillator). The STALO signal has the frequency stability required for coherent processing while the COHO can be used to introduce phase correction needed to compensate for radar platform motion or transmitter phase variations.

A description of the flow of the received signal (target signal plus clutter plus other interference such as jamming noise when present) is presented below. A detailed analysis

3
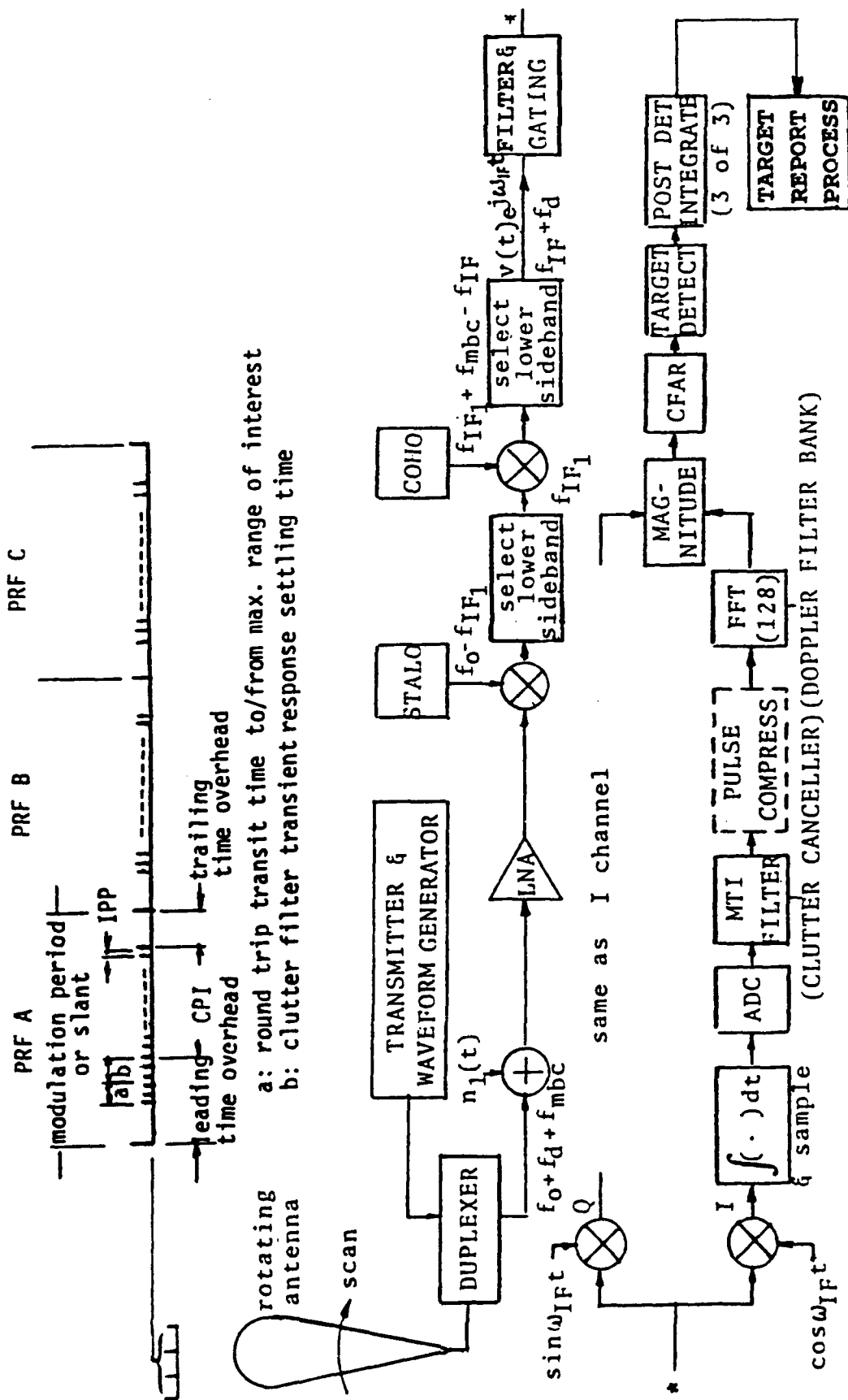
Figure 1.1-2

Simplified block Diagram for Radar Receiver/Processor

4

leading to probabilities of detection for Swerling and Marcum target models is presented in Chapter 3.

It is assumed that the carrier frequency of the received signal is $(f_0+f_d+f_{mbc})$ where f_0 is the carrier frequency of the transmitted signal, f_d is the doppler shift of a moving target as it would be observed from a motionless platform, and f_{mbc} is the doppler shift of the return from a ground patch in the direction of the main beam due to the platform motion along the line of antenna pointing direction. The thermal noise generated from all sources is modeled by the additive white Gaussian noise process, $n_1(t)$. In practice, the low noise amplifier (LNA) at the receiver front end essentially determines the noise level. The low pass filter following the first mixer separates out the signal at the difference frequency. The frequency offset f_{mbc} can be incorporated into the COHO signal so as to center the mainbeam clutter spectrum about the IF frequency, f_{IF}.

The bandwidth of the band-pass filter at f_{IF} is equal to 2B where B is the half power signal bandwidth. For analytic convenience, this filter is assumed to be an ideal band-pass filter whose gain is zero outside the pass band. This filter has no effect on the band-limited input signal but limits the bandwidth of the noise process. It forms a part of the matched filter which also includes the two paths for the quadrature components. The down-converter, sometimes referred to as a synchronous detector, converts the signal at IF to baseband while preserving both phase and amplitude   information.

The analog-to-digital converter (ADC) provides a means for signal processing in the digital domain with the attendant advantage in flexibility, reliability, repeatability and precision. Its bandwidth, linearity, and dynamic range are important factors for coherent signal processing and is often the limiting factor in the bandwidth and instantaneous dynamic range of the system. In a pulse doppler radar, particularly with a high PRF

5

waveform, the mainbeam clutter usually sets the system dynamic range requirements. The clutter canceller is another critical signal processing element in a pulse doppler radar. If not cancelled, even with an infinite dynamic range processor downstream, the mainbeam clutter will appear as residue clutter in the otherwise clutter free doppler zone as a result of integration through doppler filter sidelobes.

The clutter canceller in this radar is a cascade of two second order recursive digital filter sections, each with two poles and two zeros. This is designed to provide a desired shaped velocity response in the frequency domain. The drawback is that a significantly long time domain transient response is generated during which signal integration cannot be performed. Other forms of clutter cancellers are multistage delay line cancellers with binomial coefficients as weights, and the optimum linear filter whose weights are given by the elements of the eigen vector corresponding to the minimum eigen value of the clutter correlation matrix. Some analysis and recommendations for further work on these filters are given in chapter 6.

When a coded waveform having a long time-bandwidth product is transmitted so as to increase energy without exceeding the transmitter peak power, a pulse compressor will follow the clutter canceller. This restores the range resolution capability of the radar by generating an equivalent narrow pulse. In effect, the pulse compressor is a matched filter for the coded waveform. The doppler filter bank is implemented by a two rail pipeline FFT (fast Fourier transform) and performs a 128 point discrete Fourier transform where the input samples are windowed with a 42 dB Hamming weight. Not shown in the block diagram is the corner turning memory before the FFT which selects all of the pulses for a given range gate from the sequence of transmitted pulse returns where all of the range information is contained. The receiver/processor up to this point is assumed to be linear.

For each range gate and each doppler filter cell the inphase channel output and the quadrature channel output multiplied by -j are added together, and the real and the imaginary parts are separated, squared and summed, and then square rooted to obtain the envelope voltage. This becomes a single observation variable in the decision space. That is, all the pulses which are passed into the coherent integrator (FFT) result in a single pulse for each range-doppler cell in the radar detection context. Also, this is the sufficient statistic resulting from the Bayes likelihood ratio test for well known Swerling and Marcum target models with unknown initial phase embedded in white Gaussian noise. For these signal plus noise statistics, the above described receiver is the optimum receiver that maximizes the probability of detection. Its derivation is given by DiFranco and Rubin [2]. The test is performed separately for every azimuth-range-doppler cell.

The constant false alarm rate (CFAR) circuit provides the noise average to be used to determine the test threshold. False alarm rate is very sensitive to threshold level. For example, one dB change in the threshold can result in three orders of magnitude change in false alarm probability. To prevent fluctuations in the false alarm rate, actual noise averages are used to determine the threshold. Typically a cell averaging CFAR is used whereby envelope voltages of a predetermined number of range cells on both sides of the range cell under test are used for averaging. The two cells immediately adjacent to the test cell are excluded from the CFAR block. This average is multiplied by a fixed constant and is used as a threshold to decide whether the test statistic is signal plus noise (when above the threshold) or noise alone (when below the threshold) in the target detector.

In this radar, received radar pulses in a beam dwell are divided into three coherent processing intervals (CPI's) each operating at a different pulse repetition frequency (PRF) and each of which results in an observation variable for every range-doppler cell for detection decision making. The different PRF's are used so that range ambiguities can be

resolved by means of the Chinese remainder theorem. Before the post detection binary integration, filter normalization is performed to eliminate the variability in doppler frequency for a specific doppler cell. The M of N post detection integrator used in this radar requires that all three of the observation samples corresponding to a particular doppler filter in a beam dwell must have exceeded the threshold before the triplet can be declared as a candidate target with the velocity corresponding to that doppler filter.

Target report processing includes filter unfolding to resolve whether the velocity is opening or closing, and range ambiguity resolution to determine the unambiguous range for each candidate target. Azimuth, range and filter centroiding, deghosting to remove false target reports when more than one detection occurs in a doppler filter, and coordinate conversion to a stabilized coordinate system are part of the target report processing function. The results are sent out as radar reports which can be displayed on an operator console screen directly or after further processing by the Kalman filter tracker.

1.1.2 System Constraints

The system constraints to be observed in seeking detection performance improvement are specified in this section. Specifically, the antenna and transmitter are not allowed to be changed in the proposed modifications. As a result, the following system parameters are held fixed:

1. Antenna gain and radiation pattern

2. Transmitter power and duty factor

3. Radar operating frequency (carrier frequency and its operating frequency range).

The reason for these constraints is obvious. Changes to any of the above require a major new development with the associated cost, schedule and technical risks. Under these constraints, the potential area for investigation that would yield detection performance

8

improvement lies in signal processing changes whose implementation has been greatly facilitated by the recent breakthroughs in signal processing hardware and memory devices. As a consequence, the Scan-to-Scan Processing (SSP) concept, similar to Track Before Detect (TBD), has been promoted as a promising concept for significant detection performance improvement. However, a detailed analysis to support the projected benefits and associated drawbacks has not been carried out. A rigorous analysis of the SSP concept is one of the accomplishments of this dissertation. But first, the impact of the power-aperture product constraint is reviewed so as to provide awareness on the limits of detection performance improvement possible when the fundamental radar asset, namely the power-aperture product, is fixed.

A `rule of thumb' in radar engineering is that specification of power-aperture product, surveillance volume and the search frame time determines the detection performance against a given target, regardless of operating frequency, ignoring the secondary effects such as frequency dependent system losses, etc. The search frame time is the time it takes for the antenna beam to sweep the specified surveillance volume once at a predetermined rate. That the limit of detection performance is set by the above parameters can be seen by applying the radar range equation to the specified surveillance volume to be searched and utilizing the relationship between the solid angle subtended by the antenna beam and its aperture.

To see this, a simple radar range equation is first developed for the case where the dwell time or the number of pulses available for integration is given. If the transmitter power P_t is radiated isotropically, the power density produced at range R is given by

$$\begin{pmatrix} \text{power per unit} \\ \text{area at range R} \end{pmatrix} = \frac{P_t}{4\pi R^2} \ .$$

If a transmitting antenna of one way power gain G_t is used, the power density in the direction of this gain is

$$\begin{Bmatrix} \text{power per unit area at range} \\ \text{R in the given direction} \end{Bmatrix} = \frac{P_t G_t}{4\pi R^2} \; .$$

The signal strength reflected toward the radar per unit solid angle from a target of radar cross section (RCS) σ illuminated by the transmitted wave at range R is

$$\begin{Bmatrix} \text{reflected power per unit solid angle} \\ \text{in the direction of the radar} \end{Bmatrix} = \frac{P_t G_t}{4\pi R^2} \times \frac{\sigma}{4\pi} \; .$$

The reflected wave arrives back at the radar with a power density given by

$$\begin{Bmatrix} \text{reflected power per} \\ \text{unit area at the receiver} \end{Bmatrix} = \frac{P_t G_t}{4\pi R^2} \times \frac{\sigma}{4\pi} \times \frac{1}{R^2} \; .$$

The amount of power intercepted by the receiving antenna is this power density multiplied by the effective aperture defined by

$$\begin{Bmatrix} \text{effective} \\ \text{receiving aperture} \end{Bmatrix} = A = \frac{G\lambda^2}{4\pi} \tag{1.1-1}$$

where λ is the radar wavelength. The received signal power, S, is then expressed as

$$S = \frac{P_t G_t G_r \lambda^2 \sigma}{(4\pi)^3 R^4} \tag{1.1-2}$$

10

It is convenient to introduce a concept of equivalent input noise level, N, to arrive at the output signal-to-noise ratio at the end of the linear portion of the receiver before envelope detection. To facilitate this, the noise factor, NF, and effective noise temperature, T_e, of an amplifier or a receiver with a gain G are introduced. The noise factor is defined as

$$NF = \frac{S/N)_{in}}{(S/N)_{out}} = \frac{N_{out}}{kT_oBG}$$

where k is the Boltzman's constant, B is the bandwidth, and T_0 is the standard temperature taken to be 290°K.

The noise factor can be interpreted as the ratio of the actual available output noise power to the noise power which would be available if the receiver merely amplified the input noise. This may be expressed as

$$NF = \frac{kT_oBG + \Delta N}{kT_oBG} = 1 + \frac{\Delta N}{kT_oBG} \tag{1.1-3}$$

where ΔN is the additional noise introduced by the receiver. From equation (1.1-3), ΔN can be expressed as

$$\Delta N = (NF - 1)\, kT_oBG \;. \tag{1.1-4}$$

When two receivers are in cascade, the output noise is due to the sum of the noise from receiver 1 plus the noise introduced by receiver 2. Let the noise factor for the cascade and receivers 1 and 2 be denoted by NF, NF_1, and NF_2, respectively. Then, the output noise can be expressed as

$$N_{out} = kT_0BNFG_1G_2$$
$$= kT_0BNF_1G_1G_2 + \Delta N_2$$
$$= kT_0BNF_1G_1G_2 + (NF_2-1)kT_0BG_2 \;.$$

Dividing by $kT_0BG_1G_2$ gives

$$NF = NF_1 + \frac{(NF_2-1)}{G_1} \;. \tag{1.1-5}$$

The effective noise temperature, T_e, is defined as that temperature at the input of the receiver which would account for the noise ΔN at the output. It follows that

$$\Delta N = kT_eBG = (NF-1)kT_0BG \;,$$

and

$$T_e = (NF-1)T_0 \;. \tag{1.1-6}$$

For a cascade of two receivers, let the effective noise temperature of the cascade and receivers 1 and 2 be denoted by T_e, T_{e1}, and T_{e2}, respectively. Similar to the noise factor, the noise temperature of the cascade is given by

$$T_e = T_{e1} + \frac{T_{e2}}{G_1} \;. \tag{1.1-7}$$

If the antenna can be considered to represent a source at the reference temperature, the equivalent input noise power would be

$$N = kT_0BNF \;.$$

12

In practice, the antenna will have an effective temperature, T_a which differs from T_0. The equivalent input noise at the receiver front end can be expressed in terms of an effective input temperature T_{ei} which accounts for both the receiver and antenna noise. Note that

$$N = k[T_0(NF-1)+T_a]B = kT_{ei}B .$$

The effective input temperature is

$$T_{ei} = T_0(NF_0-1) + T_a .$$

The operating noise factor is defined to be

$$NF_0 = \frac{T_{ei}}{T_0} .$$

(1.1-8)

It follows that the equivalent input noise is

$$N = kT_0 B\ NF_0 .$$

With the introduction of NF_0, and use of Eqn. (1.1-2), the per pulse signal-to-noise ratio $(S/N)_p$ at the input to the detector assuming no multi-pulse integration becomes

$$\left(\frac{S}{N}\right)_p = \frac{P_t G^2 \lambda^2 \sigma}{(4\pi)^3\ R^4\ kT_0 B\ NF_0\ L} ,$$

(1.1-9)

where the parameters are:

P_t :   peak transmitted power which is actually the average power during the pulse duration

G :   one way antenna power gain ($G_t = G_r$ assumed)

R :   range to the target

σ :   target radar cross section

λ :   wave length at the radar operating frequency

k :   Boltzman's constant (1.38×10^{-23} W/Hz$^\circ$K)

T_0 :   standard temperature (290°K)

B :   receiver bandwidth

NF_0 :   operating noise factor as defined in Eqn.(1.1-8)

L :   total system loss factor not reflected in the operating noise factor.

The integrated signal-to-noise ratio, (S/N), is the per pulse signal-to-noise ratio, $(S/N)_p$, multiplied by N_I the number of pulses coherently integrated. To account for integration losses (i.e., the nonideality of the integrator) the loss factor, L, is increased accordingly. Then,

$$\left(\frac{S}{N}\right) = \frac{P_t G^2 \lambda^2 \sigma N_I}{(4\pi)^3 R^4 k T_0 B \, NF_0 L} .$$

$$(1.1\text{-}10)$$

If $1/B$ is replaced with the pulse width, τ, the integrated SNR is equal to the energy over noise power density, a well known matched filter equation.

When Ω, the surveillance volume in solid angle, and T_F, the frame time to search out the surveillance volume are specified, the surveillance radar range equation, (1.1-10) can be put into a different form. First, the number of antenna beam spots, n_S, to cover the entire surveillance volume is expressed as

$$n_s = \frac{\Omega}{\omega}$$

where ω is the solid angle subtended by the antenna beam. Note that

$$\omega = \frac{\lambda^2}{A}$$

where A is the effective antenna aperture. In terms of A and λ, n_s becomes

$$n_s = \frac{\Omega A}{\lambda^2} \quad .$$

Let T_r and F_r denote pulse repetition interval and pulse repetition frequency, respectively. P_A, the average power, and N_I, the number of pulses available for integration in a beam dwell, are expressed as

$$P_A = \frac{P_t \tau}{T_r} = \frac{P_t F_r}{B} \tag{1.1-11}$$

and

$$N_I = \frac{F_r T_F}{n_s} = \frac{F_r T_F \lambda^2}{\Omega A} \quad . \tag{1.1-12}$$

The peak power, P_t, can be expressed in terms of the average power, P_A, from equation (1.1-11) as

$$P_t = P_A \frac{B}{F_r} \quad . \tag{1.1-13}$$

The previously defined expression for the integrated SNR, Eqn. (1.1-10) can be rewritten by substituting Eqn. (1.1-13) for P_t, and Eqn. (1.1-12) for N_I,

$$\left(\frac{S}{N}\right) = \frac{P_t G^2 \lambda^2 \sigma N_I}{(4\pi)^3 R^4 k T_0 B NF_0 L}$$

$$= \frac{P_A B}{F_r}\left(\frac{4\pi A}{\lambda^2}\right)^2 \frac{\lambda^2 \sigma}{(4\pi)^3 R^4 k T_0 B NF_0 L}\left(\frac{F_r T_F \lambda^2}{\Omega A}\right)$$

$$= \frac{(P_A A)\sigma T_F}{4\pi R^4 \Omega k T_0 B NF_0 L} \qquad . \tag{1.1-14}$$

P_A A in the above equation is called the power-aperture product. Equation (1.1-14) is an important surveillance radar equation which shows that the integrated SNR is proportional to the power-aperture product independent of the operating frequency. It shows that when power-aperture product is fixed, radar performance is fairly well set unless its frame time and/or the surveillance volume is modified. The effect of varying these parameters is described in Chapter 5.

In addition to the power-aperture product constraint, performance improvement must be achieved without losing capability to resolve the range ambiguity inherent in a High PRF radar, and without exceeding the allowed system false alarm rate.

In a pulse doppler radar, either a range or a velocity ambiguity or both result as the consequence of a pulse repetition frequency (PRF) selection. The unambiguous range, R_u, is given by

$$R_u = \frac{c(T_r)}{2}$$

where c is the speed of light and T_r is the pulse repetition interval (PRI). For an unambiguous range of 400 nautical miles, the PRI, T_r, must be chosen such that

$$T_r \geq 2 \times 400 \times 1852/3 \times 10^8 = 4.9387 \text{ milliseconds.}$$

Hence, the PRF must be 202.4 Hz or lower.

The unambiguous radial velocity, v_{max}, is given by the doppler frequency corresponding to one-half the PRF. Note that

$$PRF/2 = f_{dmax} = 2v_{max}/\lambda.$$

Therefore, v_{max} is determined by the PRF as well as the carrier frequency of the radar chosen. For unambiguous measurements of both incoming and outgoing target velocities of up to 1800 knots, the PRF at an operating frequency of 3 GHz should be

$$PRF \geq 2f_{dmax} = 4 \times (1800 \times 1852/3600)/(3 \times 10^8/3 \times 10^9) = 37 \text{ KHz.}$$

Because of design implementation considerations some radars use PRF that is equal to just the maximum expected doppler frequency of the target. This results in an ambiguity as to opening or closing of the target velocity.

The superiority of a High PRF radar for detecting high speed airborne targets over a heavy ground traffic environment has been well demonstrated as was shown in the performance comparison between E-3 AWACS and E-2C Hawkeye radars over the European

17

continent. The E2-C radar operating at p-band (UHF frequency) has a broad antenna beam. With its low PRF waveform the largest mainbeam clutter doppler spread due to platform motion when the antenna beam is pointed normal to the platform velocity vector occupies almost 30% of the PRF interval. This PRF approximately corresponds to a 200 knot target speed. Thus, the radar cannot see targets whose speeds fall in this blind velocity zone which can be alleviated somewhat by PRF staggering. Of course, high PRF radars suffer from eclipsed range. The real difficulty with the overland performance of the E-2C radar, even with its scan-to-scan processing to suppress detections from ground vehicles and discrete land clutters, is its inability to distinguish slow moving ground vehicles from the high priority airborne threats in the portion of the PRF interval where the radar is not blinded. The high PRF radar is much more complex to build, however.

The range ambiguity in a high PRF radar is resolved by the so called Chinese remainder theorem [3, p19-16]. This approach permits a unique direct computation of the true range cell, R_c, from the multiple ambiguous range cell numbers, $A_1, A_2, --, A_n$. In particular, for the three PRF system Rc is given by

$$R_c = (C_1A_1 + C_2A_2 + C_3A_3) \; modulo(m_1m_2m_3)$$

where the m_i's are the number of range cells in each PRI and are required to be relatively prime. That is, R_c is the remainder of the term within parentheses, when divided by $m_1m_2m_3$ as many times as possible. The constants $C_1, C_2,$ and C_3 are related to $m_1, m_2,$ and m_3 by the following equations:

$$C_1 = b_1m_2m_3 = (1) \; modulo \; (m_1)$$

$$C_2 = b_2m_1m_3 = (1) \; modulo \; (m_2)$$

$$C_3 = b_3 m_1 m_2 = (1) \bmod (m_3)$$

where b_1 is the smallest positive integer which, when multiplied by $m_2 m_3$ and divided by m_1, gives unity as a remainder (and similarly for the other b's). Once m_1, m_2 and m_3 are chosen, the range, R_c, can be computed by using the C values and the ambiguous cell numbers (A_1, A_2, A_3) in which the target is detected. For example, the Chinese remainder theorem says that, given a triplet whose elements' maxima are 3, 5, and 7, any number between 1 and 105 can be uniquely specified by the triplet, {1,1,1} corresponding to 1 and {3,5,7} corresponding to 105.

To summarize, resolving range ambiguities in a High PRF system requires more than one coherent processing interval (CPI) in an antenna beam dwell with the attendant time overhead associated with each CPI. This time overhead is 50% of the available time in the example radar. This is why it is impractical, unless the scan rate is reduced to increase the dwell time, to have more than 3 CPI's in a beam dwell even though, theoretically, more CPI's can lead to improved performance of the binary post detection integrator.

Lastly, detection performance improvement is unacceptable if the false alarm rate is not kept below the minimum desired or tolerable level. Therefore, needless to say, the specified false alarm rate must not be exceeded under any condition. According to the preferred Neyman-Pearson strategy, the improvement should be in terms of maximizing the probability of detection for a fixed value of a false alarm probability that maintains the system false alarm rate at or below the allowed value.

1.1.3 Performance Improvement Criteria

Performance of the radar using the proposed modifications is compared to that of its present (baseline) configuration. A cumulative detection probability of 0.9 in a one minute time span for Swerling case 1 targets in the entire surveillance volume is adopted as the principal performance criterion under the constraint that the minimum false alarm time is 5 seconds. All suggested modifications are made within the system constraints specified in Section 1.1.2, and the Gaussian assumption for the noise and signal plus noise is assumed valid such that the receiver structure shown in Figure 1.1-2 is the optimum receiver which maximizes detection probability.

The Gaussian assumption is certainly true for the Swerling and Marcum target models in white Gaussian noise considered in this report where target doppler frequencies fall in the clutter free doppler zone after target signals are separated from the mainbeam clutter by their doppler frequencies and the mainbeam clutter is removed. This is also true in the case where target doppler frequencies coincide with doppler frequencies of sidelobe clutter. The reason for this is that the sidelobe clutter level in this radar is equal to or less than the thermal noise due to the extremely low sidelobes of the antenna. Also the sidelobe clutter is the sum of clutter returns from all ground patches whose doppler frequency and range rings fall in the ambiguous radar range-doppler cell in question such that the central limit theorem applies.

In the edge of the mainbeam clutter and in altitude-line clutter, the clutter signals can be greater than thermal noise. Even here, experimental data shows that the marginal probability density of clutter signals received through a coarse resolution radar is Gaussian within the time and spatial limit bounded by a single range-azimuth resolution cell in a beam dwell wherein a detection decision takes place. That is, even though the spatial inhomogeneity of the terrain gives rise to non-Rayleigh density functions for the amplitude

distribution of the clutter taken over a large surveillance area, the conditional density function given the local mean of the clutter voltage returning from many elemental clutter cells contained in a radar range-azimuth resolution cell is Gaussian by the central limit theorem. This random process, however, is characterized by nonzero mean and unequal variances between the quadrature components, and with a high degree of pulse to pulse correlation. This is believed to be because the sample is taken from a ground patch within a clutter spatial correlation distance and within a temporal correlation time. This is the non-stationary characterization of the clutter. More thoughts on this and some performance comparisons of several filter designs intended to maximize output signal-to-clutter ratio are presented in chapter 6.

Returning to the performance criterion, cumulative detection probability, P_c, is an important performance measure of a surveillance radar. Its definition and its relationship to the single scan probability of detection, otherwise known as the blip-scan ratio, will now be discussed. Consider the surveillance volume centered about the radar platform shown in Figure 1.1-3. The outer boundary of the horizontal coverage is defined by the range beyond which a single scan probability of detection, P_d, is less than some minimum value. Consider a radially approaching target with velocity V_R. Once the target has penetrated the boundary of the surveillance volume, let ΔR and Δt represent the maximum range penetration and the maximum time elapsed, respectively, before the target is detected by the radar at least once. Obviously, ΔR and Δt are related by

$$\Delta R = V_R \Delta t.$$

In general, several scans (say L) occur while attempting to detect the target in the interval ΔR. For analytic convenience, assume that ΔR is small compared to the range at which ΔR is measured such that the single scan detection probability (P_d) within the time Δt can be
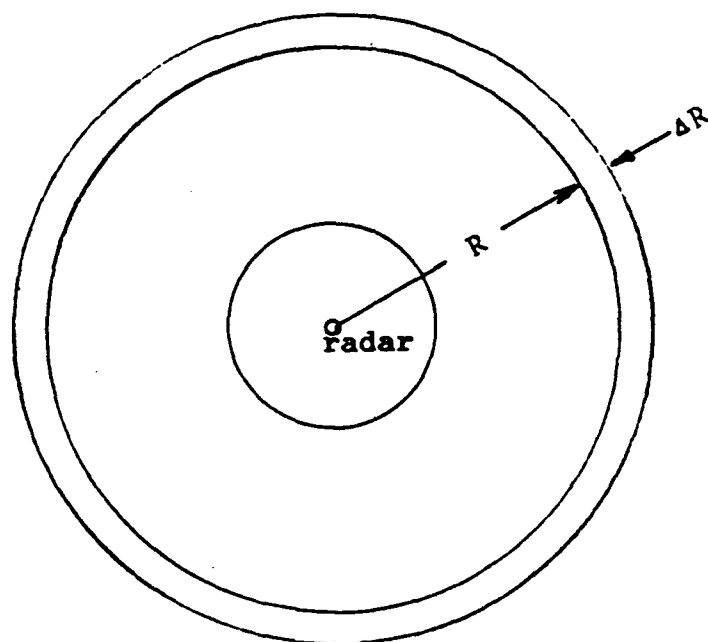
for radially approaching target
with velocity V_R

$$\Delta R = V_R \Delta t$$

Horizontal Coverage
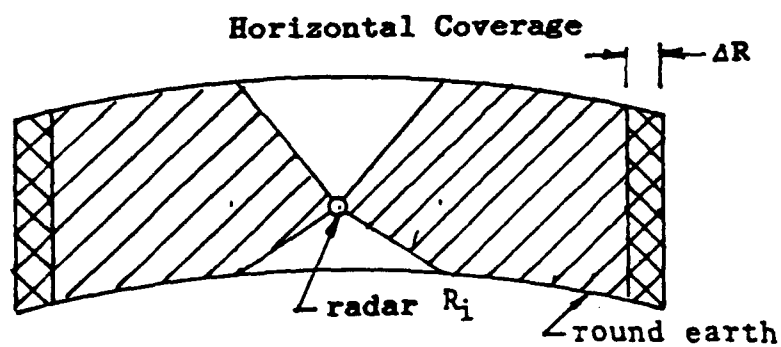
Vertical Coverage

Figure 1.1-3 Surveillance Volume for an Airborne Radar

assumed to be constant. With this assumption and the assumption of statistical independence from scan to scan, P_c in time Δt is given by

$$P_c = 1 - (1 - P_d)^L. \qquad (1.1\text{-}15)$$

In equation (1.1-15), P_d is the single scan probability of detecting the target. Thus, $(1 - P_d)$ represents the probability of a miss in any one scan and $(1 - P_d)^L$ is the probability of failing to detect the target in all L scans. Hence, Eqn. (1.1-15) gives the probability of making at least one detection in L scans.

On the surface, examination of Eqn. (1.1-15) indicates that P_c can be increased by using a larger value of L. However, for a specified Δt,

$$L = \Delta t / T_F$$

where T_F is the frame time allowed for searching out the entire surveillance volume. When Δt is held fixed, the only way to increase L is to decrease T_F. However, a reduction in T_F results in a shorter dwell time which, in turn, decreases N_I, the number of pulses to be integrated. Consequently, P_c becomes smaller as L becomes larger. It follows that there exists an optimum value for L in Eqn. (1.1-15).

A second consideration arises for fluctuating targets. It is shown in Section 3.3 that, as the signal-to-noise ratio increases, the detection probability for a fluctuating target relative to that of a nonfluctuating target degrades as shown in Figures 3.3-1 and 3.3-9. For a Swerling case 1 target, a crossover occurs when $P_d = 0.32$ in a single slant system or if an average beam shape loss is assumed for all slants in a multi-slant system. Otherwise, the crossover occurs at a point where P_d is slightly less than 0.32. For P_d less than this

value, the fluctuating target has a higher detection probability than does a nonfluctuating target. The situation is reversed for P_d greater than this value. Barton [4] states that the optimum number of scans, L, for a Swerling case 1 target is around 6 for P_c of 0.9. It is around 2 for P_c of 0.5 and around 10 for P_c of 0.99. For the radar under consideration in its baseline configuration, the specified minimum P_d is 0.32 and the maximum elapsed time Δt is one minute. This gives 6 scans in Δt at a scan rate of 36 degrees per second and P_c in Δt becomes

$$P_c = 1 - (1 - 0.32)^6 = 0.9 \qquad (1.1\text{-}16)$$

This satisfies the optimum number for L of Barton.

If the range closure during the elapsed time Δt is not negligible, then, a different P_d for each scan must be used to compute P_c. Let $\Delta R = L\Delta$ where Δ is the range closure during a single scan. Assuming a constant radial velocity, the target in a particular azimuth direction appears in the same relative position within each increment Δ, as shown in Figure 1.1-4. Let $p(R_m+r+i\Delta)$ denote the single scan P_d at range $R_m+r+i\Delta$. However, depending on the azimuth direction, r can vary anywhere from R_m to $R_m+\Delta$. Assuming r is a random variable uniformly distributed over the interval Δ, the mean cumulative detection probability, $P(R_m, \Delta)$ is given by

$$P(R_m,\Delta) = \frac{1}{\Delta} \int_{R_m}^{R_m+\Delta} \left\{ 1 - \prod_{i=0}^{L-1} [1 - p(R_m + r + i\Delta)] \right\} dr .$$

$$(1.1\text{-}17)$$

The integral in Eqn. (1.1-17) performs an averaging which takes into account the fact that the target could be anywhere in the interval $[i\Delta, (i+1)\Delta]$ with equal likelihood when

intercepted by the radar beam. Analyses based on this approach which allow determination of the optimum value of frame time is given in Sections 5.1 and 5.2. Unless otherwise specified, the definition for P_c given by Eqn. (1.1-15) will be used in this investigation.
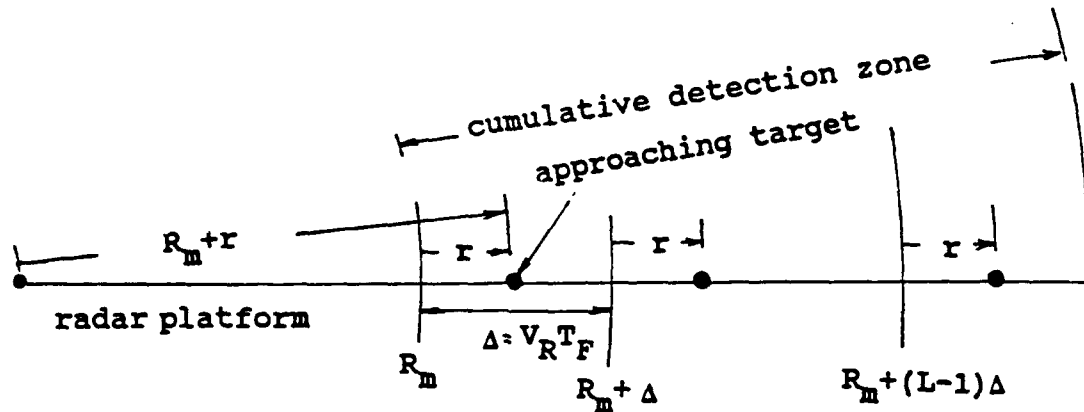
Figure 1.1-4. Detection Scenario of an Approaching Target with a Constant Radial Velocity

The relationship between P_d and P_c has been established when P_d is independent from scan to scan. As will be shown in Section 4.4, this assumption is not valid when scan-to-scan processing (SSP) is used. Therefore, for SSP, P_c cannot be computed by simply using Eqn. (1.1-15). The computation of P_c for SSP is developed in Chapter 4 which is entirely devoted to SSP.

Another term often used in radar detection is the blip-scan ratio (BSR). This is the ratio of the number of scans, J, within each of which a given target is detected to the total number of elapsed scans, L. For L large, the blip-scan ratio approximates the single scan detection probability in accordance with the relative frequency interpretation of probability [5]. Note that the average number of hits in L scans can be approximated by the product

[BSR]L. This is also equal to the number of track updates in a time interval equal to L scans.

The track update rate at the minimum critical range is another performance criterion. This is the range at which the single scan detection probability is high such that the track update rate approaches the antenna scan rate. By definition, the track update rate is the ratio of P_d to T_F. The track update interval is the reciprocal of the track update rate. For successful target tracking, a minimum track update rate must be maintained at the minimum critical range. This must be kept in mind when adjusting scan rate so as to improve cumulative detection performance. Scan rate optimization is discussed in Chapter 5 where it is shown that the cumulative detection probability can be increased by slowing the scan rate. However, the track update requirement places a lower limit on scan rate.

1.2 Dissertation Outline

The description of the radar for which performance improvement is sought was presented in Section 1.1.1. Chapter 2 contains a discussion of various considerations needed for comparison of the baseline and modified radars. These include such issues as the number of coherent processing intervals in a beam dwell, the number of available pulses in a coherent processing interval, beam shape loss, false alarm probability allocation, and target models. It is shown how two different approaches to false alarm calculations, as proposed in the radar literature, can be used to relate cell false alarms to system false alarms.

Performance analysis of the baseline radar is presented in Chapter 3. This forms the basis for comparing performance improvements of the modified configurations. It is desired to extend the range at which the specified cumulative detection probability is achieved without changing the radar's power-aperture product and operating frequency.

Scan-to-scan processing has been pursued by others as a promising technique for obtaining performance improvement. However, a detailed analysis to support this claim is not available in the literature. In Chapter 4, a careful analysis is performed and numerical results are generated for two versions of the scan-to-scan processing concept. It is shown that only marginal improvement can be attributed to scan-to-scan processing. One significant conclusion is that it is difficult to overcome the power-aperture product limitation with increased signal processing.

In an effort to overcome the limitations encountered, an alternate approach is explored in Chapter 5. This involves scan rate reduction and non-coherent integration in place of the M of N post detection integration. Trade-offs involved with reducing the search sector are also examined because the power-aperture product constraint leaves very few options. A detailed analysis reveals potential improvements over the range from 3 to 10 dB in the equivalent signal-to-noise ratio gain. The near 10 dB improvement occurs with reduction of the search sector by a factor of two, slowing down the scan rate by the same factor coupled with a non-coherent integration in lieu of the binary post detection integration, and modifying the performance requirement that $P_c=0.9$ in a 1 minute surveillance interval to the requirement that there be on the average one track update in a 10 second interval. The improvement, strictly according to the original performance criterion, can be as high as 5 dB. This requires noncoherent integration with slant-to-slant frequency agility. All these figures are for Swerling case 1 targets.

A summary of results developed in this dissertation is presented in Chapter 6. The work is focused on improving detection of targets embedded in white Gaussian noise. In addition, some thoughts on clutter statistics and their implication on receiver structure are given. Quantitative comparisons of relative performances of different classes of clutter

27

cancellers using actual high PRF radar data as test inputs are also included. Finally, suggestions for additional work are included.

CHAPTER 2

SOME CONSIDERATIONS IN PERFORMANCE COMPARISON OF
MODIFIED AND BASELINE RADAR CONFIGURATIONS

In this chapter various concepts needed for comparison of
the baseline radar configuration with proposed modifications
are discussed. After defining relevant radar terminology,
assumptions used in the analyses are presented. This is fol-
lowed by discussions of those parameters which do not remain
constant as the configuration is changed from the baseline.

2.1 Definitions of Terms

To facilitate understanding of the discussions and
analyses presented in this investigation, frequently used
terminology which may not be familiar to the nonspecialist
is defined below:

Baseline Configuration:

The radar in its present form is referred to as the
baseline configuration to distinguish it from modified con-
figurations proposed for performance improvement.

Surveillance Volume (Ω):

Surveillance volume is the volume of space to be searched

for targets of·interest. The surveillance volume of this radar was shown in Figure 1.1-3. The azimuth coverage is 360 degrees. For range less than R_i, the vertical coverage is bounded by the antenna elevation beamwidth while beyond R_i, the coverage is bounded by the surface of the earth and the maximum altitude of interest. Both coverages are bounded in range by the radar horizon and/or the maximum detection capability of the radar.

Search Frame Time (T_F):

For the radar under consideration the vertical coverage is illuminated by the single antenna beamwidth. Therefore, the antenna scan is limited to the azimuthal dimension. The search frame time is the time for the antenna fan beam to sweep through the entire 360 degree azimuth sector. The radar under consideration is equipped with a mechanically rotating antenna. The search frame time is more commonly referred to as a frame time or a scan time. For the radar in the baseline configuration, the scan time is 10 seconds. Therefore, the scan rate is 36 degrees per second or 6 revolution per minute (rpm).

Beam Spot:

For a given antenna beam, the number of beam spots required to cover the entire surveillance volume determines

the number of beam dwells in a scan and, therefore, the dwell time that results for a specified frame time. In an azimuth scan only radar, there are $360°/\theta_B$ beam spots in a $360°$ sector where θ_B is the one-way half-power azimuth beamwidth.

Dwell Time:

For the radar under consideration the antenna is mechanically rotated in azimuth at a constant rate. The dwell time is the time during a single scan that a point target in a fixed azimuth direction is within the one-way half-power beamwidth.

Pulse Repetition Frequency (PRF):

The pulse repetition frequency is the frequency of the periodic transmitted pulse train. When several different PRF's are used in order to resolve range ambiguities, the number of pulses transmitted in a given time, assuming continuous transmission at an average PRF, is used to measure time intervals of interest, e.g., dwell time, for convenience.

Coherent Processing Interval (CPI):

CPI is the time interval spanning the number of pulses used for coherent integration (i.e., number of FFT samples).

The duration of the CPI is measured in terms of the average pulse repetition frequency (PRF). CPI's in a dwell time are not contiguous. They are interleaved with intervals for time overhead.

Time Overhead (T_H):

Time overhead is the portion of the time in a modulation period that is not a part of the coherent processing interval. This includes the round trip transit time of the transmitted pulse with respect to the maximum range clutter patch and/or a target, certain house keeping overhead such as timing and control necessary to setup the CPI, and clutter canceller transient response settling time during which signal integration is prevented. In the baseline configuration, this time overhead exceeds 50% of the modulation period.

Modulation Period (T_m):

A frame time or a scan time consists of a contiguous train of modulation periods. A modulation period consists of the coherent processing interval (CPI) plus the total amount of time overhead associated with the CPI. The modulation period is depicted in Figure 2.1-1. The actual received pulses at the analog-to-digital converter output are shown in Figure 2.1-2 for range gates 33 through 36 where the interactions between first, second and multiple time around

32
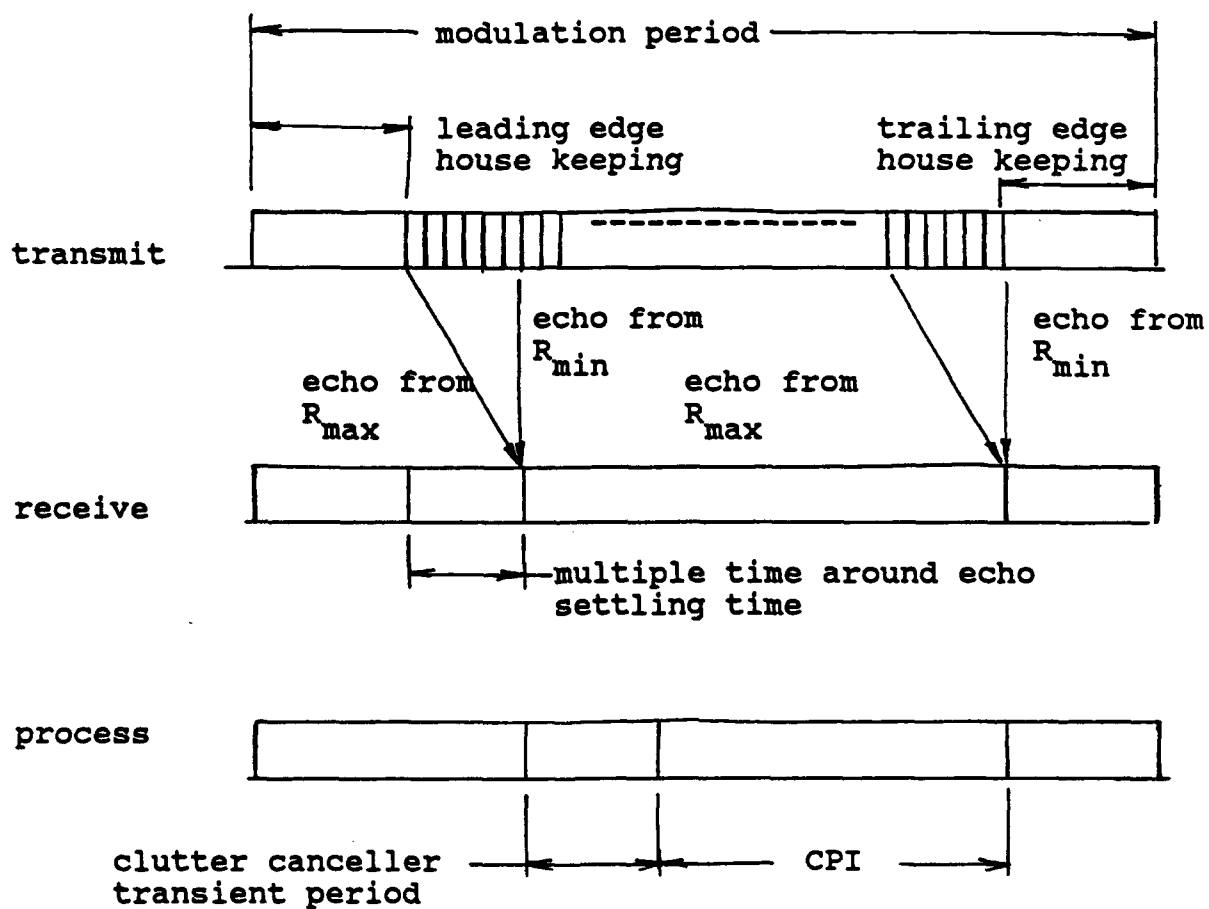
Figure 2.1-1 Modulation Period

33
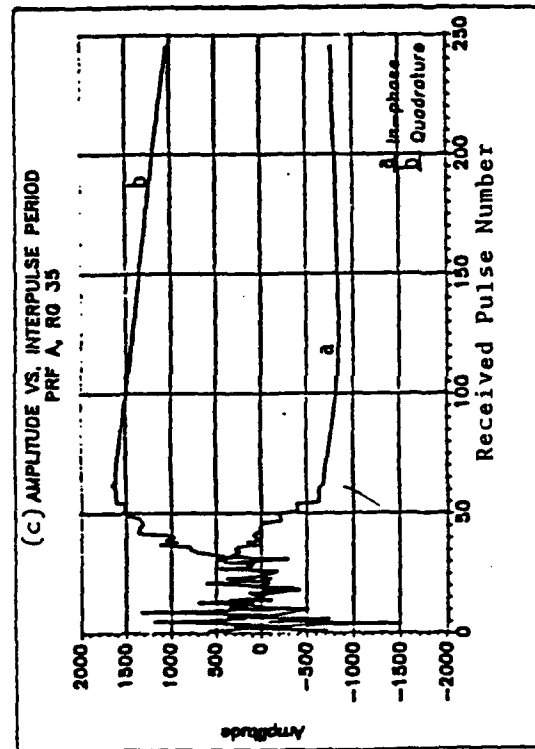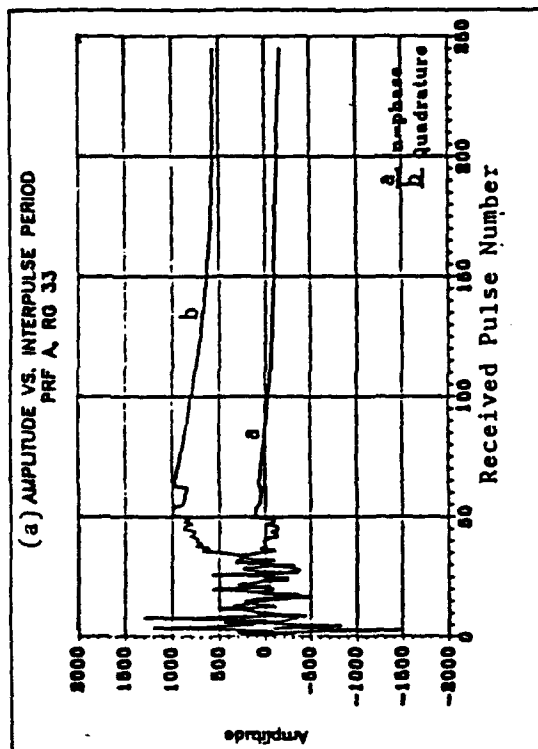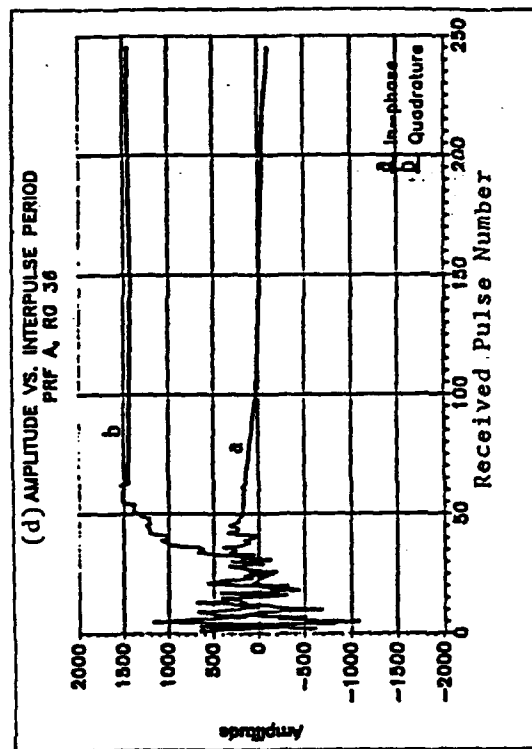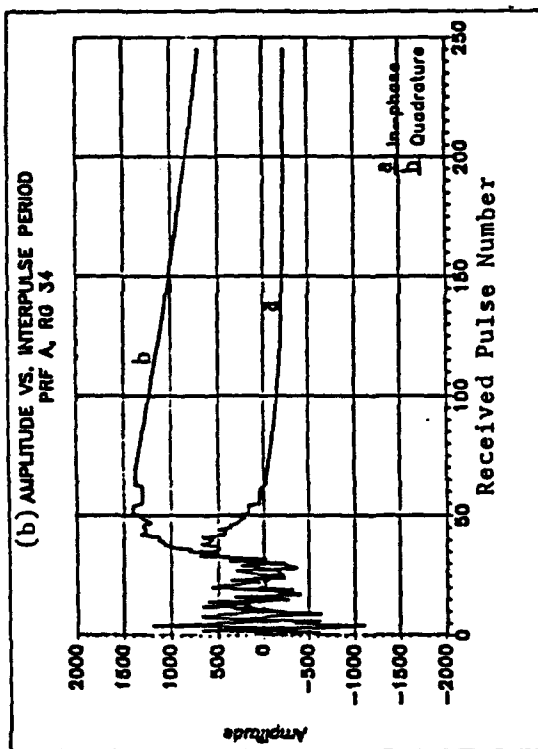
Figure 2.1-2. Received Pulse Returns in a High PRF Airborne Radar

34

echoes are clearly illustrated at the beginning of the pulse train. These pulses are discarded from further processing. This transient period lasts until returns from the clutter patch at the maximum range begins to reach the receiver. Figures 2.1-3 (a) and (b), respectively, show the output of the infinite impulse response (IIR) filter used for the clutter canceller and the steady state portion of that waveform processed through a 128 point FFT. Figures 2.1-3 (c) and (d), respectively, are the output of the finite impulse response (FIR) filter used as the clutter canceller (2-stage delay line canceller) and that waveform processed through a 256 point FFT. The absence of the transient response at the output of this FIR clutter canceller is evident and is what enables use of the longer FFT.

Slant:

A slant is synonymous with modulation period. A 2-slant or 3-slant configuration refers to the configuration wherein a dwell time is divided into the specified number of slants.

Integrated Signal-to-Noise Ratio (SNR or S/N):

As given in Eqn. (1.1-10) the integrated signal-to-noise ratio involves the average signal power over N_I pulses. Some authors use peak signal power over the N_I pulses. Consistent with DiFranco and Rubin [2] the symbol, $\mathscr{R}$, will be employed to denote the integrated signal-to-noise ratio when
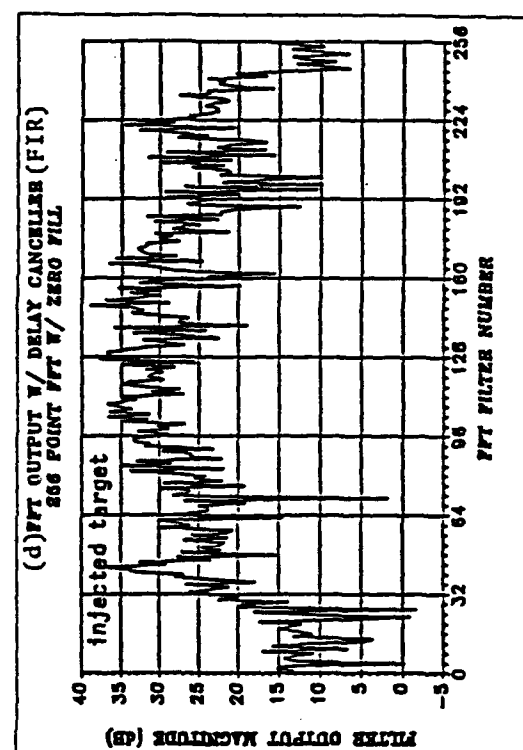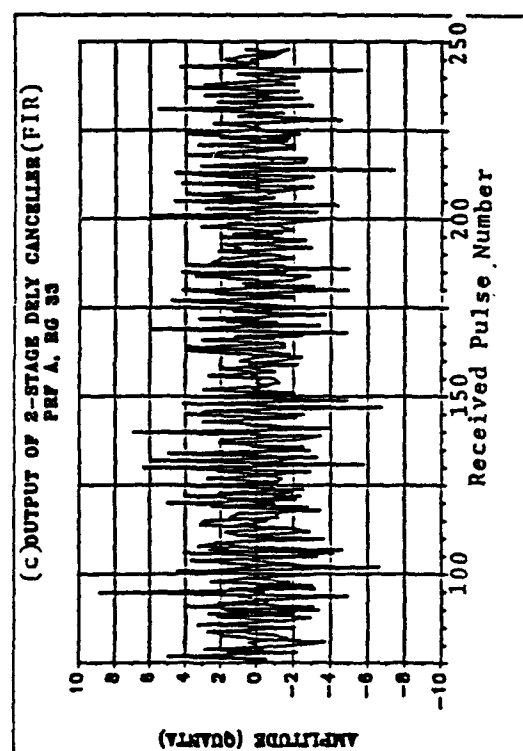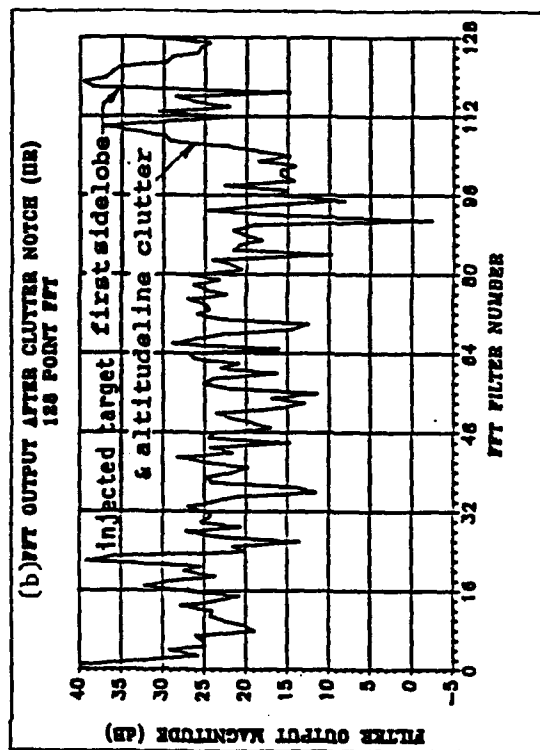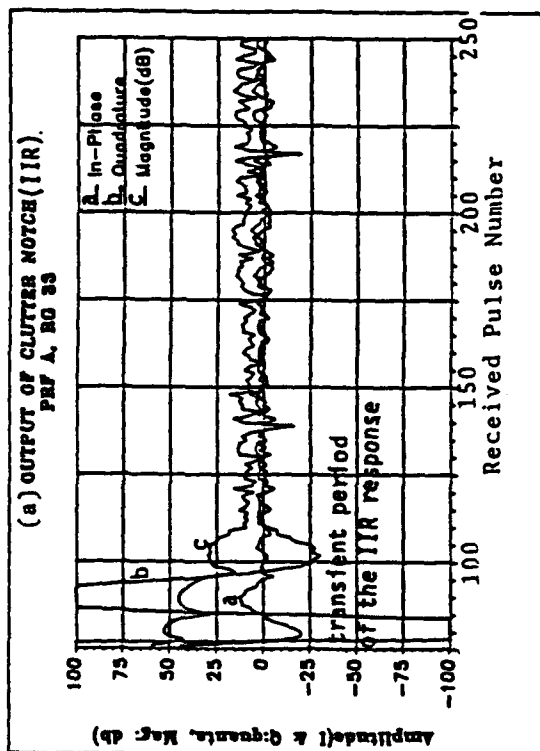
Figure 2.1-3. A Comparison of IIR and FIR Clutter Canceller in a High PRF Waveform

peak signal power is used. Note that $\mathcal{R}$ is twice SNR. Unless otherwise specified, the SNR in Tables and Figures of detection probability (P_d) will be the SNR associated with a single CPI that would appear at the detector had all the pulses in that CPI been received through the peak of the antenna beam. Hence, the notation (S_o/N) is introduced to signify this. When this is in response to an average target radar cross section (RCS), an overbar is placed above the symbol, i.e., $(\overline{S}_o/N)$. To take into account the beam shape, the P_d is computed by subtracting from the listed $(\overline{S}_o/N)$ the corresponding beam shape loss in dB for each of the CPI within a beam dwell in a given processing configuration. This allows for comparison, on a common ground, of the different processing configurations which have different beam shape losses.

Reference Range (R_o):
_____

Reference range is the range at which the specified detection performance is reached for a reference Swerling case 1 target in the baseline configuration. All other ranges are normalized to this range.

Reference Signal-to-Noise Ratio $(\overline{S}_o/N)_o$:
_____

Reference signal-to-noise ratio (reference SNR) is the integrated signal-to-noise ratio received in a CPI from a

reference target having a specified mean radar cross section (RCS) when it is located at the reference range. All reference targets have the same specified mean RCS. When the reference target is a Swerling case 1 target, the reference SNR results in a single scan detection probability of 0.32 in the baseline configuration. Since the reference target is defined only in terms of its mean RCS regardless of the target model assumed, the reference SNR has the same value for all target models in a given configuration but gives rise to different values of probability of detection. For configurations other than the baseline, the reference SNR is the SNR obtained in a CPI in each configuration from the reference target located at the reference range. Therefore, the value of the reference SNR is different for a different configuration and thus reflects the change in the configuration.

Single Scan Detection Probability (P_d):

By definition, single scan detection probability which is measured after post detection integration, does not utilize information from previous scans. Therefore, P_d is assumed to be independent from scan to scan.

Hybrid Single Scan Detection Probability (P_d(hyb)):

In contrast with single scan detection probability, the

hybrid single scan detection probability which arises in SSP uses the past scan detection history. Therefore, it is not independent from scan to scan.

Blip Scan Ratio (BSR):

Blip scan ratio is the number of scans, J, where a hit is scored from a given target divided by the total number of scans, K, elapsed. This approaches the single scan detection probability when K is large assuming that P_d remains constant.

Cumulative Detection Probability (P_c):

Cumulative detection probability and its relationship to single scan detection probability (P_d) are defined in section 1.1.3 under performance improvement criteria. Unless otherwise specified, cumulative detection probability over a fixed time interval is defined assuming that single scan detection probability is constant over that interval. This, in turn, assumes that the target range closure during the interval is negligible. Thus, in the absence of a scan-to-scan processing (SSP), P_c is given by the relationship, $P_c = 1-(1-P_d)^L$, where L is the number of antenna scans in that time interval and P_d is assumed to be independent from scan to scan. The computation of P_c under SSP is complex. This is derived in chapter 4 where SSP is discussed. Unless

otherwise specified, the time interval is taken as one minute or L is 6 scans at 6 a rpm antenna rotation rate.

2.2 Basic Assumptions

Basic assumptions under which the results of this investigation are based are presented in this Section.

1. The probability density of signal and signal plus noise voltages after removal of the mainbeam clutter is Gaussian. The noise voltages which may consist of the thermal noise and residue mainbeam clutter plus sidelobe clutter are white Gaussian with zero mean and equal variance between their quadrature components.

2. The antenna and the receiver together, including analog-to- digital converter and FFT before the detector, is linear.

3. The target model of interest belongs to one of the five Swerling and Marcum cases. In particular, the priority target is Swerling case 1.

When assumption 1 does not hold, particularly with respect

40

to the total noise remaining after the mainbeam clutter can-
cellation, the receiver structure shown in Figure 1.1-1 is
not optimum for maximizing the detection probability. Avail-
able test data shows, however, that the stated assumption
is reasonable.

2.3 Number of CPI's in a Beam Dwell and Number of Available Pulses in a CPI

As introduced in section 2.1 under definition of terms, the frame time of a radar whose antenna is scanning the surveillance sector at a constant rate is made up of contiguous modulation periods. The length of a modulation period is chosen such that there can be at least 3 modulation periods in a beam dwell in order to allow use of different PRF's to resolve the range and/or velocity ambiguities of targets. Associated with each modulation period, there is a fixed time overhead. For the baseline configuration, this is over 50% of the total modulation period. In general, for a specified beam dwell, this limits the maximum number of modulation periods in the beam dwell to 3. (For other radars, in which a smaller time overhead is possible primarily because of shorter round trip transit time for surveillance over short ranges, more modulation periods can be implemented for greater effectiveness in binary post detection integration.)

Given a system which is power limited (i.e., a transmitter which is already operating at the limit of its peak power, average power, and duty factor), the most effective operation uses the widest pulse width at its peak power con-

sistent with resolution requirements, and the maximum PRF for which the average power and duty factor are not exceeded. This, in essence, sets the maximum PRF as well. Thus, the available energy in a beam dwell is fixed for a given scan rate and pulse repetition frequency. However, usable energy is determined by the number of modulation periods chosen and the fixed time overhead associated with each modulation period. The relative figures based on these numbers are established here for the baseline and modified configurations for convenient reference.

In practice, different pulse repetition intervals (PRI's) are used in the modulation periods which reside in a beam dwell. In this investigation, relative time intervals are measured using the average PRI. For example, consider a 3-slant configuration in which the PRI's are 0.9, 1.0 and 1.1 milliseconds. (These are fictitious numbers.) Consequently, a time interval of 1 second will be said to have a duration of 1000 PRI's using the average PRI. Analogously, since there is one pulse per PRI, time can be measured in terms of the number of pulses. A dwell time is defined as

dwell time = (half power beamwidth)/(scan rate).

Let PRI and PRF denote the average pulse repetition interval and average pulse repetition frequency, respectively. Of

course, $\overline{PRF}$ is the reciprocal of $\overline{PRI}$. A dwell time is given in terms of a number of PRI's by

$$\text{dwell time (in PRI's)} = (\text{dwell time})/\overline{PRI}$$
$$= (\text{dwell time}) \times \overline{PRF}.$$

For a particular radar design, the number of modulation periods processed as a group will occupy a specified fraction of the beamwidth. (This fraction typically varies between 0.8 and a number slightly higher than unity.) Thus, an average modulation period measured in PRI's is given by

$$\text{modulation period (in } \overline{PRI}\text{'s)} = (\text{dwell time}) \times (\text{fractional}$$
$$\text{beam width used}) \times \overline{PRF} / (\text{number of modulation periods}).$$

In practice, [(dwell time)×(fractional beamwidth used)] is also referred to as dwell time for convenience.

A coherent processing interval (CPI) available in a modulation period is the time remaining after a fixed time overhead is subtracted from a given modulation period. Two different time overheads are considered in the performance analysis: One is the normal time overhead (also referred to as the maximum time overhead), and the other is a reduced time overhead. The latter is based on the assumption that under some operating conditions, where there is no clutter beyond the radar horizon, the waiting period for the multiple time around echo from the farthest clutter patch can

44

be reduced. Another factor influencing time overhead is the transient settling time of the clutter canceller. It appears possible to reduce time overhead by incorporating a canceller having a shorter settling time. The expected savings arising from the two factors are incorporated into the reduced time overhead. The relative figure proportional to the number of pulses available for integration, along with related parameters, are listed in Table 2.3-1 for a radar employing a mechanically rotating antenna with a 6 rpm scan rate.

It is assumed that N_B number PRI's occur within the antenna half-power beamwidth. Because 103.6% of the beamwidth is utilized, the total number of PRI's in a beam dwell is $1.06N_B$. Consequently, there are $1.036N_B/3 = N_{m3}$ number of pulses in a modulation period for a 3-slant configuration and $1.036N_B/2 = N_{m2}$ number of pulses for a 2-slant configuration. Because of the large time overhead, the number of useful pulses in a CPI is significantly smaller than the total number of pulses in a modulation period. The reference number of pulses per CPI is equal to (reference N_I). The relative integration gain per CPI for the various configurations is defined to be

$$\frac{\text{relative integration gain}}{\text{CPI}} \text{ (dB)} = 10 \log_{10} \frac{\text{\# of pulses in a CPI}}{(\text{reference } N_I)} \, .$$

45

Table 2.3-1

Number of Pulses Available for Integration with a 6 rpm Antenna Scan Rate

Configuration	3-slant		2-slant	
Time overhead	normal	reduced	normal	reduced
No. of pulses in 3-dB beam width	N_B	N_B	N_B	N_B
% beam width utilized for PDI*	103.6	103.6	103.6	103.6
No. of mod. periods per beam dwell	3	3	2	2
No. of pulses in a mod. period (MP)**	N_{m3}	N_{m3}	N_{m2}	N_{m2}
time overhead	$.521N_{m3}$	$.348N_{m3}$	$.347N_{m2}$	$.232N_{m2}$
CPI	$.479N_{m3}$	$.652N_{m3}$	$.653N_{m2}$	$.768N_{m2}$
Relative integration gain/CPI (dB)	Ref	1.33	3.11	3.81
Relative gain in total energy/dwell (dB)	Ref	1.33	1.35	2.05
	Baseline	Modified Configurations		

* PDI = post detection integration

** N_{mi} = (N_B)(% beamwidth utilized)/(i)

46

The reference number of pulses per beam dwell is 3x(reference N_I). Hence, the relative gain in total energy per beam dwell is given by

$$\frac{\text{relative gain in total energy}}{\text{beam dwell}} \text{ (dB)} = 10 \log_{10} \frac{(\text{\# of pulses in a CPI})(\text{\# slants})}{3\text{x}(\text{reference } N_I)} .$$

The relative integration gain/CPI is a misleading figure of merit because the larger gain for a 2-slant configuration is offset by the fact that there is one less CPI than for the 3-slant configuration. Both of these factors determine performance of the M of N binary post detection integrator. As a result, the relative gain in total energy/beam dwell is a figure of merit which more closely reflects system performance.

2.4 Beam Shape Loss

Broadly speaking, beam shape loss takes into account the variable antenna gain experienced by the transmitted and received pulses as the antenna scans by a point target during a CPI. Blake [7] has shown that a minimum two way, single dimensional beam shape loss of 1.6 dB should be used to account for the actual beam shape as compared to the constant gain over the half power beam width typically used. His

analysis assumes that a large number of pulses are centered around the peak of the beam over an optimum fraction of the beamwidth. For pulses positioned outside the 84 % beamwidth, he shows that integration results in loss of signal-to-noise ratio because more noise is added than signal beyond this optimum width. His analysis applies to a detection of a weak signal with a square-law detector followed by a post detection integrator.

Since finding an appropriate average beam shape loss depends on the percent of beamwidth utilized and the particular detection processing used, a more accurate method is to compute the actual loss per CPI. Let the two-way antenna power pattern be approximated by the Gaussian expression,

$$G(\theta) = \exp(-5.55\ \theta^2/\theta_B^2)\ .$$

Assuming a train of pulses at a constant PRF, let N_B denote the number of pulses that would be received in a beamwidth. If the pulses are centered about the peak of the beam and θ_k denotes the angular position of the kth pulse, it follows that

$$\frac{\theta_k}{\theta_B} = \frac{k}{N_B}\ . \tag{2.4-1}$$

Let N_I be the number of pulses actually integrated. For the idealized situation in which the beam pattern has a constant gain of unity, the total received power would be N_I times the power in a single pulse. Assuming the N_I pulses to be centered on the beam where N_I is an odd integer, the normalized total power received is

$$1 + 2 \sum_{k=1}^{(N_I-1)/2} \exp(-5.55 \; k^2/N_B^2) \; .$$

The beam shape loss, L_{BS}, is defined to be the ratio of these two powers, expressed in dB. Hence, as found in Skolnik [9], the beam shape loss is given by

$$L_{BS} = 10 \; \log_{10} \frac{N_I}{1 + 2 \sum_{k=1}^{(N_I-1)/2} \exp(-5.55 \; k^2/N_B^2)} \; . \tag{2.4-2}$$

For example, if there are 11 pulses to be integrated, all lying uniformly between the half-power beamwidth, the beam shape loss is 1.96 dB.

In the radar under consideration the set of modulation periods (e.g., 3 in 3-slant configuration) nearest the beam center is selected as a group, at a one slant increment on a sliding window basis, for post detection integration. The set nearest the beam center will result in the highest signal-to-noise ratio. Therefore, this particular set is the one for which the beam shape loss needs to be determined.

49

Since the antenna is continually scanning, the set can be positioned anywhere with respect to the beam center with equal likelihood from the most favorable position (centered) to the least favorable position which is one-half modulation period offset left and right from the centered position. For an offset larger than this, the next set will result in a higher signal-to-noise ratio. Therefore, the correct beam shape loss for each CPI in a set is the beam shape loss for the CPI computed per Eqn. (2.4-2) adjusted for offset from the beam center. In addition, to account for the random position of the CPI, the beam shape loss should be averaged over all possible positions of the CPI extending from one-half modulation period offset to the left and right. The centered and extreme offset positions for 2-slant and 3-slant configurations are shown in Figure 2.4-1.

Analogus to Eqn. (2.4-1), it is convenient to measure an angular offset in terms of the number of pulses that would span the offset or length. In this sense, the following notation is introduced (see Figure 2.4-1):

N_c : offset of a CPI measured from the beam centerline to the center of the CPI when the set of modulation periods is centered on the beam centerline

N_L : offset of a CPI measured from the beam centerline to the leading edge of the CPI

N_I : length of the CPI

2-Slant System:
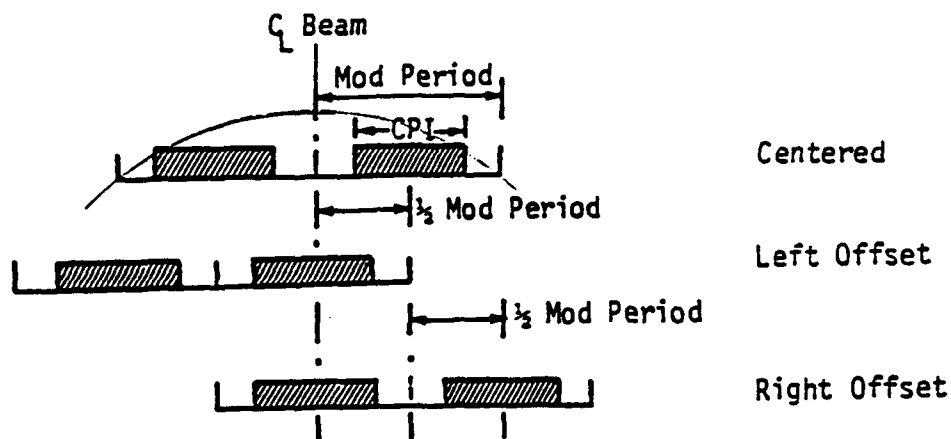
3-Slant System:
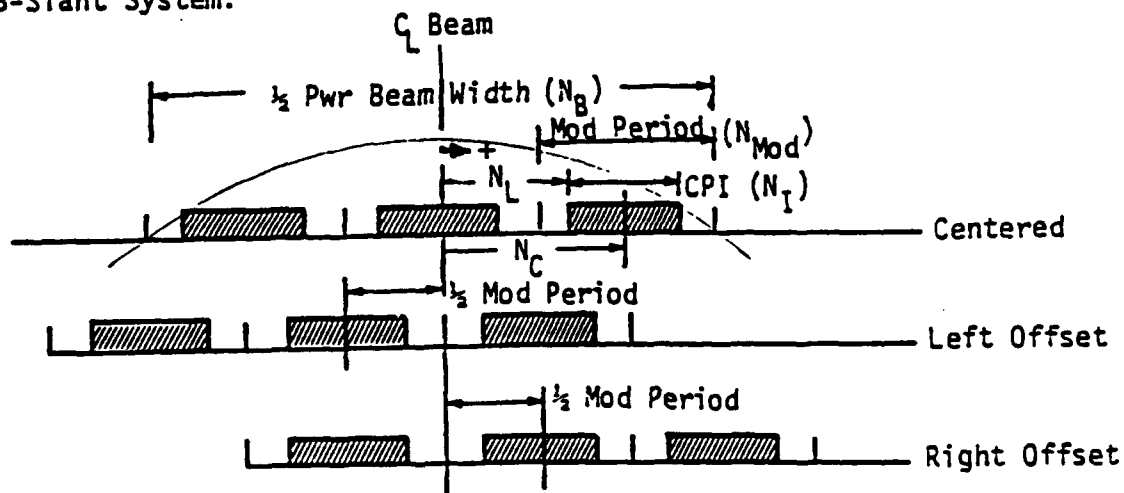
Figure   2.4-1   Possible Positions of a Set of   Modulation
         Periods w.r.t Beam Centerline

N_{mod} : length of modulation period.

For a CPI offset by N_L, the conditional beam shape loss of the CPI is

$$L_{BS|N_L} = 10 \; \log_{10} \left[\frac{N_I}{\displaystyle\sum_{k=N_L}^{N_I+N_L-1} \exp(-5.55k^2/N_B^2)} \right] .$$

To average over the random position of the CPI, let N_L be uniformly distributed over the modulation period. It follows that the beam shape loss, averaged over all possible positions of the CPI, is given by

$$L_{BS} = 10 \; \log_{10} \left[\frac{1}{N_{mod}} \sum_{N_L=-\frac{1}{2}(N_{mod}+N_I)+N_c}^{N_L=\frac{1}{2}(N_{mod}-N_I)+N_c} \left(\frac{N_i}{\displaystyle\sum_{k=N_L}^{N_I+N_L-1} \exp(-5.55k^2/N_B^2)} \right) \right] .$$

$$(2.4-3)$$

In the remainder of the investigation the term, beam shape loss, refers to the loss evaluated using Eqn. (2.4-3).

Using this method, the beam shape loss for each CPI in various 2-slant and 3-slant configurations are computed. The results are summarized in Table 2.4-1. Because of symmetry in the 2-slant configuration, the beam shape loss for both CPI's are equal. For the 3-slant configuration the loss for the center CPI is significantly less than those for the two outer CPI's. The losses with reduced time overhead are about the same as those for normal time overhead. Almost

without exception, the industry computes performance analysis using the 1.6 dB beam shape loss originally proposed by Blake [7]. When several slants are involved, the 1.6 dB loss is treated as though it applies to each of the individual CPI's. In Table 2.4-1, average beam shape losses are tabulated which are obtained by averaging the actual losses for each CPI. The increase in loss cver the 1.6 dB figure is due to both the larger percentage of beam utilization and the averaging over the random positioning of the CPI's. In the analysis of the baseline configuration, the effect of beam shape loss on the detection probability is discussed. It will be shown that use of an average beam shape loss in place of the losses for individual CPI's leads to an optimistic prediction of performance. As a final point, it is noted that the use of additional slants can be achieved by processing CPI's positioned outside the half-power beamwidth. The beam shape loss for those CPI's increases dramatically. For example, if 5 slants in a 3-slant configuration are processed, the beam shape loss for the two outer CPI's in the 5-slant set is 7.28 dB. Therefore, use of Blake's 1.6 dB figure for those CPI's would result in large errors.

Table 2.4-1 Summary of Beam Shape Loss for the 2-Slant
and 3-Slant configurations

	2-slants per beamwidth beam shape loss (dB)			3-slants per beamwidth beam shape loss (dB)			
	CPI_1	CPI_2	$(2-CPI)_{ave.}$	CPI_1	CPI_2	CPI_3	$(3-CPI)_{ave.}$
normal time overhead	2.55	2.55	2.55	3.43	0.30	3.43	2.12
reduced time overhead	2.52	2.52	2.52	3.39	0.34	3.39	2.12

2.5 False Alarm Probability Allocation and System False Alarm Verification

A system false alarm occurs when the target report generator following the post detection integrator erroneously declares the presence of a target. On the other hand, a cell false alarm before post detection integration results when the test statistic for that cell exceeds the threshold in the absence of a target. The allocation of a cell false alarm probability such that the probability of system false alarm remains below an acceptable level during actual radar operation is a complicated procedure for modern pulse doppler radars having range and/or velocity ambiguities which are resolved by post detection integration of multiple observation samples. A specification of cell false alarm probability, which is frequently done in practice, does not lead to a specific system level false alarm performance unless the underlying detection process is also specified. Two competing processing schemes should not be compared using the same cell false alarm probability because they would in general lead to different system false alarm performance.

Marcum (see Nathanson [10]) did the first work in false alarm calculation. Let P_f denote the false alarm probability

each time there is an opportunity. On the average, assume there are n' independent false alarm opportunities in a time T'_{fa}. Let P_O denote the probability of no false alarm in n' false alarm opportunities. Then, P_O is given by

$$P_0 = (1 - P_f)^{n'} . \tag{2.5-1}$$

If α denotes the average number of independent false alarm opportunities per second, then, n' is given by

$$n' \approx \alpha T'_{fa} .$$

Eqn. (2.5-1) can then be written as

$$P_0 = (1 - P_f)^{\alpha T'_{fa}} . \tag{2.5-2}$$

Given values for P_0, P_f, and α, Marcum defined the false alarm time to be that value of T'_{fa} such that Eqn. (2.5-2) is satisfied.

For large n', Eqn. (2.5-1) can be approximated by

$$P_0 \simeq e^{-n' P_f} .$$

It then follows that

56

$$P_f \simeq \frac{1}{n'} \; ln \frac{1}{P_0} \; . \tag{2.5-3}$$

Marcum selected a value of 0.5 for P_0. With this choice, the probability of having no false alarm is also equal to the probability of having one or more false alarms. Consequently, a complementary equation to Eqn. (2.5-1) is

$$0.5 = 1 - (1 - P_f)^{n'} . \tag{2.5-4}$$

Substituting $P_0 = 0.5$ into Eqn. (2.5-3) gives

$$P_f \simeq \frac{0.69}{n'} = \frac{0.69}{\alpha T'_{fa}} \; . \tag{2.5-5}$$

An alternate approach was proposed by Barton [4] and Skolnik [9]. Let n_a be the number of false alarms in time t. They defined the average false alarm time, T_{fa}, as

$$T_{fa} = \lim_{t \to \infty} \frac{t}{n_a} \; . \tag{2.5-6}$$

As before, let denote the average number of independent false alarm opportunities per second. Then, the average number of false alarm opportunities in time t is equal to t. From the relative frequency definition of probability,

the false alarm probability is given by

$$P_f = \lim_{t \to \infty} \frac{n_a}{\alpha t} = \frac{1}{\alpha} \lim_{t \to \infty} \frac{n_a}{t} . \tag{2.5-7}$$

From Eqn. (2.5-6), it follows that

$$P_f = \frac{1}{\alpha T_{f_a}} . \tag{2.5-8}$$

Equating Eqns. (2.5-5) and (2.5-8), it is seen that

$$T_{f_a}' \simeq 0.69 \ T_{f_a} . \tag{2.5-9}$$

provided $P_o = 0.5$ and n' is large.

Now a method for deriving a cell false alarm probability before post detection integration from a specified system false alarm rate requirement is developed. This is done first by using Marcum's definition for the 3 of 3 post detection integration in the baseline configuration of the radar under examination. A method for general M of N post detection integration is then derived using the Barton and Skolnik approach but suitably modified to take into account the effect of binary post detection integration, time utilization, range eclipsing, velocity blanking, and range/velocity unfolding. Finally, this is specialized for

58

the 3 of 3 processing to show that the two methods give re-
sults having the same order of magnitude.

In 3 of 3 post detection integration using a sliding win-
dow, a target is declared after each modulation period if
and only if there is a detection in each of 3 consecutive
modulation periods. Let P_3 denote the probability of one or
more false alarms occurring in each modulation period after
the 3 of 3 post detection integration for the entire set of
range-doppler cells after range and velocity unfolding. As-
sume there are n'_m decisions made by the target report gen-
erator in a false alarm time T'_{fa}. Following Marcum's
definition, let the probability equal one-half that one or
more false alarms will occur in n'_m opportunities. As in
Eqn. (2.5-4), it follows that

$$0.5 = 1 - (1 - P_3)^{n'_m} . \qquad (2.5\text{-}10)$$

With reference to Eqn. (2.5-6), let t represent the frame
time, T_F, and n_a denote the number of false alarms allowed
in one frame time. For the baseline radar, t = 10 seconds
and $n_a = 2$. Hence, the false alarm time is obtained as

$$T_{f_a} = \frac{10}{2} = 5 \text{ seconds.}$$

From Eqn. (2.5-9), Marcum's false alarm time is

$$T'_{f_a} = (0.69)(5) = 3.45 \text{ seconds.}$$

Even though the post detection integrator requires 3 modulation periods to make a decision, a sliding window is used such that decisions are made every modulation period for each range-doppler cell. Hence, the number of independent false alarm opportunities per second, α, equals the reciprocal of T_m, the time duration for a modulation period. This results in

$$n'_m = \alpha T'_{f_a} = \frac{3.45}{T_m} .$$

Let n_f be the number of doppler filter cells used to detect targets having specific doppler shifts irrespective of range. Also, before post detection binary integration, let P_{if} denote the probability of having one or more false alarms for each doppler filter arising in the ith modulation period where i = 1, 2, 3. Finally, let P_r be the probability that the resolved range falls within the target report range. The probability P_{f3} of generating one or more false

alarms in a particular doppler filter after 3 of 3 post detection integration is then given by

$$P_{f3} = P_{1f} \, P_{2f} \, P_{3f} \, P_r \, .$$
(2.5-11)

With respect to any 3 consecutive modulation periods, one or more false alarms result if one or more false alarms occur in one or more of the n_f doppler filters. As a consequence, the probability of one or more false alarms in a modulation period after post detection integration for the entire set of range-doppler cells involved is given by

$$P_s = 1 - (1 - P_{f3})^{n_f}$$
(2.5-12)

Let the average number of uneclipsed range gates in a PRI be denoted by n_r. To allow for variability in the doppler shift due either to target motion, system instability, or noise perturbations, the threshold crossing in the (i-1)th modulation period for a doppler cell centered at frequency f_j is correlated in the ith modulation period with threshold crossings from doppler cells positioned within the frequency interval, $(f_j - W_{fi}/2, \ f_j + W_{fi}/2)$ where the doppler filter

width is taken as unity and W_{fi} is a multiplicative constant greater than unity. Let p_f denote the single cell false alarm probability before post detection integration of a particular range-doppler cell. The p_{if}'s in Eqn. (2.5-11) for $i = 1, 2, 3$, are then given by

$$P_{1f} = 1 - (1 - p_f)^{n_r} \qquad\qquad (2.5\text{-}13)$$

$$P_{2f} = 1 - (1 - p_f)^{n_r W_{f2}} \qquad\qquad (2.5\text{-}14)$$

$$P_{3f} = 1 - (1 - p_f)^{n_r W_{f3}} \qquad\qquad (2.5\text{-}15)$$

Substitution of Eqn. (2.5-11) for P_{f3} and Eqns. (2.5-13) through (2.5-15) for p_{if}'s into Eqn. (2.5-12) yields

$$P_3 = 1 - \left\{ 1 - [1 - (1-p_f)^{n_r}][1 - (1-p_f)^{n_r W_{f2}}][1 - (1-p_f)^{n_r W_{f3}}] \; P_r \right\}^{n_f}. \quad (2.5\text{-}16)$$

Eqn. (2.5-16) can be simplified by use of the approximation,

$$(1-x)^k \simeq 1 - kx, \quad \text{for } x \ll 1.$$

Noting that the false alarm probabilities P_{f3} and p_f are much less than unity, it follows that

$$P_3 \simeq n_f \, n_r^3 \, W_{f2} \, W_{f3} \, P_r \, p_f^3 \qquad\qquad (2.5\text{-}17)$$

Since P_3 is much less than unity as well, Eqn. (2.5-10) also simplifies to

$$0.5 \simeq n'_m \, P_3$$

from which P_3 is obtained as

$$P_3 \simeq \frac{0.5}{n'_m} \, . \qquad\qquad (2.5\text{-}18)$$

Substitution of P_3 from Eqn. (2.5-18) into Eqn. (2.5-17) and solving for p_f yields

$$p_f \simeq \frac{1}{n_r} \left[\frac{0.5}{n'_m \, n_f \, W_{f2} \, W_{f3} P_r} \right]^{1/3} . \qquad\qquad (2.5\text{-}19)$$

Eqn. (2.5-19) is the desired result. Given the system false alarm specification, false alarm time is readily determined from which the number of opportunities in terms of number of modulation periods in that false alarm time can be determined. With n'_m so determined from the system false alarm specification and given the system parameters, n_r, n_f, W_{f2}, W_{f3}, and P_r, the cell false alarm probability, p_f, is readily determined.

An alternate expression for the single cell false alarm probability p_f before M of N post detection integration is

63

now developed. The single cell false alarm probability af-
ter M of N post detection integration is related to p_f by

$$P_{fa} = \sum_{i=M}^{N} \frac{N!}{i!(N-i)!} \ p_f^i \ (1-p_f)^{N-i} \ .$$ (2.5-20)

The development begins by assuming a simple, continuously
operating radar where a decision is made for each range gate
sample. The resulting expression for P_{fa}, obtained from
Eqn. (2.5-8), is then modified to take into account the mode
of operation of a more complicated pulse doppler radar. This
enables introduction of system factors which are useful in
radar design. The resulting expression for p_f from these
system parameters is shown to be consistent with Eqn.
(2.5-19) which was developed using Marcum's approach.

Consider a radar operating continuously at a constant PRF
where a decision is made for each range gate sample. Let

$$\tau \simeq \frac{1}{B}$$

where the radar pulse has width τ and bandwidth B. The number of range
gates in a false alarm time T_{fa} is given by

$$\frac{T_{fa}}{\tau} = BT_{fa} \ .$$

The range gates and pulse repetition intervals within the
false alarm time are illustrated in Figure 2.5-1a. Note

64
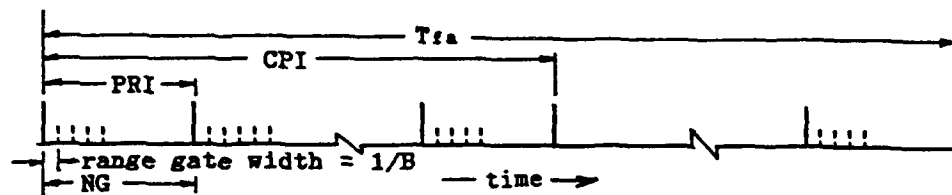
(a) range gates and PRI's in a false alarm time, Tfa, in a
continuously running radar
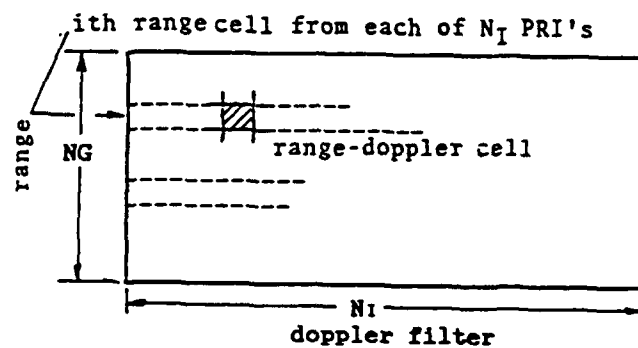
NG=total number of range gates in a PRI

(b) mapping of range gate samples onto range gate-doppler filter
cells
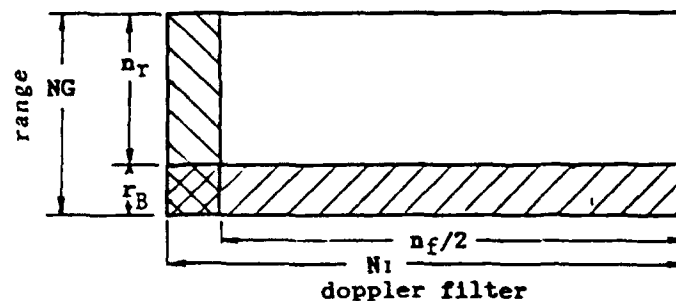
(c) time, range gate, and doppler filter utilization in a high
PRF radar

Figure 2.5-1   Process by which False Alarms Occ ur

65
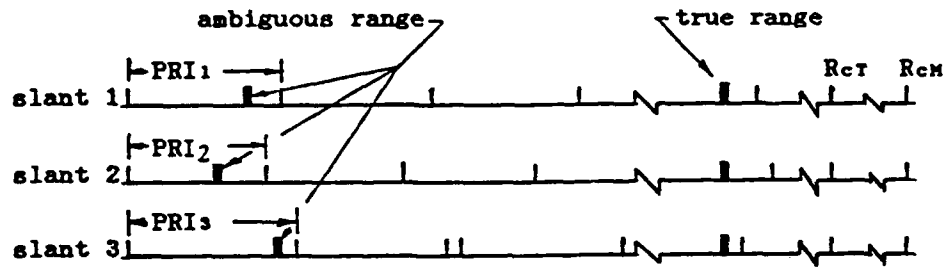
(d) range unfolding
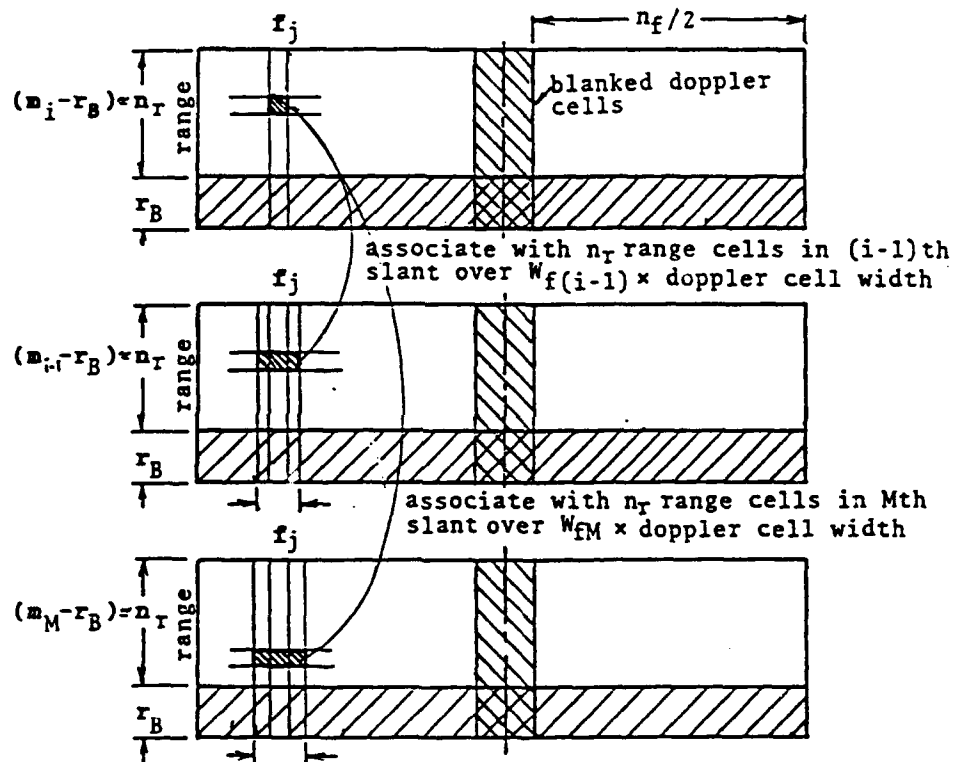
(e) actual M of N correlation process (after filter unfolding
and normalization)
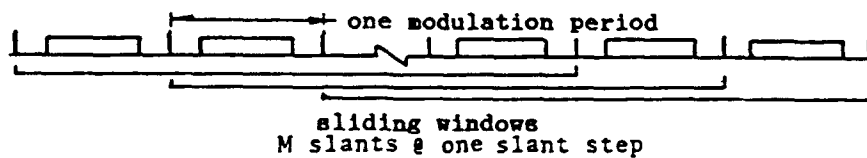
(f) sliding window

Figure 2.5-1 Process by which False Alarms Occur (cont'd)

that the average number of false alarm opportunities per second is

$$\alpha = B \ .$$

Consequently, Eqn. (2.5-8) becomes

$$P_{fa} = \frac{1}{B \ T_{fa}} \tag{2.5-21}$$

where the denominator equals the number of false alarm opportunities in a false alarm time.

Next, consider a pulse doppler radar where N_I samples for each range gate are processed through an FFT. Note that consecutive samples are separated by a PRI. Corresponding to the N_I DFT coefficients, N_I doppler filters are created for each range gate. Thus, the number of false alarm opportunities after the FFT operation remains the same as before. The total number of range gate samples before the FFT operation is transformed into an equal number of range gate-doppler filter cells. These are illustrated in Figure 2.5-1b for one modulation period.

In M of N binary integration the FFT samples from N consecutive modulation periods are jointly examined for M or more coincidence detections for each of the range-doppler cells. When decisions are made for every N nonoverlapping modulation periods, the number of false alarm opportunities in a false alarm time is reduced by this factor. As a result, Eqn. (2.5-21) is modified to read

$$P_{fa} = \frac{N}{B \, T_{fa}} \, . \tag{2.5-22}$$

In addition, for a modern pulse doppler radar, the number of false alarm opportunities in a false alarm time must be modified to take into account time overhead, range eclipsing, and doppler filter blanking. The amount of time utilization, range gate utilization, and doppler cell utilization are illustrated in Figure 2.5-1c. Furthermore, the multiplier effect of range and velocity ambiguity resolution, and the coincidence detection on a sliding window basis must be included. These factors are considered below.

Time Utilization Factor, K_1:

As explained in Section 2.1, because of time overhead, only a portion of the modulation period generates range gate

samples which are used for signal integration. The time utilization factor, denoted by K_1, is the fraction of a modulation period actually used for an FFT. It is given by

$$K_1 = \frac{(N_I)(\overline{T}_r)}{T_m}$$

where T_m and $\overline{T}_r$ are the time duration of a modulation period and the average time duration of a pulse repetition interval, respectively. Thus, $N_I \overline{T}_r$ is the average time duration of a CPI.

Range Gate Utilization Factor, K_2:

In practice, to protect against burnout, the receiver is shut down during pulse transmission and shortly thereafter. Therefore, a few range cells at the beginning of each PRI are eclipsed and do not enter into further processing. Let K_2 be the fraction of range cells which are not eclipsed. Denoting the total number of range cells in a $\overline{\text{PRI}}$ as NG, the number of eclipsed range cells as r_B, and the average number of uneclipsed range cells as n_r, K_2 is given as

$$K_2 = \frac{NG - r_B}{NG} = \frac{n_r}{NG} .$$

Velocity Ambiguity Factor, K_3:

To avoid velocity ambiguities the PRF should be greater

than or equal to twice the doppler frequency corresponding to the maximum possible target radial velocity. The radar under examination, due to design considerations, uses a PRF only half as large. Consequently, there is an ambiguity as to whether an observed doppler frequency corresponds to an opening or closing velocity. Use of different PRF's enables resolution of this ambiguity. Hence, the number of resolvable doppler frequencies is actually $2N_I$. To account for this effect, the multiplier

$$K_3 = 2$$

is introduced.

Doppler Filter Utilization Factor, K_4:

A number of doppler filter cells located around the mainbeam clutter doppler center frequency contain residue of returns from mainbeam clutter and undesirable slow moving ground targets. Therefore, these filters are blanked to prevent detection resulting from these undesirable targets and clutter. The fraction of unblanked doppler filters, K_4, is given by

$$K_4 = \frac{n_f/2}{N_I}$$

where n_f is the total number of unblanked doppler filters

69

after doppler filter unfolding and N_I, the dimension of the FFT, is the number of filter cells before correcting for the velocity ambiguity factor, K_3.

Range Correlation Factor for Range Ambiguity Resolution, K_5:

The concept of resolving range ambiguity arising from a high PRF waveform was introduced in Section 1.1.1. A set of M slants with distinct PRF's, each having m_i number of range cells in the respective PRI, is used in a beam dwell. The Chinese remainder theorem allows the resolution of the range ambiguity when the specific ambiguous range cell number in each slant is correlated over M slants. The Chinese remainder theorem requires that the m_i's are relatively prime numbers. The range ambiguity resolution process is referred to as range unfolding and is illustrated in Figure 2.5-1d.

The unambiguously resolved maximum range span, R_{cM}, measured in a range cell unit is

$$R_{cM} = m_1 m_2 -- m_M = \prod_{i=1}^{M} m_i \; .$$

Recall that NG denotes the number of range cells in a PRI. It follows that

$$NG = \frac{m_1 + m_2 + -- + m_M}{M} = \frac{1}{M} \left(\prod_{i=1}^{M} m_i \right) \; .$$

Under the condition,

$$\frac{|m_i - m_j|}{NG} \ll 1; \quad i \neq j, \quad i, j = 1, 2, \text{--}, M,$$

the m_i's are approximately equal. R_{cM} can then be approximated by

$$R_{cM} \simeq (NG)^M = (r_B + n_r)^M$$

where n_r is the number of uneclipsed range cells in a PRI. These n_r number of range cells in a particular doppler filter are correlated with n_r number of range cells in the corresponding doppler filter in the other M-1 slants. As explained before, the doppler filter width for the ith slant for correlation with the (i-1)th slant is widened by a factor, W_{fi}. Thus, the number of possible M-tuples in M slants for correlation for a particular filter is

$$(m_1 - r_B)(m_2 - r_B)W_{f2} \text{---} (m_M - r_B)W_{fM} \simeq n_r^M \prod_{i=2}^{M} W_{fi} \; .$$

Since there are n_f number of doppler filters the number of possible M-tuples in M slants for all filters becomes

$$n_f \; n_r^M \prod_{i=2}^{M} W_{fi} \; .$$

This process is shown in Figure 2.5-1e.

In particular, m_i and M are chosen so that R_{cM} is much larger than R_{cT}, the maximum reported target range, measured in a range cell unit. Because detections in unambiguous range cells beyond R_{cT} are not reported, false alarm opportunities corresponding to these cells should be excluded from the total count. Assuming the false reports after correlation of M-slants occur with equal probability in any unfolded range cell, the false alarm opportunities are effectively reduced by the factor equal to the probability P_r that the false reports fall within the reported range:

$$P_r = \frac{R_{cT}}{R_{cM}} = \frac{R_{cT}}{(n_r + r_B)^M} .$$

Let K_5 be defined as the ratio of the number of false alarm opportunities due to range unfolding to that where there is no range unfolding. Since there are exactly $(n_f n_r)$ opportunities without range unfolding, K_5 is given by

$$K_5 = \frac{n_f \, n_r^M \, \prod\limits_{i=2}^{M} W_{fi}}{n_f \, n_r} \, P_r . \qquad (2.5\text{-}23)$$

Sliding Window Factor, K_6:

The factor of N was introduced in Eqn. (2.5-22) on the assumption that a decision is made once every N nonoverlapping modulation periods. When a sliding window is

used, a decision is made once every modulation period by utilizing the previous (N-1) modulation periods along with the current modulation period as shown in Figure 2.5-1f. Consequently, the number of false alarm opportunities increases by a factor of N. To account for this effect, the multiplier

$$K_6 = \begin{cases} 1, & \text{no sliding window} \\ N, & \text{with sliding window} \end{cases}$$

is introduced.

Introduction of correction factors, K_1 through K_6, associated with practical radars into Eqn. (2.5-22) representing an ideal radar results in

$$P_{fa} = \frac{N}{BT_{fa}} \left[\prod_{i=1}^{6} K_i \right]^{-1} . \tag{2.5-24}$$

It is now shown that Eqn. (2.5-24) leads to an expression for the single cell false alarm probability p_f which is consistent with Eqn. (2.5-19). Recall that Eqn. (2.5-19) was obtained on the basis of 3 of 3 post detection integration using Marcum's method. Letting M=N=3 in Eqn. (2.5-20), it follows that

$$P_{fa} = p_f^3 .$$

Hence, Eqn. (2.5-24) can be rewritten as

$$P_{f_a} = p_f^3 = \frac{N}{BT_{f_a}\, K_1 K_2 K_3 K_4 K_5 K_6} \cdot \qquad (2.5\text{-}25)$$

Substituting M=3 into Eqn. (2.5-23) gives K_5 as

$$K_5 = \frac{n_f n_r^3 W_{f2} W_{f3}}{n_r n_f}\, P_r \cdot$$

Therefore, the factors which enter into Eqn. (2.5-25) are

$$N=3, \quad K_1 = \frac{N_I \overline{T}_r}{T_m}, \quad K_2 = \frac{n_r}{NG}, \quad K_3 = 2, \quad K_4 = \frac{n_f/2}{N_I},$$

$$K_5 = \frac{n_f\, n_r^3\, W_{f2}\, W_{f3}}{n_f\, n_r}\, P_r, \qquad K_6 = 3.$$

Hence, Eqn. (2.5-25) is given by

$$p_f^3 = \frac{3}{(BT_{f_a})\left(\frac{N_I \overline{T}_r}{T_m}\right)\left(\frac{n_r}{NG}\right)(2)\left(\frac{n_f/2}{N_I}\right)\left(\frac{n_f\, n_r^3 W_{f2} W_{f3} P_r}{n_f n_r}\right)(3)}$$

$$= \frac{1}{(BT_{f_a})\left(\frac{N_I \overline{T}_r}{T_m}\right)\left(\frac{1}{NG}\right)\left(\frac{1}{N_I}\right)(n_f n_r^3 W_{f2} W_{f3} P_r)} \cdot$$

With the sliding window, there is one false alarm opportunity per modulation period. Thus, there are

$$n_m = \frac{1}{T_m}\, T_{f_a}$$

false alarm opportunities in a false alarm time. Substitution of

$$T_{f_a} = n_m T_m, \quad B \simeq 1/\tau, \quad \text{and} \quad NG = \overline{T}_r/\tau$$

74

into Eqn. (2.5-27) gives

$$p_f^3 = \frac{1}{n_m n_f n_r^3 W_{f2} W_{f3} P_r} \qquad (2.5\text{-}28)$$

or, equivalently,

$$p_f = \frac{1}{n_r} \left[\frac{1}{n_m n_f W_{f2} W_{f3} P_r} \right]^{1/3} . \qquad (2.5\text{-}29)$$

Since

$$T_{fa}' = 0.69 T_{fa} ,$$

it follows that

$$n_m' = 0.69 n_m .$$

Therefore, Eqn. (2.5-19) can be rewritten as

$$p_f = \frac{1}{n_r} \left[\frac{0.5/0.69}{n_m n_f W_{f2} W_{f3} P_r} \right]^{1/3} \qquad (2.5\text{-}30)$$

$$= \frac{1}{n_r} \left[\frac{0.725}{n_m n_f W_{f2} W_{f3} P_r} \right]^{1/3}$$

Note that Eqn. (2.5-30) and Eqn. (2.5-29) are consistent in the sense that they yield approximately the same values for p_f. It can be concluded, therefore, that the two different approaches by Marcum and Barton produce equivalent results.

For M of N post detection integration, substitution of

Eqn. (2.5-20) into Eqn. (2.5-24) yields

$$P_{f_a} = \sum_{i=M}^{N} \frac{N!}{i!(N-i)!} \; p_f^i \; (1-p_f)^{N-i} = \frac{N}{BT_{f_a} \; K_1 K_2 K_3 K_4 K_5 K_6} \; . \qquad (2.5-31)$$

From a system designer's point of view, this equation is convenient for evaluating p_f, the cell false alarm probability before M of N post detection integration. The results obtained using Eqn. (2.5-31) are summarized in Table 2.5-1 for the 3 of 3 3-slant baseline configuration, a 2 of 3 3-slant configuration, and a 2 of 2 2-slant configuration. Relative to the 2 of 3 3-slant configuration, the value of p_f is maintained the same as that determined for the baseline configuration. This is equivalent to holding the threshold fixed for both configurations. As a result, the 2 of 3 configuration is able to achieve more detections at the expense of a higher false alarm rate. This is indicated by the larger value for P_{fa} and the smaller value for T_{fa}. With respect to the 2 of 2 configuration, the false alarm time is maintained at the same value found for the 2 of 3 configuration. This allows comparison of detection performance for the two configurations on the basis of having the same false alarm performance. The comparison is presented in Chapter 4 where it is used in conjunction with scan-to-scan processing.

As a check, it is now shown that the numerical value determined for p_f for the baseline 3 of 3 post detection integration is consistent with the baseline system requirement that there be on the average 2 false alarms per scan. Given that $p_f = 7.6 \times 10^{-4}$, it follows that

$$P_{fa} = p_f^3 = 4.39 \times 10^{-10} .$$

The total number of false alarm opportunities per scan is given by

$$n_r^3 W_{f2} W_{f3} n_f P_r\left(n_m \frac{T_F}{T_{fa}} \right)$$

$$= (42)^3 (2.2)(2)(195)\left(\frac{6173}{45^3} \right)(1040)$$

$$= 4.48 \times 10^9 .$$

The average number of false alarms per scan equals the product of P_{fa} and the total number of false alarm opportunities per scan. This yields

$$(4.39 \times 10^{-10})(4.48 \times 10^9) = 2$$

which is the expected result.

Table 2.5-1 False Alarm Probability for the Processing
Options Evaluated

	3-slant				2-slant	
M of N	3 of 3		2 of 3		2 of 2	
time overhead	normal	reduced	normal	reduced	normal	reduced
FA/scan	2	2	4.15×10^3	4.60×10^3	4.15×10^3	4.60×10^3
n_{ms} (# of MP's/ scan)	1040	1040	1040	1040	6993	693
T_{fa}(sec)	5	5	2.41×10^{-3}	2.17×10^{-3}	2.41×10^{-3}	2.17×10^{-3}
B(MHz)	1.25	1.25	1.25	1.25	1.25	1.25
K_1	0.479	0.652	0.479	0.652	0.653	0.768
K_2	0.933	0.933	0.933	0.933	0.933	0.933
K_3	2	2	2	2	2	2
K_4	0.762	0.762	0.762	0.762	0.762	0.762
K_5	533	533	282	282	282	282
K_6	3	3	3	3	2	2
$P_{fa} \times 10^{10}$	4.39×10^0	3.23×10^0	1.73×10^4	1.41×10^4	1.27×10^4	1.20×10^4
$p_f \times 10^4$	7.60×10^0	6.86×10^0	7.60×10^0	6.86×10^0	1.13×10^1	1.09×10^1

Notes:

1. For computing K_5 the following parameters are used:

   $n = 42$, $r = 3$, $R_{cT} = 6173$, $W_{f1} = 2.2$, $W_{f2} = 2.03$.

2. Explanations for the numbers under columns labeled 2 of 3 and 2 of 2 with normal time overhead are given in Section 4.3. The numbers with reduced time overhead can be found similarly. However, it should be noted that the number of range gate samples no longer matches with the total number of range-doppler cells. It is because zero filling is required to generate FFT samples when the input time samples in a CPI are not equal to integer powers of 2.

2.6 Target Models Assumed

Before presenting the target models used in the analysis

of detection performance, the concept of target radar cross

section (RCS) is reviewed. Target RCS is related to the ra-

tio of received power from a target to the power incident

on the target.   The received power is expressed in terms of

the cross sectional area of an isotropic scatterer which,

for a given incident power, would produce the same received

powe as the actual target. From this concept, the radar

cross section, σ, is given by

$$\sigma = 4\pi \frac{\text{power reflected toward source/unit solid angle}}{\text{incident power density}}$$

$$= 4\pi R^2 \left| \frac{E_r}{E_i} \right|^2$$

where the parameters are

   R: range to the target, assumed to be large enough such
        that the target is in the far field from the transmit-
        ting antenna

   E_r: reflected field strength at the radar

   E_i: incident field strength at target .

It follows that the RCS of an isotropic reflector, e.g., a

sphere, is equal to its projected area normal to the direc-

tion of radar illumination. Most targets are not isotropic

and exhibit directional preference. Objects with the same physical projected area can have considerably different values for RCS. For example, at S-band, the RCS at nose-on aspect of a cone-sphere is 30 dB smaller than the RCS of a sphere with the same projected area while a corner reflector can have an RCS 30 dB greater than that of the sphere, all having the same projected area of 1 m^2.

Skolnik [9] and Nathanson [10] each have a good summary of work by various investigators on target RCS and commonly used statistical target models.

The RCS of a large complex target may be approximated by assuming that the target is composed of individual reflectors such that the total value of σ is related to the vector sum of the individual cross sections, σ_k, in the following manner:

$$\sigma = \left| \sum_k \sqrt{\sigma_k} \exp\left(\frac{j4\pi d_k}{\lambda} \right) \right|^2$$

where d_k is the distance from the radar to the kth reflector with RCS, σ_k.

The RCS of a complex target is a strong function of the aspect angle. Since the precise aspect angle is unknown in a

given situation, the RCS is best described statistically. A summary of the frequently used target models is presented below:

1. Marcum case (nonfluctuating target):

For nonfluctuating targets, σ is a deterministic constant. Let A denote the envelope amplitude of the received signal voltage. Since the average power during the duration of the pulse, $A^2/2$, is proportional to σ, it follows that

$$K_a \sigma = A^2$$

where K_a is the constant of proportionality. A constant value of σ implies a constant value of A.

2. Swerling case 1:

This model assumes that a target is composed of many reflectors where none is dominant. For this case, σ remains constant over all N slants within a scan. However, σ varies randomly from scan to scan. The probability density function of the RCS is given by

$$p(\sigma) = \begin{cases} \frac{1}{\sigma_{av}} \exp\left(-\frac{\sigma}{\sigma_{av}}\right) & \sigma \geq 0 \\ 0 & \sigma < 0 \end{cases} \qquad (2.6\text{-}1)$$

where σ_{av} denotes the expected value of σ. To represent the

variation of signal-to-noise ratio from scan to scan due to a target's RCS fluctuation, it is convenient to have an expression for the probability density function of the integrated signal-to-noise ratio, (S/N). It is the ratio of the received time averaged signal power to the mean noise power during the duration of the received pulse train integrated in a slant. Let S_o denote the received signal power assuming no beam shape loss. Since the mean noise power is assumed to be constant, (S_o/N) is directly proportional to RCS. It follows that

$$\left(\frac{S_0}{N}\right) = K_b \sigma . \tag{2.6-2}$$

Averaging over the fluctuations from scan to scan, the average signal-to-noise ratio is

$$\left(\frac{\bar{S}_0}{N}\right) = K_b \sigma_{av} . \tag{2.6-3}$$

Therefore, Eqn. (2.6-1) can be transformed according to

$$p\left(\frac{S_0}{N}\right) = p(\sigma) \left| \frac{d\sigma}{d\left(\frac{S_0}{N}\right)} \right|_{\sigma = \frac{1}{K_b}\left(\frac{S_0}{N}\right), \ \sigma_{av} = \frac{1}{K_b}\left(\frac{\bar{S}_0}{N}\right)}$$

$$= \begin{cases} \dfrac{1}{(\bar{S}_0/N)} \exp\left(-\dfrac{S_0/N}{\bar{S}_0/N}\right), & S_0/N \geq 0 \\ 0, & S_0/N < 0 . \end{cases} \tag{2.6-4}$$

82

The probability density function for the envelope ampli-
tude can be similarly derived using the transformation,

$$K_a \sigma = A^2$$

from which it is found that

$$\sigma = \frac{A^2}{K_a} \ , \quad \left| \frac{d\sigma}{dA} \right| = \frac{2A}{K_a} \ , \quad \sigma_{av} = \frac{\overline{A}^2}{K_a} \ . \tag{2.6-5}$$

Then, $p(A)$ becomes

$$p(A) = \begin{cases} p(\sigma) \left| \dfrac{d\sigma}{dA} \right|_{\sigma = A^2/K_a, \ \sigma_{av} = \overline{A}^2/K_a} = \dfrac{2A}{\overline{A}^2} \exp\left(- \dfrac{A^2}{\overline{A}^2} \right) \ , & A \geq 0 \\[4mm] 0 \ , & A < 0 \ . \end{cases} \tag{2.6-6}$$

3. <u>Swerling case 2</u>:

This target model is assumed to be composed of many re-
flectors where none is dominant as with Swerling case 1.
Therefore, the probability density function for σ is identi-
cal to that in Swerling case 1. However, now the RCS is as-
sumed to fluctuate from slant to slant while the amplitude
of the received pulses within a CPI remains constant. This
rapid fluctuation is not encountered with practical targets.
However, it can be induced by slant-to-slant frequency agil-
ity.

4. Swerling case 3:

This target model is assumed to be composed of many equal size scatterers plus one dominant reflector which fluctuates slowly from scan-to-scan. As with Swerling case 1, σ remains constant over all N slants within a scan. The probability density function of this model's target RCS is given by

$$
p(\sigma) = \begin{cases} \dfrac{4\sigma}{\sigma_{av}^2} \, \exp\left(-\dfrac{2\sigma}{\sigma_{av}} \right) \,, & \sigma > 0 \\[3mm] 0 \,, & \sigma < 0 \end{cases}
\qquad (2.6\text{-}7)
$$

where, as before, σ_{av} denotes the expected value of σ. The probability density function for the integrated signal-to-noise ratio , $p(S_0/N)$, is obtained from Eqn. (2.6-7) with the transformation given by Eqn. (2.6-3). Making the substitution, $|d\sigma/d(S_0/N) = 1/K_b$, into Eqn. (2.6-3) gives

$$
p\left(\frac{S_0}{N} \right) = \begin{cases} \dfrac{4(S_0/N)}{(\overline{S_0}/N)^2} \, \exp\left(-\dfrac{2(S_0/N)}{(\overline{S_0}/N)} \right) \,, & S_0/N \geq 0 \\[3mm] 0 \,, & S_0/N < 0 \,. \end{cases}
\qquad (2.6\text{-}8)
$$

The probability density function for the envelope amplitude A is again obtained from Eqn. (2.6-7) with the

variable transformation

$$K_a \sigma = A^2, \quad \text{and} \quad K_a \sigma_{av} = \overline{A^2}. \tag{2.6-9}$$

Use of σ, $|d\sigma/dA|$, and σ_{av}, given by Eqn (2.6-5), yields

$$p(A) = \begin{cases} \dfrac{8A^3}{\overline{A^2}} \exp\left(-\dfrac{2A^2}{\overline{A^2}}\right), & A > 0 \\ \\ 0, & A < 0. \end{cases} \tag{2.6-10}$$

5. <u>Swerling case 4</u>:

Swerling case 4 has the same probability density function for σ as Swerling case 3. As in case 2, the RCS is assumed to fluctuate from one slant to the next while the amplitude of the pulses in a CPI remains constant. Swerling case 4 is related to Swerling case 3 as Swerling case 2 is related to Swerling case 1.

These probability density functions are used for determining detection probabilities in the baseline and modified radar configurations described in the Chapters to follow.

CHAPTER 3

PERFORMANCE OF THE AIRBORNE SURVEILLANCE RADAR IN ITS BASELINE CONFIGURATION

Detection probabilities in the baseline configuration for the five target models introduced in Chapter 2 are determined in this chapter. This is done by taking into account the number of pulses available for integration in each slant, the beam shape loss, and the cell false alarm probability also established in Chapter 2.

3.1 Sufficient Statistic and the Likelihood Ratio Test (LRT)

With reference to the receiver/processor block diagram of Figure 1.1-2, it is assumed that the analog-to-digital converter (ADC) and the clutter canceller are both ideal with their characteristics as shown in Figure 3.1-1 (a) and (b), respectively.

(a) ADC response   (b) clutter canceller response
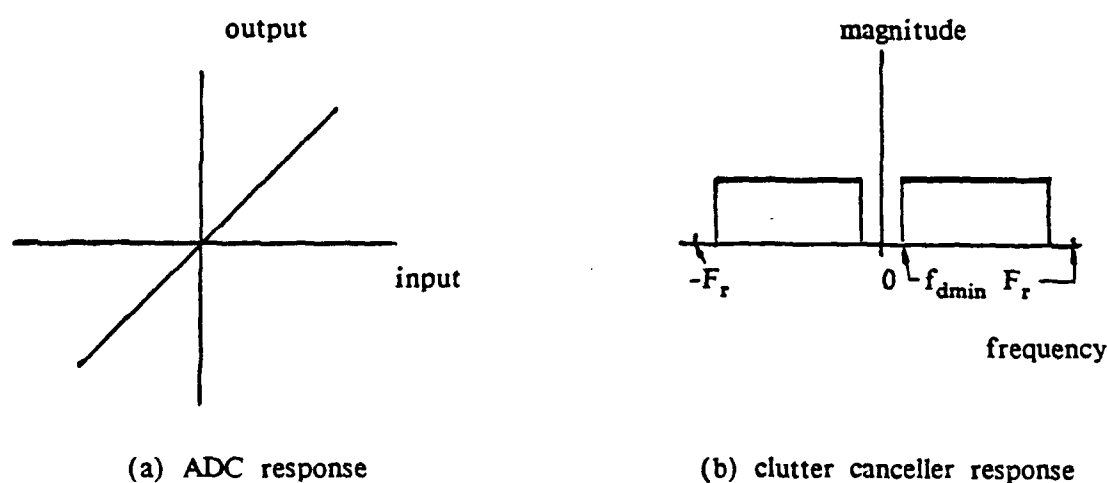
Figure 3.1-1   Assumed ADC and clutter Canceller Characteristics

Let $v(t)$ denote the received waveform at the IF filter output. Then, $v(t)$ is given by

$$v(t) = \begin{cases} n(t) & :H_0 \\ s(t-t_d')p(t-t_d')+n(t) & :H_1 \end{cases} \qquad (3.1\text{-}1)$$

where H_0 and H_1 denote the null hypothesis (target absent) and the alternate hypothesis (target present), respectively. Under H_0, $v(t)$ consists of the noise $n(t)$ alone. The rectangular gating function $p(t)$ in the expression of $v(t)$ under H_1 is of unit amplitude and duration r. The clutter $c(t)$ is not included in Eqn. (3.1-1) since the clutter spectrum is assumed to be confined in the stop band of the clutter canceller. Therefore, the detection problem under consideration is for target signals with doppler frequencies greater than f_{dmin} which are embedded in thermal noise. The delayed signal $s(t-t_d')$ can be written as

$$s(t-t_d') = A\cos[(\omega_{IF}+\omega_d)(t-t_d') + \theta(t-t_d') + \phi] \qquad (3.1\text{-}2)$$

where A is the signal amplitude, $\theta(t)$ is the signal phase modulation, ϕ is the unknown initial phase, and t_d' is the round trip delay for a point target located at range R. The time delay is given by

$$t_d' = \frac{2R}{c}$$

where c is the speed of light.

Corresponding to the received signal with delay t_d', there is a time gating pulse $p(t-t_d)$ which effectively multiplies the incoming signal. In general,

t_d' is not equal to t_d. The mismatch between t_d' and t_d gives rise to a range gate straddling loss, the average value of which is included in the system loss factor. Having accounted for the straddling loss in this manner, it is assumed in the subsequent analysis that $t_d'=t_d$. Since the integrator following the multiplier (mixer) is synchronized to t_d and performs the integration over the duration of $p(t-t_d)$, $p(t-t_d)$ equals unity during the entire integration period and can be dropped without effect. For the radar under consideration, there is no phase modulation. Hence, $\theta(t) = 0$. The radar receiver under consideration implements the Bayes strategy by performing the likelihood ratio test (LRT) in each range, angle, and doppler frequency resolution cell. Thus, without loss in generality, the delay in the expression for $s(t)$ can be dropped. Then, $v(t)$ becomes

$$v(t) = \begin{cases} n(t) & : \text{under } H_0 \\ \\ s(t)+n(t) & : \text{under } H_1 \end{cases} \quad ; \quad 0 < t < \tau . \qquad (3.1\text{-}3)$$

The expression for $s(t)$ can be written in terms of its quadrature components $s_I(t)$ and $s_Q(t)$ as

$$s(t) = A\cos[(\omega_{IF}+\omega_d)t+\phi]$$

$$= \text{Re}\left\{ \tilde{s}(t)\ e[j(\omega_{IF}t+\phi)] \right\}$$

$$= \text{Re}\left\{ [s_I(t)+js_Q(t)]\ \exp[j(\omega_{IF}t+\phi)] \right\}$$

$$= s_I(t)\cos(\omega_{IF}t+\phi) - s_Q(t)\sin(\omega_{IF}t+\phi) \qquad (3.1\text{-}4)$$

where

$$\tilde{s}(t) = A\ e^{j\omega_d t} = s_I(t) + js_Q(t) = A\cos\omega_d t + jA\sin\omega_d t$$

is the complex envelope of s(t). The narrowband noise process n(t) can also be expressed by its quadrature components as

$$n(t) = n_I(t)\cos\omega_{IF}t - n_Q(t)\sin\omega_{IF}t. \qquad (3.1\text{-}5)$$

The receiver that maximizes the output signal-to-noise ratio is the correlation receiver as shown in Figure 3.1-2. This also maximizes the probability of detection when v(t) is Gaussian distributed.
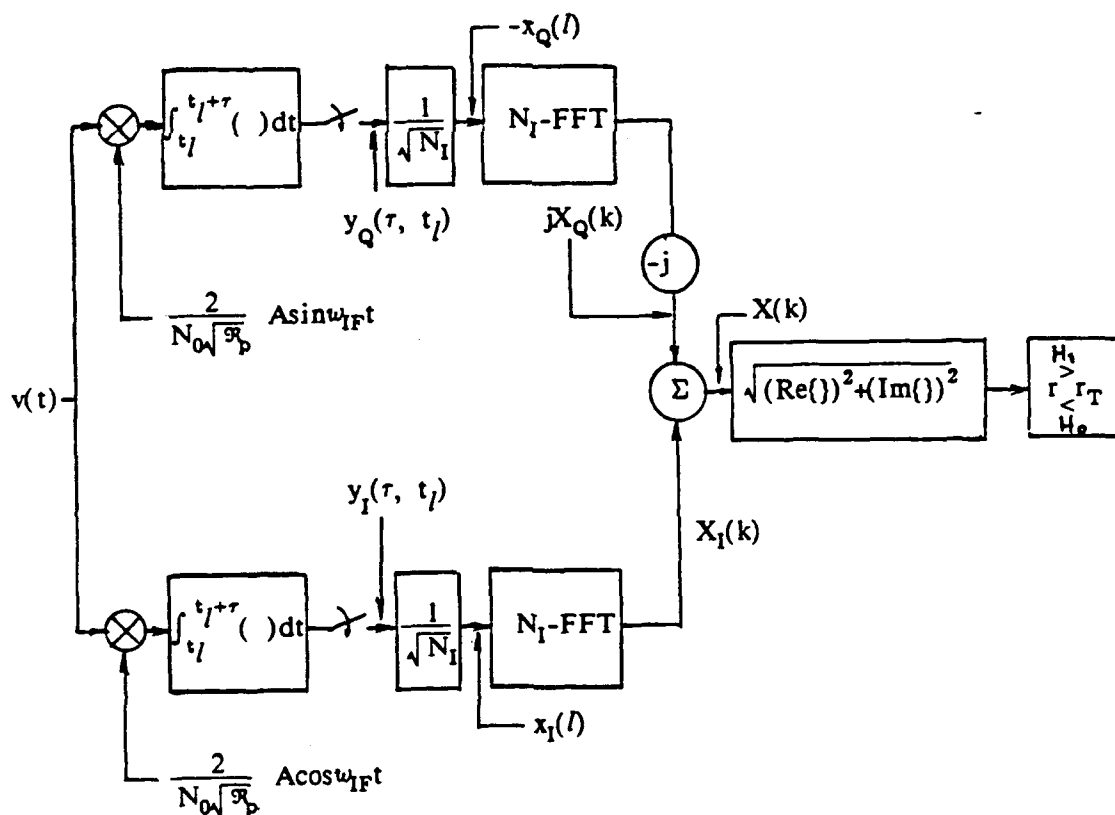
Figure 3.1-2 Equivalent Receiver block diagram

In Figure 3.1-2, the constant $\dfrac{2A}{N_0\sqrt{\mathfrak{R}_p}}$ in the reference signal going into the product

mixer is chosen such that the variances of $y_I(\tau, t_l)$ and $y_Q(\tau, t_l)$ are unity where $N_0/2$

is the two sided noise power spectral density and $\mathfrak{R}_p$ is the single pulse

peak signal-to-noise ratio. The noise power contained in a video bandwidth B is

equal to $N_0 B$. Thus, the single pulse signal-to-noise ratio $(S/N)_p$ at the input

to the FFT before correction for the loss factor is

$$\left(\frac{S}{N}\right)_p = \frac{(1/2)A^2}{N_0 B} = \frac{(1/2)A^2 \tau}{N_0} = \frac{E}{N_0} = \frac{\mathfrak{R}_p}{2} \ . \tag{3.1-6}$$

The multiplier $1/\sqrt{N_I}$ before the FFT in Figure 3.1-2 is introduced so that

the variances of $X_I(k)$ and $X_Q(k)$, appearing at the FFT outputs, are each unity.

Returning to Figure 3.1-2, the output of the product mixer is described by

first considering the signal and noise separately. Let the constant K represent

$$K = \frac{2A}{N_0\sqrt{\mathfrak{R}_p}} \ .$$

In each of the I and Q channels, repectively, the output of the product mixer for the

signal is

$$Ks(t)\cos(\omega_{IF}t) = K\{s_I(t) \tfrac{1}{2}[\cos\phi + \cos(2\omega_{IF}t+\phi)]$$

$$-s_Q(t) \tfrac{1}{2}[\sin\phi + \sin(2\omega_{IF}t+\phi)]\} \tag{3.1-7}$$

and

$$Ks(t)\sin(\omega_{IF}t) = K\{s_I(t) \tfrac{1}{2}[-\sin\phi + \sin(2\omega_{IF}t+\phi)]$$

$$-s_Q(t) \tfrac{1}{2}[\cos\phi - \cos(2\omega_{IF}t+\phi)]\} \ . \qquad (3.1\text{-}8)$$

Similarly, the output of the product mixer for the noise is

$$Kn(t)\cos(\omega_{IF}t) = K\{ \tfrac{1}{2}n_I(t)[1+\cos(2\omega_{IF}t)] - \tfrac{1}{2}n_Q(t)\sin(2\omega_{IF}t)\} \qquad (3.1\text{-}9)$$

and

$$Kn(t)\sin(\omega_{IF}t) = K\{-\tfrac{1}{2}n_Q(t)[1-\cos(2\omega_{IF}t)] + \tfrac{1}{2}n_I(t)\sin(2\omega_{IF}t)\} \ . \qquad (3.1\text{-}10)$$

The sampled output of the integrator is obtained by recognizing that the double frequency terms integrate to zero while the narrowband signal and noise do not appreciably change during the integration period τ. Thus, the sampled output of the integrator is closely approximated by

$$K\int_{t_l}^{t_l+\tau} s(t)\cos(\omega_{IF}t)dt = \frac{K\tau}{2}\left\{ s_I(t_l)\cos\phi - s_Q(t_l)\sin\phi \right\}$$

$$= \frac{K}{2}A\tau\left\{ \cos(\omega_d t_l)\cos\phi - \sin(\omega_d t_l)\sin\phi \right\}$$

$$= \frac{K}{2}A\tau\,\cos(\omega_d t_l + \phi) \qquad (3.1\text{-}11)$$

and

91

$$K \int_{t_l}^{t_l + \tau} s(t) \sin(\omega_{IF} t) \, dt = -\frac{K\tau}{2} \left\{ s_I(t_l) \sin\phi + s_Q(t_l) \cos\phi \right\}$$

$$= -\frac{K}{2} A\tau \left\{ \cos(\omega_d t_l) \sin\phi + \sin(\omega_d t_l) \cos\phi \right\}$$

$$= -\frac{K}{2} A\tau \sin(\omega_d t_l + \phi) . \tag{3.1-12}$$

The sampled output of the integrator for noise is

$$K \int_{t_l}^{t_l + \tau} n(t) \cos(\omega_{IF} t) \, dt = \frac{K\tau}{2} n_I(t_l) \tag{3.1-13}$$

and

$$K \int_{t_l}^{t_l + \tau} n(t) \sin(\omega_{IF} t) \, dt = -\frac{K\tau}{2} n_Q(t_l) . \tag{3.1-14}$$

Thus, the sampled output of the integrator is

$$y_I(\tau, t_l) = \begin{cases} \dfrac{K}{2} \tau n_I(t_l) & : \text{ under } H_0 \\[2em] \dfrac{K}{2} A\tau \cos(\omega_d t_l + \phi) + \dfrac{K}{2} \tau n_I(t_l) & : \text{ under } H_1 \end{cases} \tag{3.1-15}$$

and

$$y_Q(\tau, t_l) = \begin{cases} -\dfrac{K}{2} \tau n_Q(t_l) & : \text{ under } H_0 \\[2em] -\dfrac{K}{2} A\tau \sin(\omega_d t_l + \phi) - \dfrac{K}{2} \tau n_Q(t_l) & : \text{ under } H_1 \end{cases} \tag{3.1-16}$$

The mean and variance of y_I and y_Q are

$y_I(\tau, t_l)$:

under H_0:

mean $= 0$

variance $= \left(\dfrac{2A\tau}{2N_0\sqrt{\mathfrak{R}_p}} \right)^2 \overline{n_I^2(t_l)} = 1$.

under H_1:

mean $= \dfrac{2A^2\tau}{2N_0\sqrt{\mathfrak{R}_p}} \cos(\omega_d t_l + \phi) = \sqrt{\mathfrak{R}_p} \cos(\omega_d t_l + \phi)$

variance $= 1$.

$y_Q(\tau, t_l)$:

under H_0:

mean $= 0$

variance $= 1$.

under H_1:

mean $= -\sqrt{\mathfrak{R}_p} \sin(\omega_d t_l + \phi)$

variance $= 1$.

As shown in Figure 3.1-2, let

$x_I(l) = \dfrac{1}{\sqrt{N_I}} y_I(\tau, t_l)$

and

$x_Q(l) = \dfrac{-1}{\sqrt{N_I}} y_Q(\tau, t_l)$.

93

It is convenient to consider the FFT process for noise and signal separately. Let $n_I^{\cdot}(l)$ and $n_Q^{\cdot}(l)$ denote the lth in-phase and quadrature noise sample in a sequence for $l = 0, 1, - -, N_I-1$:

$$n_I^{\cdot}(l) = \frac{K\tau}{2\sqrt{N_I}} \, n_I(lT_r)$$

and

$$n_Q^{\cdot}(l) = \frac{K\tau}{2\sqrt{N_I}} \, n_Q(lT_r) \; .$$

The kth output coefficient $N_I(k)$ of the N_I-point FFT in response to the input sequence $n_I^{\cdot}(l)$ is given by

$$N_I(k) = \sum_{l=0}^{N_I-1} n_I^{\cdot}(l) \, e^{-j\frac{2\pi k l}{N_I}} \, , \qquad k = 0, 1, - -, N_I-1 \; . \tag{3.1-17}$$

Note that $n_I^{\cdot}(l)$ is a zero mean white Gaussian noise sequence. Hence,

$$E[n_I^{\cdot}(l)] = 0 \quad \text{and} \quad E[n_I^{\cdot}(l)n_I^{\cdot}(m)] = \frac{1}{N_I} \, \delta_{lm} \; .$$

The first and second moments of $N_I(k)$ are given by

$$E[N_I(k)] = \sum_{l=0}^{N_I-1} E[n_I^{\cdot}(l)] \, e^{-j\frac{2\pi k l}{N_I}} = 0 \tag{3.1-18}$$

and

$$E[N_I(k)N_I^*(p)] = \sum_{l=0}^{N_I-1} \sum_{m=0}^{N_I-1} E[n_I^{\cdot}(l)n_I^{\cdot}(m)] \, e^{-j\frac{2\pi k l}{N_I}} \, e^{+j\frac{2\pi p m}{N_I}} \, , \tag{3.1-19}$$

94

respectively. Note that the variance of $n_I^*(l)$ is $\sigma_{n_I}^2 = \frac{1}{N_I}$. Letting k=p, the

variance of $N_I(k)$ is given by

$$\text{var } [N_I(k)] = \sum_{l=0}^{N_I-1} \sum_{m=0}^{N_I-1} \frac{1}{N_I} \delta_{lm} \, e^{-j\frac{2\pi k(l-m)}{N_I}}$$

$$= \sum_{l=0}^{N_I-1} \frac{1}{N_I} = 1 \ .$$

For k≠p, Eqn. (3.1-19) becomes

$$E[N_I(k)N_I^*(p)] = \frac{1}{N_I} \frac{1-\exp\left[-j\frac{2\pi(k-p)}{N_I}\right]N_I}{1-\exp\left[-j\frac{2\pi(k-p)}{N_I}\right]}$$

$$= 0 \text{ for } k\neq p \ .$$

Identical results apply to the quadrature component $N_Q(k)$. Hence, the noise outputs

in different doppler cells are orthogonal. Because they are also zero mean, they

are uncorrelated. $N_I(k)$ and $N_Q(k)$ are also Gaussian random variables because they

are each linear combinations of jointly Gaussian random variables. Therefore, $N_I(k)$

and $N_I(p)$ as well as $N_Q(k)$ and $N_Q(p)$ are independent for k≠p.

The expected value of the cross term, $E[N_I(k)N_Q^*(p)]$, is given by

$$E[N_I(k)N_Q^*(p)] = \sum_{l=0}^{N_I-1} \sum_{m=0}^{N_I-1} E[n_I^*(l)n_Q^*(m)] \, e^{-j\frac{2\pi kl}{N_I}} e^{+j\frac{2\pi pm}{N_I}} \ .$$

A property of a stationary narrowband noise process of bandwidth B is that

the crossspectral density $S_{N_IN_Q}(f)$ of its quadrature components is purely imaginary

and is given by [13]

$$S_{N_I N_Q}(f) = -S_{N_Q N_I}(f)$$

$$= \begin{cases} j[S_N(f+f_0) - S_N(f-f_0)] \; ; & -B < f < B \\ \\ 0 & ; \quad \text{elsewhere} . \end{cases}$$

If the bandpass noise n'(t) is Gaussian with zero mean, and its power spectral density $S_N(f)$ is locally symmetrical about the midband frequency $\pm f_0$, then $S_{N_I N_Q}(f)$ equals zero. It follows that the in-phase noise $n_I'(t)$ and the quadrature noise $n_Q'(t)$ are orthogonal, i.e., $E[n_I'(l) n_Q'(m)] = 0$ for all l, m. Therefore, $N_I(k)$ and $N_Q(p)$ are also orthogonal. Since both are zero mean Gaussian distributed, they are statistically independent.

Next, the kth output coefficient S(k) of a DFT in response to the input signal sequence $s_I'(l) + j s_Q'(l)$, $l = 0, 1, - -, N_I - 1$, is considered where l denotes the signal sample taken at $t = l T_r = l/F_r$. From Eqns. (3.1-15) and (3.1-16) and Figure 3.1-2, observe that

$$s_I'(l) = \frac{K}{2\sqrt{N_I}} A\tau \cos(2\pi l f_d/F_r + \phi)$$

$$s_Q'(l) = \frac{K}{2\sqrt{N_I}} A\tau \sin(2\pi l f_d/F_r + \phi) .$$

Let s'(l) denote the weighted sum

$$s'(l) = s_I'(l) + j s_Q'(l)$$

$$= \frac{K}{2\sqrt{N_I}} A\tau \, e^{j\phi} \, e^{j2\pi l f_d/F_r}$$

$$= d \, e^{j\phi} \, e^{j2\pi l f_d/F_r} \qquad\qquad (3.1-20)$$

where

$$d = \frac{K}{2\sqrt{N_I}} \, A\tau \ .$$

The DFT output $S(k)$ coresponding to the input sequence $s'(l)$, $l = 0, 1, - -$, N_I-1, is

$$
\begin{aligned}
S(k) &= \sum_{l=0}^{N_I-1} \left(d \, e^{j\phi} \, e^{j2\pi f_d/F_r} \right) e^{-j2\pi kl/N_I} \\
&= d \, e^{j\phi} \, \frac{1 - e^{j2\pi(f_d/F_r - k/N_I)N_I}}{1 - e^{j2\pi(f_d/F_r - k/N_I)}} \\
&= d \, e^{j\phi} \, e^{j\pi(f_d/F_r - k/N_I)(N_I-1)} \, \frac{\sin\pi(f_d/F_r - k/N_I)N_I}{\sin\pi(f_d/F_r - k/N_I)} \ .
\end{aligned}
\tag{3.1-21}
$$

Let α and β denote

$$\alpha = \pi(f_d/F_r - k/N_I)$$

$$\beta = \pi(f_d/F_r + k/N_I) \ .$$

Note that the DFT outputs, $S_I(k)$ and $S_Q(k)$ corresponding to input sequences, $s_I'(l)$ and $s_Q'(l)$, respectively, are

$$S_I(k) = \frac{d}{2} \left[e^{j\phi} e^{j\alpha(N_I-1)} \frac{\sin N_I \alpha}{\sin\alpha} + e^{-j\phi} e^{-j\beta(N_I-1)} \frac{\sin N_I \beta}{\sin\beta} \right] \tag{3.1-22}$$

$$S_Q(k) = \frac{d}{2j} \left[e^{j\phi} e^{j\alpha(N_I-1)} \frac{\sin N_I \alpha}{\sin\alpha} - e^{-j\phi} e^{-j\beta(N_I-1)} \frac{\sin N_I \beta}{\sin\beta} \right] \ . \tag{3.1-23}$$

Clearly, the sum, $S_I(k) + jS_Q(k)$, is equal to $S(k)$.

97

When $f_d/F_r = k/N_I$, $\alpha = 0$, $N_I\beta = 2\pi k$, and the DFT becomes the matched filter for the corresponding doppler frequency. Under this condition, the DFT outputs become

$$S(k)|_{f_d/F_r=k/N_I} = d\,N_I\,e^{j\phi} \qquad\qquad (3.1\text{-}24)$$

$$S_I(k)|_{f_d/F_r=k/N_I} = \frac{d\,N_I}{2}\,e^{j\phi}$$

$$= \frac{d\,N_I}{2}\,(\cos\phi + j\sin\phi) \qquad\qquad (3.1\text{-}25a)$$

$$S_Q(k)|_{f_d/F_r=k/N_I} = \frac{d\,N_I}{2j}\,e^{j\phi}$$

$$= \frac{d\,N_I}{2j}\,(\cos\phi + j\sin\phi) \; . \qquad\qquad (3.1\text{-}25b)$$

With reference to Figure 3.1-2, the output $X(k)$ of the summer following the FFT's is given by

$$X(k) = X_I(k) + jX_Q(k)$$

$$= \begin{cases} N_I(k)+jN_Q(k) = N(k) & : \text{ under } H_0 \\ S_I(k)+jS_Q(k) + N_I(k)+jN_Q(k) = S(k)+N(k) & : \text{ under } H_1 \; . \end{cases} \qquad (3.1\text{-}26)$$

For the remainder of the discussion, it is assumed that $f_d/F_r = kN_I$. The real and imaginary parts of $S(k)$ are determined from

$$S(k) = S_I(k) + jS_Q(k)$$

$$= \text{Re}\{S_I(k)\} - \text{Im}\{S_Q(k)\} + j[\,\text{Im}\{S_I(k) + \text{Re}\{S_Q(k)\}\}\,]$$

$$= d\,N_I\,\cos\phi + j\,d\,N_I\,\sin\phi \; .$$

Hence, the real and imaginary parts of $X(k)$ are

$$Re\{X(k)\} = \begin{cases} Re\{N_I(k)\} - Im\{N_Q(k)\} & : \text{under } H_0 \\ d \ N_I \cos\phi + Re\{(N_I(k)\} - Im\{N_Q(k)\} & : \text{under } H_1 \end{cases} \qquad (3.1\text{-}27a)$$

and

$$Im\{X(k)\} = \begin{cases} Im\{(N_I(k)\} + Re\{N_Q(k)\} & : \text{under } H_0 \\ d \ N_I \sin\phi + Im\{(N_I(k)\} + Re\{N_Q(k)\} & : \text{under } H_1. \end{cases} \qquad (3.1\text{-}27b)$$

It will now be shown that $X(k)$ under H_0, which is given by

$$X(k) = N(k) = Re\{N(k)\} + jIm\{N(k)\}$$

is a zero mean complex Gaussian random variable. To prove this, the following must be verified:

1) $Re\{N(k)\}$ is a zero mean Gaussian random variable

2) $Im\{N(k)\}$ is a zero mean Gaussian random variable

3) $Var[Re\{N(k)\}] = Var[Im\{N(k)\}]$

4) $E[Re\{N(k)\}Im\{N(k)\}] = 0$.

From Eqn.(3.1-27), $Re\{N(k)\}$ and $Im\{N(k)\}$ are given by

$$Re\{N(k)\} = Re\{N_I(k)\} - Im\{N_Q(k)\}$$

$$= \sum_{l=0}^{N_I-1} \left[n_I'(l)\cos\frac{2\pi kl}{N_I} + n_Q'(l)\sin\frac{2\pi kl}{N_I} \right] \qquad (3.1\text{-}28a)$$

and

$$Im\{N(k)\} = Im\{N_I(k)\} + Re\{N_Q(k)\}$$

$$= -\sum_{l=0}^{N_I-1} \left[n_I'(l)\sin\frac{2\pi kl}{N_I} + n_Q'(l)\cos\frac{2\pi kl}{N_I} \right] . \qquad (3.1\text{-}28b)$$

Since $n_I^{\cdot}(l)$, $n_Q^{\cdot}(l)$ are both zero mean jointly Gaussian random variables, $\text{Re}\{N(k)\}$ and $\text{Im}\{N(k)\}$, which are linear combinations of $n_I^{\cdot}(l)$, $n_Q^{\cdot}(l)$, are zero mean Gaussian random variables. In particular,

$$E[\text{Re}\{N(k)\}] = E[\text{Im}\{N(k)\}] = 0 \ . \tag{3.1-29a}$$

From Eqn. (3.1-28), the variance of the $\text{Re}\{N(k)\}$ can be written as

$$\text{var}[\text{Re}\{N(k)\}] = E[\ \Big(\ \sum_{l=0}^{N_I-1}\ \Big[\ n_I^{\cdot}(l)\cos\frac{2\pi kl}{N_I} + n_Q^{\cdot}(l)\sin\frac{2\pi kl}{N_I}\ \Big]\ \Big)^2\ ] \ .$$

Since $E[n_I^{\cdot}(l)n_I^{\cdot}(m)] = 0$ for $l \neq m$ and $E[n_I^{\cdot}(l)n_Q^{\cdot}(m)] = 0$ for all l, m, $\text{var}[\text{Re}\{N(k)\}]$ becomes

$$\text{var}[\text{Re}\{N(k)\}] = \sum_{l=0}^{N_I-1}\ E[n_I^{\cdot 2}(l)]\cos^2\Big(\frac{2\pi kl}{N_I}\Big) + \sum_{l=0}^{N_I-1}\ E[n_Q^{\cdot 2}(l)]\ \sin^2\Big(\frac{2\pi kl}{N_I}\Big)$$

$$= 1 \ . \tag{3.1-29b}$$

Similarly, $\text{var}[\text{Im}\{N(k)\}]$ can be shown to be 1. To prove that $\text{Re}\{N(k)\}$ and $\text{Im}\{N(k)\}$ are orthogonal, $E[\text{Re}\{N(k)\}\text{Im}\{N(k)\}]$ is carried out as follows:

$$E[\text{Re}\{N(k)\}\text{Im}\{N(k)\}]$$

$$= E[\ \Big(\ \text{Re}\{N_I(k)\} - \text{Im}\{N_Q(k)\}\ \Big)\ \Big(\ \text{Im}\{N_I(k)\} + \text{Re}\{N_Q(k)\}\ \Big)\ ]$$

$$= -\sum_{l=0}^{N_I-1}\ \sum_{m=0}^{N_I-1}\ E[n_I^{\cdot}(l)n_I^{\cdot}(m)]\ \cos\frac{2\pi kl}{N_I}\ \sin\frac{2\pi km}{N_I}$$

$$+\sum_{l=0}^{N_I-1}\ \sum_{m=0}^{N_I-1}\ E[n_I^{\cdot}(l)n_Q^{\cdot}(m)]\ \cos\frac{2\pi kl}{N_I}\ \cos\frac{2\pi km}{N_I}$$

$$-\sum_{l=0}^{N_I-1}\ \sum_{m=0}^{N_I-1}\ E[n_I^{\cdot}(l)n_Q^{\cdot}(m)]\ \sin\frac{2\pi kl}{N_I}\ \sin\frac{2\pi km}{N_I}$$

$$+\sum_{l=0}^{N_I-1}\ \sum_{m=0}^{N_I-1}\ E[n_Q^{\cdot}(l)n_Q^{\cdot}(m)]\ \sin\frac{2\pi kl}{N_I}\ \cos\frac{2\pi km}{N_I}\ \ .$$

Since $E[n_I^\cdot(l)n_I^\cdot(m)] = E[n_Q^\cdot(l)n_Q^\cdot(m)] = 0$ for $l \neq m$, $E[n_I^\cdot(l)n_Q^\cdot(m)] = 0$ for all l and m, and $E[n_I^{\cdot 2}(l)] = E[n_Q^{\cdot 2}(l)]$, the above quantity evaluates to zero. Thus,

$$E[\text{Re}\{N(k)\}\text{Im}\{N(k)\}] = 0 \ . \tag{3.1-29c}$$

It is concluded that $N(k)$ is a zero mean complex Gaussian random variable.

With the above preliminaries, the mean and variance of the real and imaginary parts of $X(k)$ under both hypotheses are given as follows:

$\text{Re}\{X(k)\}$

    under H_0:

        mean $= 0$

        variance $= 1$.

    under H_1:

        mean $= \sqrt{N_I \Re_p} \, \cos\phi = \sqrt{\Re} \, \cos\phi$

        variance $= 1$.

$\text{Im}\{X(K)\}$

    under H_0:

        mean $= 0$

        variance $= 1$.

    under H_1:

        mean $= \sqrt{\Re} \, \sin\phi$

        variance $= 1$.

Recall that $\Re = N_I \Re_p = 2N_I(S/N)_p$ is the integrated peak signal-to-noise ratio.

Define the envelope voltage r and the phase angle ν such that r and ν are related to Re{X(k)} and Im{X(k)} by

$$r = \sqrt{[Re\{X(k)\}]^2 + [Im\{X(k)\}]^2} \ . \tag{3.1-30a}$$

$$\nu = \tan^{-1}\left(\frac{Im\{X(k)\}}{Re\{X(k)\}} \right) \ . \tag{3.1-30b}$$

It follows that

$$Re\{X(k)\} = r \ cos\nu \tag{3.1-31a}$$

$$Im\{X(k)\} = r \ sin\nu \ , \tag{3.1-31b}$$

Note that Re{X(k)} and Im{X(k)} are statistically independent due to the independence of Re{N(k)} and Im{N(k)}.

Under H_0, the joint probability densty of Re{X(k)} and Im{X(k)} is

$$
\begin{aligned}
p(Re\{X\}, \ Im\{X\}) &= p(Re\{X\}) \ p(Im\{X\}) \\
&= \left(\frac{1}{2\pi}\right) \ \exp\left(-\frac{(Re\{X\})^2 + (Im\{X\})^2}{2} \right) \\
&= \frac{1}{2\pi} \ e^{-r^2/2} \ . \tag{3.1-32}
\end{aligned}
$$

By the transformation of variables given in Eqn. (3.1-31), the joint probability density $p(r, \ \nu)$ can be shown to be

$$p(r, \ \nu) = \frac{r}{2\pi} \ \exp\left(-\frac{r^2}{2} \right) \ . \tag{3.1-33}$$

The marginal density function p(r) is obtained by integrating Eqn. (3.1-33) over

$\mathcal{V}$ which becomes

$$p(r) = \frac{1}{2\pi} \int_0^{2\pi} r\, e^{-\frac{r^2}{2}}\, d\nu = r\, \exp\left(-\frac{r^2}{2}\right) \ . \tag{3.1-34}$$

Under hypothesis H_1, the joint probability density function of $\text{Re}\{X(k)\}$ and $\text{Im}\{X(k)\}$ given ϕ and $\Re$ is

$$p(\text{Re}\{X\},\ \text{Im}\{X\}|\phi,\Re) = \frac{1}{2\pi} \exp\left(-\frac{(\text{Re}\{X\} - \sqrt{\Re}\,\cos\phi)^2 + (\text{Im}\{X\} + \sqrt{\Re}\,\sin\phi)^2}{2}\right) \ .$$
$$\tag{3.1-35}$$

By the transformation of variables given in Eqn. (3.1-31), $p(r,\ \nu|\phi,\ \Re)$ can be obtained as

$$p(r,\ \nu|\phi,\ \Re) = \frac{r}{2\pi} \exp\left[-\frac{r^2 + \Re - 2r\sqrt{\Re}\,\cos(\phi+\nu)}{2}\right] \ . \tag{3.1-36}$$

Integration of Eqn. (3.1-36) with respect to ν gives the conditional marginal density function $p(r|\phi,\ \Re)$ as

$$p(r|\phi,\ \Re) = re^{-(r^2+\Re)/2} \frac{1}{2\pi} \int_0^{2\pi} e^{r\sqrt{\Re}\,\cos(\phi+\nu)}\, d\nu$$

$$= re^{-(r^2+\Re)/2}\, I_0(r\sqrt{\Re}) \ , \tag{3.1-37}$$

where I_0 is the modified Bessel function of the first kind, zero order. Note that Eqn. (3.1-37) is not a function of ϕ. Assuming ϕ is uniformly distributed between 0 and 2π, the conditional density function of r given $\Re$ is

$$p(r|\Re) = \int_0^{2\pi} p(r,\phi|\Re)d\phi = \int_0^{2\pi} \frac{1}{2\pi}\, p(r|\phi,\Re)d\phi$$

$$= re^{-(r^2+\Re)/2}\, I_0(r\sqrt{\Re}) \ . \tag{3.1-38}$$

The envelope voltage r is the sufficient statistic. Under the null hypothesis, the probability density function for r, $p(r|\mathfrak{R})$, is Rayleigh as agiven by Eqn. (3.1-34). Under the alternate hypothesis, $p(r|\mathfrak{R})$ is Rician as given by Eqn. (3.1-38), for all target models assumed. The likelihood ratio test (LRT) decides that a target is present when the test statistic r exceeds the threshold r_T. Otherwise, it decides that a target is not present:

$$r \underset{H_0}{\overset{H_1}{\gtrless}} r_T \, .$$

The detection probability arising from the probability density of r given $\mathfrak{R}$ must be properly averaged over target RCS fluctuations which is carried out in the next Section.

3.2 Detection Threshold and Probabilities of Detection

The detection threshold is determined from the cell false alarm probability p_f prior to the binary post detection integration, and the probability density function $p(r)$ for the test statistic r under the null hypothesis H_0. The false alarm probability is determined in Section 2.5 from the given system false alarm rate and the specific post detection integration involved. The probability density function for the test statistic under H_0 is Rayleigh as given by Eqn. (3.1-34). Hence, the cell false alarm probability p_f is

$$p_f = \int_{r_T}^{\infty} r e^{-r^2/2} = \exp\left(-\frac{r_T^2}{2}\right) . \tag{3.2-1}$$

The detection threshold r_T follows from Eqn. (3.2-1) and is

$$r_T = \sqrt{2 \ln \frac{1}{p_f}} . \tag{3.2-2}$$

The probability of detection p_{di} in the ith slant conditioned on the integrated peak signal-to-noise ratio for the ith slant, denoted by $\mathcal{R}_i$, is obtained by integrating the probability density function $p(r|\mathcal{R}_i)$ under hypothesis H_1. Let $(S/N)_i = N_I (S/N)_{pi}$ denote the integrated signal-to-noise ratio for the ith slant. Since $\mathcal{R}_i = 2N_i (S/N)_{pi}$,

105

$$\left(\frac{S}{N}\right)_i = \frac{\mathcal{R}_i}{2}.$$

Let $(S_0/N) = \mathcal{R}_0/2$ denote the integrated signal-to-noise ratio assuming all pulses are received through a rectangular beam at its peak gain. Taking into account, L_{BSi}, the beam shape loss for the ith slant, the integrated signal-to-noise ratio for the ith slant is expressed as

$$\left(\frac{S}{N}\right)_i = \left(\frac{S_0}{N}\right)(L_{BS_i}) = \left(\frac{\mathcal{R}_0}{2}\right)(L_{BS_i}).$$

The actual beam shape losses, in dB, are determined and tabulated in Section 2.4.

The conditional density function $p(r|\mathcal{R}_i)$ is Rician for all Swerling and Marcum target models assumed. Thus, for a specified value of $\mathcal{R}_i$, p_{di} is given as

$$p_{di} = \int_{r_T}^{\infty} r \, \exp(-r^2 + \mathcal{R}_i)/2 \; I_0(r\sqrt{\mathcal{R}_i})dr = Q(r_T, \sqrt{\mathcal{R}_i}) \qquad (3.2\text{-}3)$$

where $Q(\cdot)$ is Marcum's Q function [2].

For specified value of $\mathcal{R}_i$; $i=1,2,--,N$, the detection probability $P'_d(M,N)$ after M of N binary post detection integration is a function of p_{d1}, p_{d2}, $--$ p_{dN}, M, and N. This is written as

$$P'_d(M,N) = f(p_{d_1}, p_{d_2}, \text{--}, p_{d_N}, M, N); \qquad 1 \leq M \leq N. \qquad (3.2\text{-}4)$$

For an idealized rectangular antenna beam where $p_{di} = p_{dj}$, $i = j$, $P'_d(M,N)$ is given by

$$P'_d(M,N) = \sum_{i=M}^{N} \frac{N!}{i!(N-i)!} \, p_{d_j}^i (1-p_{d_j})^{N-i} .$$

In general, $p_{di} \neq p_{dj}$ because the antenna beam is not rectangular and $L_{BSi} \neq L_{BSj}$. Then, Eqn. (3.2-4) consists of product terms of the form

$$\prod_{k=1}^{i} p_{d_k} \prod_{j=1}^{N-i} (1-p_{d_{(i+j)}}); \qquad M \leq i \leq N-1 \qquad (3.2\text{-}5a)$$

or

$$\prod_{k=1}^{N} p_{d_k}; \qquad i = N . \qquad (3.2\text{-}5b)$$

The unconditioned detection probability P_d is obtained by averaging $P'_d(M,N)$ over the random variations of $(S/N)_1$, $(S/N)_2$, - - , $(S/N)_N$. This process is illustrated in Figure 3.2-1. The unconditioned detection probability is given by

$$P_d = [\overline{P'_d(M,N)}] \qquad (3.2\text{-}6)$$

where the overbar indicates an N-dimensional expectation
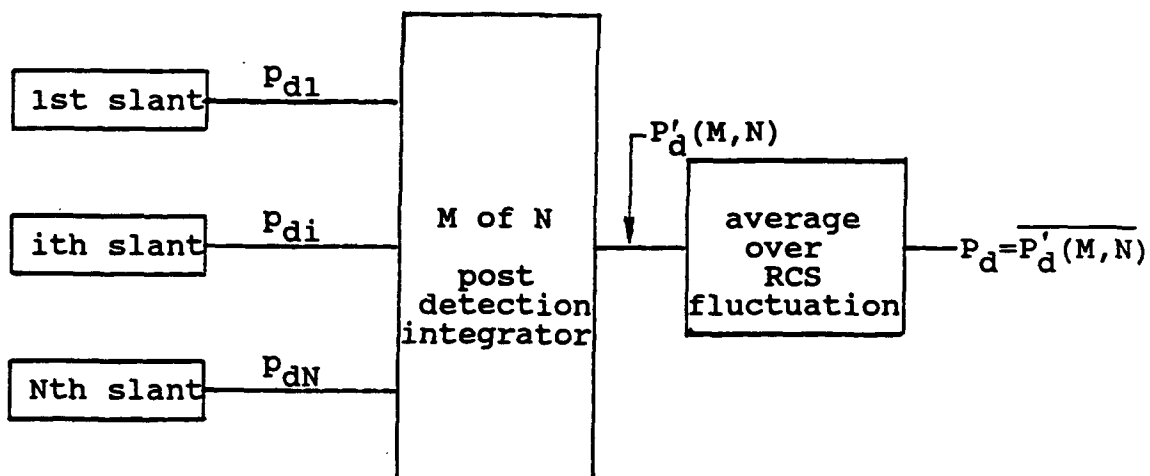
Figure 3.2-1 Process for Determining Probabilities of Detection after M of N Post Detection Binary Integrator
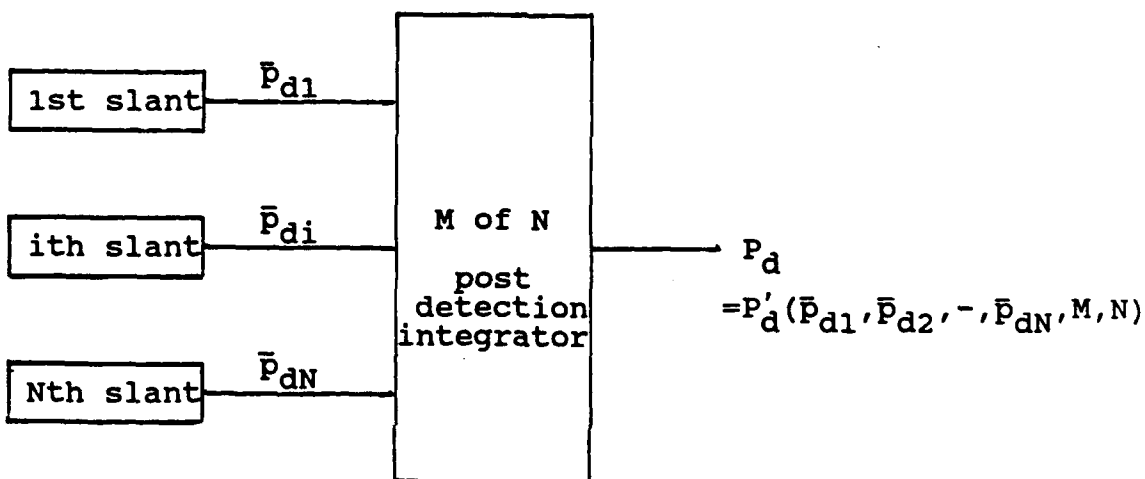
Figure 3.2-2 Process for Determining Probabilities of Detection after M of N Post Detection Binary Integrator (slant-to-slant RCS fluctation)

with respect to $(S/N)_1$, $(S/N)_2$, - - , $(S/N)_N$.

For scan-to-scan fluctuation, the signal-to-noise ratio remains constant over each slant and Eqn. (3.2-6) can be written as

$$P_d = [\overline{P_d'(M,N)}] = \int_0^\infty P_d'(M,N) \; p(S_0/N) \; d(S_0/N) \; . \tag{3.2-7}$$

For slant-to-slant fluctuations, the signal-to-noise ratio varies from one slant to another. Assuming the variations to be statistically independent, each factor in Eqns. (3.2-5a) and (3.2-5b) can be averaged separately. The N-dimensional expectation of Eqn. (3.2-6) then involves product terms of the form

$$[\overline{\prod_{k=1}^{i} p_{d_k} \prod_{j=1}^{N-i} (1-p_{d_{(i+j)}})}] = \prod_{k=1}^{i} \overline{p}_{d_k} \prod_{j=1}^{N-i} (1-\overline{p}_{d_{(i+j)}}) \; ; \qquad M \leq i \leq N-1$$

and

$$[\overline{\prod_{k=1}^{N} p_{d_k}}] = \prod_{k=1}^{N} \overline{p}_{d_k} \; ; \qquad i = N,$$

respectively. Hence, the expression for P_d corresponding to slant-to-slant fluctuation can be written as

$$P_d = [\overline{P_d^j(M,N)}] = g(\overline{P}_{d_1}, \overline{P}_{d_2}, \cdots, \overline{P}_{d_N}, M, N) . \qquad (3.2\text{-}8)$$

The detection process for slant-to-slant fluctuating target cases is redrawn in Figure 3.2-2.

The probability of detection for the five target models introduced in section 2.6 is developed below for the baseline 3 of 3 post detection integration. For this purpose, the center slant is designated with a subscript 1, and each of the two outer slants is designated with a subscript 2.

1. Marcum (Nonfluctuating) case:

For this model, the probabilities of detection in the center and outer slants are:

$$P_{d_1} = Q(r_T \sqrt{\Re_1}) \qquad (3.2\text{-}9a)$$

$$P_{d_2} = Q(r_T \sqrt{\Re_2}) \qquad (3.2\text{-}9b)$$

where

$$\Re_i = 2\left(\frac{S_0}{N}\right)(L_{BS_i}) ; \qquad i = 1, 2 .$$

Since this model assumes no fluctuation, there is no averaging with respect to RCS fluctuation. Thus, the detection probability after 3 of 3 post detection integration becomes

$$P'_d(3,3) = P_d = p_{d_1} p_{d_2}^2 .$$ \hfill (3.2-10)

2. Swerling case 1:

For this model, p_{di}, and $P'_d(3,3)$ are identical to the Marcum case given above. P_d is obtained by averaging $P'_d(3,3)$ over the scan-to-scan variations of (S_0/N). Hence, P_d is given by

$$P_d = \int_0^\infty [P'_d(3,3)] \; p(S_0/N) \; d(S_0/N)$$

$$= \int_0^\infty [P'_d(3,3)] \frac{1}{\overline{S_0/N}} \exp\left(-\frac{S_0/N}{\overline{S_0/N}}\right) \; d(S_0/N)$$ \hfill (3.2-11)

where $(\overline{S}_0/N)$ is the mean integrated signal-to-noise ratio corresponding to the mean target radar cross section. Further simplification is not possible and the integrand must be evaluated numerically.

3. Swerling case 2:

For this model, p_{di} is the same as for the Marcum case. Hence, Eqns. (3.2-9a,b) are applicable. $\overline{p}_{di}$ for the ith slant is obtained by averaging $\dot{p}_{di}$ over the slant-to-slant

111

variations of $(S/N)_i$ due to target RCS fluctuation:

$$\bar{P}_{d_i} = \int_0^\infty [P_{d_i}] \, p([S/N]_i) \, d([S/N]_i) \, .$$
(3.2-12)

Substitution of Eqn. (3.2-3) for P_{di} in Eqn. (3.2-12) results in

$$\bar{P}_{d_i} = \int_0^\infty \left\{ \int_{r_T}^\infty r \, \exp\left[-(r^2 + 2(S_0/N)(L_{BS_i})/2 \right] \right.$$

$$\left. \cdot I_0 \left[r\sqrt{2(S_0/N)(L_{BS_i})} \right] dr \right\} \, p(S_0/N) d(S_0/N)$$

where $p(S_0/N)$ is given by Eqn. (2.6-4). Interchanging the order of integration transforms the above to a product of a gamma function and a confluent hypergeometric function [2]. Using the power series expansion of the confluent hypergeometric function leads to a simple closed form solution given by

$$\bar{P}_{d_i} = \exp\left(\frac{\ln p_f}{1 + (\overline{S/N})_i} \right) \, ; \quad i = 1, \, 2 \, ,$$
(3.2-13)

where $(\overline{S/N})_i = (\bar{S}_0/N)(L_{BSi})$. The probability of detection P_d after post detection integration is

$$P_d = [\overline{P_d'(3,3)}] = g(\bar{P}_{d_1}, \bar{P}_{d_2}, \bar{P}_{d_2}, M, N) = \bar{P}_{d_1} \bar{P}_{d_2}^2 \, .$$
(3.2-14)

112

4. Swerling case 3:

The procedure in this case is exactly the same as that used for Swerling case 1 except the density function for (S_0/N) corresponds to one dominant plus Rayleigh (exponential power) scatterers. As with Swerling case 1, p_{di} and $P'_d(3,3)$ are identical to the Marcum case. P_d is given by

$$P_d = \int_0^\infty [P'_d(3,3)] \, p(S_0/N) \, d(S_0/N)$$

$$= \int_0^\infty [P'_d(3,3)] \frac{4S_0/N}{(\overline{S_0/N})^2} \exp\left(-\frac{2S_0/N}{\overline{S_0}/N}\right) \, d(S_0/N) \qquad (3.2\text{-}15)$$

The above integral must be evaluated numerically.

5. Swerling case 4:

Exactly the same steps are used for this model as in Swerling case 2. However, the form of the probability density function for the variation of (S_0/N) is identical to that of Swerling case 3. From DiFranco and Rubin [2], p_{di} for this case is given by

$$\overline{P}_{d_i} = \int_0^\infty [p_{d_i}] \, p([S/N]_i) \, d([S/N]_i)$$

$$= \frac{1}{1+\dfrac{(S/N)_i}{2}} \left[1 + \frac{(S/N)_i}{2} - \frac{\ln p_f}{1+\dfrac{2}{(S/N)_i}} \right] \exp\left[\frac{\ln p_f}{1+\dfrac{(S/N)_i}{2}} \right] ,$$

$$(3.2\text{-}16)$$

where $(\overline{S/N})_i$ equals $(\overline{S_0}/N)(L_{BSi})$. The detection probability after 3 of 3 post detection integration is

$$P_d = [\overline{P_d'(3,3)}] = g(\overline{P}_{d_1}, \overline{P}_{d_2}, \overline{P}_{d_2}, M, N) = \overline{P}_{d_1} \overline{P}_{d_2}^2 . \qquad (3.2\text{-}14)$$

Plots of P_d versus $(\overline{S}_0/N)$ for the baseline configuration are shown in Section 3.3 for the five target models.

114

3.3 Detection Performance for the Baseline Configuration

The detection performance for the baseline configuration is presented in this section by developing probability of detection versus $(\overline{S}_0/N)$ plots. To accomplish this, a cell false alarm probability before 3 of 3 post detection integration corresponding to the given system false alarm specification is first required. Procedures for obtaining this are presented in Section 2.5. Next, the detection threshold is determined per Eqn. (3.2-2). For each slant in a beam dwell, the beam shape loss given in Section 2.4 is then subtracted in dB from the stated $(\overline{S}_0/N)$ before the conditional detection probability, p_{di}, is computed for each target model. The number of pulses available for integration for the baseline and modified configurations were determined in Section 2.3. Finally, the detection probability after post detection binary integration is determined according to the procedures outlined in Section 3.2.

Figure 3.3-1 shows the probabilities of detection averaged over the respective target fluctuations assumed for the five target models described in Section 2.6. For these detection probabilities, the threshold is set such that the resulting system false alarm rate is 2 per each antenna scan which takes ten seconds. When $(\overline{S}_0/N)$ is 12.2 dB, the
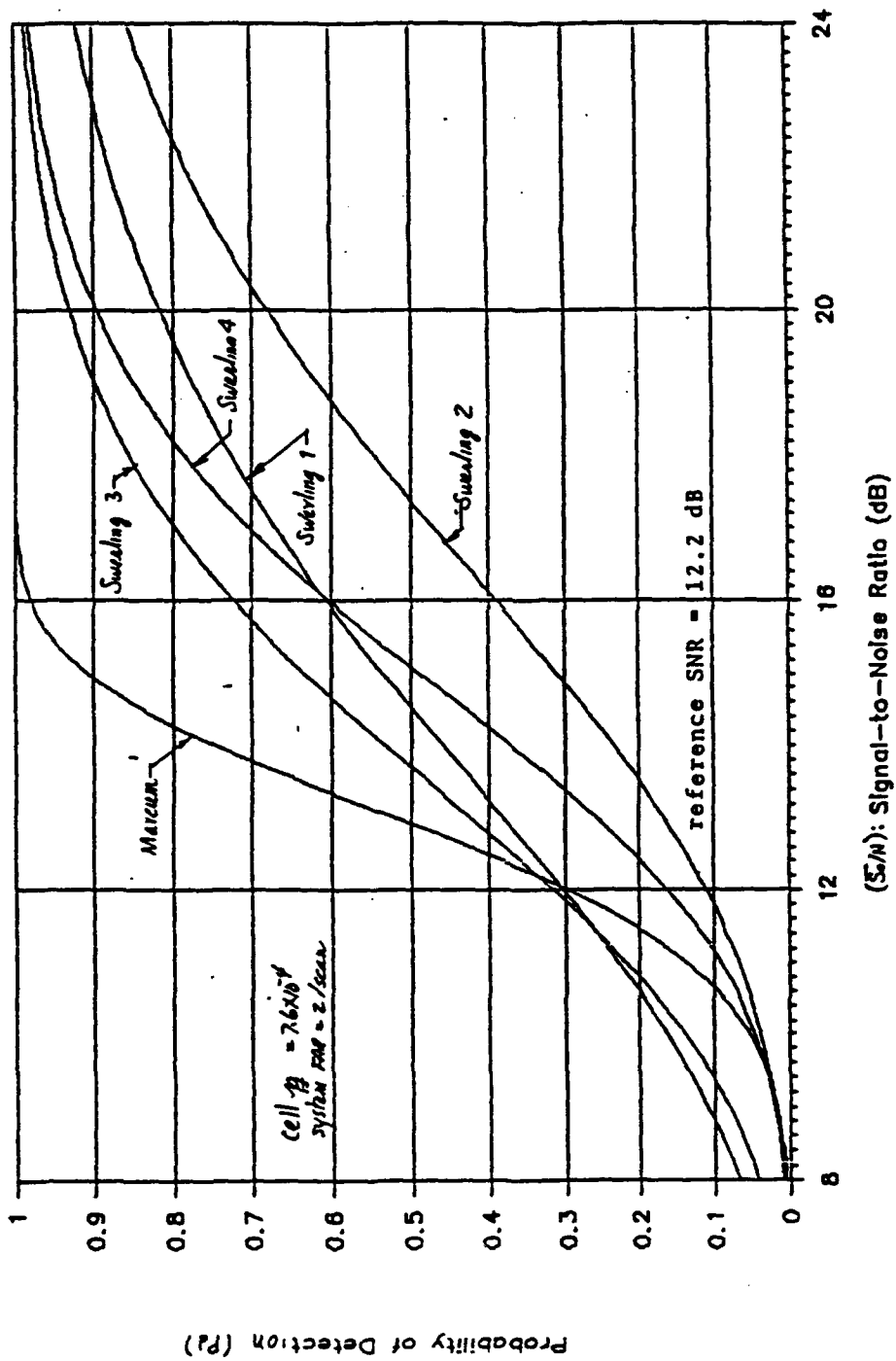
Figure 3.3-1

Detection Performance of the Baseline

Swerling and Marcum Target Models

baseline yields the single scan detection probability of 0.32 for a Swerling case 1 reference target when it is located at the reference range. Note that this is equivalent to the cumulative detection probability of 0.9 in 6 antenna scans as explained in Section 1.1.3. The cumulative detection probability curves for the five target models are shown in Figure 3.3-2. Given single scan detection probabilities of Figure 3.3-1, the cumulative detection probabilities of Figure 3.3-2 for 6 antenna scans arise as a natural consequence. Therefore, the curves of Figure 3.3-2 are those to which performance under scan-to-scan processing using 6 scans should be compared. It is evident from these figures that fluctuating target models yield poorer detection performance than a nonfluctuating target model in the region of high SNR. Also evident is the influence of correlation properties on detection performance. Swerling case 1 and Swerling case 3 are more alike in their detection performance than those for Swerling case 1 and Swerling case 2 even though Swerling case 1 and 2 have the same probability density function for their RCS fluctuations.

Figures 3.3-3 through 3.3-7 are detection performance plots for Swerling cases 1, 2, 3, 4, and the Marcum model, respectively, for various cell false alarm probabilities. With reference to Eqn. (2.5-25), note that an increase by a

Cumulative Detection Probability

of the Baseline
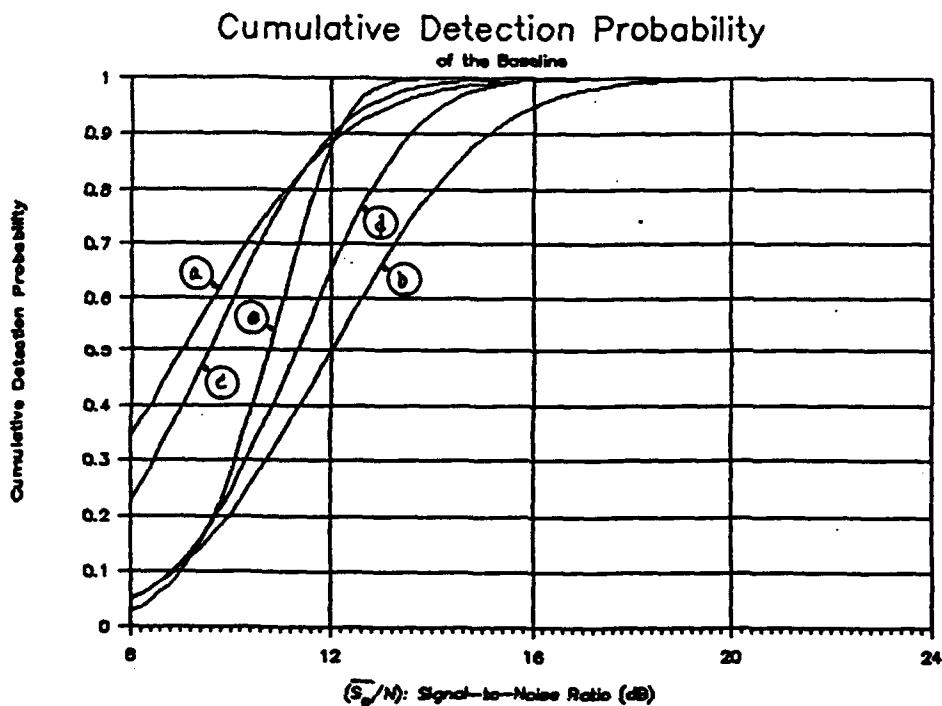
(a) Swerling case 1

(b) Swerling case 2

(c) Swerling case 3

(d) Swerling case 4

(e) Marcum

cell false alarm probability: 7.6×10^{-4}

normal time overhead: 5 milliseconds

individual beam shape losses: 0.3/3.43 dB

reference SNR: 12.2 dB

Figure 3.3-2 Cumulative Detection Probabilities for Swerling
and Marcum Target Models - Baseline
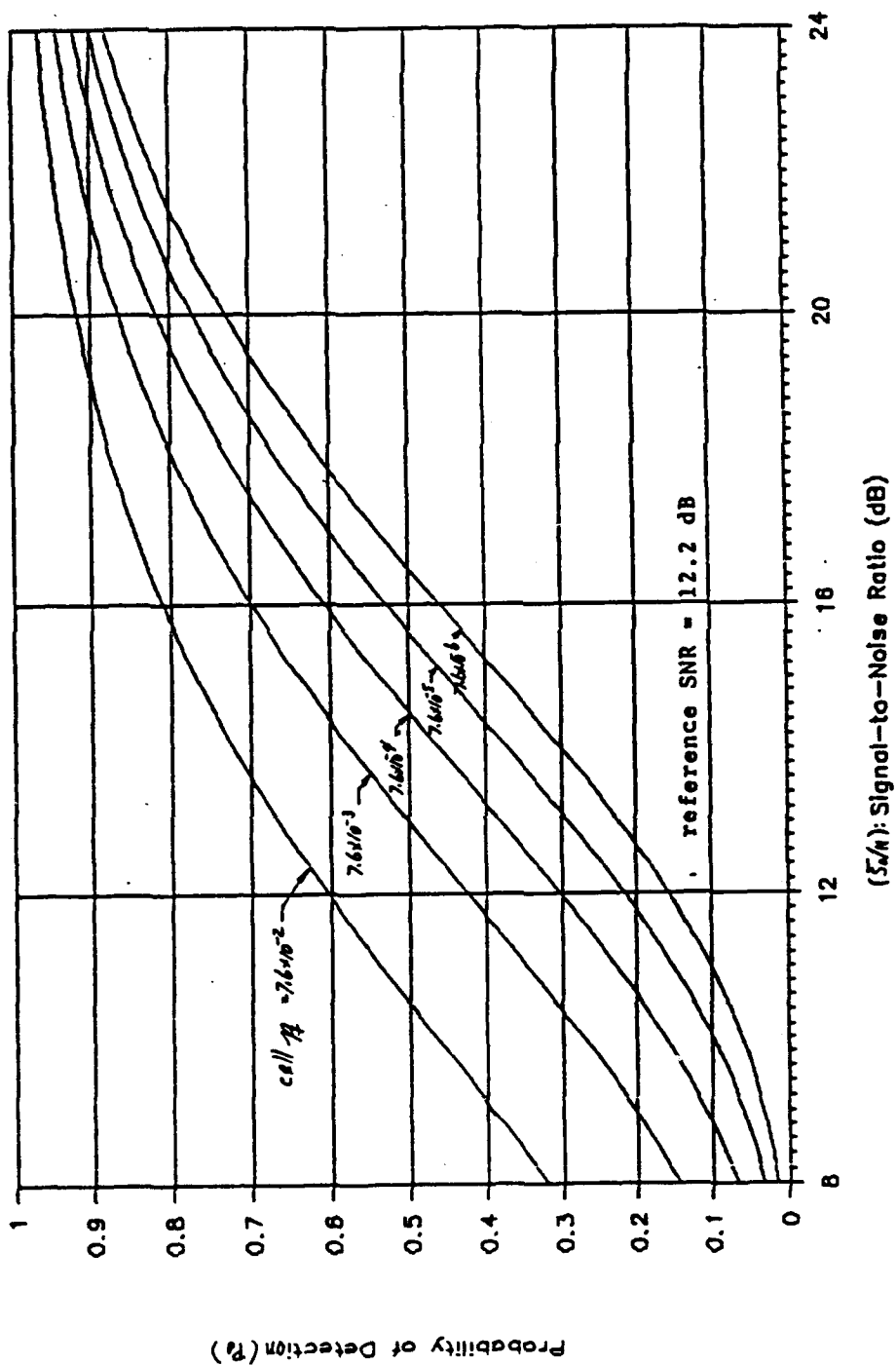
Figure 3.3-3

Detection Performance of the Baseline

Swerling Case 1 Target Model
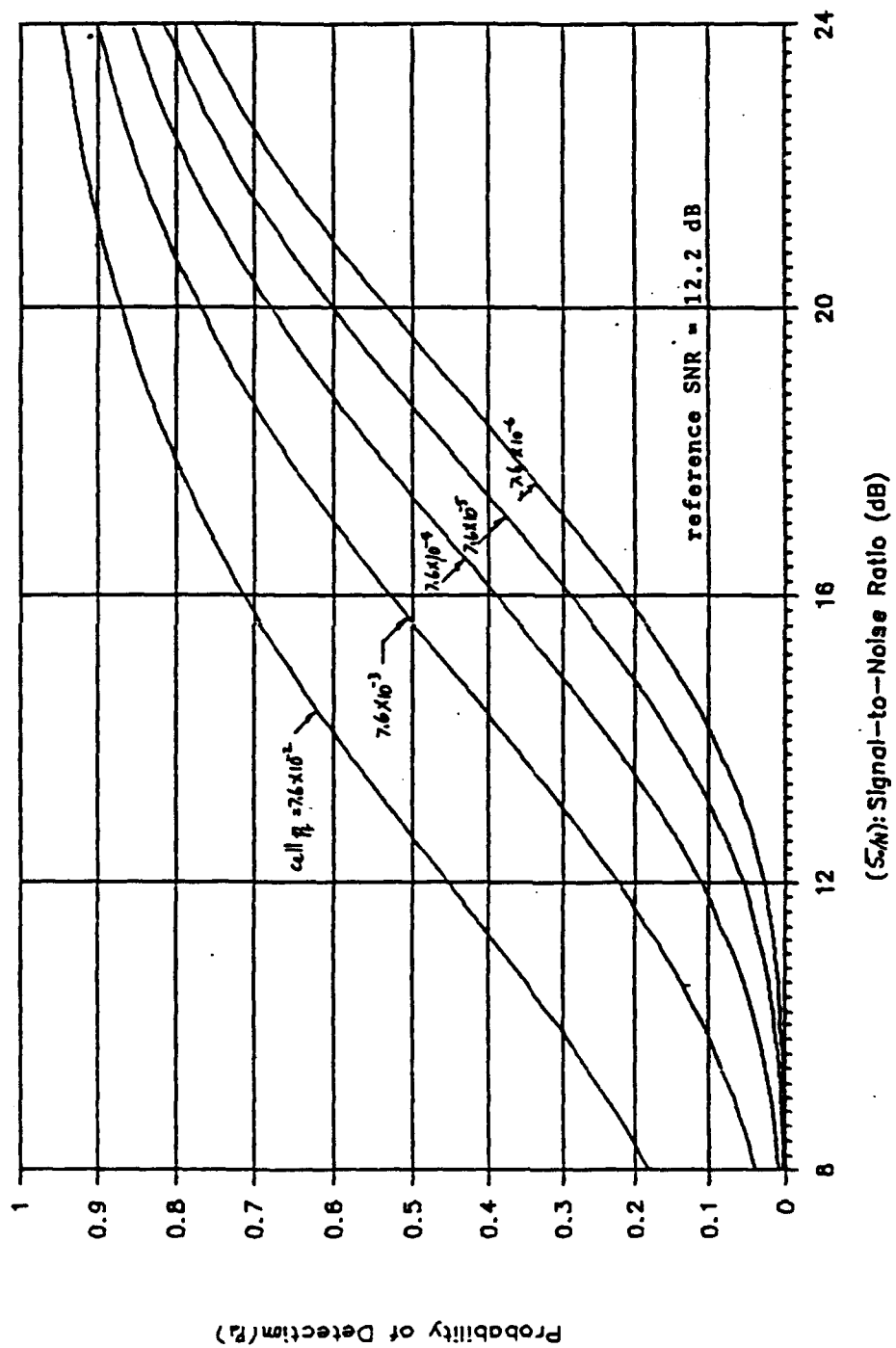
Figure 3.3-4.

Detection Performance of the Baseline

Swerling Case 2 Target Model
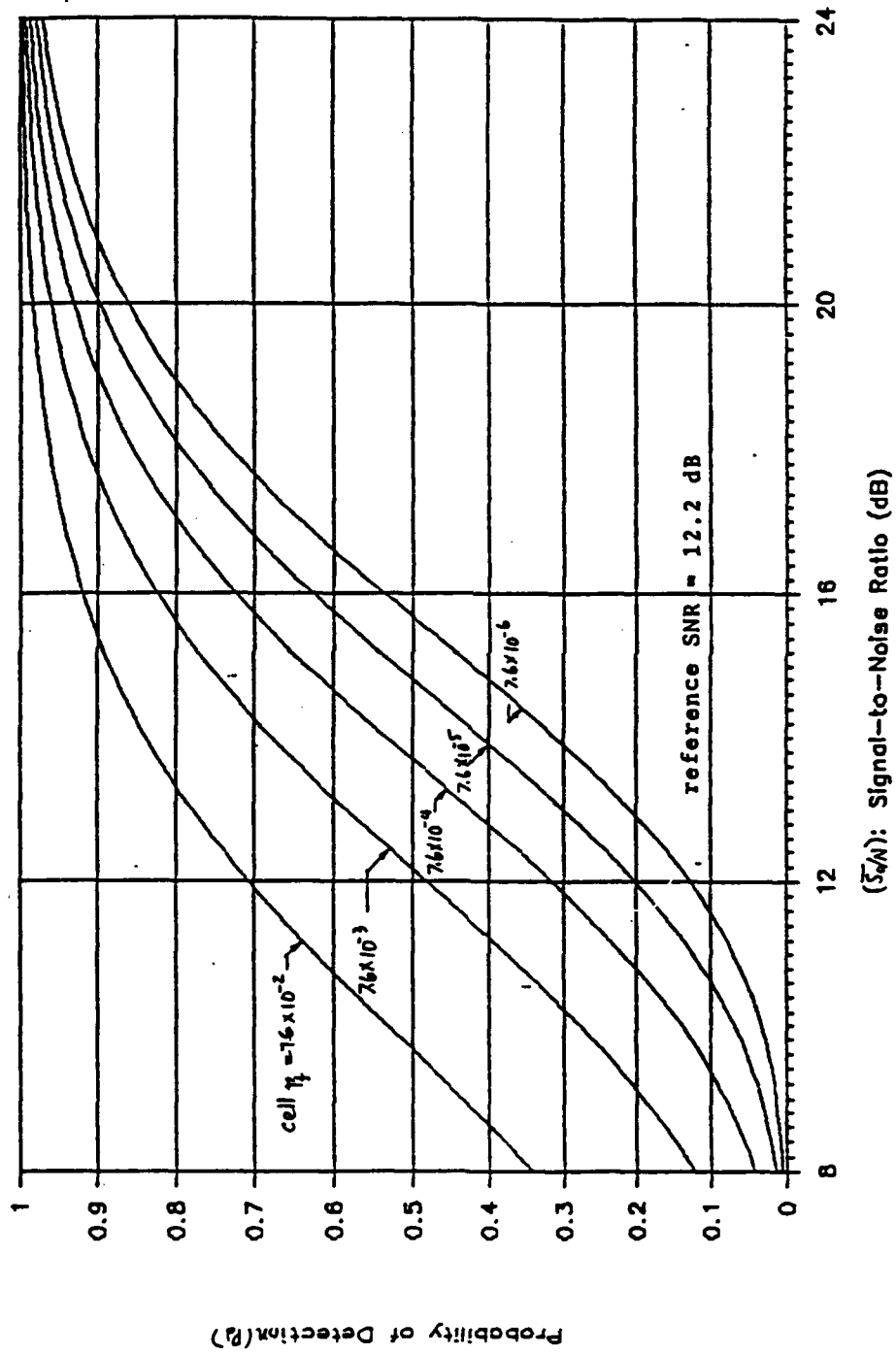
Figure 3.3-5

Detection Performance of the Baseline

Swerling Case 3 Target Model

(S/N): Signal-to-Noise Ratio (dB)

Probability of Detection (Pd)
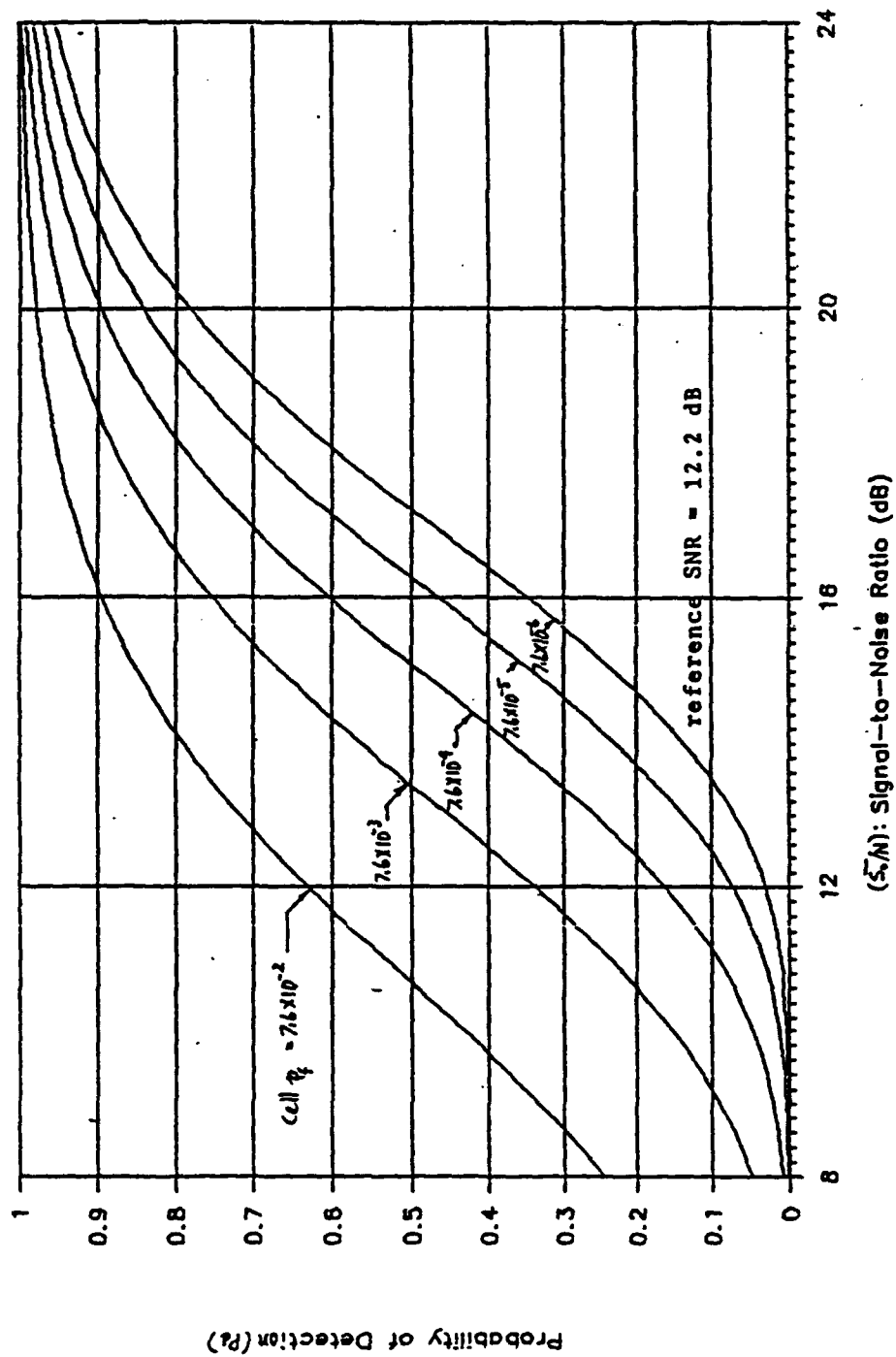
Figure 3.3-6
Detection Performance of the Baseline
Swerling Case 4 Target Model

122
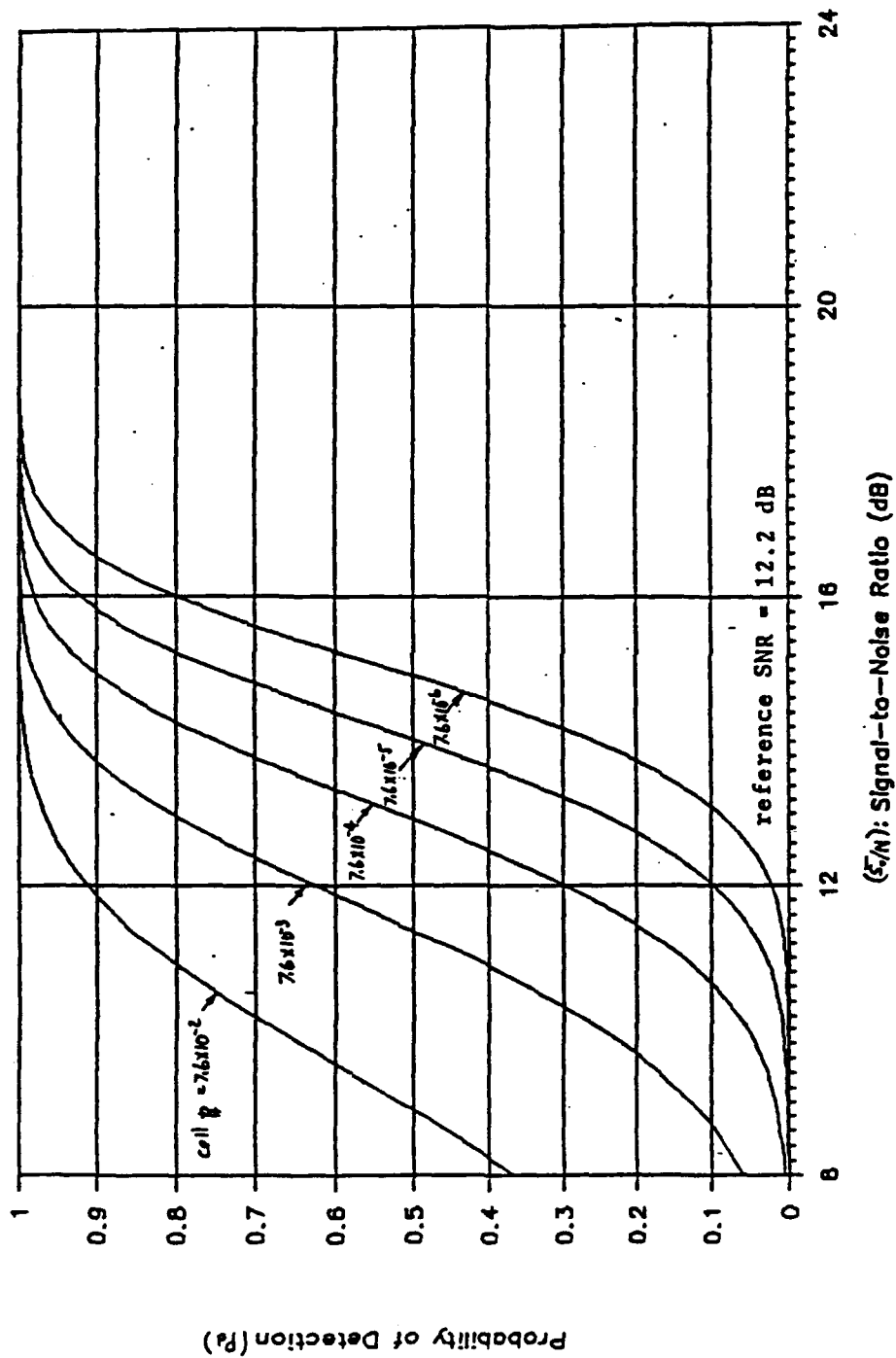
Figure 3.3-7

Detection Performance of the Baseline
Nonfluctuating (Marcum) Target Model

123

factor of 10 in the cell false alarm probability results in an increase of 1000 in the system false alarm rate because $P_{fa} = p_f^3$. Consequently, one must be careful in lowering the threshold in an attempt to enhance detection. The baseline performance presented here will provide the basis for measuring performance improvements in the modified configurations discussed in the next two Chapters.

It should be noted that a separate beam shape loss is used for each slant in the computation of $(S/N)_i$. It is a common practice in radar engineering to evaluate P_d by using for each slant the average value of $(S/N)_i$ obtained by computing an average value of beam shape loss. However, this yields optimistic results for P_d of 0.7 dB for Swerling case 1 and 0.4 dB for Swerling case 2 in the vicinity of $(\bar{S}_0/N)$ = 12 dB. These numbers were obtained by comparing two sets of detection performance results where individual beam shape losses were used in one set and one average beam shape loss was used in the other. The results for Swerling case 1, 2, and Marcum target models are plotted in Figures 3.3-8 and 3.3-9 for individual and average beam shape losses, respectively. This is very important in comparing the performance of the modified configurations to the baseline performance. The performance of the modified configurations would appear pessimistic by the respective amount if one average beam

SNR VS. PROBABILITY OF DETECTION
3 OF 3 PROCESSING @ 6 RPM
NORMAL TIME OVERHEAD (5 millisec)

Probability of Detection

$(\overline{S_o}/N)$ Signal-to-Noise Ratio (dB)

ⓐ Swerling 1
ⓑ Swerling 2
ⓒ Marcum

reference SNR + 12.2 dB

Beam Shape Loss = 0.30/3.43 dB
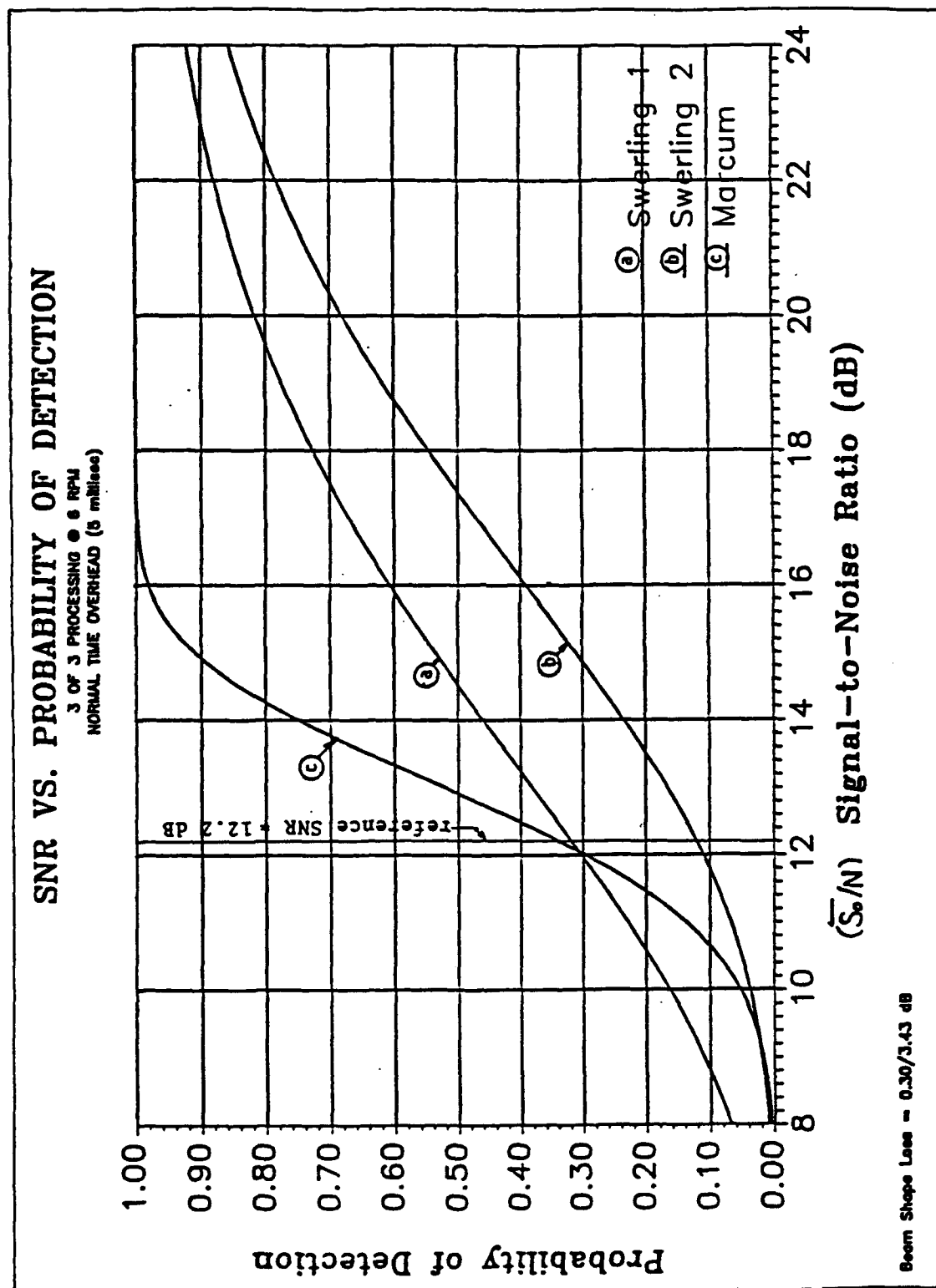
Figure 3.3-8. SNR vs. Probability of Detection, 3 of 3 Processing @ 3 rpm, Normal Time Overhead

SNR VS. PROBABILITY OF DETECTION

3 OF 3 PROCESSING @ 6 RPM
NORMAL TIME OVERHEAD (5 millisec)
with Averaged Beam Shape Loss

(a) Swerling 1
(b) Swerling 2
(c) Marcum

reference SNR = 12.1 dB

$(\overline{S}_o/N)$ Signal-to-Noise Ratio (dB)

Probability of Detection

Beam Shape Loss = 2.12 dB
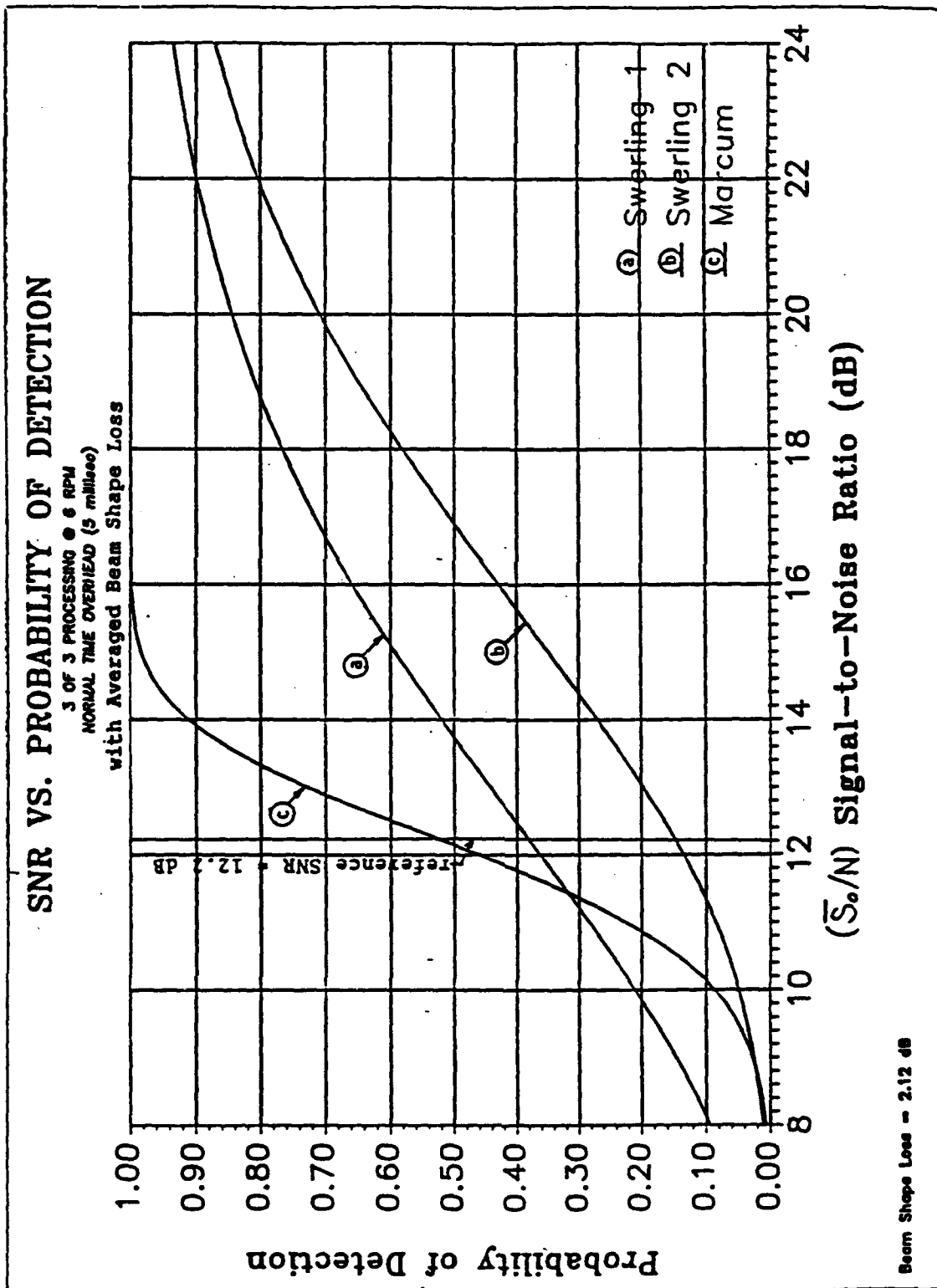
Figure 3.3-9. SNR vs. Probability of Detection, 3 of 3 Processing
@ 3 rpm, Normal Time Overhead, with Average Beam Shape Loss

126

shape loss had been used in the evaluation of the baseline performance.

It should also be noted, in Figures 3.3-1 through 3.3-9, that the normal time overhead per each slant of 5 milliseconds was used in the performance evaluation. When a modified configuration includes a reduction of time overhead, unless this reduction is a direct consequence of a certain unique feature of the modification, the measure of improvement should be by comparison of its performance to the baseline performance which also includes the reduction of time overhead. This is so that the improvement imparted by the specific processing modification can be quantified separately. For this purpose, plots of the baseline performance with a reduced time overhead to 3.5 milliseconds per each slant are shown in Figure 3.3-10 for Swerling case 1, 2, and Marcum target models.

Additional details on how the two different approaches to beam shape loss affect detection probability estimates are included in Section 3.4. What happens to the beam shape loss when the 3 of 3 post detection integration is changed to a 2 of 3 post detection integration all within a 3-slant configuration is also discussed in Section 3.4.

SNR VS. PROBABILITY OF DETECTION

3 OF 3 PROCESSING @ 6 RPM
REDUCED TIME OVERHEAD (3.35 mSec)

Probability of Detection

1.00
0.90
0.80
0.70
0.60
0.50
0.40
0.30
0.20
0.10
0.00

Reference SNR = 13.5 dB

ⓐ
ⓑ
ⓒ

8   10   12   14   16   18   20   22   24

$(\overline{S_o}/N)$ Signal-to-Noise Ratio (dB)

ⓐ Swerling 1
ⓑ Swerling 2
ⓒ Marcum

Beam Shape Loss = 0.34/3.38
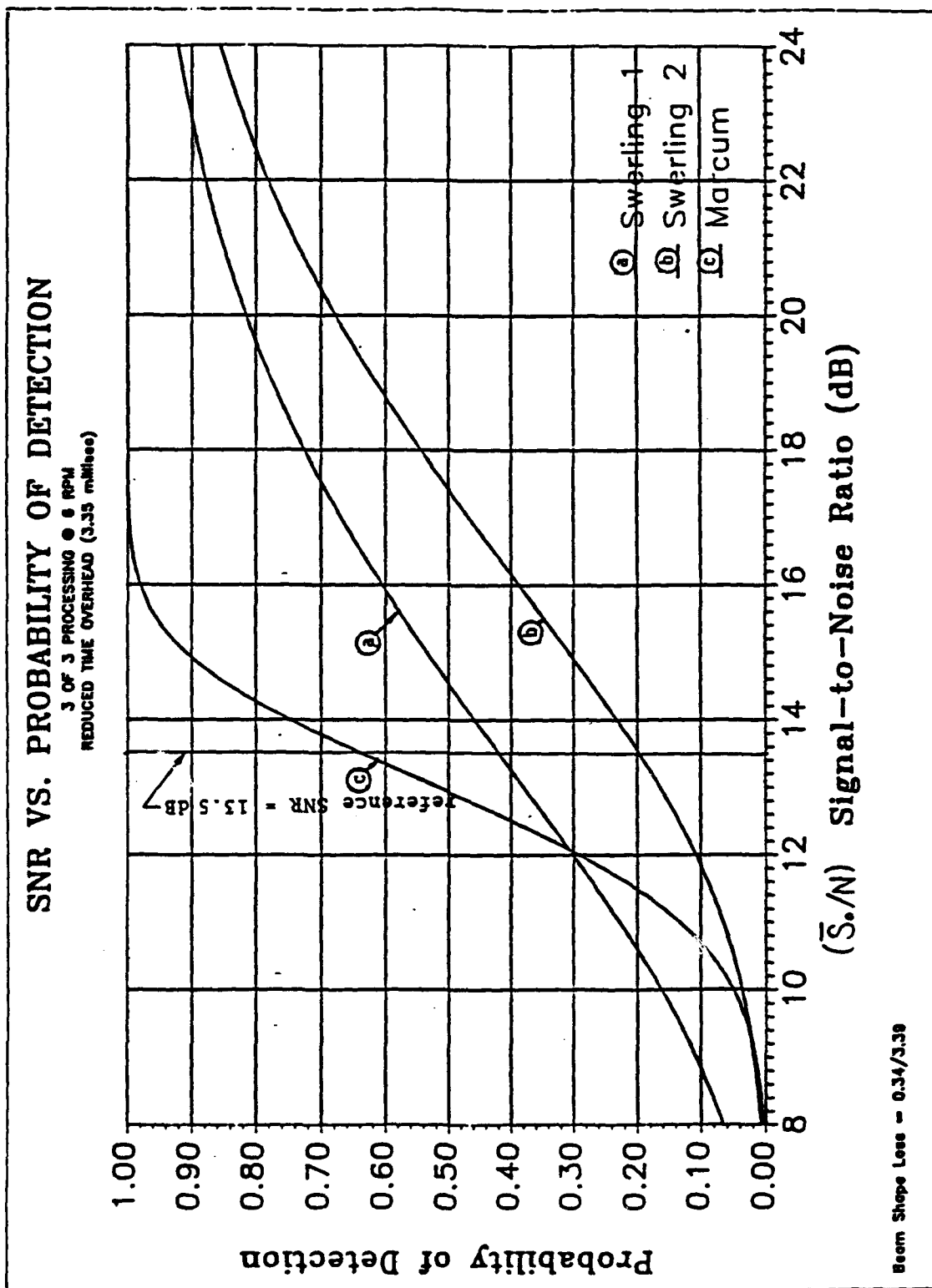
Figure 3.3-10. SNR vs. Probability of Detection, 3 of 3 Processing @ 3 rpm,
Reduced Time Overhead

128

3.4 Effect of Beam Shape Loss on Detection Probability

In the analysis of detection probabilities for the baseline 3-slant configuration, it was found that a noticeably different performance prediction results when a single average beam shape loss is used instead of the individual beam shape loss for each slant. When one average beam shape loss is used, the resulting detection probability for $(\bar{S}_0/N)$ in the neighborhood of 12.0 dB is more optimistic by 0.4 dB for Swerling case 2 and by 0.7 dB for Swerling case 1. This is with the threshold for cell false alarm probability of 7.6×10^{-4} which, in conjunction with the 3 of 3 post detection integration, yields the system false alarm rate of 2 for each antenna scan covering a 360 degree azimuth sector in 10 seconds.

The above result is illustrated for a Swerling case 2 target below. A comparison for Swerling case 1 developed using numerical integration is included in Section 3.3. The actual beam shape losses of 0.3 dB for the center slant and 3.43 dB for the two outer slants can be converted to one average loss by first converting these dB's to equivalent power levels referenced to a unit power level, obtaining the average of these power levels, and taking the ratio with respect to unity. The average beam shape loss so computed for

the 3-slant configuration is 2.12 dB.

The actual SNR in each CPI, given $(\bar{S}_0/N)=12.0$ dB is 12.0 dB minus the respective beam shape loss. These are 11.7 dB for the center slant and 8.57 dB for each of the two outer slants. When the average loss is used instead, it is 9.88 dB. The corresponding detection probability in the ith slant for a Swerling case 2 target can be obtained from Eqn. (3.2-13).

Let the detection probabilities in the center slant and the two outer slants by $\bar{p}_{d1}$, and $\bar{p}_{d2}$, respectively. Also, let the detection probability in any slant when the average beam shape loss is used be denoted by $\bar{p}_d$. Letting $(\overline{S/N})_i = 10^{\overline{SNR}(dB)/10}$ and using 7.6×10^{-4} for p_f in Eqn. (3.2-13) yields the following detection probabilities:

$$\mathcal{P}_{d_1} = 0.635$$

$$\mathcal{P}_{d_2} = 0.416$$

$$\mathcal{P}_d = 0.518 \ .$$

With these probability values, P_d, the overall detection probability after post detection integration is computed for the two cases: one using the actual beam shape loss for each individual slant, and the other using one average beam

shape loss for all 3 slants for 2 of 3, and 3 of 3 post detection integration.

2 of 3 Post Detection Integration:

Let $P_d(2/3)$ and $P_d^*(2/3)$ denote the detection probability after post detection integration with actual beam shape losses and with an average beam shape loss, respectively. Then, $P_d(2/3)$ and $P_d^*(2/3)$ are given by

$$P_d(2/3) = 2P_{d_1}\bar{P}_{d_2}(1-\bar{P}_{d_2}) + P_{d_2}{}^2(1-\bar{P}_{d_1}) + \bar{P}_{d_1}\bar{P}_{d_2}{}^2 \qquad (3.4\text{-}1a)$$

and

$$P_d^*(2/3) = 3\bar{P}_d^2(1-\bar{P}_d) + \bar{P}_d^3 . \qquad (3.4\text{-}1b)$$

Substituting values of $\bar{P}_{d1}$, $\bar{P}_{d2}$, and $\bar{P}_d$ previously determined into the above equations yields

$P_d(2/3) = 0.482$

$P_d^*(2/3) = 0.527$.

Using the average beam shape loss resulted in a detection probability which is more optimistic by 0.4 dB than the one with actual losses as explained below. This was determined by substituting for the $(\overline{S/N})_i$ in Eqn. (3.2-13) a value 0.4

dB less than the one based on the average beam shape loss and obtaining a $\bar{p}_d$ value of 0.484. Next, substituting this value for $\bar{p}_d$ in Eqn. (3.4-1b) yields a value that is the same as the one obtained by Eqn. (3.4-1a) using actual losses.

3 of 3 Post Detection Integration:

Let $P_d(3/3)$ and $P_d^*(3/3)$ denote the detection probability after 3 of 3 post detection integration with actual beam shape losses and with an average beam shape loss, respectively. These probabilities are given by

$$P_d(3/3) = \bar{p}_{d_1}\bar{p}_{d_2}^2 = 0.11 , \qquad (3.4\text{-}2a)$$

and

$$P_d^*(2/3) = \bar{p}_d^3 = 0.139 \qquad (3.4\text{-}2b)$$

where use was made of the values for $\bar{p}_{d1}$, $\bar{p}_{d2}$, $\bar{p}_d$ previously determined. Again, the result based on the average beam shape loss is optimistic by an amount of 0.4 dB. This was determined by following the same procedure used for the 2 of 3 post detection integration example.

Thus, a simplification in computing by use of an average

beam shape loss resulted in an optimistic prediction by 0.4 dB for Swerling case 2 targets. An optimistic prediction by an amount of 0.7 dB resulted for Swerling case 1 targets when the detection evaluation is based on 3 of 3 post detection integration. This difference is obtained by comparing the numerical integration results of Eqn. (3.2-11) for Swerling case 1 with two different approaches to the beam shape loss. The difference in detection prediction was also computed for the Marcum target model. These results were plotted in Figures 3.3-8 and 3.3-9 in Section 3.3 using individual and average beam shape losses, respectively.

Next, the following questions is considered: What happens to the beam shape loss when the post detection integration rule is changed from 3 of 3 to 2 of 3 in a 3-slant configuration? There is a common misconception that the beam shape loss would be reduced under a 2 of 3 rule. This notion is based on the observation that if the binary post detection rule requires only two hits, the two contiguous slants that could provide these hits would be found more favorably centered about the peak of the antenna beam than would be for 3 slants. While this observation is correct, the detection rule under this situation approaches a 2 of 2, not a 2 of 3 rule since the 3rd (and the 4th) slant is too far from beam center to contribute significantly. The detection

probability based on a 2 of 2 rule with less beam shape loss is inferior to a 2 of 3 rule with slightly higher beam shape loss. Alternatively, one can correctly observe that there are two 3-slant sets on a sliding window providing 2 of 3 detection opportunities when 4 slants are symmetrically situated about the peak of the beam even though the beam shape losses for the two outer slants are high. This observation is again correct. But, the 4 slants with higher beam shape loss produces inferior performance, as will be shown, to that produced by 3 slants symmetrically situated about the peak of the beam.

Fortunately, the differences can be readily quantified. To this end, a snap shot of the train of modulation periods passing by a point target at an instant of the most favorable placement for 3 slants, and 2 (or 4) slants are depicted in Figure 3.4-1 (a) and (b), respectively.

	₵ of beam toward a point target			₵ of beam toward a point target			
L_{BSi} (dB)	3.40	0.30	3.40	7.29	1.08	1.08	7.29
	$\bar{P}_{di}$	$\bar{P}_{d2}$	$\bar{P}_{d1}$ $\bar{P}_{d2}$	$\bar{P}_{d2}$	$\bar{P}_{d2}$	$\bar{P}_{d1}$	$\bar{P}_{d2}$

(a) 3 slants   (b) 2 or 4 slants
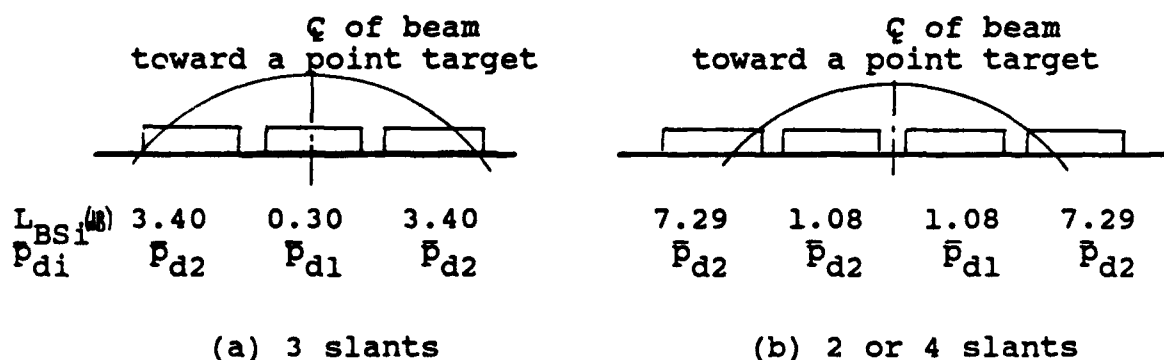
Figure 3.4-1 Beam Shape Loss for 2 of 2, 2 of 3 and 2 of 4 Processing given 3 Slants in a Beamwidth

134

The beam shape loss for each slant is computed according to the method described in Section 2.4 and is indicated under the slant for which it applies in the Figure.

As before, the detection probability in each slant for the 3-slant case is denoted p_{d1} for the center and p_{d2} for the two outer slants. For the 4-slant case, they are denoted p_{d1} for the two inner slants and p_{d2} for the two outer slants. The Swerling case 2 model is again used for simplicity to determine the detection probabilities based on the calculated beam shape losses so as to establish which placement of the slants results in the minimum loss. We are still dealing with a 3 slant configuration meaning there are only 3 slants in a half power beam width and the detection rule is 2 of 3 hits from a set of 3 contiguous slants selected on a sliding window which advances at one slant increment. An overall detection probability given 4 slants and using a 3-slants at a time sliding window with a 2 of 3 rule is first established. Since the two 3-slant sliding windows are overlapping, the probabilities of detection are not independent, and a careful sorting is required before determining the overall detection probability. This is best accomplished by establishing the matrix of all possible combinations of only 2 of 4, only 3 of 4, and 4 of 4 detection possibilities within the 4 slants given, and eliminating the

ones which do not have the 2 or 3 required hits within the 3 slant sliding window. Note that an M of N means M or more hits in N trials while only M of N means exactly M hits in N trials. This matrix of hits and misses along with the sliding window is shown in Figure 3.4-2.

Now, the expression for the probability of detecting 2 of 3 in 4 slants on a 3-slant sliding window can be written down by inspection of the matrix of Figure 3.4-2. The number of ways a detection can occur is all the possible combinations shown in the Figure less those excluded by the 3-slant sliding window test. The sum of different numbers of ways a detection can occur multiplied by the corresponding probabilities gives the overall detection probability:

$P_d(2/4)$ (on a 3-slant sliding window)

$$= 4p_{d_1}\bar{p}_{d_2}(1-\bar{p}_{d_1})(1-\bar{p}_{d_2}) + \bar{p}_{d_1}^2(1-\bar{p}_{d_2})^2 + 2\bar{p}_{d_1}^2\bar{p}_{d_2}(1-\bar{p}_{d_2}) + \bar{p}_{d_1}^2\bar{p}_{d_2}^2 .$$

Obviously, the probability of detecting 2 of 2 from a 2-slant set is

$$P_d(2/2) = \bar{p}_{d_1}^2 .$$

The probability of detecting 2 of 3 in a 3-slant set was derived before in Eqns. (3.4-1a,b).

```
                          center line
                           of beam
                              |
                    ┌─ outer slants ─┐    case rejected by
                    │  inner slants  │      3-slant window
                    ↓       ↓     ↓     ↓
                    |       |     |     |
      1 way to get  ─────────────────────
  4 hits in 4 slants    x       x     x     x
                    ─────────────────────
                        x       x     x     o
      4 ways to get     x       x     o     x              x
  3 hits and 1 miss     x       o     x     x              x
      in 4 slants       o       x     x     x
                    ─────────────────────
                        x       x     o     o
                        x       o     x     o
      6 ways to get     x       o     o     x              x
  2 hits and 2 misses   o       x     x     o
      in 4 slants       o       x     o     x
                        o       o     x     x
                    ─────────────────────
  prob. of detection   P̄d2     P̄d1   P̄d1   P̄d2
                        └_____┘

                            ┼_____┼

                    3-slant sliding windows
```

Figure 3.4-2 Matrix of Possible Combinations of 2 of 4
               Detections on a 3-Slant Sliding Window

137

The probabilities of detection after 2 of 2, 2 of 3, and 2 of 4 binary post detection integration are computed as a function of $(\bar{S}_0/N)$ according to the equations derived for the Swerling case 2 model. The results are listed in Table 3.4-1. It can be seen from the table that the detection probability based on the 2 of 3 rule with 3 slants centered about the beam center is superior to the result based on 2 of 2 or 2 of 4 rules using 2 slants or 4 slants centered about the peak of the beam. This is in spite of the smaller beam shape loss for the center 2 slants in these cases. As a final point, it is noted that the average beam shape loss depends on the number of slants within a half power beamwidth. It has nothing to do with the values of M and N selected for M of N binary integration. Those slants falling outside of the half power beamwidth contribute very little to detection performance in the small signal region. Actually, Blake [7] determined that the optimum beam utilization is 84 % of the half power beamwidth.

Table 3.4-1

Detection Probabilities with 2 of 2, 2 of 3, and 2 of 4 Processing for a Swerling Case 2 Target

$(\overline{S}_o/N)$	P (2/2)	P (2/4)*	P (2/3)
10.4	.222717	.308167	.312528
10.5	.236682	.328043	.332856
10.8	.250970	.348318	.353562
11.0	.265551	.368923	.374578
11.2	.280395	.389785	.395834
11.4	.295472	.410828	.417259
11.6	.310748	.431975	.438782
11.8	.326191	.453147	.460333
12.0	.341769	.474263	.481840
12.2	.357450	.495247	.503239
12.4	.373202	.516021	.524463
12.6	.388994	.536512	.545452
12.8	.404797	.556649	.566148
13.0	.420580	.576367	.586496
13.2	.436315	.595605	.606448
13.4	.451976	.614308	.625959
13.6	.467538	.632429	.644990
13.8	.482975	.649925	.663504

* 2 of 4 on a 3-slant sliding window as explained
  in the text.

CHAPTER 4

SYSTEM PERFORMANCE WITH SCAN-TO-SCAN PROCESSING

A description of scan-to-scan processing (SSP) and a detailed analysis of the modified radar configuration with scan-to-scan processing is presented in this Chapter. A considerable amount of effort has been spent in industry in seeking a detection performance improvement by means of scan-to-scan processing. Surprisingly, however, there is little written material on scan-to-scan processing in the open literature[1] in spite of more than a decade of industrial independent research and development efforts that went into investigation of the concept. Evidently, the only documentation that exists are proprietary internal company reports not available to the general public. These reports document interim results of trials with various flight test samples and some simulations. Optimistic improvement claims as much as 12 dB in equivalent signal-to-noise ratio are made without accompanying analytical verification[2] Similar work named Track before Detect (TBD) [11, 12] was carried out under the auspices of RADC[3] This is not to be confused with the TBD term used in the moving target indication algorithm in infrared imaging [13].

---

1. as applies to airborne surveillance radars
2. Upon careful examination, this 12 dB includes improvement projections arising mostly from other radar processing changes not directly attributable to SSP.
3. for a ground surveillance radar

In view of the primarily experimental nature of industry's investigation, a need for an independent theoretical review of the concept arose as a consequence. This investigation provides one such review. The analysis presented will show that only a marginal improvement is directly attributable to SSP when correct comparisons are made.

4.1 Description of Scan-to-Scan Processing

As the effective range of avionics systems continually increases, so does the need for increasing the effective range of sensor systems. Because of the enormous cost and risk involved in developing and deploying a new radar system, increasing emphasis is being placed on improving a proven existing system capitalizing on recent technology breakthroughs in signal processing. Thus, scan-to-scan processing became one of the most appealing concepts for improving performance. The improvement sought is to maintain the same detection capability for targets whose radar cross section (RCS) is continually being reduced. Equivalently, an alternate aim is to extend the detection range for conventional targets.

As described in Chapter 3, detection performance is directly related to the threshold setting. The philosophy behind SSP is to lower the threshold to enhance detection. The resulting increase in system false alarm is expected to be managed through data processing over many radar scans whereby detection histories of true and false targets in past scans are correlated and those detections which do not result in realistic trajectories are rejected as false targets. According to this notion, there is no limit as to how much the achievable improvement can be. It is only a matter of how much data processing is to be performed to be able to reject all false targets.

On the other hand, there is a theoretical approach for determining the upper bound on performance improvement which is possible through SSP. Recall Barton's result on surveillance radar performance quoted in Section 1.1.3 when the surveillance objective is to detect a target within a specified interval of time with a high probability of success. Given the total number of pulses available for integration during this time interval and an option to adjust the scan rate, Barton compared the resulting performance between using the available pulses all in a single scan with a slow scan rate and, alternatively, dividing these into many scans with a faster scan rate. He

considered the integration loss, scan distribution loss, and target fluctuation loss, and concluded that it was more advantageous to use more than one scan to achieve the goal. However, his analysis is based on some ideal assumptions, e.g., a stationary target which falls in the same radar resolution cell in every scan, and operation of the radar in a low PRF mode such that division of the available number of pulses into many scans does not increase the total time overhead.

Barton's integration loss is the loss incurred in video integration when compared to what can be achieved in an ideal coherent integration. His scan distribution loss is the additional number of pulses that are required for a nonfluctuating target using many scans to achieve the same detection probability as for a nonfluctuating target using a single scan. The fluctuation loss is the additional signal-to-noise ratio required, on the average, for a fluctuating target in a single scan to achieve the same level of detection probability as for a nonfluctuating target. In Barton's multi-scan strategy, detection probability in each scan is assumed independent from any other scan.

Suppose now a storage device is introduced to accumulate the results of several successive scans and a hit is

declared when the same target is detected in the same resolution cell in J out of K successive scans. This, then, would reduce the scan distribution loss. This, in essence, is the scan-to-scan processing concept. In terms of mathematical expressions, given a total number of K scans in the baseline without SSP, the cumulative detection probability P_c, that is the probability of detecting the same target in one or more scans, was given as

$$P_c = 1-(1-P_d)^K \qquad\qquad (4.1-1)$$

where P_d is the single scan detection probability assumed to be independent from scan to scan. With SSP, the cumulative detection probability, that is the probability of detecting the same target in J out of a total number of K scans, is given by

$$P_c = \sum_{i=J}^{K} \frac{K!}{i!(K-i)!} P_d^i (1-P_d)^{K-i} . \qquad\qquad (4.1-2)$$

Of course, both detection rules should be subject to the same system false alarm requirement. For J>1, the effect of SSP is to lower false alarms relative to the J=1 case. Therefore, for maintaining the same levels of system false alarms, the detection threshold can be lowered with SSP thus enhancing the detection probability.

The extent to which the threshold can be lowered for a moving target, with the resulting large increase in interim system false alarms per scan prior to SSP, depends on the size of the correlation window which determines the number of cells per scan where reports are correlated with those of other scans. If sufficient information about the target trajectory is known such that correlation could be performed on a single resolution cell for each scan over the number of scans in which correlation is performed, false alarm suppression by the J of K integrator in SSP would be great. However, the likelihood is small of correctly estimating the resolution cell for each scan in which the target is located. To account for the radar platform motion and target maneuver during the scan-to-scan correlation period, the correlation window for each scan is made larger for successively earlier scans as shown in Figure 4.1-1.

Note that, even with SSP, M of N post detection integration still takes place within each scan so as to resolve target range ambiguity at least partially in each scan. Otherwise, target range (and velocity) information would not be available and there would be no basis to correlate present scan detections with those of the past scans.

correlation window for
the Kth scan

correlation window for
the ith scan

resolution cell in which target
is reported in the current scan
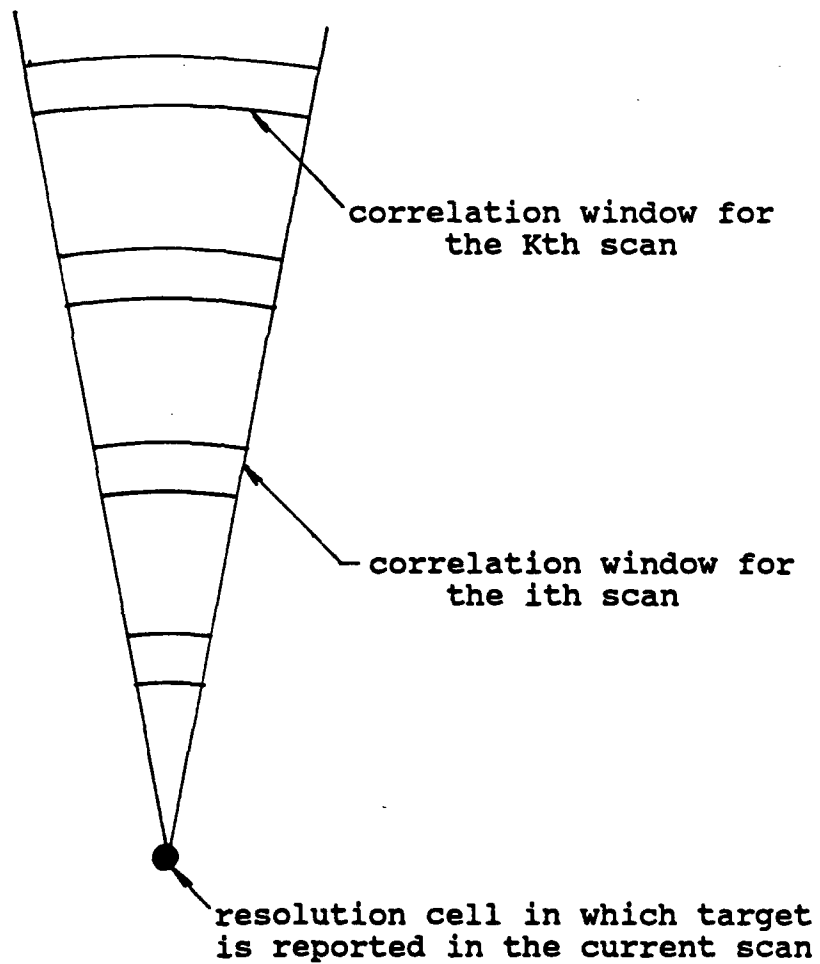
Note: Azimuth and range correlation windows only are shown.
      Velocity correlation window is not shown.

Figure 4.1-1 Correlation Windows for Successively Earlier
               Scans

Two specific SSP concepts are examined in this investigation. One uses the 3-slant configuration, as in the baseline, and employs a modified version of scan-to-scan processing. As a result, this approach is referred to as the modified J of K SSP. The other is based on a 2-slant configuration and uses conventional J of K SSP. In both versions, a sliding window is used with respect to the K scans such that a decision is made after each scan.

In the modified J of K SSP, the threshold level is kept the same as in the 3 of 3 baseline configuration and a full success is declared when threshold crossings occur in all 3 slants of a given scan. All range and velocity ambiguities can be resolved and operation is the same as for the baseline configuration. Hence, SSP is bypassed for a scan in which a full success occurs for the given target in that particular resolution cell. A partial success is declared within a single scan if and only if 2 threshold crossings in any of the 3 slants in a particular doppler filter occur. Note that this constitutes a failure in the baseline 3 of 3 post detection rule. In the modified J of K SSP rule, a detection is declared when either a full success occurs in the present scan, which is the same as the baseline, or both a partial success occurs in the present scan and (J-1) or more partial or full successes have occurred in the past

(K-1) scans. For J=3 and K=8, this SSP is referred to as the modified 3 of 8 SSP. For the modified J of K SSP, the probability of detection at the end of each scan is called a hybrid single scan detection probability since it can arise from either a full success which is independent from scan-to-scan or from partial successes in a number of scans which makes the P_d based on them no longer independent from scan-to-scan. Since the threshold level is kept the same as in the 3 of 3 baseline configuration, the 2 of 3 post detection integration generates in each scan an increase in false alarms of more than 3 orders of magnitude. The association from scan-to-scan is an attempt to reduce the false alarms to an acceptable level.

The conventional J of K SSP concept is based on a 2-slant configuration. By using 2 slants within a scan, it is possible to integrate more pulses per slant although the number of slants is reduced. In this concept, the threshold level is adjusted to maintain the same false alarm rate per scan, before SSP, as in the modified J of K SSP described above. This is done so that the two concepts can be compared on a common basis. When there are only 2 slants, 1 of 2 detections cannot be considered as a partial success because range and velocity information is unavailable for correlation purposes due to unresolved ambiguities. Also,

2 of 2 detections cannot be treated as a full success because the false alarm rate would be too high and the range ambiguity could only be partially resolved. For conventional J of K SSP, J or more partial successes in K scans are required to declare a detection. Because of the sliding window, a decision is made after each scan. However, the detection probability associated with these decisions should be compared with a cumulative detection probability based on K scans as opposed to a single scan detection probability.

4.2 The Scan-to-Scan Correlation Window

The size and position of the correlation window allocated for each scan is a function of the target parameters. In particular, the correlation window for each scan is designed to be large enough such that a maneuvering target appears within the window. For this purpose, it is necessary to account for the target's tangential velocity and acceleration. In determining the window size, it is assumed that the maximum linear acceleration is 1-g (i.e., 9.8 m/sec.) along the radial velocity vector, and the maximum tangential velocity is given by

$$
V_T = \begin{cases} 5V_R \; ; & 5v_R \leq V_{max} \\ V_{max} \; ; & 5V_R > V_{max} \end{cases}
$$

where V_R is the measured radial velocity in the present scan and V_{max} is the maximum possible velocity assumed.

The geometry for the correlation window in the ith scan is shown in Figure 4.2-1. The procedure consists of selecting a candidate target report which has the potential of being included in the window, constructing the window ussing its position and that of the present target report under test, rejecting the candidate target report if it falls outside of the window, and retaining the candidate target report if it falls inside. This procedure is repeated for all candidate target reports in the ith scan. With reference to Figure 4.2-1, define the following notation:

W_R:	range correlation window width along the radial direction
W_T:	cross range correlation window measured normal to the radial direction
V_R:	measured target radial velocity
V_A:	platform velocity
a_1:	linear acceleration of the target along its radial velocity vector
θ_i :	measured target azimuth angle in ith past scan

150
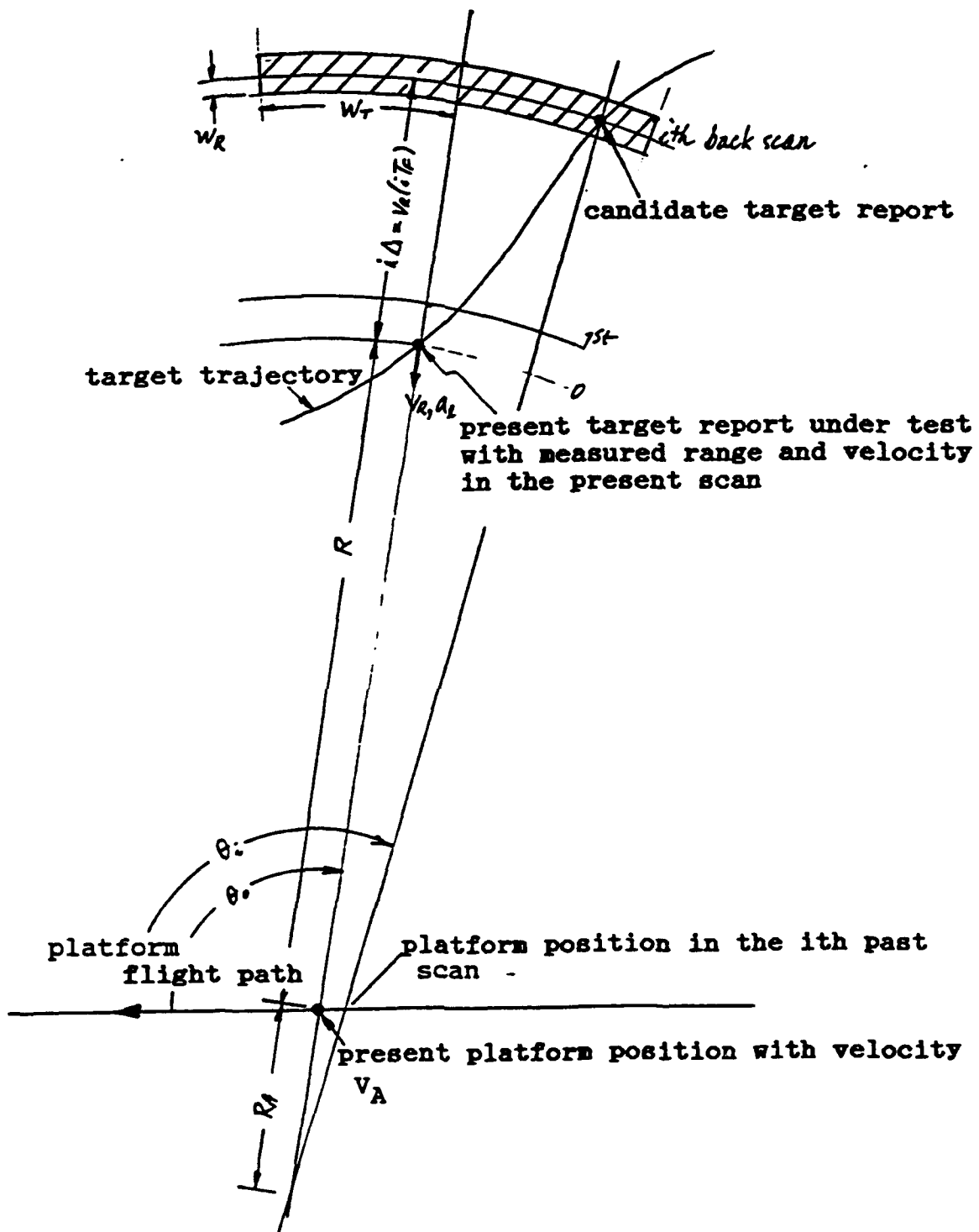
Figure 4.2-1

Correlation Window for the 1th Scan

θ_0 : measured target azimuth angle in the present scan

R: measured range to the target in the present scan

R_A: · radial distance from the platform position to the point where the radial lines to target positions in the present scan and i^{th} past scan intersect

$i\Delta R$: estimated difference in range to the target between the present scan and i^{th} past scan ($\Delta R = iT_F V_R$) .

Also, introduce the notation:

σ_r : range measurement error

σ_θ : azimuth angle measurement error

σ_p : platform position error .

For the ith scan,

$$i\Delta R = iT_F V_R$$

where T_F is the frame time. From the law of sines, the distance R_A is related to target azimuth angles by

$$\frac{R_A}{\sin(\pi - \theta_i)} = \frac{V_A(iT_F)}{\sin(\theta_i - \theta_0)} ; \qquad \theta_i > \theta_0$$

$$\frac{R_A}{\sin\theta_i} = \frac{V_A(iT_F)}{\sin(\theta_i - \theta_0)} ; \qquad \theta_0 > \theta_i .$$

For the ith scan, the spatial size of the correlation window extends over

$$\pm \ W_R \ = \left[(a_i(iT_F)^2/2)^2 \ + \ 2(\sigma_R)^2 \ + \ 2(\sigma_p)^2 \ + 2\bigl((R+R_A+i\Delta R)\sigma_\theta \sin|\theta_i - \theta_0| \bigr)^2 \right]^{1/2}$$

$$\pm \ W_T \ = \left[(V_T(iT_F))^2 \ + \ 2[(R+R_A+i\Delta R)\sigma_\theta]^2 \ + \ 2(\sigma_p)^2 \right]^{1/2} \ .$$

Because of variations and uncertainties in the present target velocity, it is necessary to extend the correlation window into the velocity domain. The correlation window size for the velocity is

$$\pm \ W_V \ = \left[(a_i(iT_F))^2 \ + \ (V_T \sin|\theta_i - \theta_0|)^2 \right]^{1/2} \ .$$

Having determined the (K-1) correlation windows related to the present target report, the next step is to calculate the false alarm multiplier associated with these windows. Let n_i denote the number of resolution units in the correlation window for the ith back scan. The false alarm multiplier for the (K-1) correlation windows is given by

$$M_k \ = \ (n_1)(n_2) - \ - \ - \ (n_{K-1}) \ .$$

With SSP the total number of false alarm opportunities equals M_K times the conventional number of false alarm opportunities for a radar without SSP.

To determine a realistic value for M_K, it is necessary to specify a typical target maneuver[1] For this purpose, con-

---

1. as worst case

sider a target making a 6-g coordinated turn with a speed of 450 knots at a range of 150 nautical miles. The maneuver scenario is illustrated in Figure 4.2-2. Also, let

$$V_A = 360 \text{ knots}$$

$$\sigma_R = 0.8 \text{ nmi}$$

$$\sigma_\theta = 0.003 \text{ radians}$$

$$\sigma_p = 0.04 \text{ nmi}$$

For this maneuver, the flight path is circular and $a_1 = 0$. The corresponding correlation window size, in terms of azimuth angle expressed in degrees and the number of range and doppler cells, is listed in Table 4.2-1. On the average, there are 3 slants contained in 1 degree azimuth. The number of resolution units, n_i, for the ith scan is listed in the column labeled $n_i(1)$ where a resolution unit is 1 slant by 1 range cell by 1 doppler cell. The false alarm multiplier for K scans, $K = 2,3,--,8$, is listed in the column labeled $M_K(1)$.

If it were possible to estimate past target positions down to a single resolution cell for each back scan, then, the false alarm multiplier arising from SSP would be unity. As shown in Table 4.2-1, the false alarm multiplier increases dramatically as the window size is made large enough so as to yield a high likelihood of covering the target.

Turn Radius: $r = V^2/a$

Centripetal Acceleration: a

Turn Rate: $\dot{\gamma} = Vt/r$

Target Position: $X = X_0 - r \cos \gamma$
$Y = Y_0 + r \sin \gamma$

Target Range: $R = ((X - V_a t)^2 + Y^2)^{\frac{1}{2}}$

Range Rate: $\dot{R}(t) = \dfrac{R(t) - R(t + \Delta t)}{\Delta t}$

platform moving @ 360 kts

Figure 4.2-2 Maneuver Scenario used for testing the SSP
Correlation Window

155

Table 4.2-1

SSP Correlation Window and False Alarm Opportunity Multiplier

back scan scan depth		correlation window			# of resolution units		multiplier	
l	K	(deg.) azimuth	(cell) range	(cell) doppler	$n_i(1)$	$n_i(2)$	$M_K(1)$	$M_K(2)$
1	2	1.58	12.35	6.0	352.2	2.0	3.52×10^2	2.0
2	3	2.46	36.73	6.0	1,628.3	9.0	5.73×10^5	1.77×10^1
3	4	3.33	77.62	6.0	4,658.6	25.9	2.67×10^9	4.59×10^2
4	5	4.21	134.72	6.0	10,199.8	56.7	2.72×10^{13}	2.60×10^4
5	6	5.15	208.18	6.0	19,286.5	107.2	5.25×10^{17}	2.79×10^6
6	7	5.94	297.99	6.0	31,843.9	176.9	1.67×10^{22}	4.93×10^8
7	8	6.80	404.32	6.0	49,478.0	274.9	8.28×10^{26}	1.35×10^{11}

Because this number is unacceptably large, a bigger resolution unit composed of 3 azimuth slants by 10 range cells by 6 doppler cells will be used in this analysis. (Any grouping which is reasonable for the particular application can be used.) Multiple threshold crossings in this larger resolution unit now count as one. The corresponding number of resolution units is listed under the column labeled $n_i(2)$ and the resulting multiplier is listed under the column labeled $M_K(2)$. Observe that $M_8(1) = 8.28 \times 10^{26}$ while $M_8(2) = 1.35 \times 10^{11}$. Even though $M_8(2)$ is 15 orders of magnitude smaller than $M_8(1)$, it is still a very large number.

4.3 Determination of threshold Setting and Depth of Scan from False Alarm Considerations

The procedure for determining the cell false alarm probability p_f from the system false alarm specification was developed for a general M of N post detection integrator in Section 2.5. This procedure requires determination of the false alarm time, which follows directly from the system false alarm specification, and the determination of false alarm opportunities which takes into account utilization factors for time, range cells, and doppler cells, and correlation factors due to range and velocity unfolding for ambiguity resolution, and use of sliding windows for M of N binary integration. From the false alarm time T_{fa} and the number of false alarm opportunities in a false alarm time n, the false alarm probability after post detection integration P_{fa} is determined. From the knowledge of the specific binary post detection rule, the cell false alarm probability before the post detection integration p_f is then determined from P_{fa}.

In the modified J of K SSP in a 3-slant configuration, SSP is invoked if and only if a threshold crossing occurs in 2 of the 3 slants. This is called a partial success. When threshold crossings occur in all 3 slants, which constitutes

a full success, SSP is bypassed. The modified J of K processor then becomes identical to the baseline processor. For this bypass feature to perform as in the baseline, the threshold setting for each slant should remain the same as that set for the 3 of 3 processing in the baseline. This is equivalent to a lowering of the threshold for the 2 of 3 processing such that the false alarm rate per scan before SSP increases by 3 orders of magnitude, as shown in Table 2.5-1.

To demonstrate the 3 orders of magnitude increase in the false alarm rate before SSP and to facilitate evaluation of the false alarm rate after SSP, the following events relative to false alarm occurrences are defined:

F1: false alarms occur in all 3 slants of a scan

F2: false alarms occur in 2 of the 3 slants of a scan with no false alarm in the remaining slant

F3: false alarm occurs in at most one of the 3 slants of a scan with no false alarm in the remaining slants

F4: event F1 for the present scan

F5: event F2 for the present scan

F6: event F1 or F2 for J-1 or more of the past K-1 scans and event F3 in the remaining scans

F7: intersection of event F5 and F6.

Let $n(F1)$ and $n(F2)$ denote the number of false alarm opportunities in a false alarm time associated with F1 and F2, respectively. The average number of false alarms per scan before SSP is then given by

$$FA/scan_{|before\ SSP} = P(F1)n(F1)\frac{T_F}{T_{fa_1}} + P(F2)n(F2)\frac{T_F}{T_{fa_2}} \qquad (4.3-1)$$

The first term in Eqn. (4.3-1) is the average number of false alarms in a scan for the baseline which is specified to be 2. The second term results by allowing partial successes to also be counted. Note that

$$P(F2) = \frac{3!}{2!\ 1!}\ p_f^2(1-p_f) \simeq 3p_f^2. \qquad (4.3-2)$$

In Section 2.5 it is shown that the cell false alarm rate, p_f, equals 7.6×10^{-4} for the baseline. Consequently,

$$P(F2) \simeq 3p_f^2 = 1.73 \times 10^{-6}. \qquad (4.3-2a)$$

Analogous to the derivation of Eqn. (2.5-32), the total number of false alarm opportunities per scan for event F2 is

$$n(F2)\frac{T_F}{T_{fa_2}} = n_r(n_r W_{f2})n_f P_r n_{ms}$$

$$= n_r^2 W_{f2} n_f \frac{R_c T}{(n_r + r_B)^2}\left(n_m \frac{T_F}{T_{fa}}\right).$$

160

For the system under consideration

$$n_r=42, \quad W_{f2}=2.2, \quad n_r=195, \quad R_{cT}=6173, \quad r_B=3, \quad n_{ms}=n_m\frac{T_F}{T_{fa_2}}=1040 .$$

It follows that

$$n(F2)\frac{T_F}{T_{fa_2}} = 2.40 \times 10^9 . \qquad\qquad (4.3\text{-}2b)$$

Hence,

$$P(F2)n(F2)\frac{T_F}{T_{fa_2}} = (1.73 \times 10^{-6})(2.40 \times 10^9) = 4.15 \times 10^3 . \qquad (4.3\text{-}2c)$$

The large predicted number of false alarms before SSP agrees with the flight test result illustrated in Figure 4.3-1.

Having introduced the false alarm multiplier $M_K(2)$ in Section 4.2 to account for the expanding correlation window as a function of scan depth, the analysis can be carried out by 1) considering correlation between single resolution units over K scans for which the false alarm multiplier is unity, and 2) applying $M_K(2)$ to account for the actual correlation window. With respect to step 1, the size of the correlation window in each scan is one resolution unit. The corresponding SSP process can be thought of as a combined experiment of K identical and independent subexperiments where the kth subexperiment, $k = 1, 2, - - , K$, consists of

Ground stabilized range
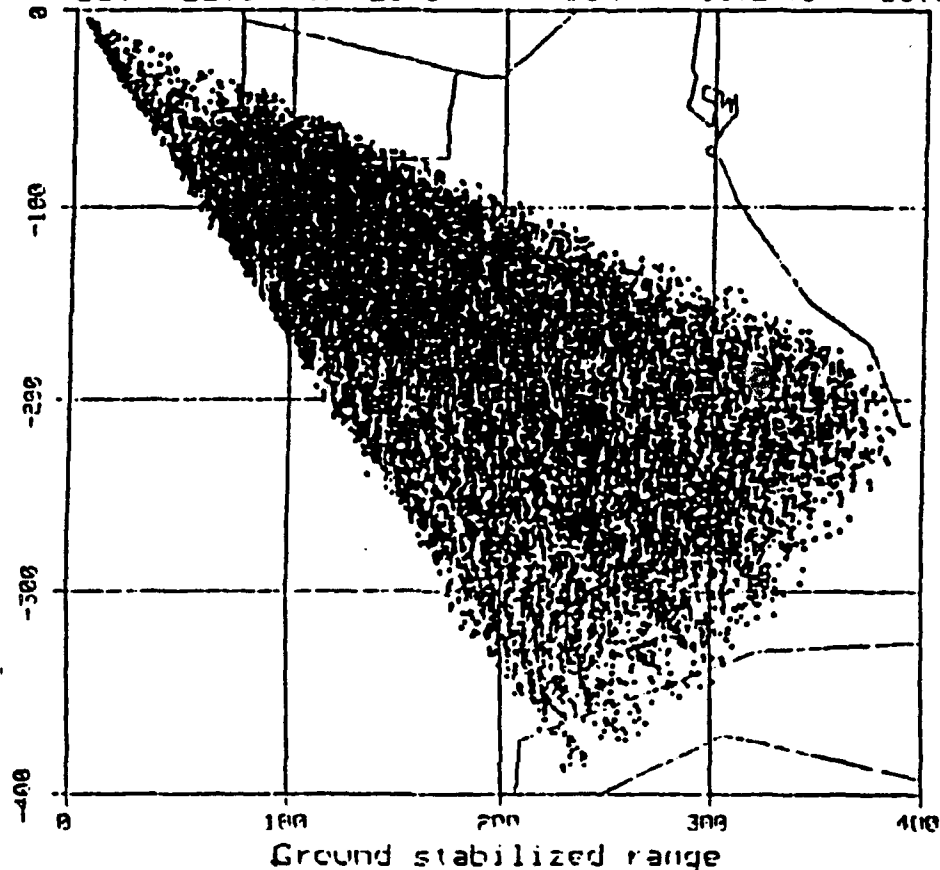
21,134 false alarms / 57 scans
= 371 false alarms / scan over a 34 degree azimuth
  sector

(371 x 360/34)
= 3,928 false alarms per scan before SSP

predicted number of false alarms / scan before SSP
= 4,150

Figure 4.3-1

Flight Test Verification of the Prediction of False Alarms
before SSP with 2 of 3 Post Detection Integration

162

a detection trial in the kth scan for the resolution unit in question. The sample space S for the combined experiment can be represented by the product space

$$S = S_1 \times S_2 \times S_3 \times -- \times S_K \qquad (4.3-3)$$

where the kth sample space, S_K, can be partitioned into the three mutually exclusive events, F1, F2, and F3. Let the outcome of the kth experiment be denoted by the event A_k where A_k is either F1, F2, or F3. Then, the outputs of the K subexperiments can be represented in the product space as

$$A_1 \times A_2 \times A_3 \times -- \times A_K .$$

For the case of statistical independence,

$$P(A_1 \times A_2 \times A_3 \times -- \times A_K) = P(A_1)P(A_2) -- P(A_K) . \qquad (4.3-4)$$

That is, with independent experiments, the probabilities for events defined on S are completely determined from probabilities of events defined in the subexperiments [5].

By the rule established, a 'hit' in the modified J of K SSP is a union of events F4 and F7. The probabilities of these events are

$$P(F4) = P(F1) \tag{4.3-5a}$$

$$P(F7) = P(F5 \cap F6) = P(F2)P(F6) , \tag{4.3-5b}$$

respectively. Note that

$$P(F1) = p_f^3 \tag{4.3-6a}$$

$$P(F2) = \frac{3!}{2!}p_f^2(1-p_f) = 3p_f^2 - 3p_f^3 \simeq 3p_f^2 \tag{4.3-2}$$

$$P(F6) = \sum_{i=(J-1)}^{K-1} \frac{(K-1)!}{i!(K-1-i)!} \left[P(F1)+P(F2) \right]^i \left[P(F3) \right]^{K-1-i} . \tag{4.3-6b}$$

The equivalent cell false alarm probability after SSP is given by

$$P_{fa|\text{after SSP}} = P(F4 \cup F7) . \tag{4.3-7}$$

Since events F4 and F7 are mutually exclusive,

$$P_{fa|\text{after SSP}} = P(F4) + P(F7) = P(F4) + P(F5)P(F6)$$

$$= P(F1) + P(F2)P(F6) . \tag{4.3-8}$$

$P_{fa|\text{after SSP}}$ is referred to as an equivalent cell false alarm probability because it applies to the situation in which the size of the correlation window in each scan is one

164

resolution unit. The system false alarms after SSP are now determined by suitably modifying Eqn. (4.3-1). The first term remains unchanged since this accounts for the SSP by-pass. The second term is modified by replacing P(F2) with P(F7) and multiplying the result by the false alarm multiplier $M_K(2)$. Consequently, the average number of false alarms in a scan after SSP becomes

$$FA/scan_{|\,after\ SSP} = P(F1)n(F1)\frac{T_F}{T_{fa_1}} + P(F7)M_K(2)n(F2)\frac{T_F}{T_{fa_2}} \quad (4.3-9)$$

The first term in Eqn. (4.3-9) is equal to 2 false alarms per scan. Recall that it is required to be 2 or less by the baseline specification. For the modified J of K SSP to meet the same specification, the second term in Eqn. (4.3-9) must be negligible. With $p_f=7.6 \times 10^{-4}$, it follows from Eqns. (4.3-5b), (4.3-2), and (4.3-6b) that

$$P(F7) = \begin{cases} 1.08 \times 10^{-16} & \text{for J=3, K=8} \\ 5.18 \times 10^{-17} & \text{for J=3, K=6} . \end{cases}$$

The number of false alarm opportunities, $[n(F2)T_F/T_{fa}]$, was found in Eqn. (4.3-2b) to be 2.40×10^9. From Table 4.2-1, the false alarm multiplier $M_K(2)$ is

$$M_K(2) = \begin{cases} 1.35 \times 10^{11} & \text{for J=3, K=8} \\ 2.79 \times 10^6 & \text{for J=3, K=6} . \end{cases}$$

Thus, the second term in Eqn. (4.3-9) yields

$$P(F7)M_K(2)[n(F2)]\frac{T_F}{T_{f_{a_2}}} = \begin{cases} (1.08 \times 10^{-16})(1.35 \times 10^{11})(2.40 \times 10^9) = 3.49 \times 10^4 \\ \text{for } J=3, \ K=8 \\ \\ (5.18 \times 10^{-17})(2.79 \times 10^6)(2.40 \times 10^9) = 0.345 \\ \text{for } J=3, \ K=6 \ . \end{cases}$$

The above results indicate that a suitable choice for the target scenario described in Section 4.2 and the modified J of K SSP is J=3, and K=6.

The conventional J of K SSP is considered next. For this SSP, the number of slants in a beam dwell is changed from 3 to 2 in the hope of enhancing detection probability. This change is intended to increase the SNR per slant by increasing the number of pulses coherently integrated. The overall time overhead per each beam dwell is also reduced because of one less slant. The threshold is set, somewhat arbitrarily, such that the resulting false alarms in a single scan before SSP are equal to those arising from the 2 of 3 post detection integration used with the modified J of K SSP, as given in Eqn. (4.3-2c). This enables comparison of the two SSP's on a common ground.

The average number of false alarms per scan before SSP in

the modified J of K SSP with 2 of 3 post detection integration is approximately 4.15×10^3. This is equivalent to the false alarm time of

$$T_{fa} = \frac{T_F}{FA/scan_{|before\ SSP}} = 2.41 \times 10^{-3} \ \text{seconds} \ .$$

Now, two additional false alarm events are introduced:

    F8: false alarms occur in a scan in both slants of a
           2-slant configuration

    F9: event F8 in J or more of the K scans.

A false alarm occurs after SSP only if event F9 occurs.

An expression for $P_{fa}(M/N)$ is given by Eqn. (2.5-24). Letting $M = N = 2$, it follows that

$$P_{fa}^{-1} = P(F8)^{-1} = \frac{T_{fa}B}{N} \prod_{i=1}^{6} (K_i) \ .$$

Substituting the numerical values found in Table 2.5-1 gives

$$P_{fa}^{-1} = \frac{(2.41 \times 10^{-3})(1.25 \times 10^6)}{2} (0.479) \ (0.933) \ (2) \ (0.762) \ (282) \ (2)$$

$$= 7.89 \times 10^5 \ .$$

Hence, $P(F8)$ equals 1.27×10^{-6}. Since $P(F8) = p_f^2$, p_f equals 1.13×10^{-3}.

Let $n(F8)$ denote the number of false alarm opportunities in a false alarm time associated with event F8. The average number of false alarms per scan, which is equal to 4.15×10^3, can be written as

$$FA/scan_{|before\ SSP} = P(F8)[n(F8)]\frac{T_F}{T_{fa}} = 4.15 \times 10^3 .$$

It follows that the number of false alarm opportunities in a scan is

$$[n(F8)]\frac{T_F}{T_{fa}} = 3.27 \times 10^9 . \tag{4.3-10}$$

On the other hand, the number of false alarms per scan after SSP is

$$FA/scan_{|after\ SSP} = P(F9)M_K(2)[n(F8)]\frac{T_F}{T_{fa}} . \tag{4.3-11}$$

$P(F9)$ is given by

$$P(F9) = \sum_{i=J}^{K} \frac{K!}{i!(K-i)!} P(F8)^i (1-P(F8))^{K-i}$$

$$= \begin{cases} 2.41 \times 10^{-11} & \text{for } J=2,\ K=6 \\ 4.09 \times 10^{-17} & \text{for } J=3,\ K=6 . \end{cases}$$

From Table 4.2-1, the false alarm opportunity multiplier for a scan depth of 6 is 2.79×10^6. Substitutions of these numbers into Eqn. (4.3-11) yields

$$FA/scan_{|\text{after SSP}} = \begin{cases} 2.19 \times 10^5 & \text{for } J=2, \ K=6 \\ \\ 0.37 & \text{for } J=3, \ K=6 \ . \end{cases}$$

It is evident that 2 of 6 SSP does not meet the system false alarm requirement. Suitable values of J and K for the target scenario described in Section 4.2 and the conventional J of K SSP are J = 3, K = 6.

4.4 Detection Performance under Modified J of K SSP

Detection performance under the modified J of K SSP using a 3-slant configuration with 2 of 3 post detection integration is evaluated in this Section. The performance evaluation is based on the cumulative detection probability under a one minute time constraint. Let L denote the number of scans within this constraint. For a 6 revolution per minute antenna rotational rate for 360 degrees azimuth coverage, the value of L equals 6. Recall from Sections 4.2 and 4.3 that extending the depth of correlation in SSP beyond 6 scans results in the average number of false alarms grossly exceeding the system specification when adaptive correlation windows are designed to accommodate target maneuvers up to 6-g coordinated turns at moderate speeds. Thus, even without the time constraints, associating targets beyond 6 scans would be impractical, if not impossible, when ordinary target maneuvers are considered. In addition, the problem that arises in a dense target environment is the possibility of incorrect correlation of target tracks.

As with the computation of system false alarms presented in Section 4.3, the following events are defined to facilitate the analysis:

D1: detections occur in all 3 slants of a scan

D2: detections occur in 2 of the 3 slants of a scan with no detection in the remaining slant

D3: detection occurs in at most one of the 3 slants of a scan with no detections occurring in the remaining slants

D4: event D1 for the present scan

D5: event D2 for the present scan

D6: event D1 or D2 for J-1 of the past K-1 scans

D7: intersection of event D5 and D6

D8: event D1 in one or more of the L scans

D9: event D2 without event D1 in J or more scans of a K scan deep sliding window where the window is one or more subsets of the L scans

D10: complement to the union of events D8 and D9

D11: event D2 without event D1 in J or more of the L scans

D12: complement to the union of events D8 and D11

D13: J or more partial successes occurring in L scans without the occurrence of a full success but these partial successes do not occur within a K scan deep sliding window.

The probability of detection is a conditional probability which is conditioned on the hypothesis that a target is present. Consequently, it is assumed for SSP that the resolution cell occupied by the target in each scan is known a priori. Therefore, the correlation window used in false alarm calculations is not applicable to evaluation of the detection probability.

As was done for false alarms in Section 4.3, cumulative detection can be viewed as an event in a combined experiment having a sample space S. The combined experiment without SSP consists of L independent and identical subexperiments, each with its sample space S_l, where the lth subexperiment is a detection trial in the lth scan for the resolution cell in question; $l = 1, 2, --, L$. The combined sample space is given by

$$S = S_1 \times S_2 \times -- \times S_L .$$

The lth sample space can be partitioned into the three mutually exclusive events D1, D2, and D3. Let the output of the lth experiment be denoted by the event B_l where B_l is either D1, D2, or D3. Then, the outputs of the L subexperiments can be represented in the product space as

$$B_1 \times B_2 \times -- \times B_L .$$

For the case of statistical independence,

$$P(B_1 \times B_2 \times -- \times B_L) = P(B_1)P(B_2) -- P(B_L) .$$

That is, with independent experiments, the probabilities for events defined on S are completely determined from probabilities of events defined in the subexperiments.

Without SSP the detection in each scan is independent from scan to scan. Let P_d denote the detection probability for a single scan. The cumulative detection probability P_c is defined to be the probability of detecting a target in one or more of the L scans. Assuming that the range closure during this time span is negligible, P_c is given by

$$P_c = 1-(1-P_d)^L .$$ (4.4-1)

With the modified J of K SSP the cumulative detection probability cannot be determined from the single scan detection probability since correlations are involved with detections in previous scans. As a result, independence no longer exists from a detection in one scan to the next. Under the modified SSP rule, recall that a 'hit' is declared in a scan if the event (D4 U D7) occurs. However, because of the above mentioned dependence between detection trials, the cumulative detection probability over L scans is not readily determined in terms of P(D4 U D7). The latter probability is referred to as the hybrid detection probability after SSP and is given by

$$P_d(hyb) = P(D4) + P(D7) .$$ (4.4-2)

A little thought leads to the conclusion that the cumulative

detection probability for the modified J of K SSP is the probability of the event (D8 U D9). Note that events D8 and D9 are mutually exclusive events. Hence,

$$D8 \cap D9 = \emptyset \qquad\qquad (4.4\text{-}3)$$

where $\emptyset$ denotes the null set. Also, because D10 is the complement of D8 U D9,

$$D8 \cup D9 \cup D10 = S .$$

In addition, note that D1, D2, and D3, which form a partition of the sample space S_ℓ, are also mutually exclusive. For convenience, P, p, and q will be used to designate the probabilities P(D1), P(D2), and P(D3), respectively. It follows that

$$P = P(D1) = P_d(3/3) = \overline{\left(p_{d1}p_{d2}^2\right)} \qquad\qquad (4.4\text{-}4a)$$

$$p = P(D2) = \overline{\left[2p_{d1}p_{d2}(1-p_{d2}) + p_{d2}^2(1-p_{d1})\right]} \qquad\qquad (4.4\text{-}4b)$$

$$q = P(D3) = \overline{\left[(1-p_{d1})(1-p_{d2})^2 + 2p_{d2}(1-p_{d1})(1-p_{d2}) + p_{d1}(1-p_{d2})^2\right]}$$

$$= 1 - P - p . \qquad\qquad (4.4\text{-}4c)$$

where the overbar denotes averaging with respect to target RCS fluctuations. The detection probability in the ith slant p_{di} and the method of averaging are developed in Chap-

ter 3.

From the above discussion, the cumulative detection probability for the modified J of K SSP is

$$P_{c \mid w/ SSP} = P(D8 \cup D9)$$

$$= 1 - P(D10) . \tag{4.4-5}$$

Since D8 and D9 are mutually exclusive, Eqn. (4.4-5) becomes

$$P_{c \mid w/ SSP} = P(D8) + P(D9) . \tag{4.4-6}$$

Observe that

$$P(D8) = 1 - \left(1 - P_d(3/3) \right)^L = 1 - (p + q)^L . \tag{4.4-7}$$

This corresponds to the cumulative detection probability for the baseline configuration. Therefore, the second term in Eqn. (4.4-6) is recognized as the SSP gain. While Eqn. (4.4-6) reveals some insight into performance, it is simpler to use Eqn. (4.4-5) for computing $P_{c \mid w/ SSP}$ where P(D10) represents the probability of failure (i.e., missing the target). A failure can arise by having either 1) less than J partial successes and no full success occurring in L scans (event D12), or 2) J or more partial successes occurring in L scans without the occurrence of a full success but the partial successes do not occur within the K scan deep slid-

ing window (event D13). Since event D12 and D13 are mutually exclusive, it follows that

$$P(D10) = P(D12) + P(D13).$$

Note that the probability of event D12 is given by

$$P(D12) = \sum_{i=0}^{J-1} \binom{L}{i} p^i q^{L-i} . \qquad (4.4-8)$$

To count the number of ways to fail in the second case for $1 < J \leq K$, $J \leq K \leq L$, the outcomes in events D11 and D9 are considered for each J, K, and L as appropriate. The difference in the number of outcomes in D11 and D9 when there are $i \geq J$ partial successes is denoted by $N_L^i(J,K)$. This difference is the number of ways to fail when at least J partial successes occur in L scans without the occurrence of a full success. For each J and given L, P(D11) is given by

$$P(D11) = \sum_{i=J}^{L} \binom{L}{i} p^i q^{L-i} .$$

This shows, for a given J, that there are exactly $L!/(i!(L-i)!)$, $i = J$, --, L, possible ways for a partial success to occur in i scans with neither a partial nor a full success occurring in (L-i) scans. Event D9 is clearly a subset of event D11. For $i \geq J$, the number of elements in D11 but not in D9, which we have denoted by $N_L^i(J,K)$, is most readily counted by forming a table of all possible outcomes

176

for event D11 and applying the K scan deep sliding window to identify those which do not belong to the event D9. Such tables for J=2 and K≤L=6, and J=3 and K≤L=6 are shown in Tables 4.4-1 and 4.4-2, respectively. Having determined $N_L^i(J,K)$, the probability of event D13 is

$$P(D13) = \sum_{i=J}^{L} N_L^i(J,K)p^i q^{L-i} \qquad (4.4-9)$$

An example illustrates the procedure for computing $P_{c|w/ SSP}$ when J=3 and K=L=6. From Eqn. (4.4-8), the number of ways to fail when i<3 is L!/[i!(L-i)!], i = 0, 1, 2. The corresponding probabilities of failure for these values of i are

i=0: q^6

i=1: $6pq^5$

i=2: $15p^2 q^4$.

From Table 4.4-2, the number of ways to fail when i=3 and i=4 are:

i=3:   0

i=4:   0.

It is obvious that the number of ways to fail when partial successes occur in 5 or more scans is zero. Hence, P(D10) = P(D11) for i≥5. Using the above results in Eqn. (4.4-5)

177

Table 4.4-1 Ways to Fail in J=2 of K≤L=6 SSP

Combinations of i=2 Partial Successes and 4 Failures over L=6
Scans (15 possible ways for the p^2q^4 term)

```
Scan No.
   1    1 1 1 1 1 0 0 0 0 0 0 0 0 0 0
   2    1 0 0 0 0 1 1 1 1 0 0 0 0 0 0
   3    0 1 0 0 0 1 0 0 0 1 1 1 0 0 0
   4    0 0 1 0 0 0 1 0 0 1 0 0 1 1 0
   5    0 0 0 1 0 0 0 1 0 0 1 0 1 0 1
   6    0 0 0 0 1 0 0 0 1 0 0 1 0 1 1
```

$N_6^2(2,K)$

Scan Depth (K)		Number of Ways to Fail
2	x x x x x x x x x x	10
3	x x x x x x	6
4	x x x	3
5	x	1
6 or more		0

Combinations of i=3 Partial Successes and 3 Failures over L=6
Scans (20 possible ways for the p^3q^3 term)

```
Scan No.
   1    1 1 1 1 1 1 1 1 1 1 0 0 0 0 0 0 0 0 0 0
   2    1 1 1 1 0 0 0 0 0 0 1 1 1 1 1 1 0 0 0 0
   3    1 0 0 0 1 1 1 0 0 0 1 1 1 0 0 0 1 1 1 0
   4    0 1 0 0 1 0 0 1 1 0 1 0 0 1 1 0 1 1 1 1
   5    0 0 1 0 0 1 0 1 0 1 0 1 0 1 0 1 1 0 0 1
   6    0 0 0 1 0 0 1 0 1 1 0 0 1 0 1 1 0 1 1 1
```

$N_6^3(2,K)$

Scan Depth (K)		Number of Ways to Fail
2	x x x x	4
3 or more		0

178

Table 4.4-2 Ways to Fail in J=3 of K≤L=6 SSP

Combinations of i=3 Partial Successes and 3 Failures over L=6
Scans (20 possible ways for the $p^3 q^3$ term)

```
Scan No.
   1    1 1 1 1 1 1 1 1 1 1 0 0 0 0 0 0 0 0 0 0
   2    1 1 1 0 0 0 0 0 0 0 1 1 1 1 1 1 1 0 0 0 0
   3    1 0 0 0 1 1 1 0 0 0 1 1 1 0 0 0 1 1 1 0
   4    0 1 0 0 1 0 0 1 1 0 1 0 0 1 1 0 1 1 1 1
   5    0 0 1 0 0 1 0 1 0 1 0 1 0 1 0 1 1 0 0 1
   6    0 0 0 1 0 0 1 0 1 1 0 0 1 0 1 1 0 1 1 1
```

	$N_6^3(3,K)$
Scan	Number of Ways
Depth (K)	to Fail

```
Scan
Depth (K)                                              to Fail
   3        x x x x x x x x x   x  x x x x   x x        16
   4          x x   x x x x x       x   x x             10
   5            x       x     x x                        4
 6 of more                                               0
```

Combinations of i=4 Partial Successes and 2 over L=6 Scans
(15 possible ways for the $p^4 q^2$ term)

```
Scan No.
   1    1 1 1 1 1 1 1 1 1 1 0 0 0 0 0
   2    1 1 1 1 1 1 0 0 0 0 1 1 1 1 0
   3    1 1 1 0 0 0 1 1 1 0 1 1 1 0 1
   4    1 0 0 1 1 0 1 1 0 1 1 1 0 1 1
   5    0 1 0 1 0 1 1 0 1 1 1 0 1 1 1
   6    0 0 1 0 1 1 0 1 1 1 0 1 1 1 1
```

	$N_6^4(3,K)$
Scan	Number of Ways
Depth(K)	to Fail

```
Scan
Depth(K)                                      to Fail
   3          x x x   x x         x              6
   4            x                                1
 5 or more                                       0
```

yields

$$P_{c\,|w/\,SSP} = 1 - P(D10) = 1 - (q^6 + 6pq^5 + 15p^2q^4) \ . \qquad (4.4\text{-}10)$$

The alternate form of $P_{c|w/\,SSP}$ by Eqn. (4.4-6) is

$$P_{c\,|w/\,SSP} = P(D8) + P(D9) = 1 - (1-P)^L + P(D9)$$

$$= 1 - (1-P)^6 + \left[\ 20p^3q^3 + 15p^4q^2 + 6p^5q + p^6/ \right]/ \ . \quad (4.4\text{-}11)$$

That the above two expressions yield the same numerical result is illustrated in Table 4.4-3. In this example, it is assumed that $p_{d1} = p_{d2}$ for simplicity such that the detection probabilities in all 3 slants are identical. This is equivalent to using one average beam shape loss for each of the 3 slants. The result of the example is of course expected. That Eqns. (4.4-10) and (4.4-11) are identical can be shown by substituting $(p+q)$ for P in Eqn. (4.4-10) and carrying out the algebra:

$$P_{c\,|w/\,SSP} = P(D8) + P(D9) = 1 - (1-P)^L + P(D9)$$

$$= 1 - \left[\ p^6 + 6p^5q + 15p^4q^2 + 20p^3q^3 + 15p^2q^4 + 6pq^5 + q^6 \right]$$

$$+ \left[\ 20p^3q^3 + 15p^4q^2 + 6p^5q + p^6 \right]$$

$$= 1 - (q^6 + 6pq^5 + 15p^2q^4) \ .$$

Following the same procedure, the expressions for $P_{c|w/\,SSP}$ for J=2 and for J=3, and k$\leq$L=6 are determined.

Table 4.4-3

An Illustration for Computing $P_{|w/\ SSP}$ by Two Formulas

(3-Slant Configuration with 6-Scan Deep SSP)

P	P(D8)	$P_{|w/\ SSP}$ Eqn.4.4-5	$P_{|w/\ SSP}$ Eqn.4.4-6
0.1177031	0.0664269	0.0902742	0.0902744
0.1406250	0.0901633	0.1280342	0.1280342
0.1644844	0.1184709	0.1744983	0.1744984
0.1890000	0.1514509	0.2294627	0.2294628
0.2138907	0.1890810	0.2920931	0.2920930
0.2388750	0.2312025	0.3609468	0.3609468
0.2636719	0.2775120	0.4340711	0.4340711
0.2880000	0.3275578	0.5091608	0.5091610
0.3115782	0.3807418	0.5837611	0.5837610
0.3341251	0.4363300	0.6554816	0.6554816
0.3553594	0.4934678	0.7222001	0.7222000
0.3750000	0.5512050	0.7822266	0.7822268
0.3927657	0.6085276	0.8344148	0.8344150
0.4083750	0.6643983	0.8782052	0.8782053
0.4215469	0.7177992	0.9136057	0.9136057
0.4320000	0.7677816	0.9411144	0.9411142
0.4394531	0.8135140	0.9616017	0.9616016
0.4436250	0.8543281	0.9761709	0.9761709
0.4442344	0.8897591	0.9860174	0.9860175
0.4410001	0.9195747	0.9923041	0.9923042

program used for computation:

```
10   P1 = .2
20   PRINT "        P       PC        PC1        PC2"
30   FOR I = 1 TO 20
40 P1 = P1 + .025
50   PP = P1^3
60   P = 3*P1^2*(1 - P1)
70   Q = 1 - P - PP
80   PC1 = 1 - (Q^6 + 6*P*Q^5 + 15*P^2*Q^4)
90   PC = 1 - (1 - PP)^6
100  PC2 = PC + 20*P^3*Q^3 + 15*P^4*Q^2 + 6*P^5*Q + P^6
110 PRINT USING " #.#######"; P, PC, PC1, PC2
120 NEXT
```

The results are listed in Table 4.4-4. Using these formulas and Eqn. (4.4-4), cumulative detection probabilities as a function of scan depth K for the 5 target models are computed by numerical integration. The results are shown in Table 4.4-5 (a) through (f) for Swerling cases 1 through 4 and Marcum target models.

Recognizing that the baseline configuration corresponds to a scan depth of unity, it is evident from Table 4.4-5 that a only a modest improvement is achieved by SSP. In an attempt to explain more optimistic projections by other investigators, both the interim detection probabilities arising from 2 of 3 post detection integration before SSP and the hybrid detection probabilities after SSP, defined by Eqn. (4.4-2) are computed. The former is given by

$$P_d(3/3) = P(D1) + P(D2)$$

while the latter is given by

$$P_d(hyb) = P(D4) + P(D7) .$$

Values of J=3 and K=8 were used for evaluating P_d(hyb) in order to get more optimistic results. Numerical results for these quantities are shown in Table 4.4-6 (a) through (e) for Swerling cases 1 through 4 and Marcum target models. Cumulative detection probabilities under the scan limit of L=6 for both with and without SSP are also shown. These results are

Table 4.4-4 Expressions for Cumulative Detection Probability with Scan-to-Scan Processing

Scan Depth K for SSP	2 of K SSP	3 of K SSP
1	$1 - (1-P)^6$	$1 - (1-P)^6$
2	$1 - (q^6 + 6pq^5 + 10p^2q^4 + 4p^3q^3)$	$1 - (1-P)^6$
3	$1 - (q^6 + 6pq^5 + 6p^2q^4)$	$1 - (q^6 + 6pq^5 + 15p^2q^4 + 16p^3q^3 + 6p^4q^2)$
4	$1 - (q^6 + 6pq^5 + 3p^2q^4)$	$1 - (q^6 + 6pq^5 + 15p^2q^4 + 10p^3q^3 + p^4q^2)$
5	$1 - (q^6 + 6pq^5 + p^2q^4)$	$1 - (q^6 + 6pq^5 + 15p^2q^4 + 4p^3q^3)$
6	$1 - (q^6 + 6pq^5)$	$1 - (q^6 + 6pq^5 + 15p^2q^4)$

Table 4.4-5. Cumulative Probability of Detection vs. SNR, 3-Slant, Normal Time Overhead, as a Function of Scan Depth Used

a. Swerling Case 1

So/N (dB)	Pd(3/3)	Pc w/ ssp in 6 scans for 2 of K SSP scan depth used						Pc w/ ssp in 6 scans for 3 of K SSP scan depth used					
		1	2	3	4	5	6	1	2	3	4	5	6
10.0	.163	.66	.71	.74	.75	.77	.77	.66	.66	.67	.67	.68	.69
10.2	.175	.69	.74	.76	.78	.79	.80	.69	.69	.69	.70	.71	.72
10.4	.188	.71	.76	.79	.80	.81	.82	.71	.71	.72	.73	.74	.75
10.6	.201	.74	.79	.81	.83	.83	.84	.74	.74	.75	.76	.77	.77
10.8	.215	.77	.81	.83	.85	.85	.86	.77	.77	.77	.78	.79	.80
11.0	.229	.79	.83	.85	.86	.87	.88	.79	.79	.80	.81	.81	.82
11.2	.243	.81	.85	.87	.88	.89	.89	.81	.81	.82	.83	.83	.84
11.4	.257	.83	.87	.89	.90	.90	.91	.83	.83	.84	.85	.85	.86
11.6	.272	.85	.89	.90	.91	.92	.92	.85	.85	.86	.87	.87	.88
11.8	.287	.87	.90	.91	.92	.93	.93	.87	.87	.88	.88	.89	.89
12.0	.302	.88	.91	.93	.93	.94	.94	.88	.88	.89	.90	.90	.91
12.2	.318	.90	.93	.94	.94	.95	.95	.90	.90	.91	.91	.92	.92
12.4	.333	.91	.94	.95	.95	.96	.96	.91	.91	.92	.92	.93	.93
12.6	.349	.92	.95	.95	.96	.96	.96	.92	.92	.93	.93	.94	.94
12.8	.365	.93	.95	.96	.97	.97	.97	.93	.93	.94	.94	.95	.95
13.0	.381	.94	.96	.97	.97	.97	.97	.94	.94	.95	.95	.95	.96

b. Swerling Case 2

So/N (dB)	Pd(3/3)	Pc w/ ssp in 6 scans for 2 of K SSP scan depth used						Pc w/ ssp in 6 scans for 3 of K SSP scan depth used					
		1	2	3	4	5	6	1	2	3	4	5	6
10.0	.037	.20	.39	.47	.52	.55	.57	.20	.20	.24	.28	.31	.33
10.2	.042	.23	.43	.51	.56	.59	.61	.23	.23	.27	.32	.35	.37
10.4	.048	.25	.47	.56	.60	.63	.65	.25	.25	.31	.35	.39	.42
10.6	.054	.28	.51	.60	.64	.68	.69	.28	.28	.34	.39	.43	.46
10.8	.060	.31	.55	.64	.68	.71	.73	.31	.31	.37	.43	.48	.50
11.0	.067	.34	.59	.68	.72	.75	.76	.34	.34	.41	.47	.52	.55
11.2	.075	.37	.63	.71	.75	.78	.80	.37	.37	.45	.51	.56	.59
11.4	.083	.40	.67	.75	.79	.81	.83	.40	.40	.49	.55	.60	.63
11.6	.091	.44	.70	.78	.82	.84	.85	.44	.44	.53	.59	.64	.67
11.8	.100	.47	.74	.81	.84	.87	.88	.47	.47	.56	.63	.68	.71
12.0	.110	.50	.77	.84	.87	.89	.90	.50	.50	.60	.67	.72	.75
12.2	.120	.54	.80	.86	.89	.91	.92	.54	.54	.64	.71	.75	.78
12.4	.131	.57	.83	.88	.91	.92	.93	.57	.57	.67	.74	.79	.81
12.6	.142	.60	.85	.90	.92	.94	.94	.60	.60	.71	.77	.82	.84
12.8	.154	.63	.87	.92	.94	.95	.96	.63	.63	.74	.80	.84	.87
13.0	.166	.66	.89	.93	.95	.96	.96	.66	.66	.77	.83	.87	.89

Table 4.4-5 Cumulative Probability of Detection vs. SNR, 3-Slant, Normal Time Overhead, as a Function of Scan Depth Used (Continued)

c. Swerling Case 3

So/N (dB)	Pd(3/3)	Pc w/ ssp in 6 scans for 2 of K SSP scan depth used						Pc w/ ssp in 6 scans for 3 of K SSP scan depth used					
		1	2	3	4	5	6	1	2	3	4	5	6
10.0	.139	.59	.69	.73	.75	.77	.78	.59	.59	.61	.63	.65	.66
10.2	.153	.63	.72	.76	.79	.80	.81	.63	.63	.65	.67	.69	.70
10.4	.168	.67	.76	.80	.82	.83	.84	.67	.67	.69	.71	.73	.74
10.6	.184	.71	.79	.83	.84	.86	.86	.71	.71	.73	.75	.76	.77
10.8	.201	.74	.82	.85	.87	.88	.89	.74	.74	.76	.78	.79	.80
11.0	.219	.77	.85	.88	.89	.90	.91	.77	.77	.79	.81	.82	.83
11.2	.237	.80	.87	.90	.91	.92	.92	.80	.80	.82	.84	.85	.86
11.4	.256	.83	.89	.92	.93	.93	.94	.83	.83	.85	.86	.87	.88
11.6	.275	.86	.91	.93	.94	.95	.95	.86	.86	.87	.89	.90	.90
11.8	.295	.88	.93	.94	.95	.96	.96	.88	.88	.89	.91	.91	.92
12.0	.316	.90	.94	.96	.96	.97	.97	.90	.90	.91	.92	.93	.94
12.2	.337	.92	.95	.96	.97	.97	.98	.92	.92	.93	.94	.94	.95
12.4	.358	.93	.96	.97	.98	.98	.98	.93	.93	.94	.95	.96	.96
12.6	.380	.94	.97	.98	.98	.98	.99	.94	.94	.95	.96	.96	.97
12.8	.402	.95	.98	.98	.99	.99	.99	.95	.95	.96	.97	.97	.97
13.0	.424	.96	.98	.99	.99	.99	.99	.96	.96	.97	.98	.98	.98

d. Swerling Case 4

So/N (dB)	Pd(3/3)	Pc w/ ssp in 6 scans for 2 of K SSP scan depth used						Pc w/ ssp in 6 scans for 3 of K SSP scan depth used					
		1	2	3	4	5	6	1	2	3	4	5	6
10.0	.045	.24	.46	.55	.60	.63	.65	.24	.24	.30	.34	.38	.41
10.2	.053	.28	.51	.60	.65	.68	.70	.28	.28	.34	.39	.44	.46
10.4	.061	.31	.57	.65	.70	.73	.74	.31	.31	.38	.44	.49	.52
10.6	.070	.35	.62	.70	.75	.77	.79	.35	.35	.43	.50	.55	.58
10.8	.080	.39	.67	.75	.79	.81	.83	.39	.39	.48	.55	.60	.63
11.0	.091	.44	.71	.79	.83	.85	.86	.44	.44	.53	.60	.65	.68
11.2	.103	.48	.76	.83	.86	.88	.89	.48	.48	.58	.65	.70	.73
11.4	.116	.52	.80	.86	.89	.91	.92	.52	.52	.63	.70	.75	.78
11.6	.130	.57	.83	.89	.91	.93	.94	.57	.57	.68	.75	.79	.82
11.8	.146	.61	.86	.91	.93	.95	.95	.61	.61	.72	.79	.83	.86
12.0	.162	.65	.89	.93	.95	.96	.96	.65	.65	.77	.83	.86	.89
12.2	.179	.69	.91	.95	.96	.97	.97	.69	.69	.80	.86	.89	.91
12.4	.197	.73	.93	.96	.97	.98	.98	.73	.73	.84	.89	.92	.93
12.6	.217	.77	.95	.97	.98	.99	.99	.77	.77	.87	.91	.94	.95
12.8	.237	.80	.96	.98	.99	.99	.99	.80	.80	.90	.93	.95	.96
13.0	.257	.83	.97	.99	.99	.99	.99	.83	.83	.92	.95	.97	.97

Table 4.4-5 Cumulative Probability of Detection vs. SNR, 3-Slant, Normal Time Overhead, as a Function of Scan Depth Used (Continued)

e. Marcum (Non-Fluctuating Case)

So/N (dB)	Pd(3/3)	Pc w/ ssp in 6 scans for 2 of K SSP scan depth used						Pc w/ ssp in 6 scans for 3 of K SSP scan depth used					
		1	2	3	4	5	6	1	2	3	4	5	6
10.0	.052	.28	.54	.64	.69	.72	.73	.28	.28	.35	.42	.47	.50
10.2	.064	.33	.62	.71	.75	.78	.80	.33	.33	.42	.49	.55	.58
10.4	.079	.39	.69	.78	.82	.84	.85	.39	.39	.50	.57	.65	.66
10.6	.095	.45	.76	.83	.87	.89	.90	.45	.45	.57	.65	.71	.74
10.8	.115	.52	.82	.88	.91	.92	.93	.52	.52	.65	.73	.78	.81
11.0	.137	.59	.87	.92	.94	.95	.96	.59	.59	.72	.79	.84	.86
11.2	.162	.65	.91	.95	.96	.97	.98	.65	.65	.79	.85	.89	.91
11.4	.191	.72	.94	.97	.98	.98	.99	.72	.72	.85	.90	.93	.94
11.6	.223	.78	.96	.98	.99	.99	.99	.78	.78	.89	.93	.96	.97
11.8	.258	.83	.98	.99	.99	1.00	1.00	.83	.83	.93	.96	.97	.98
12.0	.296	.88	.99	1.00	1.00	1.00	1.00	.88	.88	.96	.98	.99	.99
12.2	.336	.91	.99	1.00	1.00	1.00	1.00	.91	.91	.97	.99	.99	1.00
12.4	.379	.94	1.00	1.00	1.00	1.00	1.00	.94	.94	.99	.99	1.00	1.00
12.6	.425	.96	1.00	1.00	1.00	1.00	1.00	.96	.96	.99	1.00	1.00	1.00
12.8	.471	.98	1.00	1.00	1.00	1.00	1.00	.98	.98	1.00	1.00	1.00	1.00
13.0	.519	.99	1.00	1.00	1.00	1.00	1.00	.99	.99	1.00	1.00	1.00	1.00

Table 4.4-6

Probability of Detection vs. SNR, 3-Slant,
Normal Time Overhead

P_{fa}	P_f	r_T(dB)	L_{BS1}(dB)	L_{BS1}(dB)
0.339×10^{-9}	0.760×10^{-3}	8.5626	0.296	3.429

a. Swerling Case 1

$\overline{So}/N$ (dB)	Pd (3/3)	Pd (2/3)	Pd (hyb)	Pc w/o ssp	Pc w/ ssp
10.00	.16	.33	.28	.66	.69
10.20	.18	.34	.30	.69	.72
10.40	.19	.36	.32	.71	.75
10.60	.20	.37	.34	.74	.77
10.80	.21	.39	.36	.77	.80
11.00	.23	.40	.38	.79	.82
11.20	.24	.42	.40	.81	.84
11.40	.26	.44	.41	.83	.86
11.60	.27	.45	.43	.85	.88
11.80	.29	.47	.45	.87	.89
12.00	.30	.48	.47	.88	.91
12.20	.32	.50	.49	.90	.92
12.40	.33	.51	.50	.91	.93
12.60	.35	.53	.52	.92	.94
12.80	.36	.54	.53	.93	.95
13.00	.38	.56	.55	.94	.96

b. Swerling Case 2

$\overline{So}/N$ (dB)	(3/3)	(2/3)	(hyb)	Pc w/o ssp	Pc w/ ssp
10.00	.04	.27	.18	.20	.33
10.20	.04	.29	.21	.23	.37
10.40	.05	.31	.23	.25	.42
10.60	.05	.33	.26	.28	.46
10.80	.06	.35	.29	.31	.50
11.00	.07	.37	.31	.34	.55
11.20	.07	.40	.34	.37	.59
11.40	.08	.42	.37	.40	.63
11.60	.09	.44	.40	.44	.67
11.80	.10	.46	.43	.47	.71
12.00	.11	.48	.45	.50	.75
12.20	.12	.50	.48	.54	.78
12.40	.13	.52	.51	.57	.81
12.60	.14	.55	.53	.60	.84
12.80	.15	.57	.55	.63	.87
13.00	.17	.59	.58	.66	.89

Table 4.4-6

Probability of Detection vs. SNR, 3-Slant, Normal Time Overhead (cont'd)

c. Swerling Case 3

$\overline{So}/N$ (dB)	Pd(3/3)	Pd(2/3)	Pd(hyb)	Pc w/o ssp	Pc w/ ssp
10.00	.13901	.34930	.29988	.59264	.65821
10.20	.15332	.37020	.32661	.63159	.69785
10.40	.16846	.39135	.35342	.66941	.73537
10.60	.18444	.41268	.38011	.70573	.77043
10.80	.20120	.43411	.40654	.74021	.80276
11.00	.21873	.45558	.43256	.77259	.83220
11.20	.23697	.47702	.45805	.80264	.85864
11.40	.25588	.49836	.48294	.83022	.88209
11.60	.27540	.51954	.50718	.85525	.90263
11.80	.29547	.54050	.53072	.87770	.92039
12.00	.31602	.56118	.55354	.89761	.93555
12.20	.33700	.58153	.57563	.91507	.94834
12.40	.35832	.60149	.59701	.93019	.95900
12.60	.37992	.62103	.61766	.94315	.96779
12.80	.40171	.64010	.63760	.95414	.97492
13.00	.42363	.65867	.65683	.96334	.98066

d. Swerling Case 4

$\overline{So}/N$ (dB)	Pd(3/3)	Pd(2/3)	Pd(hyb)	Pc w/o ssp	Pc w/ ssp
10.00	.04540	.31140	.23005	.24329	.40765
10.20	.05270	.33725	.26435	.27735	.46364
10.40	.06087	.36390	.29999	.31397	.51890
10.60	.06997	.39120	.33646	.35287	.57526
10.80	.08003	.41902	.37321	.39375	.63052
11.00	.09108	.44721	.40979	.43617	.68353
11.20	.10317	.47562	.44578	.47968	.73327
11.40	.11629	.50409	.48088	.52374	.77891
11.60	.13048	.53247	.51486	.56779	.81986
11.80	.14571	.56060	.54757	.61127	.85578
12.00	.16197	.58834	.57894	.65361	.88658
12.20	.17924	.61554	.60893	.69430	.91240
12.40	.19748	.64208	.63755	.73297	.93357
12.60	.21665	.66784	.66481	.76893	.95054
12.80	.23668	.69273	.69075	.80219	.96385
13.00	.25750	.71663	.71537	.83243	.97406

Table 4.4-6

Probability of Detection vs. SNR, 3-Slant,

Normal Time Overhead (cont'd)

e. Marcum (Non-Fluctuating Case)

$\overline{So}/N$ (dB)	Pd (3/3)	Pd (2/3)	Pd (hyb)	Pc w/o ssp	Pc w/ ssp
10.00	.05	.36	.29	.28	.53
10.20	.06	.40	.35	.33	.58
10.40	.08	.44	.40	.39	.66
10.60	.10	.49	.46	.45	.74
10.80	.11	.53	.51	.52	.81
11.00	.14	.58	.57	.59	.86
11.20	.16	.62	.61	.65	.91
11.40	.19	.66	.66	.72	.94
11.60	.22	.71	.70	.78	.97
11.80	.26	.75	.74	.93	.98
12.00	.30	.78	.78	.88	.99
12.20	.34	.82	.82	.91	1.00
12.40	.38	.85	.85	.94	1.00
12.60	.42	.88	.88	.96	1.00
12.80	.47	.90	.90	.96	1.00
13.00	.52	.92	.92	.99	1.00

also plotted in Figures 4.4-1 through 4.4-5. The measure of improvement can be obtained by drawing a horizontal line passing through the ordinate at 0.9 and comparing the difference in $(\bar{S}_0/N)$ for cumulative detection probabilities with and without SSP for each of the models. The improvement measured this way is 0.2 dB, 2.0 dB, and 0.9 dB for Swerling case 1, case 2, and Marcum target models, respectively. A larger improvement can be claimed if a similar comparison is made between $P_d(3/3)$ and $P_d(2/3)$ or $P_d(hyb)$ at a level of 0.32 probability or at any other level. Even a larger improvement can be claimed if the cumulative detection probability with SSP is compared against $P_d(3/3)$.

A set of computations were also made using the reduced time overhead. The result for Swerling case 1 is given in Table 4.4-7. The difference in detection performance between the two cumulative detection probabilities, one with and the other without SSP, is almost identical to that based on the normal time overhead as expected.
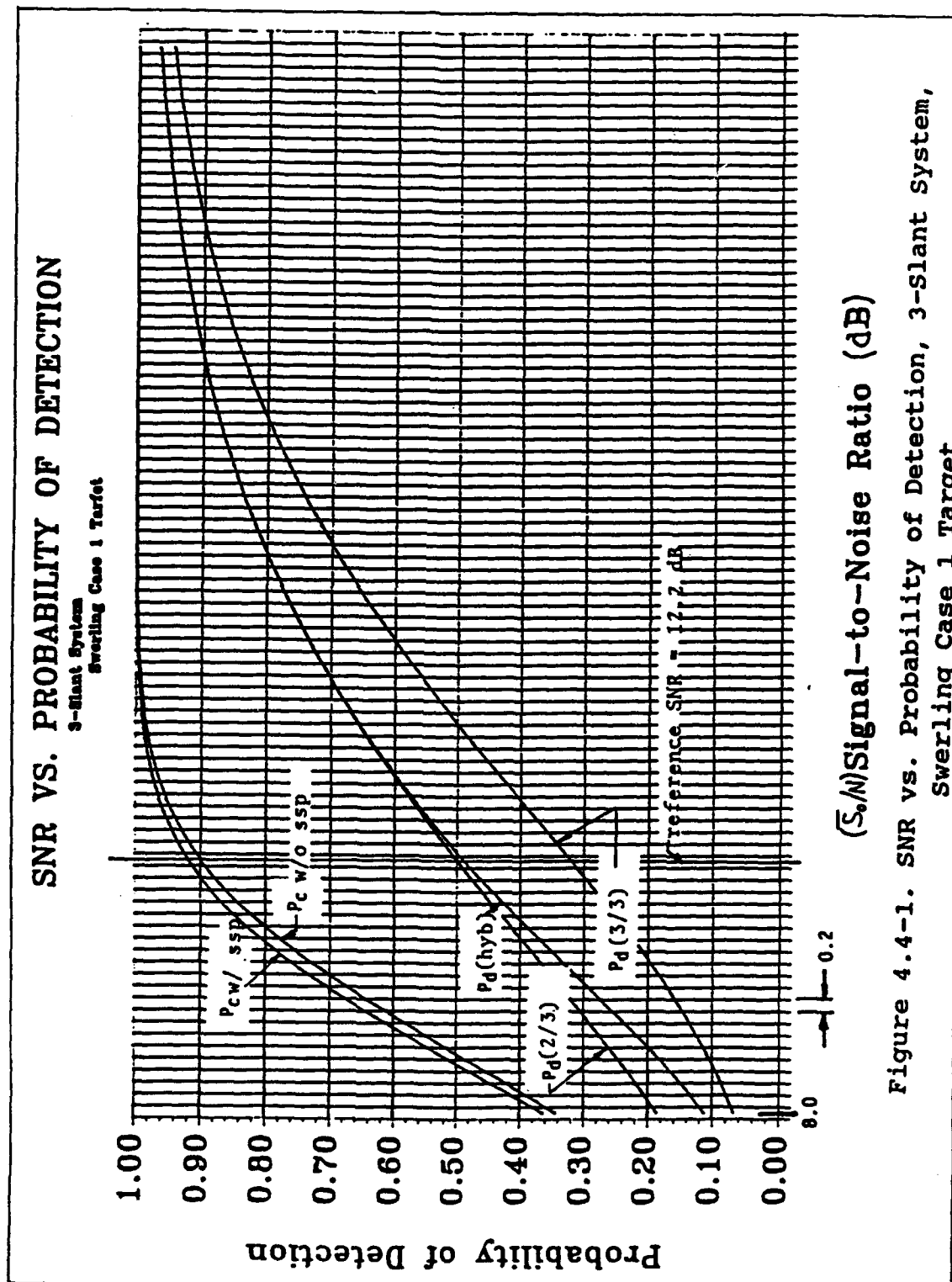
Figure 4.4-1. SNR vs. Probability of Detection, 3-Slant System, Swerling Case 1 Target

Figure 4.4-2. SNR vs. Probability of Detection, 3-Slant System, Swerling Case 2 Target

Figure 4.4-3. SNR vs. Probability of Detection, 3-Slant System, Swerling Case 3 Target

SNR VS. PROBABILITY OF DETECTION

3-Slant System
Swerling Case 4 Target

Figure 4.4-4. SNR vs. Probability of Detection, 3-Slant System,
Swerling Case 4 Target

$(\overline{S}_o/N)$ Signal-to-Noise Ratio (dB)
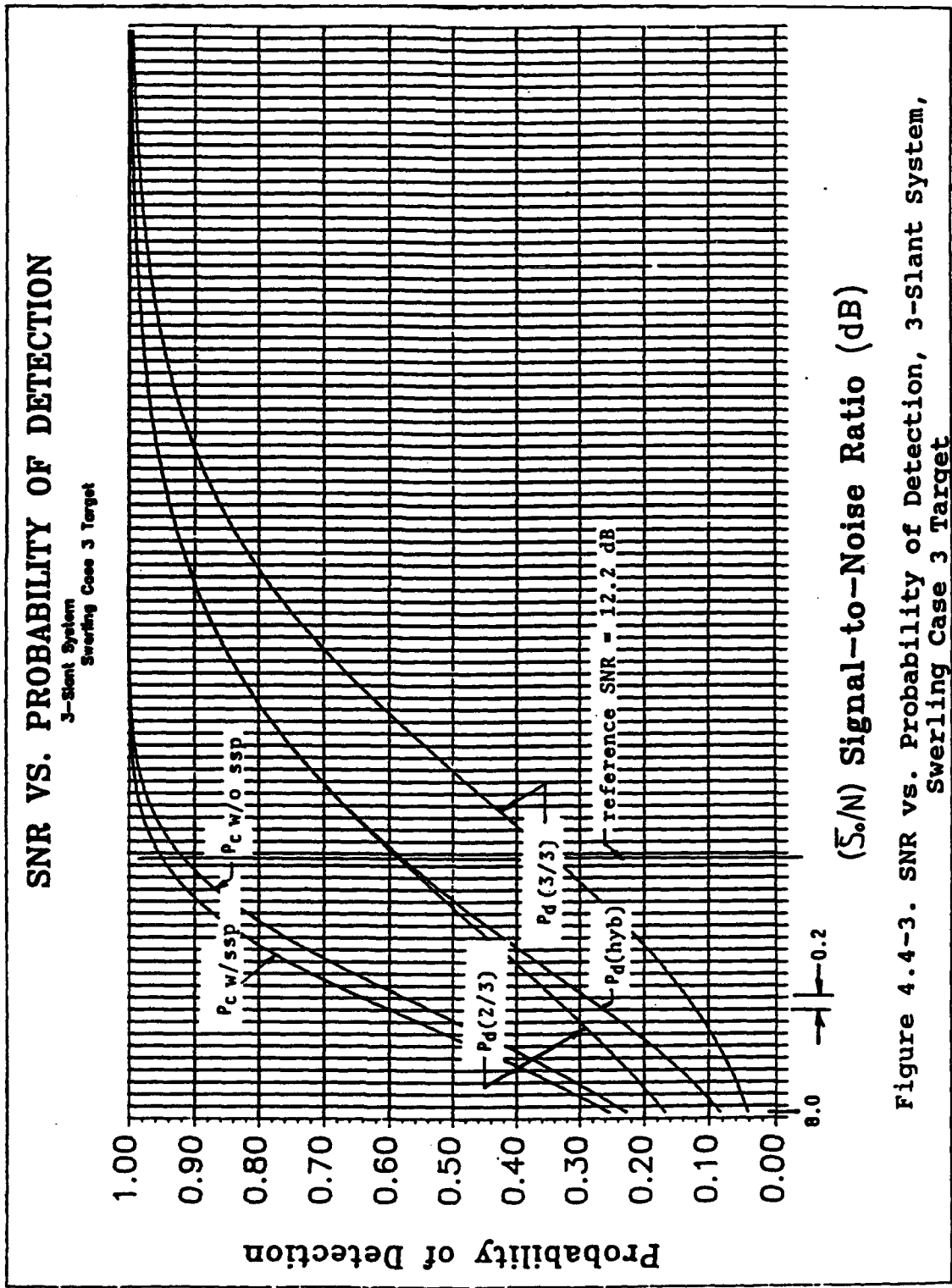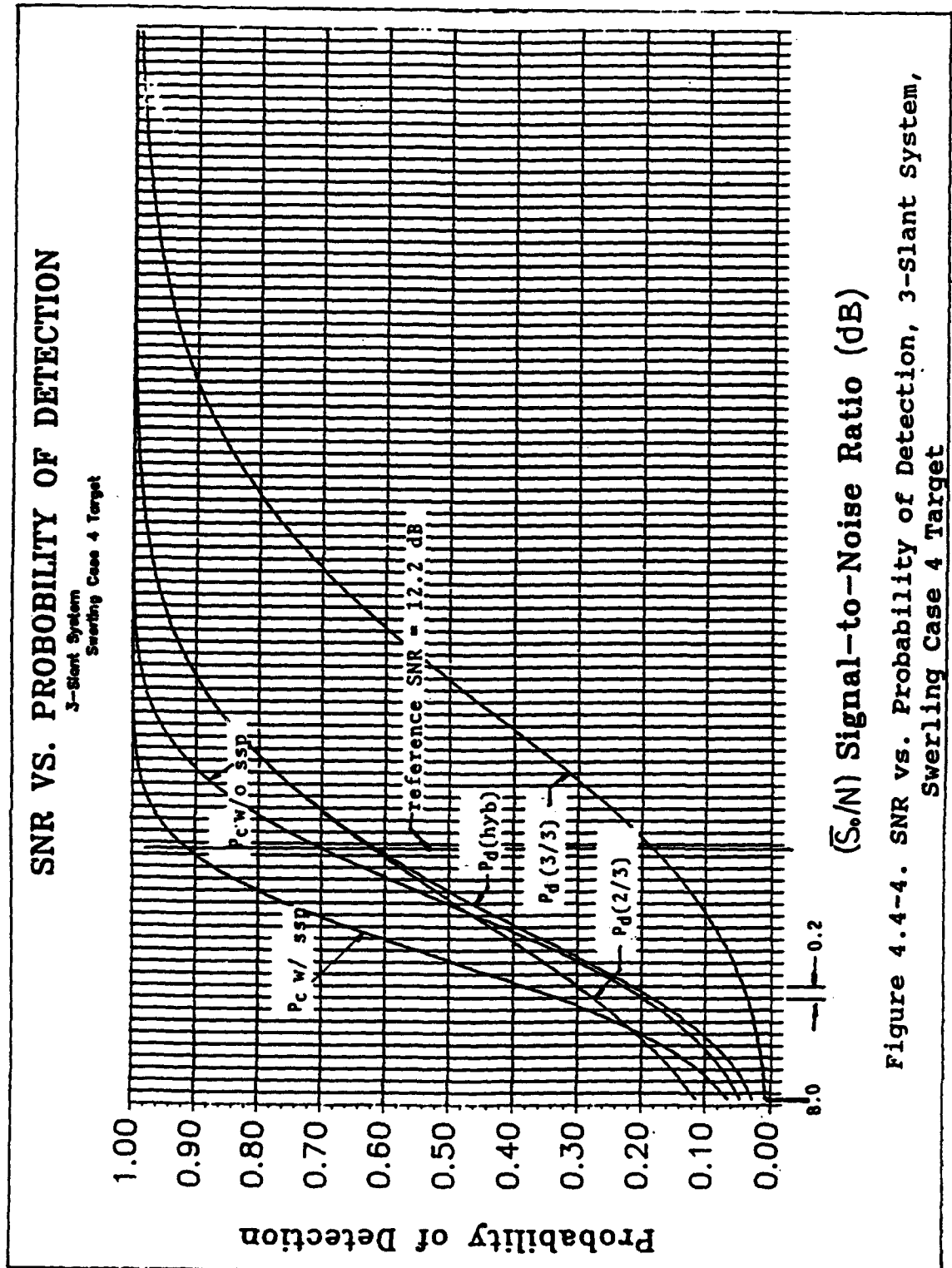
Probability of Detection

Figure 4.4-5 SNR VS. PROBABILITY OF DETECTION
3-Slant System
Non-Fluctuating Target
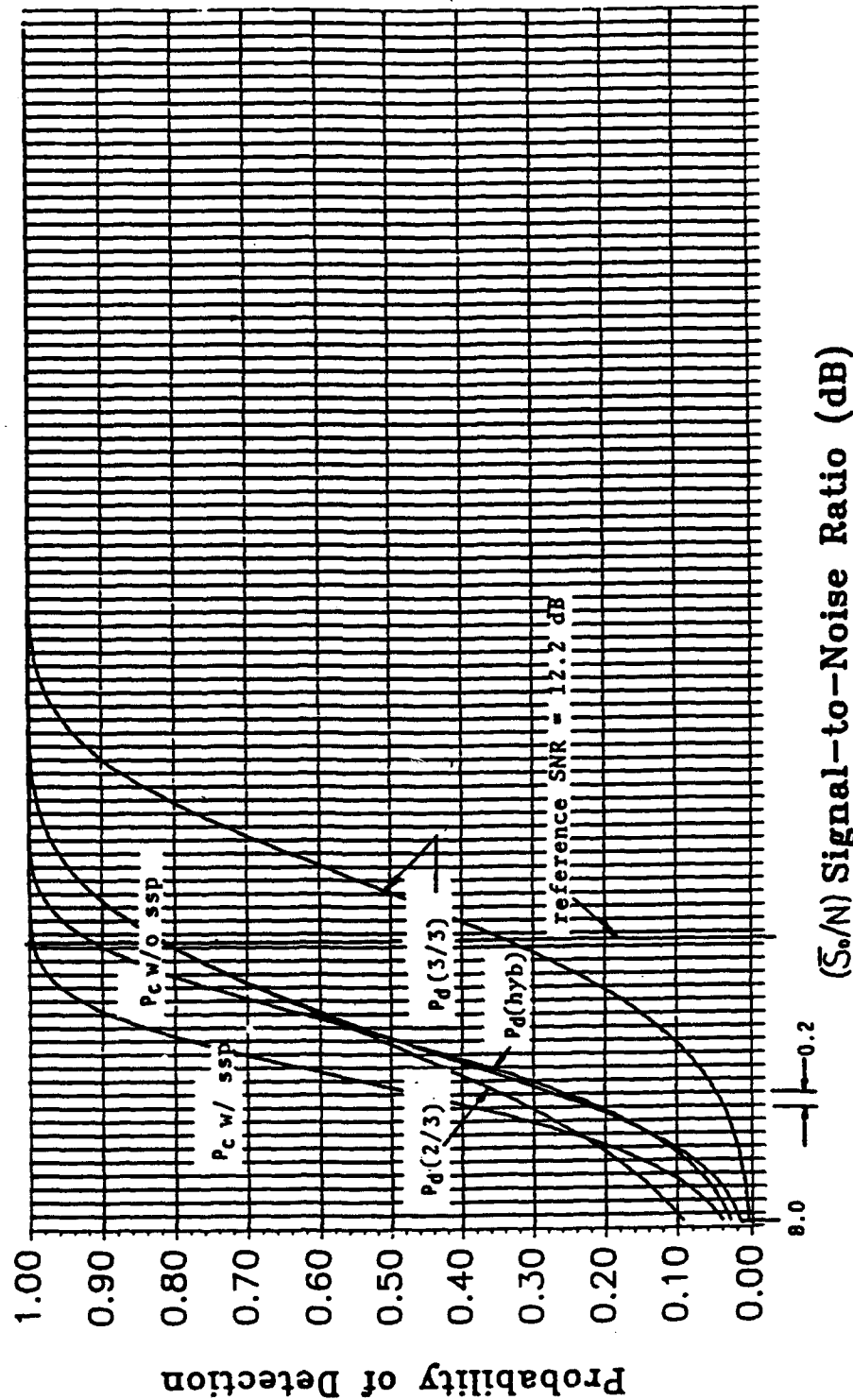
Figure 4.4-5. SNR vs. Probability of Detection, 3-Slant System, Nonfluctuating (Marcum) Target

Table 4.4-7 Probability of Detection vs. SNR, 3-Slant,
Reduced Time Overhead, Swerling Case 1

So/N (dB)	Pd(3/3)	Pd(2/3)	Pd(hyb)	Pc w/o ssp	Pc w/ ssp
8.50	.08526	.21392	.14460	.41414	.43747
8.70	.09375	.22749	.16027	.44602	.47107
8.90	.10276	.24140	.17671	.47827	.50490
9.10	.11229	.25562	.19384	.51066	.53866
9.30	.12234	.27012	.21157	.54296	.57213
9.50	.13290	.28487	.22980	.57497	.60504
9.70	.14396	.29984	.24843	.60647	.63716
9.90	.15550	.31500	.26738	.63725	.66828
10.10	.16750	.33032	.29653	.66712	.69820
10.30	.17996	.34577	.30579	.69591	.72676
10.50	.19285	.36132	.32509	.72348	.75383
10.70	.20614	.37693	.34434	.74971	.77929
10.90	.21982	.39258	.36346	.77449	.80308
11.10	.23385	.40823	.38240	.79775	.82515
11.30	.24819	.42387	.40111	.81944	.84550
11.50	.26284	.43946	.41953	.83954	.86412
11.70	.27775	.45497	.43765	.85805	.88105
11.90	.29289	.47039	.45542	.87499	.89636
12.10	.30822	.48568	.47282	.89040	.91013
12.30	.32373	.50083	.48966	.90434	.92237
12.50	.33937	.51581	.50650	.91687	.93326
12.70	.35511	.53061	.52276	.92807	.94297
12.90	.37092	.54521	.53862	.93802	.95130
13.10	.38677	.55959	.55409	.94682	.95866
13.30	.40263	.57373	.56917	.95456	.96504
13.50	.41847	.58763	.58387	.96132	.97056
13.70	.43426	.60127	.59818	.96721	.97530
13.90	.44997	.61465	.61212	.97231	.97935
14.10	.46558	.62774	.62569	.97670	.98281
14.30	.48107	.64055	.63889	.98047	.98573
14.50	.49641	.65308	.65173	.98369	.98820
14.70	.51158	.66530	.66422	.98642	.99027
14.90	.52657	.67722	.67636	.98874	.99200
15.10	.54134	.68884	.68816	.99069	.99345
15.30	.55590	.70016	.69961	.99233	.99465
15.50	.57021	.71116	.71073	.99370	.99564
15.70	.58428	.72187	.72153	.99484	.99646
15.90	.59808	.73226	.73199	.99578	.99714
16.10	.61160	.74235	.74214	.99657	.99769
16.30	.62485	.75214	.75198	.99721	.99814
16.50	.63780	.76163	.76150	.99774	.99850
16.70	.65045	.77082	.77072	.99818	.99880
16.90	.66281	.77972	.77964	.99853	.99904
17.10	.67486	.78832	.78827	.99882	.99923
17.30	.68659	.79665	.79661	.99905	.99939
17.50	.69802	.80470	.80466	.99924	.99951

4.5 Detection Performance under Conventional *J* of *K* *SSP*

Finally, detection performance using conventional J of K SSP is examined where K equals the number of scans L. This is based on 2-slant, 2 of 2 post detection integration for the reasons stated in Section 4.3. In addition to the events introduced in Sections 4.3 and 4.4, the following two are defined:

D14: detections occur in both of the 2 slants in the 2-slant configuration

D15: event D14 occurs in J or more of the K=L scans

The single scan detection probability P(D14) is given by

$$P(D14) = P_d(2/2) = \overline{p_{d1}^2}$$
(4.5-1)

where p_{d1} denotes the single slant detection probability and the method for averaging with respect to target RCS fluctuation is as described in Chapter 3.

The cumulative detection probability is

$$P_{c| \ w/ \ SSP} = P(D15)$$

$$= \sum_{i=J}^{K} \binom{K}{i} P_d^i (1-P_d)^{K-i} .$$
(4.5-2)

Results for the single scan detection probabilities P(D14),

obtained by numerical integration, are listed in Table 4.5-1 and are plotted in Figure 4.5-1 for the 5 target models. The cumulative detection probabilities P(D15) for J=2 and J=3 with K=6 are shown in Table 4.5-2 for the same target models. They are plotted in Figures 4.5-2 and 4.5-3 for J=2 and J=3, respectively. Recall from Section 4.3 that the choice J=2 and K=6 results in increased false alarms beyond an acceptable level. Therefore, comparison with the baseline configuration is made for the case where J=3.

The above results are based on using the reduced time overhead. Hence, they should be compared with the baseline results which are also based on the reduced time overhead. Because the integrated signal-to-noise ratio is configuration dependent (i.e., depends on the number of slants in a beam dwell), it is necessary to introduce a reference range so that a common reference point in signal-to-noise ratio can be established for different configurations. The reference SNR for the baseline is 12.2 dB. This means that the received $\bar{S}_0/N$ from the reference target located at the reference range is 12.2 dB for the baseline. When the reduced time overhead is assumed in the baseline, the number of pulses for integration increases such that the received $\bar{S}_0/N$ from the reference target at the reference range increases to 13.5 dB. In the 2-slant configuration, SNR per slant is

Table 4.5-1 Single Scan Probability of Detection vs. SNR, 2-Slant with a Reduced Time Overhead

Pfa	P_f	M	N	T_T	LBS
1.197×10^{-6}	1.094×10^{-3}	2	2	8.4374	2.520

$\overline{So}/N$ (dB)	SW1	SW2	SW3	SW4	MARCUM
11.00	.311	.177	.328	.222	.315
11.20	.326	.189	.348	.240	.354
11.40	.342	.202	.369	.260	.395
11.60	.358	.215	.391	.280	.438
11.80	.373	.229	.412	.300	.483
12.00	.389	.243	.434	.322	.529
12.20	.405	.258	.456	.343	.575
12.40	.420	.272	.477	.365	.621
12.60	.436	.287	.499	.388	.666
12.80	.452	.302	.520	.410	.710
13.00	.467	.318	.542	.433	.751
13.20	.483	.333	.562	.456	.790
13.40	.498	.349	.583	.478	.825
13.60	.513	.364	.603	.501	.857
13.80	.528	.380	.623	.523	.885
14.00	.543	.396	.642	.545	.909
14.20	.557	.412	.661	.567	.930
14.40	.571	.427	.679	.588	.947
14.60	.585	.443	.696	.609	.961
14.80	.599	.459	.713	.630	.971
15.00	.612	.474	.730	.649	.980
15.20	.626	.489	.746	.669	1.000
15.40	.638	.505	.761	.687	1.000
15.60	.651	.520	.775	.705	1.000
15.80	.663	.535	.789	.722	1.000
16.00	.675	.549	.802	.739	1.000
16.20	.687	.564	.815	.755	1.000
16.40	.699	.578	.827	.770	1.000
16.60	.710	.592	.838	.785	1.000
16.80	.720	.605	.849	.799	1.000
17.00	.731	.619	.859	.812	1.000
17.20	.741	.632	.868	.824	1.000
17.40	.751	.644	.877	.836	1.000
17.60	.760	.657	.886	.847	1.000
17.80	.770	.669	.894	.858	1.000
18.00	.779	.681	.901	.868	1.000
18.20	.787	.693	.909	.877	1.000
18.40	.796	.704	.915	.886	1.000
18.60	.804	.715	.921	.894	1.000
18.80	.811	.725	.927	.902	1.000
19.00	.819	.736	.933	.909	1.000
19.20	.826	.746	.938	.916	1.000
19.40	.833	.755	.942	.922	1.000

Figure 4.5-1. SNR vs. Single Scan Probability of Detection, 2-Slant System, Reduced Time Overhe

Table 4.5-2 CUMULATIVE PROBABILITY OF DETECTION VS. SNR, 2-SLANT, PULSE NORMAL WITH A REDUCED TIME OVERHEAD

| So/N (dB)	2 of 6 SSP					3 of 6 SSP				
	SW1	SW2	SW3	SW4	MARCUM	SW1	SW2	SW3	SW4	MARCUM
8.00	.1492	.0280	.0970	.0258	.0141	.0244	.0018	.0122	.0015	.0006
8.20	.1709	.0340	.1162	.0328	.0196	.0304	.0024	.0163	.0022	.0010
8.40	.1934	.0418	.1386	.0418	.0269	.0372	.0033	.0216	.0033	.0016
8.60	.2188	.0502	.1643	.0517	.0378	.0457	.0043	.0285	.0045	.0028
8.80	.2472	.0608	.1934	.0656	.0517	.0560	.0058	.0372	.0066	.0045
9.00	.2761	.0722	.2259	.0808	.0689	.0675	.0076	.0482	.0091	.0071
9.20	.3054	.0861	.2592	.0989	.0915	.0802	.0101	.0607	.0126	.0111
9.40	.3373	.1008	.2956	.1202	.1202	.0952	.0130	.0759	.0172	.0172
9.60	.3692	.1182	.3348	.1428	.1556	.1115	.0167	.0940	.0227	.0251
9.80	.4035	.1365	.3766	.1709	.2003	.1305	.0211	.1155	.0304	.0395
10.00	.4350	.1578	.4205	.2026	.2520	.1494	.0267	.1406	.0402	.0579
10.20	.4708	.1798	.4637	.2353	.3127	.1726	.0330	.1679	.0516	.0836
10.40	.5036	.2049	.5082	.2713	.3815	.1955	.0410	.1989	.0655	.1182
10.60	.5379	.2306	.5513	.3127	.4542	.2213	.0499	.2320	.0836	.1616
10.80	.5711	.2568	.5948	.3545	.5334	.2483	.0597	.2688	.1039	.2178
11.00	.6033	.2883	.6382	.3986	.6116	.2763	.0727	.3091	.1277	.2839
11.20	.6342	.3176	.6772	.4422	.6884	.3052	.0858	.3489	.1539	.3610
11.40	.6657	.3496	.7154	.4896	.7589	.3368	.1014	.3916	.1856	.4453
11.60	.6957	.3815	.7525	.5356	.8212	.3691	.1182	.4370	.2196	.5341
11.80	.7224	.4156	.7849	.5798	.8739	.3998	.1377	.4806	.2557	.6239
12.00	.7492	.4494	.8159	.6261	.9155	.4329	.1585	.5259	.2974	.7089
12.20	.7744	.4849	.8437	.6676	.9463	.4660	.1823	.5706	.3388	.7845
12.40	.7965	.5174	.8675	.7083	.9679	.4971	.2057	.6122	.3834	.8485
12.60	.8185	.5513	.8897	.7476	.9820	.5300	.2320	.6544	.4308	.8952
12.80	.8389	.5841	.9083	.7819	.9907	.5625	.2594	.6930	.4764	.9372
13.00	.8565	.6179	.9252	.8145	.9954	.5925	.2897	.7313	.5239	.9629
13.20	.8739	.6482	.9386	.8437	.9980	.6239	.3190	.7642	.5706	.9798
13.40	.8887	.6790	.9506	.8686	.9992	.6525	.3509	.7965	.6141	.9896
13.60	.9023	.7065	.9604	.8916	.9997	.6803	.3814	.8249	.6581	.9951
13.80	.9147	.7343	.9687	.9107	.9999	.7072	.4143	.8511	.6983	.9978
14.00	.9259	.7604	.9752	.9274	1.0000	.7330	.4474	.8737	.7364	.9991
14.20	.9354	.7849	.9807	.9416	1.0000	.7562	.4806	.8942	.7721	.9997
14.40	.9440	.8064	.9850	.9532	1.0000	.7783	.5115	.9116	.8038	.9999
14.60	.9517	.8276	.9884	.9630	1.0000	.7994	.5443	.9263	.8330	1.0000
14.80	.9586	.8473	.9911	.9712	1.0000	.8194	.5766	.9394	.8596	1.0000
15.00	.9643	.8643	.9933	.9774	1.0000	.8370	.6063	.9508	.8815	1.0000
15.20	.9698	.8800	9950	.9827	1.0000	.8548	.6354	.9603	.9022	1.0000
15.40	.9740	.8952	.9963	.9867	1.0000	.8691	.6656	.9679	.9187	1.0000
15.60	.9780	.9083	.9972	.9899	1.0000	.8837	.6930	.9741	.9334	1.0000
15.80	.9812	.9201	.9979	.9923	1.0000	.8962	.7194	.9794	.9456	1.0000
16.00	.9841	.9301	.9985	.9943	1.0000	.9079	.7431	.9836	.9563	1.0000

SNR VS. CUM PROBABILITY OF DETECTION

2-Slant System (2 of 6 SSP)
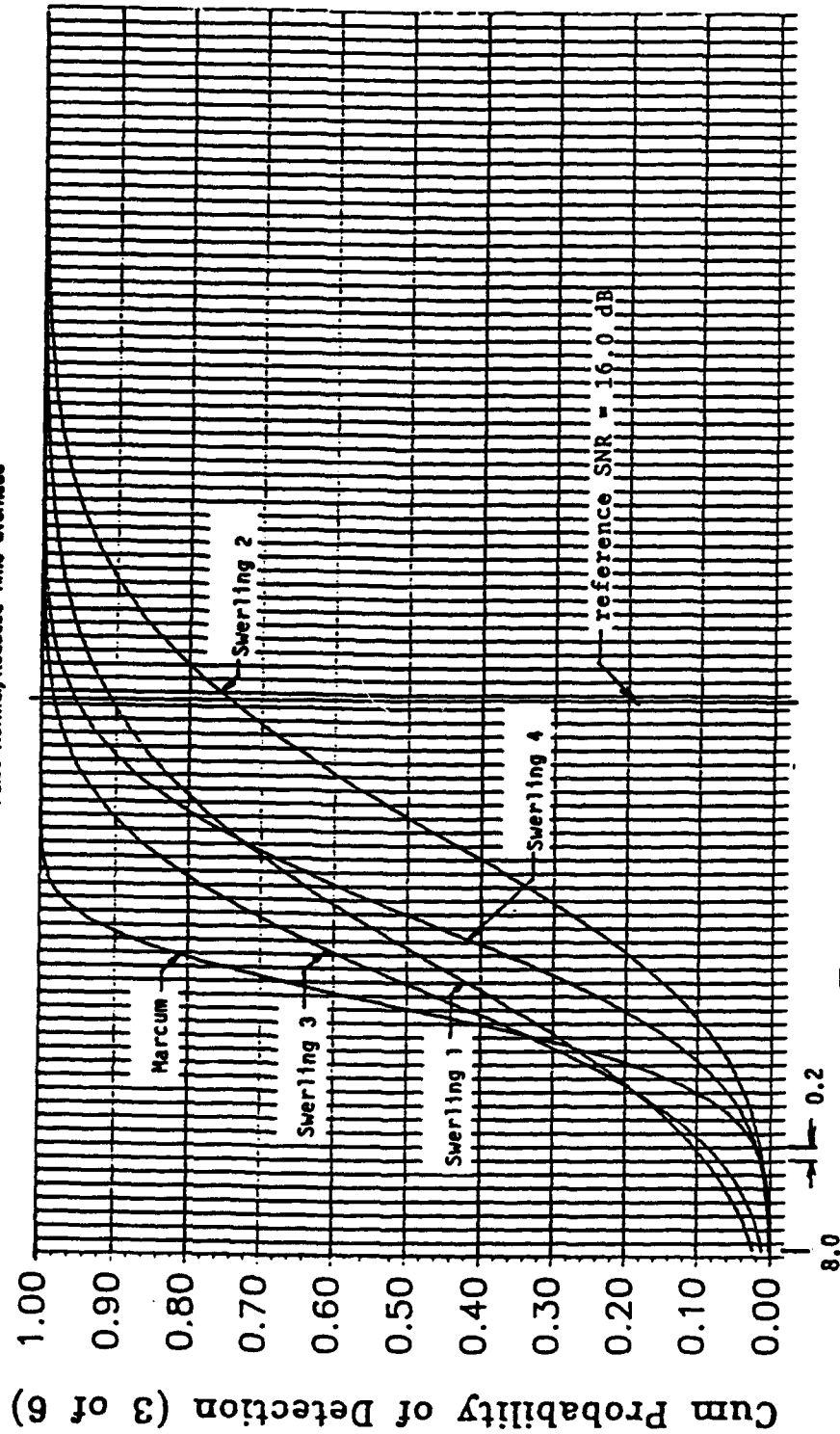Pulse Normal/Reduced Time Overhead
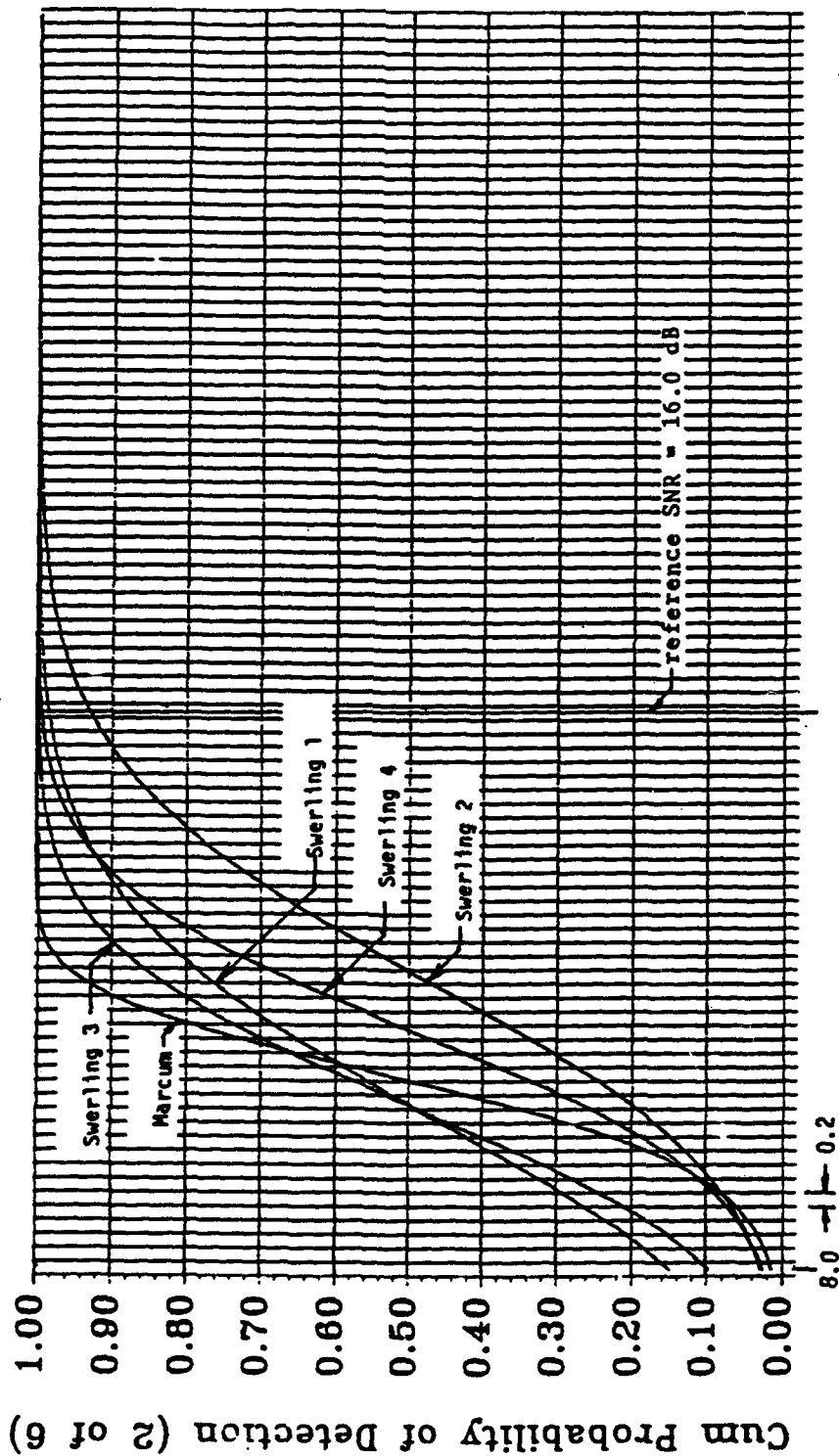
Figure 4.5-2. SNR vs. Cumulative Probability of Detection (2 of 6 SSP), 2-Slant System, Reduced Time Overhead

Figure 4.5-3. SNR vs. Cumulative Probability of Detection (3 of 6 SSP), 2-Slant System, Reduced Time Overhead

higher because of one less slant into which the available number of pulses must be divided and the reduction of the number of fixed time overheads from 3 to 2. The net effect is that $\overline{S}_0/N$ for the reference target at the reference range increases to 16.0 dB. To make a performance comparison at a specific cumulative detection probability level, e.g., at 0.9, the SNR margin for each of the competing configurations is first determined. The margins are compared and the configuration having the larger positive margin is superior by an amount equal to the margin difference. Figure 4.5-4 illustrates this procedure using some fictitious numbers.
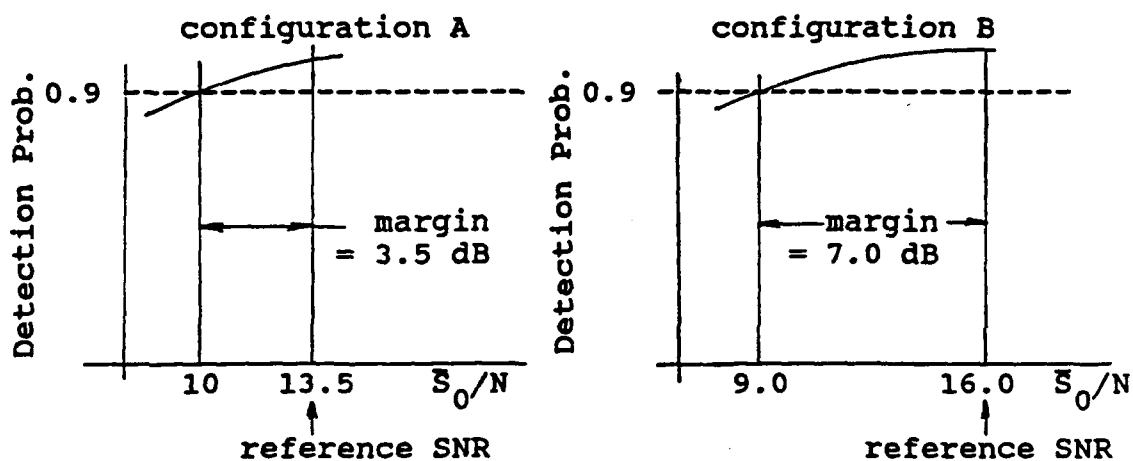
Configuration B is superior to configuration A by

$$\text{margin}_{|\text{config. B}} - \text{margin}_{|\text{config. A}} = 7.0 - 3.5 = 3.5 \text{ dB}$$

Figure 4.5-4

Illustration of Performance Comparison Method

The SNR margin for $P_c=0.9$ for the baseline using reduced time overhead is 1.3 dB for a Swerling case 1 target. Similarly, for the conventional SSP with J=3, K=6, the SNR margin is 0.1 dB as can be seen from Table 4.5-2. Therefore, the performance under the conventional 3 of 6 SSP is inferior to the baseline performance by 1.2 dB!

A totally different conclusion can be drawn if the cumulative detection probability under SSP is compared with the single scan detection probability of the baseline. In the 3 of 6 SSP, $P_c=0.9$ was reached at $\bar{S}_0/N = 15.9$ dB for a Swerling case 1 target giving the margin of 0.1 dB. The values of $\bar{S}_0/N$ required to reach $P_d = 0.9$ in a single scan of the baseline for Swerling case 1 target is 23.0 dB. The SNR margin is 13.5 less 23.0 dB, or -9.5 dB. The difference between the two is 9.6 dB in favor of the 3 of 6 SSP. This form of comparison is made by some investigators. Obviously, this results in an erroneous conclusion.

The correct assessment[1] is that there is marginal improvement with SSP. This conclusion confirms Barton's assertion that the simple single scan approach is preferred even for a stationary target when the scan depth used for correlation is less than 6 [4]. Scan depth beyond 6 is impractical in most realistic target environments where targets can pop

1. for the cases examined in this report

in and out of terrain masking and move in and out of blind velocity doppler cells or eclipsed range cells either inadvertently or intentionally by clever maneuvers. Target maneuvers at 6-g level at a moderate speed would require a large correlation window which results in false alarm rates far greater than the baseline specification if the scan depth used for correlation is larger than 6 as shown in Section 4.3.

CHAPTER 5

PERFORMANCE IMPROVEMENT WITH SCAN RATE REDUCTION AND NONCOHERENT INTEGRATION

The radar range equation was introduced in Section 1.1.2. When the transmitter power P, wavelength at the radar ooperating frequency λ, antenna gain G, target RCS σ, number of pulses for coherent integration N_I and system losses are specified, the SNR in the coherent processing interval (CPI) for a target at range R is proportional to the ratio of the energy received in a single pulse to the noise power density multiplied by the number of pulses coherently integrated. This is indicated by Eqn. (1.1-10). Of course, the number of pulses available for integration in a CPI and the number of CPI's in a given antenna beam direction within a scan is proportional to the dwell time of the antenna beam over a point target. This in turn depends on the frame time T_F.

To resolve the range ambiguity in a high PRF radar, multiple looks with distinct PRF's are required in each beam dwell in a scan. For the radar under consideration, 3 looks are required for the bandwidth chosen. Because of the practical fixed time overhead associated with each slant, it is not beneficial to form more than 3 slants for post detection integration within the given scan rate constraint even

though, in theory, 8 slants with 3 of 8 processing would perform better. A performance comparison of 2 of 2 post detection integration in a 2 slant configuration, and 2 of 3 and 3 of 3 processing in a 3 slant configuration showed that the baseline 3 of 3 post detection integration was a good choice when time overhead, scan rate constraint and range resolution requirements were taken into account. An improvement on the order of 1 dB in equivalent signal-to-noise ratio can be associated with 2 of 2 or 2 of 3 processing when the respective cell false alarm probabilities are adjusted to yield the same level of system false alarms. However, the cost for a 3 fold range ambiguity with these processing options must be weighted in the comparison.

Under a careful examination (see Chapter 4), scan-to-scan processing also failed to show the performance improvement that was hoped for. When the dwell time specification is expressed in terms of the solid angle Ω subtending the search volume and the frame time T_F needed to completely cover the volume once, Eqn. (1.1-14) shows that the SNR for a target at range R is proportional to the power-aperture product independent of the operating frequency. When the power-aperture product is held fixed, it follows that the variation of T_F for a given Ω is the only remaining option for additional performance improvement.

In Section 1.1.3, and in the introduction of Chapter 4, the concept of cumulative detection probability P_c is introduced. Because of the loss associated with target RCS fluctuations, it is explained there that it is more efficient to achieve one or more detections with high probability by using several scans rather than a single scan. According to Barton [4], about 6 scans are optimum for detecting a fluctuating target at $P_c = 0.9$ if the pulses available in a scan are noncoherently integrated. DiFranco and Rubin [2] show that the number is 4 for Swerling case 1 and 2 or 3 for Swerling case 3 when the available pulses in a scan are coherently integrated. These results assume that the change in target range is negligible during the cumulative detection period. In this chapter the optimum frame time needed to maximize the range at which the specified P_c is achieved for a radar with a uniformly scanning antenna is determined for a target approaching with a constant radial velocity.

First, the classical works by Mallett and Brennan [6] and DiFranco and Rubin [2] are examined. Based on their results, a performance test with a slow scan rate ($T_F=50$ seconds) was tried with the consequence that the range was extended at which $P_c = 0.9$. The equivalent sensitivity improvement was 7 to 8 dB. It is very significant that the cumulative detection probability for a low observable target

whose RCS is less than the reference target by 7-8 dB can be detected at the same range as the reference target by increasing the frame time. This is a result of a trade-off between detection and track update. Their work is then extended in this chapter for a high PRF radar application where the frame time affects both the SNR per slant and the system false alarm rate.

Finally, because of the track update requirement, the extension of the frame time is limited to twice that of the baseline. 3 and 6 slant configurations with either the binary or noncoherent post detection integration are then analyzed. The performance relative to P_c = 0.9 is determined for detecting a target within time durations of 60, 20, and 10 seconds. Performance, in terms of track update rate, for targets both in the outer and inner range with respect to the reference range is also examined. With noncoherent integration of 3 slants and slant-to-slant frequency agility, significant improvement is achieved in terms of P_c and track update rate in the outer range. Compared to the baseline, the track update rate suffers degradation in the inner range.

5.1 Scan Rate Optimization

The surveillance radar equation relating SNR to the radar power-aperture product when the surveillance volume Ω and search frame time T_F are specified was presented in Section 1.1.2 as

$$\frac{S}{N} = \frac{P_A \, A \, \sigma \, T_F}{4\pi R^4 \, kT_0 \, NF_0 \, L \, \Omega} \,.$$

(1.1-14)

When the target approach velocity V_R and the desired cumulative detection probability P_C are specified instead of T_F, Eqn. (1.1-14) can be put into a form suitable for scan rate optimization. The optimization is in the sense of maximizing the range at which the specified P_C is achieved. Let R_Z denote the range at which (S/N) becomes unity. Then, setting (S/N) = 1 and $R = R_Z$ in Eqn. (1.1-14) and solving for R_Z gives

$$R_z^4 = \frac{P_A \, A \, \sigma \, T_F}{4\pi \, kT_0 \, NF_0 \, L \, \Omega} \,.$$

(5.1-1)

Let Δ denote the range interval traversed in T_F by a target closing in with a constant radial velocity V_R. The scenario is shown in Figure 5.1-1.
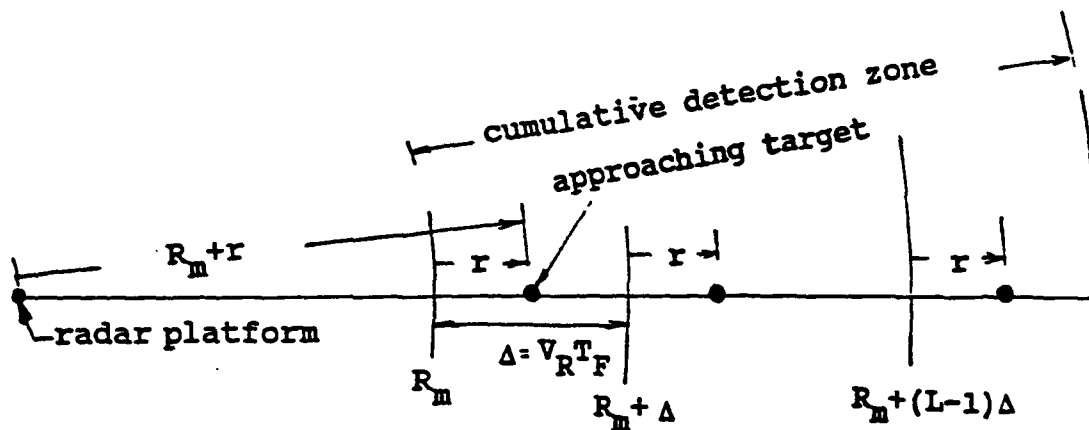
Figure 5.1-1

**Detection Scenario of an Approaching Target with a constant
Radial Velocity**

Note that

$$\Delta = V_R T_F . \qquad\qquad (5.1\text{-}2)$$

Expressing T_F in terms of V_R and Δ from Eqn. (5.1-2) and substituting into Eqn. (5.1-1) yields,

$$R_z^4 = \left(\frac{P_A \; A \; \sigma}{4\pi \; kT_0 \; NF_0 \; L \; \Omega \; V_R}\right) \Delta \; . \qquad\qquad (5.1\text{-}3)$$

Let R_1 be defined such that R_z is expressed in terms of R_1 and Δ by

$$R_z^4 \; \triangle \; R_1^3 \Delta \; . \qquad\qquad (5.1\text{-}4)$$

In terms of R_1, Eqn. (5.1-3) becomes

$$R_1^3 = \frac{P_A \; A \; \sigma}{4\pi \; kT_0 \; NF_0 \; L \; \Omega \; V_R} \; . \qquad\qquad (5.1\text{-}5)$$

R_1^3 represents the fixed set of radar parameters (P_A, A, kT_0, NF_0, L, Ω) and target characteristics (σ, V_R).

For determining the cumulative detection probability, let L denote the number of times a target will be illuminated (i.e., the number of scans) during the period in which it is to be detected one or more times before it reaches the range R_m. The first illumination of the target is assumed to occur in the range ring extending from $R_m + (L-1)\Delta$ to $R_m + L\Delta$. Let $R_m + (L-1)\Delta + r$ denote the range to the target when it is first illuminated where $0 \le r \le \Delta$. By Eqn. (5.1-2), the target will be at the range $R_m + i\Delta + r$ when it is illuminated while in the range ring extending from $R_m + i\Delta$ to $R_m + (i+1)\Delta$; $1=0,--,(L-1)$. The position of the target during each scan when illuminated is indicated in Figure 5.1-1.

Let $P_d(R)$ denote the probability of detecting the target in a single scan at range R. The cumulative detection probability P_c of detecting the target by the final range (R_m+r) is given by

$$P_c = 1-\prod_{i=0}^{L-1} [1-P_d(R_m+r+i\Delta)] \ .$$ (5.1-6)

Assuming r is uniformly distributed between $(R_m, R_m+\Delta)$, the average cumulative detection probability P_c can be written as

$$\overline{P}_c = \frac{1}{\Delta} \int_{R_m}^{R_m+\Delta} \left\{ 1-\prod_{i=0}^{L-1} [1-P_d(R_m+r+i\Delta)] \right\} dr \ .$$ (5.1-7)

Given that the power-aperture product of the radar is fixed, for a specified target velocity V_R and search angle Ω, it is sought to optimize the search frame time T_F so as to maximize R_m, the range by which the target is detected at least once with a probability of 0.9.

Mallett and Brennan [6, 10] normalized all distances in Eqn. (5.1-7) with respect to R_1. For different values of $\overline{P}_c$, they solved Eqn. (5.1-7) by numerical evaluation for all possible pairs of Δ/R_1 and R_m/R_1 while letting L and, hance, the outer range limit get large enough for each trial such that $P_d(R_m+r+(L-1)\Delta)$ becomes negligibly small. For a given

$\bar{P}_c$, the Δ/R_1 which corresponds to the maximum R_m/R_1 is the optimum Δ/R_1. Their result shows, for a given target velocity, that the larger the detection range the longer the frame time should be. Eqn. (5.1-4) can be written as

$$R_z^4 = \Delta R_1^3 = \left(\frac{\Delta}{R_1}\right) R_1^4$$

where

$$R_z = R\big|_{(S/N)_z=1} .$$

In general, the range R is related to R_z by

$$\frac{R^4}{R_z^4} = \frac{(S/N)_z}{(S/N)} = (S/N)^{-1} .$$

As a result, R_m can be expressed as

$$R_m^4 = \frac{\left(\frac{\Delta}{R_1}\right)R_1^4}{\left(\frac{S}{N}\right)_m}$$

where $(S/N)_m$ is the SNR per scan for a target located at R_m. Assuming all the pulses in a beam dwell are coherently integrated, Mallett and Brennan solved numerically for the optimum values of Δ/R_1 and R_m/R_1 for $P_{fa} = 1\times10^{-6}$ for different values of $\bar{P}_c$. The optimum values for $\bar{P}_c = 0.9$ for a Swerling case 1 target are

$$\frac{\Delta}{R_1} = 0.042$$

$$\frac{R_m}{R_1} = 0.155 .$$

Using these optimum values in Eqn. (5.1-2) gives T_F as

$$T_F = \frac{(\Delta/R_l)R_l}{V_R} = \frac{(\Delta/R_l)R_m}{V_R(R_m/R_l)}$$

$$= \frac{0.27R_m}{V_R} . \qquad\qquad (5.1\text{-}8)$$

Typical values for R_m and V_R are 200 nautical miles and 1600 knots, respectively. The optimum frame time according to the above equation is then 121 seconds. This contrasts with the baseline frame time of 10 seconds.

Because the above results suggest that an improvement is possible by slowing down the scan rate, many detection performance trade-off analyses are carried out in this investigation using a frame time longer than that of the baseline and either M of N binary or noncoherent post detection integration as options. The same fixed time overhead as in the baseline is used for each slant and the cell false alarm rate was adjusted so that the system false alarm rate is the same as in the baseline. One sample run with the frame time close to 50 seconds and a post detection processing consisting of 6 slants of signals noncoherently integrated is shown in Figures 5.1-2 and 5.1-3 for the single scan and cumulative detection probabilities, respectively. In this simulation, V_R = Mach 1 was assumed and the maximum range where the cumulative detection process began was 400 nauti
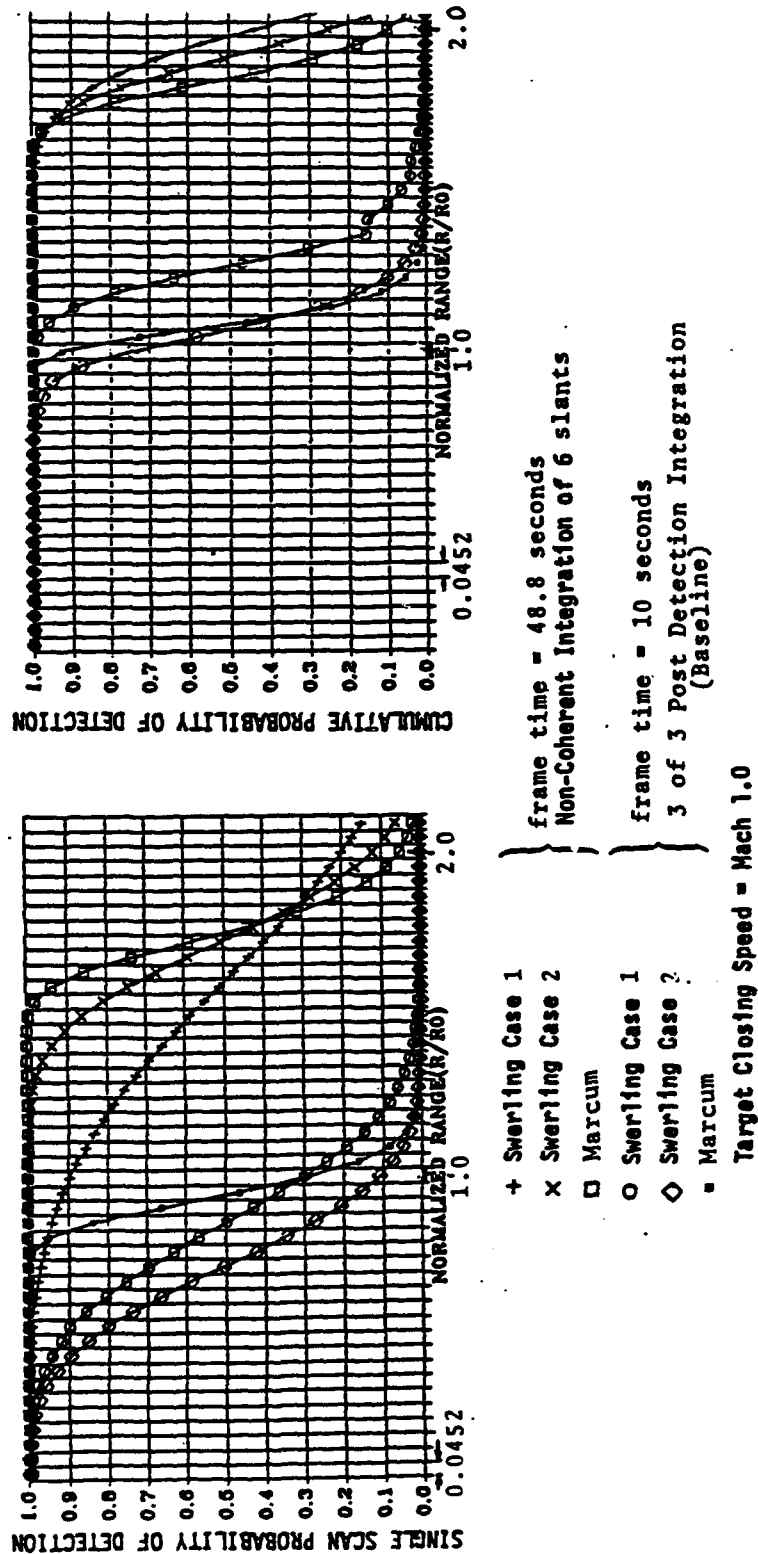
Figure 5.1-2
Single Scan Probability of Detection vs SNR
1.2 RPM Antenna Scan Rate

Figure 5.1-3
Cumulative Probability of Detection vs SNR
1.2 RPM Antenna Scan Rate

+ Swerling Case 1
× Swerling Case 2   } frame time = 48.8 seconds
□ Marcum   Non-Coherent Integration of 6 slants

○ Swerling Case 1
◇ Swerling Case 2   } frame time = 10 seconds
■ Marcum   3 of 3 Post Detection Integration
                                  (Baseline)

Target Closing Speed = Mach 1.0

cal miles. The time limit of 1 minute to achieve the cumulative detection probability was ignored in this case. The cumulative detection probability comparison indicates that a performance improvement equivalent to an increase of approximately 7 to 8 dB SNR is achieved by slowing down the scan rate by a factor of approximately 5. If $\bar{P}_c$ were the only performance criterion, the longer frame time would be very beneficial.

DiFranco and Rubin [2] followed a slightly different approach. For a given R_m, they solved for values of Δ and L which minimize the power-aperture product. To make the solution to Eqn. (5.1-7) more tractable, they let $r = \Delta/2$ and $\bar{R}_i = R_m + \Delta/2 + i\Delta$. It follows that $P_d(R_m + r + i\Delta) = P_d(\bar{R}_i)$. They also normalized Δ such that

$$d = \frac{\Delta}{2R_m} = \frac{V_R T_F}{2R_m} . \tag{5.1-9}$$

Then, carrying out the integration in Eqn. (5.1-7), $\bar{P}_c$ can be approximated as

$$P_c \simeq 1 - \prod_{i=0}^{L-1} (1 - P_d(R_i))$$

$$= 1 - \prod_{i=0}^{L-1} \left[1 - P_d \left\{ R_m[1 + d(2i+1)] \right\} \right] . \tag{5.1-10}$$

Swerling [2, 13] has shown that the detection probability for noncoherent integration of an incoherent pulse train can be approximately expressed as

$$P_d \simeq \begin{cases} \exp(-x) \; ; & \text{for Swerling case 1} \\ (1+2x) \, \exp(-2x) \; ; & \text{for Swerling case 3} \end{cases}$$

where

$$x = f(P_{f_a}, \; N_I)/\mathfrak{R}_p$$

and $\mathfrak{R}_p$ is the expected peak SNR per pulse. Let R_2 be the range at which $x = 1 = f(P_{f_a}, \; N_I)/(\mathfrak{R}_p)_2$. Then, from the radar range equation

$$\frac{\mathfrak{R}_p}{(\mathfrak{R}_p)_2} = \left(\frac{R_2}{R}\right)^4 ,$$

and

$$\mathfrak{R}_p = (\mathfrak{R}_p)_2 \left(\frac{R_2}{R}\right)^4 = f(P_{f_a}, \; N_I)\left(\frac{R_2}{R}\right)^4 .$$

Consequently, x can be expressed as

$$x = f(P_{f_a}, \; N_I)/\mathfrak{R}_p = \left(\frac{R_2}{R}\right)^{-4} = \left(\frac{R}{R_2}\right)^4 .$$

With the above identity, P_d is approximately given by

219

$$P_d \simeq \begin{cases} \exp\left[-\left(\dfrac{R}{R_2}\right)^4\right] & \text{; for Swerling case 1} \\ \\ \left[1+2\left(\dfrac{R}{R_2}\right)^4\right]\exp\left[-2\left(\dfrac{R}{R_2}\right)^4\right] & \text{; for Swerling case 3 .} \end{cases} \qquad (5.1\text{-}11)$$

DiFranco and Rubin substitute Eqn. (5.1-11) into Eqn. (5.1-10) to obtain the following expression for $\bar{P}_c$:

$$\bar{P}_c = 1 - \prod_{i=0}^{L-1} \left\{ 1 - \left[1+2\left(\frac{R_m}{R_2}\right)^4 \right]\left(1+d(2i+1)\right)^4 \right]^{l-1} \right.$$
$$\left. \cdot \exp[-l\left(\frac{R_m}{R_2}\right)^4 (1+d(2i+1))^4] \right\} \qquad (5.1\text{-}12)$$

where $l=1$ and $l=2$ applies to Swerling case 1 and 3, respectively.

Note that Eqn. (1.1-14) can be rearranged to obtain an expression for the power-aperture product. Substituting

$$\frac{S}{N} = f(P_{fa}, N_I)\left(\frac{R_2}{R_m}\right)^4 \left(\frac{N_I}{2}\right) = k_1\left(\frac{R_2}{R_m}\right)^4, \quad T_F = \frac{\Delta}{V_R}\frac{2R_m d}{V_R}, \quad \text{and} \quad R = R_m$$

into Eqn. (1.1-14), where k_1 is a constant, and rearranging for $P_A A$ yields

$$P_A A = \frac{k_1 (R_2/R_m)^4 4\pi R_m^4 k T_0 N F_0 L \Omega}{\sigma(2R_m d/V_R)}$$

$$= \left[\frac{k_1 2\pi k T_0 N F_0 L \Omega V_R R_m^3}{\sigma d} \right] \left(\frac{R_2}{R_m} \right)^4$$

$$= k_2 \frac{(R_2/R_m)^4}{d} \qquad\qquad (5.1\text{-}13)$$

where all of the terms in coefficient k_2 are constants that must be specified for a search radar.

For a specified R_m, DiFranco and Rubin find values of d and L which satisfy Eqn. (5.1-12) for a specified $\bar{P}_C$ and also minimize $P_A A$ in Eqn. (5.1-13). Their steps are:

1. For a specified $\bar{P}_C$, select values of d and L, L=1, 2, 3, --, and solve Eqn. (5.1-12) for R_2/R_m. A plot of R_2/R_m, as a function of d, is generated for each integer value of L.

2. For each value of L, solve Eqn. (5.1-13) for $P_A A$ using pairs of d and R_2/R_m as obtained from step 1. A plot of $P_A A$ as a function of d is then plotted for each value of L.

3. Select that pair of values for L an d which yields the minimum value of $P_A A$.

Minimizing the power-aperture product for a specified R_m is equivalent to maximizing R_m for a specified

221

power-aperture product. It follows that the values of L and d which yield a minimum power-aperture product for a specified R_m also result in a maximum value of R_m when that minimum power-aperture is specified. The system frame time is then given by

$$T_F = \frac{2R_m d}{V_R} .$$
(5.1-14)

Their results show that the approximate optimum frame time and the number of scans to achieve the required $\bar{P}_C$ are such that the cumulative detection zone is equal to R_m. In particular,

$$LV_R T_F = R_m .$$
(5.1-15)

That is, the detection zone is equal to the minimum detection range. Thus, once the optimum L is known, the optimum T_F follows. From the work of DiFranco and Rubin the optimum L for different $\bar{P}_C$ levels are given in Table 5.1-1.

Table 5.1-1 Optimum L for the P_C Level Specified

	$\bar{P}_C = 0.9$	$\bar{P}_C = 0.95$	$\bar{P}_C = 0.99$
Swerling 1	4	5	6
Swerling 3	2	3	4

Returning to the previous example where $\overline{P}_c=0.9$, $R_m=200$ nautical miles and $V_R=1600$ knots, the optimum T_F becomes

$$T_F = \frac{R_m}{V_R L} = \frac{(200)(3600)}{(1600)(4)} = 112.5 \text{ seconds} .$$

This is almost the same result as obtained earlier using the Mallett and Brennan approach.

Both the Mallett and Brennan and DiFranco and Rubin teams assume that there is no radar line of sight limit and, therefore, L can be as large as necessary. Also, without stating it, the radar is assumed to be operating in a low PRF mode so that the time overhead, assuming it is entirely due to the round trip transit time for the radar wave with respect to the target at the maximum range of interest, does not affect the division of the available radar energy into M number of slants and L number of scans.

In the next section, scan rate optimization is carried out for a high PRF radar. To effectively utilize the various slants needed to resolve the range ambiguity associated with the high PRF radar under consideration, post detection processing, either an M of N binary integration where $M \geq 3$ or a noncoherent integration where $N \geq 3$ is required in each scan. Unlike the low PRF radar studied by others,

in a high PRF radar, there is a fixed time overhead associated with each of the N slants and L scans which includes one round trip transit time for the entire pulse group in a slant. This affects in a nonlinear way the SNR and cell false alarm probability and complicates determination of the optimum frame time. Imposing a line of sight limitation or time constraint in achieving the stated P_c further complicates the problem.

5.2 Scan Rate Optimization for a High PRF Radar

In this Section, scan rate optimization for a high PRF radar is carried out by extending the work of the Mallett and Brennan team. The extension is in the form of taking into account the effect of a fixed time overhead on the coherent integration gain and the cell false alarm probability allocation as a function of antenna scan rate. As the scan rate decreases, it will be shown that the variation in detection performance due to the fixed time overhead can be ignored once the coherent integration gain and the cell false alarm probability allocation in a multi-slant system are properly assigned taking into account the effect of the fixed time overhead for the particular post detection integration chosen at its maximum antenna scan rate assumed. The procedures for computing integration gain, allocating the false alarm probability, and translating these to the single scan detection probability after the post detection integration are developed in Chapters 2 and 3.

To take into account the effect of the fixed time overhead, the following reference parameters for the baseline system are introduced:

T_{F_0} = frame time in the baseline

$$V_{R_0} = 450 \text{ knots}$$

$$\Delta_0 = T_{F_0} V_{R_0} .$$

The optimization is carried out for the 3 of 3 post detection integration scheme as used in the baseline. Let T_H denote the fixed time overhead. In the baseline with

$$T_{F_0} = 10 \text{ seconds}$$

and

$$T_H = 0.52 \ T_m ,$$

where T_m is the time duration of a modulation period, an increase in dwell time proportional to an increase in T_{FO} by a factor of c_1 results in an increase in SNR per slant by the ratio, c_2, as given by

$$c_2 = \frac{(c_1 - T_H/T_m)T_m}{(1 - T_H/T_m)T_m} .$$

Consequently, Eqn. (1.1-14) is modified to read

$$\left(\frac{S}{N}\right) = c_2 \frac{P_A \ A \ \sigma \ T_{F_0}}{4\pi \ R^4 \ kT_0 \ NF_0 \ L\Omega} .$$

As before, let R_z denote the range at which (S/N) becomes unity. Recalling that $T_{FO} = \Delta_0/V_{RO}$, it follows that

$$R_z^4 = c_2 \frac{P_A \ A \ \sigma}{4\pi \ kT_0 \ NF_0 \ L \ \Omega \ V_{R_0}} \Delta_0 = c_2 \ R_1^3 \ \Delta_0$$

$$= R_1^3 \frac{(c_1 - T_H/T_m)}{(1 - T_H/T_m)} \Delta_0 . \qquad (5.2\text{-}1)$$

Substitution of $T_H/T_m = 0.52$ in the above equation yields

$$R_2^4 = R_1^4 \frac{(1-0.52/c_1)}{0.48} \left(\frac{c_1 \Delta_0}{R_1} \right) . \qquad (5.2\text{-}2)$$

Since $\Delta = c_1 \Delta_0$, Eqn. (5.1-4) can be written as

$$R_2^4 = R_1^3 c_1 \Delta_0 = R_1^4 \left(\frac{c_1 \Delta_0}{R_1} \right) . \qquad (5.1\text{-}4)$$

Note that Eqn. (5.2-2) differs from Eqn. (5.1-4) only by the factor of

$$\frac{c_2}{c_1} = \left(\frac{1-0.52/c_1}{0.48} \right) .$$

Hence, the range at which SNR becomes unity is extended by the factor of c_2/c_1.

To correct for the cell false alarm probability change as a result of an increased dwell time, note that, once the cell false alarm probability corresponding to the system false alarm rate specification has been determined, the cell false alarm probability is affected only by the time utilization factor K_1 according to Eqn. (2.5-25). The effect of this change on R_z depends on the particular post detection integration chosen.

The detection probability after post detection integra-

tion for Swerling case 1 and 3 targets is given in Section 3.2 as

$$P_d = \int_0^\infty P_d'(M,N) \; p(S_0/N) d(S_0/N) \; . \tag{3.2-7}$$

This is in the same form as Eqn. (3.2-12), the single slant detection probability before post detection integration for Swerling case 2 and 4 targets. For Swerling case 2, p_{di} is given by

$$\bar{P}_{di} = \exp\left(\frac{\ln p_f}{1+(S/N)_i}\right) \; . \tag{3.2-13}$$

Therefore, for a Swerling case 1 target we try for the purpose of approximating Eqn. (3.2-7) an equation of the form

$$P_d = \exp\left[\frac{\ln P_{fa}}{c_4(1+(\bar{S}_0/N))}\right] \tag{5.2-3a}$$

where P_{fa}, the cell false alarm probability after 3 of 3 post detection integration, is given by

$$P_{fa} = p_f^3$$

and $(\bar{S}_0/N)$ is the signal-to-noise ratio per CPI if all the pulses are received through the antenna beam at its peak gain. Taking the natural logarithm of Eqn. (5.2-3a) and re-

230

arranging yields

$$c_4 \left[1 + \left(\frac{\bar{S}_0}{N} \right) \right] = \frac{\ln p_f^3}{\ln P_d} .$$

(5.2-3b)

The value of c_4 can be obtained from Eqn. (5.2-3b) and a point from a P_d versus $(\bar{S}_0/N)$ plot for a given value of p_f. Referring to Figure 3.3-3, the following values for two points, each for two different values of p_f, are read off from the plots of P_d versus $(\bar{S}_0/N)$ for Swerling case 1 after 3 of 3 post detection integration .

	$(\bar{S}_0/N)$ @ $P_d=0.3$	(S_0/N) @ $P_d=0.5$
@ $p_f=7.6 \times 10^{-4}$	15.85 (12.00 dB)	28.31 (14.52 dB)
@ $p_f=7.6 \times 10^{-5}$	20.61 (13.14 dB)	36.64 (15.64 dB)

For $p_f=7.6 \times 10^{-4}$, substitution of $(\bar{S}_0/N)=15.85$ and $P_d=0.3$ into Eqn. (5.2-3b) gives $c_4=1.062$. Inserting this value of c_4 and $(\bar{S}_0/N)=28.31$ into Eqn. (5.2-3a) yields $P_d=0.5$. This agrees with the plot of Figure 3.3-3 which is obtained by numerical integration. Trying still other values of $(\bar{S}_0/N)$ for $p_f=7.6 \times 10^{-4}$ reveals that Eqn. (5.2-3a) is an excellent approximation for P_d as a function of (S_0/N) and p_f. However, a different value of c_4 is required for each value of p_f. The value of c_4 corresponding to $p_f=7.6 \times 10^{-5}$ is 1.0935.

Since what is sought is an approximate equation for interpolation between two values of $(\widetilde{S}_0/N)$ at a given value of P_d due to a change in p_f, an expression that is slightly different from Eqn. (5.2-3b) which is less sensitive to changes in p_f is tried. The equation is of the form:

$$P_d \simeq c_5 \exp\left[\frac{\ln P_{fa}}{1+(S_0/N)}\right] . \qquad (5.2\text{-}3c)$$

Associating points from the plots of Figure 3.3-3 with the corresponding terms in Eqn. (5.2-3c), the value of c_5 corresponding to $p_f = 7.6 \times 10^{-4}$ and $p_f = 7.6 \times 10^{-5}$ at a P_d level of 0.3 becomes 1.078 and 1.119, respectively. Using the average of these two values for c_5 in Eqn. (5.2-3c) is found to give accurate results relating changes in p_f to the corresponding changes in $(\widetilde{S}_0/N)$ for a fixed value of P_d over a range of change in p_f by a factor of 10. This relationship can be expressed as

$$P_d \simeq c_5 \exp\left[\frac{\ln (p_{f1})^3}{1 + (S_0/N)_1}\right] = c_5 \exp\left[\frac{\ln (p_{f2})^3}{1 + (S_0/N)_2}\right]$$

Dividing both sides of the above equation by c_5 and taking a natural logarithm gives

$$\left[\frac{\ln(p_{f_1})^3}{1+(S_0/N)_1}\right] = \left[\frac{\ln(p_{f_2})^3}{1+(S_0/N)_2}\right]$$

or

$$\frac{\ln(p_{f_1})^3}{\ln(p_{f_2})^3} = \frac{\ln P_{fa_1}}{\ln P_{fa_2}} = \frac{1+(S_0/N)_1}{1+(S_0/N)_2} \simeq \frac{(S_0/N)_1}{(S_0/N)_2} , \text{ for } (\overline{S}_0/N)_1, (\overline{S}_0/N)_2 \gg 1 . \quad (5.2\text{-}3)$$

Note from Eqn. (2.5-25) that the ratio of false alarm probabilities after 3 of 3 post detection integration equals the inverse of the ratio of time utilization factors. Since the optimization is to determine how much to slow down the antenna scan rate with respect to the scan rate in the baseline, p_f must be reduced to maintain the same system false alarm rate as the scan rate is reduced and, therefore, the time utilization factor is increased.

In the vicinity of $(\overline{S}_0/N) = 12.2$ dB and $p_f = 7.6 \times 10^{-4}$, a decrease in p_f by a factor of 10 results in a corresponding decrease in the detection probability. This is equivalent to maintaining p_f at 7.6×10^{-4} and reducing SNR by 1.2 dB, a factor of approximately 1.32 as can be seen in Figure 3.3-3. Another way of putting it is that an increase in SNR by a factor of 1.32 is required to maintain the P_d level the same as before. This can be verified by substituting these p_f values into Eqn. (5.2-3).

As mentioned previously, the ratio of false alarm probabilities after 3 of 3 post detection integration equals the

inverse of the ratio of time utilization factors. Note that c_2 is equal to the ratio of time utilization factors. Substitution of $(1/c_2)$ for (P_{fa_2}/P_{fa_1}) in Eqn. (5.2-3) yields

$$\frac{\ln P_{fa_1}}{\ln (\frac{1}{c_2} P_{fa_1})} \simeq \frac{(S_0/N)_1}{(S_0/N)_2} \Delta c_3 . \qquad (5.2\text{-}4)$$

For values of c_1 equal to 1.1 and 10, the values of c_2 are 1.098 and 1.975, respectively. The corresponding values of c_3 are 0.996 and 0.969. These values are the ratios by which SNR is effectively reduced. Or equivalently, SNR must be increased by the inverse of these values to maintain the original level of P_d. Thus, it is seen that once the cell false alarm probability is determined for the particular post detection integration according to the procedure established in Section 2.4, the false alarm probability change as a consequence of an increase in dwell time has a small effect on the SNR. Hence, as a first approximation, it can be ignored in the scan rate optimization using 3 of 3 post detection integration. The effect of time overhead on other post detection integration can be determined in the same way.

When the dwell time is increased by a large factor, the time overhead becomes a negligible portion of the modulation period. Returning to Eqn. (5.2-2), note that

234

$$\lim_{c_1 \to \infty} \left(\frac{1 - 0.52/c_1}{0.48} \right) = 2.08 \ .$$

Its impact on R_z is $(2.08)^{1/4} = 1.2$ in the limit. This represents a 20 % increase in the detection range. However, the maximization peaks are very broad. As a result, this factor can be dropped for simplicity from Eqn. (5.2-1). Even so, the effect of time overhead in the multi-slant processing is included in evaluation of the detection and false alarm probabilities for a specified post detection integration.

With respect to Eqn. (5.1-10) for $\overline{P}_c$, all range units are normalized by R_1 which includes all fixed radar and target parameters. Note that $P_d(\overline{S}_0/N)$ can be converted to $P_d(R/R_z)$ by using the relationship

$$\left(\frac{R}{R_z} \right)^4 = \frac{(S_0/N)_z}{(S_0/N)} \ .$$

Using Eqn. (5.1-4) R/R_z can be converted to R/R_1 once Δ/R_1 is specified:

$$\left(\frac{R}{R_z} \right)^4 = \left(\frac{R}{R_1} \right)^4 \frac{1}{(\Delta/R_1)}$$

and

$$\left(\frac{R_1}{R_z} \right)^4 = \frac{1}{(\Delta/R_1)} = \frac{1}{(S_0/N)_1} \ .$$

Hence, when $R = R_1$,

$$(S_0/N)_1 = \frac{\Delta}{R_1} \ .$$

The above conversion allows the computation of P_d as a function of the normalized range, R/R_1. A set of values for $P_d(R/R_1)$ is computed according to the procedure outlined in Chapter 3 for the normalized range increment, Δ/R_1, ranging from 0.01 to 0.1. $\bar{P}_c(R/R_1)$ is then computed for each value of the normalized range increment chosen. From a set of these values, the optimum Δ/R_1 and the corresponding R_m/R_1 are selected for $\bar{P}_c = 0.9$.

These optimum values for $\bar{P}_c = 0.9$ are listed in Table 5.2-1 for Swerling case 1 through 4 and Marcum target models.

Table 5.2-1

Optimum Values Δ/R_1 and the Corresponding Values of
R_m/R_1 - 3 of 3 Post Detection Integration

$$\bar{P}_c = 0.9; \quad P_{fa} = 4.39 \times 10^{-10}$$

| | Swerling case | | | | Marcum nonfluctuating |
	1	2	3	4	
Δ/R_1	0.050	0.058	0.060	0.080	0.078
R_m/R_1	0.157	0.132	0.171	0.171	0.223

236

The optimum values derived by Mallett and Brennan are listed in Table 5.2-2 for $\bar{P}_c = 0.9$ for easy comparison.

Table 5.2-2

Optimum Values Δ/R_1 and the Corresponding Values of R_m/R_1 by Mallett and Brennan

$$\bar{P}_c = 0.9; \quad P_{fa} = 1\times10^{-6}$$

| | Swerling case | | | | Marcum |
	1	2	3	4	nonfluctuating
Δ/R_1	0.042	---	0.053	---	0.080
R_m/R_1	0.155	---	0.169	---	0.196

Note that the referenced values assume a single slant system for which computation of P_d is fairly straightforward. It should be observed that in a single slant system there is no difference between a Swerling case 1 and a Swerling case 2 (nor a Swerling case 3 and a Swerling case 4). Hence, their result does not show values for Swerling cases 2 and 4. Still, the optimum values determined here for a system with a particular post detection integration are found to be very close to the corresponding values found by Mallett and Brennan even though they are evaluated at different false alarm probabilities. Therefore, performance improvement based on cumulative detection probability at a level of 0.9

237

for a radially approaching target with a speed of Mach 1 can be 7-8 dB as shown by an example in Section 5.1 when the antenna scan rate is reduced by a factor of approximately 5. In this example, note that the one minute time constraint is not observed. Instead, the outer boundary of the cumulative detection zone is taken as 400 nautical miles.

5.3 Detection Probability with Noncoherent Integration in Lieu of Binary Integration

The Bayes likelihood ratio test for detecting targets based on noncoherent integration of multiple observations in white Gaussian noise is discussed in <u>Radar Detection</u> by DiFranco and Rubin [2]. Specific forms of integral expressions for the probabilities of detection resulting from binomial post detection integration were derived and presented in Chapter 3. The integral expressions describing the probability of false alarm and probabilities of detection under noncoherent integration are summarized below following the work by Difranco and Rubin.

The optimum receiver structure in the region of small signal-to-noise ratio is the matched filter for each pulse followed by a square law detector and a noncoherent summer or a video integrator for all four Swerling cases and Marcum target models. Let Y denote the sufficient statistic. The sufficient statistic, Y, is one half the sum of the square of the envelop voltage r_i,

$$Y = \sum_{i=1}^{N} (1/2) r_i^2 \qquad (5.3-1)$$

where N is the number of observation samples noncoherently integrated. For the kth doppler cell, note that the DFT coefficient X(k) which arises from an N_I-point FFT constitutes a single sample for the noncoherent integration.

In the absence of the signal, the probability density of Y under hypothesis 0 (target absent) assumes the form,

$$p(Y|0) = \begin{cases} Y^{N-1} e^{-Y} / (N-1)!, & Y \geq 0 \\ 0, & Y < 0. \end{cases} \qquad (5.3-2)$$

This is a chi-square density with 2N degrees of freedom. It arises because Y is the sum of 2N statistically independent squared Gaussian random variables. That is, it is the sum of N pairs of squared in-phase and quadrature Gaussian noise components each having zero mean and unit variance (i.e., normalized). Thus, the probability of false alarm is given by

$$P_{fa} = 1 - \int_{0}^{Y_b} Y^{N-1} e^{-Y}/(N-1)! \, dY = 1 - I(Y_b/\sqrt{N}, N-1). \qquad (5.3-3)$$

where Y_b is the threshold and $I(u,s)$ is the incomplete gamma function defined by

$$I(u,s) = \int_{0}^{u\sqrt{1+s}} (e^{-v} v^{s}/s!) \, dv.$$

The probability of detection is given by

$$P_d = \int_{Y_b}^{\infty} p(Y|1) \, dY \qquad (5.3-4)$$

where $p(Y|1)$ is the probability density of Y for $Y \geq 0$ under hypothesis 1 (target present) with peak SNR per pulse, $\mathcal{R}_p$. The relationship of the peak SNR to the envelope amplitude A, and the probability densities of A and $\mathcal{R}_p$ for Marcum and Swerling target models were given in Section 2.6.

240

The probability density of Y, $p(Y|1)$, and the probability of detection for Marcum (nonfluctuating) and Swerling target models are:

Marcum (nonfluctuating)

for $Y \geq 0$

$$p(Y|1) = (2Y/N\mathcal{R}_p)^{(N-1)/2} \, e^{-Y-N\mathcal{R}_p/2} \, I_{N-1}(\sqrt{2N\mathcal{R}_p Y}), \quad (5.3-5)$$

$$P_d = 1 - \int_0^{Y_b} (2Y/N\mathcal{R}_p)^{(N-1)/2} \, e^{-Y-N\mathcal{R}_p/2} \, I_{N-1}(\sqrt{2N\mathcal{R}_p Y}) \, dY$$

$$= 1 - T_{\sqrt{Y_b}} (2N-1, N-1, \sqrt{N\mathcal{R}_p/2}). \quad (5.3-6)$$

$I_{N-1}(x)$ is the modified Bessel function of the first kind, order N-1 and $T_B(m,n,r)$ is the incomplete Toronto function,

$$T_B(m,n,r) = 2r^{n-m+1} \, e^{-r^2} \int_0^B t^{m-n} \, e^{-t} \, I_n(2rt) \, dt.$$

Swerling case 1

for $Y \geq 0$

$$p(Y|1) = \frac{(1 + 1/N\overline{\mathcal{R}}_p/2)^{N-2} \, e^{-Y/(1+N\overline{\mathcal{R}}_p/2)}}{N\overline{\mathcal{R}}_p/2}$$

$$\cdot I[\frac{Y}{\sqrt{N-1}(1+1/N\overline{\mathcal{R}}_p/2)}, \, N-2], \quad (5.3-7)$$

241

$$P_d = 1 - I(Y_b/\sqrt{N-1}, N-2) + (1+1/N\bar{\mathcal{R}}_p/2)^{N-1} e^{-Y_b/(1+N\bar{\mathcal{R}}_p/2)}$$

$$\cdot I[Y_b/(\sqrt{N-1}(1+1/N\bar{\mathcal{R}}_p/2)), N-2]. \qquad (5.3-8)$$

Swerling case 2

for $Y \geq 0$

$$p(Y|1) = 1/(1+\bar{\mathcal{R}}_p/2)^N [1/(N-1)!] Y^{N-1} e^{-Y/(1+\bar{\mathcal{R}}_p/2)}, \qquad (5.3-9)$$

$$P_d = 1 - \int_0^{Y_b/(1+\bar{\mathcal{R}}_p/2)} (x^{N-1} e^{-x})/(N-1)! dx$$

$$= 1 - I[Y_b/(\sqrt{N}(1+\bar{\mathcal{R}}_p/2)), N-1]. \qquad (5.3-10)$$

Swerling case 3

for $Y \geq 0$

$$p(Y|1) = \frac{(1+1/N\bar{\mathcal{R}}_p/4)^{N-2}}{(1+N\bar{\mathcal{R}}_p/4)^2} Y e^{-Y/(1+N\bar{\mathcal{R}}_p/4)}$$

$$\cdot I[(Y/(1+1/N\bar{\mathcal{R}}_p/4)\sqrt{N-1}), N-2]$$

$$- \frac{(N-2)(1+1/N\bar{\mathcal{R}}_p/4)^{N-1}}{(1+N\bar{\mathcal{R}}_p/4)^2} e^{-Y/(1+N\bar{\mathcal{R}}_p/4)}$$

$$\cdot I[(Y/(1+1/N\bar{\mathcal{R}}_p/4)\sqrt{N-1}), N-2] + \frac{Y^{N-1} e^{-Y}}{(N-1)!(1+N\bar{\mathcal{R}}_p/4)^2},$$

$$(5.3-11)$$

242

$$P_d = \int_{Y_b}^{\infty} p(Y) \, dY.$$

Swerling 4

for $Y \geq 0$

$$p(Y|1) = \frac{Y^{N-1} \, e^{-Y/(1+\bar{\mathscr{R}}_p/4)} \, N!}{(1+\bar{\mathscr{R}}_p/4)^{2N}} \sum_{k=0}^{N} \left((\bar{\mathscr{R}}_p/4)/(1+\bar{\mathscr{R}}_p/4) \right)^k$$

$$\cdot \frac{Y^k}{k! \, (N+k-1)! \, (N-k)!}, \qquad (5.3\text{-}12)$$

$$P_d = 1 - N!/(1+\bar{\mathscr{R}}_p/4)^N \sum (\bar{\mathscr{R}}_p/4)^k \frac{I[(Y_b/(1-\bar{\mathscr{R}}_p/4)\sqrt{N+k}), N+k-1]}{k! \, (N-k)!}. \qquad (5.3\text{-}13)$$

Numerical integration of above equations is used in Section 5.4 to determine the threshold and probabilities of detection under noncoherent integration.

243

5.4 Probabilities of Detection with Slower Scan Rate

In this section, M of N binary post detection integration is compared with noncoherent integration (NCI) along with a 2 to 1 increase in dwell time as a means for detection enhancement. The 2 to 1 increase in dwell time is achieved by reducing the antenna scan rate by a factor of 2. Enhancement options examined include slant-to-slant frequency agility and back-to-back antennas. When used, the back-to-back antennas are assumed to be switched to the single receiver/ transmitter one at a time every 180 degree rotation of the rotodome so that the azimuth coverage is reduced from 360 to 180 degrees and the same 180 degree azimuth sector is covered with twice the dwell time. It was shown in Section 5.1 and 5.2 that scan rate optimization called for a considerably slower scan rate. Reduction of the scan rate by more than a factor of 2, however, is prevented by track update considerations for near-in targets. For post detection integration, it is well known that noncoherent integration is more efficient than binary integration. Only recent advances in signal processing hardware make it feasible to implement NCI in a high PRF radar.

The single scan detection probabilities for 3 of 3, and 3 of 6 post detection binary integration, and noncoherent in-

tegration with 3 and 6 observation samples, all within the same false alarm time constraints but with the antenna scan rate at 3 rpm, are first determined for the Swerling case 1, 2, and Marcum target models. The false alarm constraint is such that the system false alarm rate is 2 or less in a 10 second interval on the average. It should be noted that Swerling case 2 results apply to Swerling case 1 when slant-to-slant frequency agility is used in the radar operation. Under this condition, Swerling case 1 is transformed to Swerling case 2. The single scan detection probabilities for the four processing options are plotted for the Swerling case 1, 2 and Marcum target models in Figures 5.4-1 through 5.4-4. The numerical results with the same processing options for Swerling case 1 and 2 along with the baseline performance are also shown in Table 5.4-1. For generating these results, an average beam shape loss is used for all cases, first, to facilitate the detection probability evaluation with NCI where equal signal-to-noise ratios are assumed for all samples, and second, to generate results on the same basis for all processing options considered.

The same reference target located at the reference range, as was used previously, is employed in this chapter for establishing the reference SNR for the particular processing configuration. For the baseline 3-slant configuration with a

SNR VS. PROBABILITY OF DETECTION

3 NONCOHERENT INTEGRATION @ 3 RPM
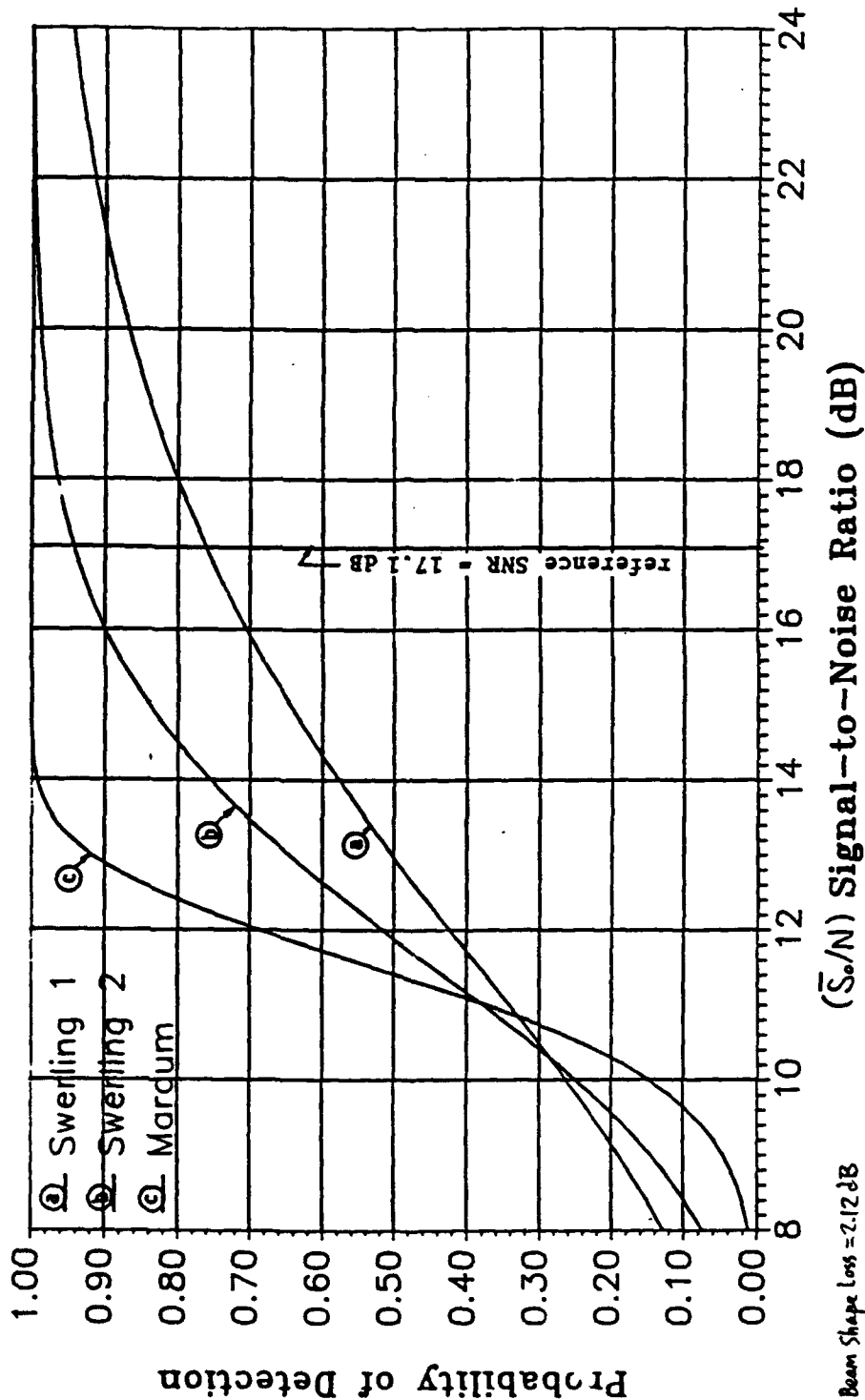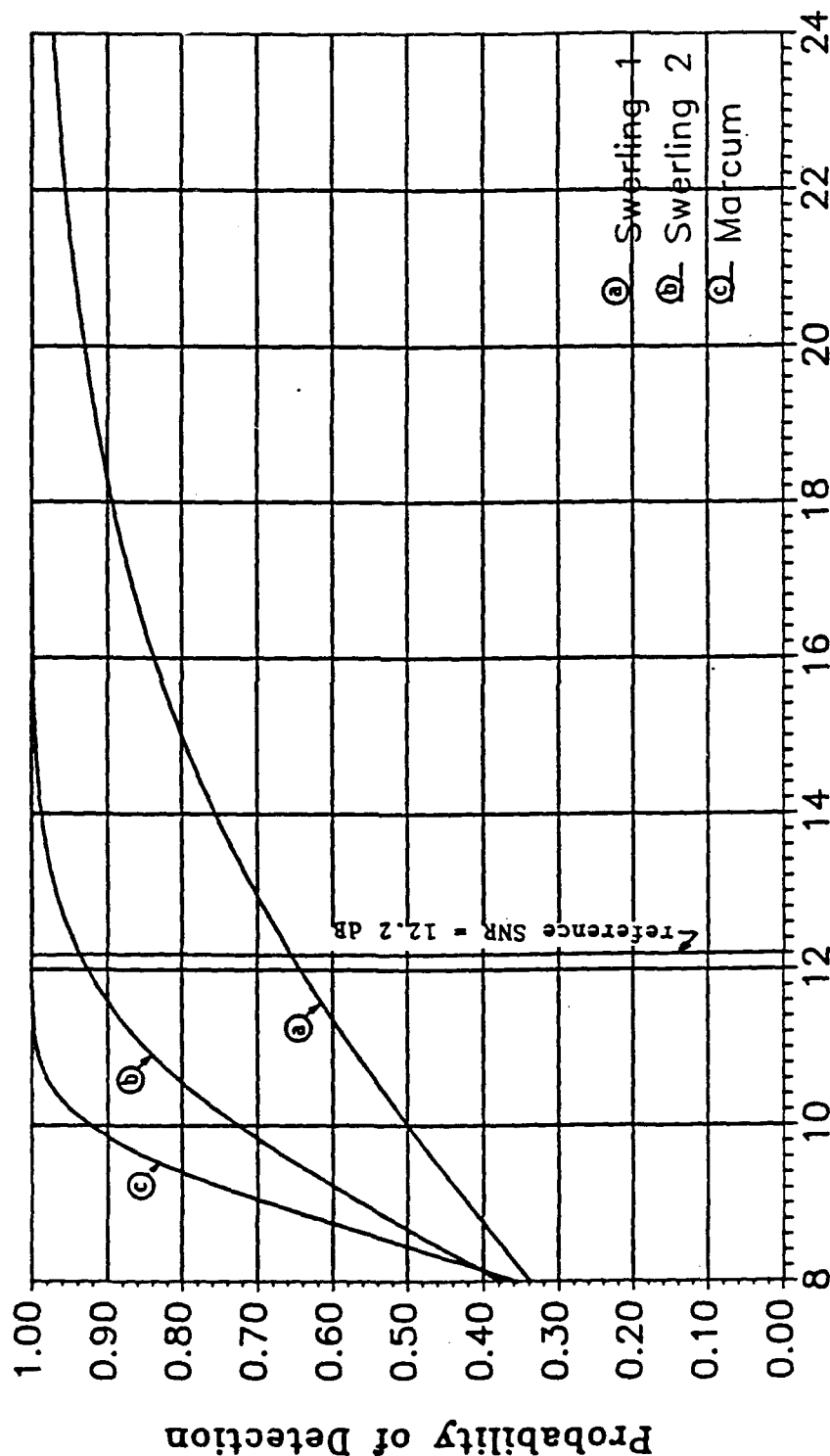NORMAL TIME OVERHEAD (5 MILLISEC)

ⓐ Swerling 1
ⓑ Swerling 2
ⓒ Marcum

reference SNR = 17.1 dB

Beam Shape Loss = 2.12 dB

Probability of Detection

1.00
0.90
0.80
0.70
0.60
0.50
0.40
0.30
0.20
0.10
0.00

8   10   12   14   16   18   20   22   24

$(\bar{S}_o/N)$ Signal-to-Noise Ratio (dB)

Figure 5.4-1. SNR vs. Probability of Detection, 3-NCI @ 3 rpm,
Normal Time Overhead

SNR VS. PROBABILITY OF DETECTION

@ NONCOHERENT INTEGRATION @ 3 RPM
NORMAL TIME OVERHEAD (5 millisec)

Beam Shape Loss = 1.6 dB

reference SNR = 12.2 dB

ⓐ Swerling 1
ⓑ Swerling 2
ⓒ Marcum

Probability of Detection

$(\bar{S}_o/N)$ Signal-to-Noise Ratio (dB)

Figure 5.4-2. SNR vs. Probability of Detection, 6-NCI @ 3 rpm,
Normal Time Overhead

247

SNR VS. PROBABILITY OF DETECTION

3 OF 3 PROCESSING @ 3 RPM
NORMAL TIME OVERHEAD (5 millisec)

Probability of Detection

$(\bar{S}_o/N)$ Signal-to-Noise Ratio (dB)

- ⓐ Swerling 1
- ⓑ Swerling 2
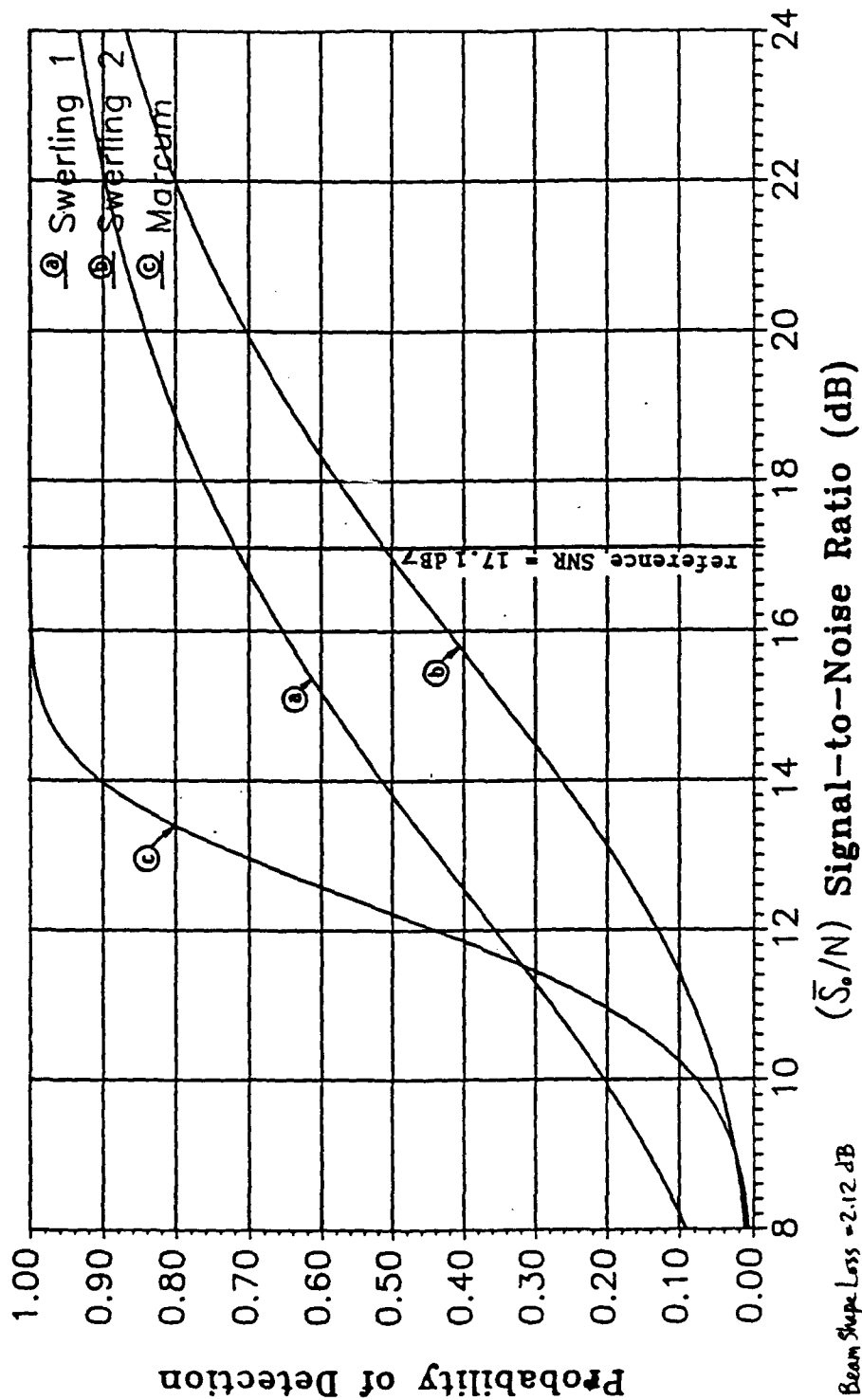- ⓒ Marcum

reference SNR = 17.1 dB?

Beam Shape Loss = 2.12 dB

Figure 5.4-3. SNR vs. Probability of Detection, 3 of 3 Processing @ 3 rpm, Normal Time Overhead

SNR VS. PROBABILITY OF DETECTION

3 OF 6 PROCESSING @ 3 RPM
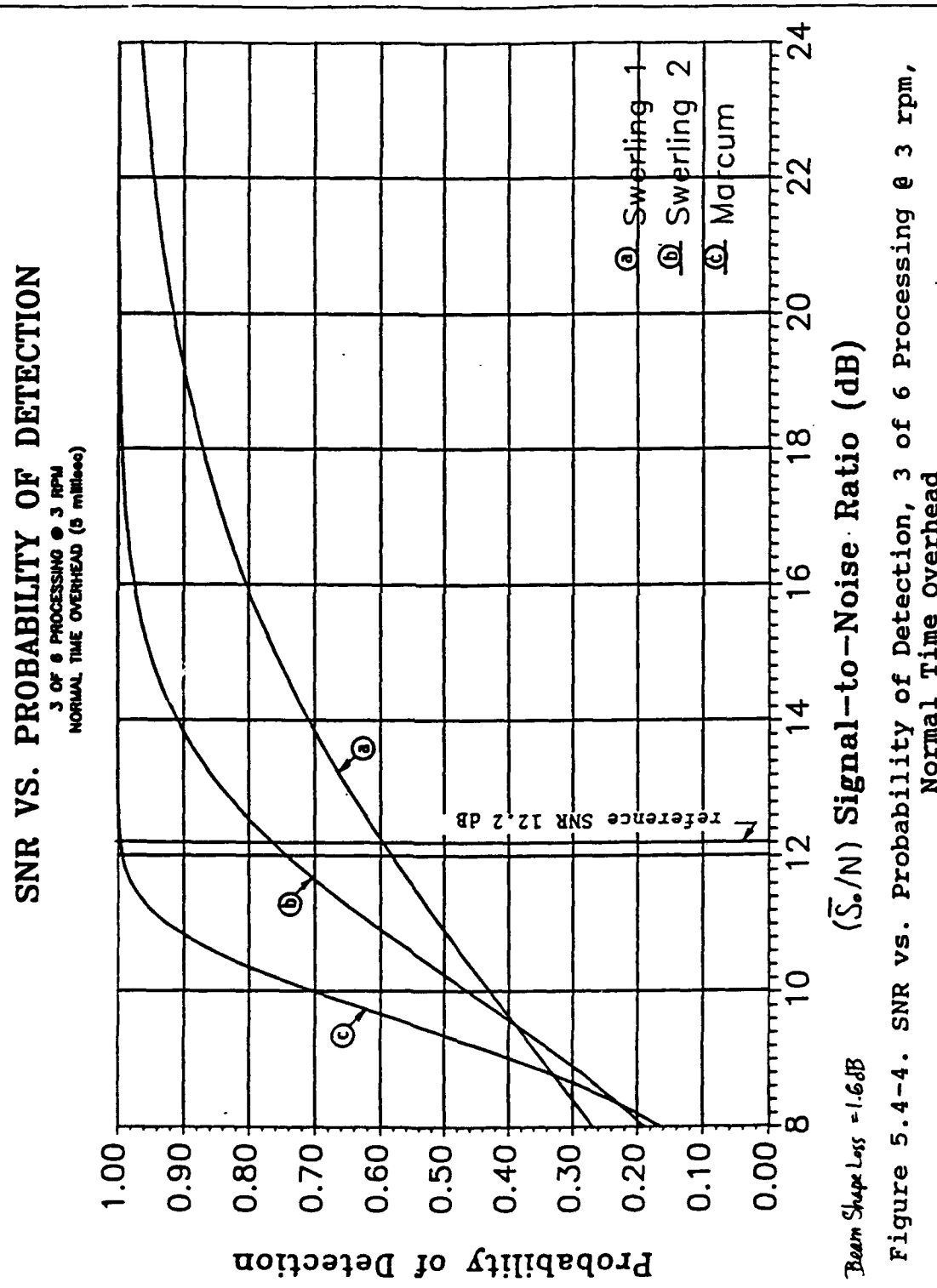**NORMAL TIME OVERHEAD (5 milliSec)**

Figure 5.4-4. SNR vs. Probability of Detection, 3 of 6 Processing @ 3 rpm, Normal Time Overhead

Table 5.4-1 Single Scan Detection Probabilities @ 3 rpm Antenna Scan Rate with Normal Time Overhead

	+++++++++Reference SNR = 17.1dB+++++++++				----------------------Reference SNR = 12.2 dB----------------					
	--------3 NCI-------	zzzzzzzz3 OF 3zzzzzzz			6 NCI		--------3 OF 6------		3 of 3 / 6 rpm (baseline)	
$(\overline{S_o/N})$	SW-1	SW-2	SW-1	SW-2	SW-1	SW-2	SW-1	SW-2	SW-1	SW-2
8.00	0.128	0.074	0.090	0.011	0.337	0.376	0.269	0.189	0.094	0.012
8.20	0.139	0.086	0.099	0.013	0.354	0.411	0.284	0.212	0.103	0.014
8.40	0.151	0.099	0.109	0.015	0.370	0.448	0.300	0.236	0.113	0.016
8.60	0.164	0.113	0.119	0.018	0.386	0.485	0.316	0.261	0.123	0.019
8.80	0.177	0.128	0.130	0.021	0.403	0.522	0.332	0.287	0.134	0.022
9.00	0.190	0.145	0.141	0.024	0.419	0.558	0.348	0.315	0.146	0.026
9.20	0.204	0.164	0.153	0.028	0.435	0.594	0.364	0.343	0.158	0.029
9.40	0.218	0.183	0.165	0.032	0.451	0.628	0.380	0.373	0.170	0.034
9.60	0.232	0.204	0.178	0.036	0.467	0.662	0.397	0.403	0.183	0.038
9.80	0.247	0.226	0.191	0.041	0.483	0.694	0.413	0.433	0.196	0.043
10.00	0.262	0.249	0.204	0.046	0.499	0.724	0.429	0.463	0.210	0.049
10.20	0.278	0.273	0.218	0.052	0.514	0.753	0.445	0.494	0.224	0.055
10.40	0.293	0.298	0.232	0.059	0.529	0.780	0.461	0.524	0.238	0.062
10.60	0.309	0.324	0.247	0.066	0.544	0.805	0.477	0.554	0.253	0.069
10.80	0.325	0.351	0.262	0.073	0.559	0.828	0.492	0.584	0.268	0.076
11.00	0.341	0.377	0.277	0.081	0.574	0.849	0.508	0.613	0.283	0.085
11.20	0.358	0.405	0.292	0.090	0.588	0.868	0.523	0.641	0.299	0.093
11.40	0.374	0.432	0.308	0.099	0.602	0.885	0.538	0.668	0.314	0.103
11.60	0.390	0.460	0.324	0.109	0.616	0.900	0.553	0.694	0.330	0.113
11.80	0.406	0.488	0.340	0.119	0.629	0.914	0.568	0.719	0.346	0.123
12.00	0.423	0.515	0.356	0.130	0.642	0.926	0.582	0.743	0.362	0.134
12.20	0.439	0.542	0.372	0.141	0.655	0.937	0.596	0.765	0.378	0.146
12.40	0.455	0.569	0.388	0.153	0.667	0.946	0.610	0.786	0.394	0.158
12.60	0.471	0.595	0.404	0.165	0.679	0.955	0.623	0.806	0.410	0.170
12.80	0.487	0.621	0.420	0.178	0.691	0.962	0.636	0.824	0.426	0.183
13.00	0.502	0.645	0.436	0.191	0.702	0.968	0.649	0.842	0.442	0.197
13.20	0.517	0.669	0.452	0.205	0.714	0.973	0.662	0.858	0.458	0.210
13.40	0.533	0.692	0.467	0.219	0.724	0.978	0.674	0.872	0.473	0.225
13.60	0.548	0.714	0.483	0.234	0.735	0.981	0.686	0.886	0.489	0.239
13.80	0.562	0.735	0.499	0.248	0.745	0.985	0.697	0.898	0.504	0.254
14.00	0.577	0.755	0.514	0.263	0.755	0.987	0.709	0.909	0.520	0.269
14.20	0.591	0.774	0.529	0.279	0.764	0.990	0.720	0.919	0.535	0.285
14.40	0.605	0.792	0.544	0.294	0.774	0.991	0.730	0.929	0.549	0.300
14.60	0.618	0.809	0.558	0.310	0.782	0.993	0.740	0.937	0.564	0.316
14.80	0.632	0.825	0.573	0.326	0.791	0.994	0.750	0.945	0.578	0.332
15.00	0.645	0.840	0.587	0.342	0.799	0.995	0.760	0.951	0.592	0.348
15.20	0.657	0.854	0.601	0.358	0.807	0.996	0.769	0.957	0.606	0.364
15.40	0.670	0.867	0.614	0.374	0.815	0.997	0.778	0.963	0.619	0.380
15.60	0.682	0.879	0.628	0.390	0.823	0.998	0.787	0.967	0.633	0.396
15.80	0.693	0.890	0.641	0.407	0.830	0.998	0.796	0.971	0.645	0.413
16.00	0.705	0.900	0.653	0.423	0.837	0.998	0.804	0.975	0.658	0.429
16.20	0.716	0.909	0.666	0.439	0.844	0.999	0.812	0.978	0.670	0.445
16.40	0.726	0.918	0.678	0.455	0.850	0.999	0.819	0.981	0.682	0.461
16.60	0.737	0.926	0.689	0.471	0.856	0.999	0.827	0.984	0.694	0.476
16.80	0.747	0.933	0.701	0.486	0.862	0.999	0.834	0.986	0.705	0.492
17.00	0.757	0.940	0.712	0.502	0.868	0.999	0.840	0.988	0.716	0.507
17.10	0.760	0.943	0.717	0.509						

Table 5.4-1

Single Scan Detection Probabilities @ 3 rpm Antenna Scan Rate with Normal Time Overhead (cont'd)

	++++++++Reference SNR = 17.1dB++++++++				----------------Reference SNR = 12.2 dB----------------					
	--------3 NCI--------		:::::::::3 OF 3:::::::		6 NCI		--------3 OF 6------		3 of 3 / 6 rpm (baseline)	
(S₀/N)	SW-1	SW-2	SW-1	SW-2	SW-1	SW-2	SW-1	SW-2	SW-1	SW-2

$(\overline{S_o}/N)$	SW-1	SW-2	SW-1	SW-2	SW-1	SW-2	SW-1	SW-2	SW-1	SW-2
17.20	0.766	0.946	0.723	0.517	0.873	1.000	0.847	0.990	0.727	0.523
17.40	0.775	0.952	0.733	0.532	0.879	1.000	0.853	0.991	0.737	0.538
17.60	0.784	0.957	0.743	0.547	0.884	1.000	0.859	0.992	0.747	0.553
17.80	0.793	0.961	0.753	0.562	0.889	1.000	0.865	0.993	0.757	0.567
18.00	0.801	0.965	0.763	0.576	0.893	1.000	0.871	0.994	0.766	0.581
18.20	0.809	0.969	0.772	0.590	0.898	1.000	0.876	0.995	0.775	0.595
18.40	0.817	0.972	0.781	0.604	0.902	1.000	0.881	0.996	0.784	0.609
18.60	0.824	0.975	0.789	0.618	0.906	1.000	0.886	0.996	0.793	0.623
18.80	0.831	0.978	0.798	0.631	0.910	1.000	0.891	0.997	0.801	0.636
19.00	0.838	0.980	0.806	0.644	0.914	1.000	0.896	0.997	0.809	0.649
19.20	0.845	0.983	0.814	0.657	0.918	1.000	0.900	0.998	0.816	0.661
19.40	0.851	0.984	0.821	0.669	0.922	1.000	0.905	0.998	0.824	0.673
19.60	0.857	0.986	0.828	0.681	0.925	1.000	0.909	0.998	0.831	0.685
19.80	0.863	0.988	0.835	0.693	0.928	1.000	0.913	0.999	0.838	0.697
20.00	0.869	0.989	0.842	0.704	0.931	1.000	0.916	0.999	0.845	0.708
20.20	0.874	0.990	0.849	0.715	0.934	1.000	0.920	0.999	0.851	0.719
20.40	0.880	0.992	0.855	0.726	0.937	1.000	0.923	0.999	0.857	0.729
20.60	0.885	0.992	0.861	0.736	0.940	1.000	0.927	0.999	0.863	0.740
20.80	0.890	0.993	0.867	0.746	0.942	1.000	0.930	0.999	0.869	0.750
21.00	0.894	0.994	0.872	0.756	0.945	1.000	0.933	1.000	0.874	0.759
21.20	0.899	0.995	0.877	0.765	0.947	1.000	0.936	1.000	0.879	0.769
21.40	0.903	0.995	0.883	0.775	0.950	1.000	0.939	1.000	0.884	0.778
21.60	0.907	0.996	0.888	0.783	0.952	1.000	0.941	1.000	0.889	0.787
21.80	0.911	0.996	0.892	0.792	0.954	1.000	0.944	1.000	0.894	0.795
22.00	0.915	0.997	0.897	0.800	0.956	1.000	0.946	1.000	0.899	0.803
22.20	0.919	0.997	0.901	0.808	0.958	1.000	0.949	1.000	0.903	0.811
22.40	0.922	0.998	0.905	0.816	0.960	1.000	0.951	1.000	0.907	0.819
22.60	0.925	0.998	0.910	0.823	0.962	1.000	0.953	1.000	0.911	0.826
22.80	0.929	0.998	0.913	0.831	0.963	1.000	0.955	1.000	0.915	0.833
23.00	0.932	0.998	0.917	0.837	0.965	1.000	0.957	1.000	0.918	0.840
23.20	0.935	0.999	0.921	0.844	0.966	1.000	0.959	1.000	0.922	0.846
23.40	0.938	0.999	0.924	0.851	0.968	1.000	0.961	1.000	0.925	0.853
23.60	0.940	0.999	0.927	0.857	0.969	1.000	0.962	1.000	0.929	0.859
23.80	0.943	0.999	0.930	0.863	0.971	1.000	0.964	1.000	0.932	0.865
24.00	0.945	0.999	0.933	0.868	0.972	1.000	0.966	1.000	0.935	0.870
24.20	0.948	0.999	0.936	0.874	0.973	1.000	0.967	1.000	0.937	0.876
24.40	0.950	0.999	0.939	0.879	0.974	1.000	0.969	1.000	0.940	0.881
24.60	0.952	0.999	0.942	0.884	0.976	1.000	0.970	1.000	0.943	0.886
24.80	0.954	0.999	0.944	0.889	0.977	1.000	0.971	1.000	0.945	0.891
25.00	0.956	1.000	0.947	0.894	0.978	1.000	0.973	1.000	0.948	0.895
25.20	0.958	1.000	0.949	0.898	0.979	1.000	0.974	1.000	0.950	0.900
25.40	0.960	1.000	0.951	0.903	0.980	1.000	0.975	1.000	0.952	0.904
25.60	0.962	1.000	0.953	0.907	0.981	1.000	0.976	1.000	0.954	0.908
25.80	0.964	1.000	0.955	0.911	0.981	1.000	0.977	1.000	0.956	0.912
26.00	0.965	1.000	0.957	0.915	0.982	1.000	0.978	1.000	0.958	0.916

scan rate of 6 rpm, this results in a single slant reference SNR, $(\bar{S}_0/N)_0$, of 12.2 dB. Note that the reference SNR for a 6-slant configuration with a scan rate of 3 rpm is also 12.2 dB. For a 3-slant configuration with a scan rate of 3 rpm, $(\bar{S}_0/N)_0$ equals 17.1 dB. The increase in $(\bar{S}_0/N)_0$ when the scan rate is reduced by a factor of 2 is more than 3 dB because the number of pulses integrated increases without an increase in the time overhead.

The analysis result shows that a considerable improvement is possible in the single scan detection probability with NCI and slant-to-slant frequency agility when they are accompanied with an increased dwell time. Frequency agility renders a rapid fluctuation to Swerling case 1 (and case 3) targets such that they behave as Swerling case 2 (or case 4) targets. Single scan detection probability with NCI improves rapidly for Swerling case 2 targets in the high SNR region. Increased dwell time, as a consequence of slower scan rate, places the returned signal from the reference target at the reference range in the higher SNR region. Since a different processing configuration gives rise to a different level of SNR per slant for a given target situation, the reference SNR for each configuration is used to identify one point in the P_d versus $(\bar{S}_0/N)$ curve to a

252

particular detection range, namely, the reference range of the reference target. Then, the remaining values of $(\bar{S}_0/N)$ can be converted to the corresponding range using the radar range equation.

Improvements in single scan detection probabilities with an increase in dwell time are, of course, expected since SNR is proportional to the dwell time. Whether the improvement in single scan detection probability with slower revisit rates leads to improvement in cumulative detection probability and track update rates is the real question. Since a slower scan rate results in fewer opportunities for the cumulative detection process and track updates, a back-to-back antenna configuration is also included as an option which is used to cover a reduced surveillance sector of 180 degree azimuth. In the following investigation, the target is assumed to be an aircraft whose RCS fluctuates according to the Swerling case 1 model. Results for other target models can be determined in the same manner.

The improvement in cumulative detection performance is determined on the basis of achieving $P_c = 0.9$ in 60, 20, and 10 seconds using the single scan detection probabilities shown in Table 5.4-1. The track update performance is deter-

mined on the basis of the average number of 'hits' in a 5 minute time interval. It will be shown that the slower scan rate improves performance in both cumulative detection probability and track update rate for the outer ranges at the expense of a poorer track update rate in the inner ranges when compared to the result with normal scan rate used in the baseline. This is because update rate can never exceed the antenna scan rate.

Assuming that target range closure is negligible during the interval over which a specified value of P_c is achieved, P_c is given by

$$P_c = 1-(1-P_d)^L$$

where L is the number of revisits to or scans by the target in question during the cumulative detection interval. It follows that the necessary level of P_d to achieve a specified value for P_c can be expressed as

$$P_d = 1-\exp[(1/L)\ln(1-P_c)] \ . \tag{5.4-1}$$

The required P_d that yields $P_c = 0.9$ is calculated from Eqn. (5.4-1) as a function of L and is listed in Table 5.4-2.

Table 5.4-2

Required P_d to achieve P_c = 0.9 in L scans

L	P_d
1	0.900
2	0.683
3	0.535
4	0.437
5	0.369
6	0..318

The improvement in dB is the differential margin in SNR relative to the baseline for the reference target located at the reference range for each processing option. By definition, the SNR margin is the amount by which the reference SNR is higher than the SNR required to yield a level of P_d that will translate to the specified P_c. This method of performance comparison was also used in Section 4.5. The concept is illustrated in Figure 4.5-4.

At an antenna scan rate of 3 rpm, the number of scans in 20 and 60 seconds are 1 and 3, respectively. These values of

L require P_d levels of 0.9 and 0.535, respectively, to yield P_c = 0.9 in 20 and 60 seconds. As an illustration of the margin computation, it is seen from Table 5.4-1 under 3 NCI for Swerling case 2 (which would apply to Swerling case 1 when slant-to-slant frequency agility is used) that the required $(\bar{S}_0/N)$ for P_d = 0.9 and P_d = 0.535 is 16.0 dB and 12.1 dB. These translate to SNR margins relative to the reference SNR of 17.1-16.0=1.1 dB and 17.1-12.1=5.0 dB. In the baseline with 3 of 3 post detection integration and with the antenna scan rate of 6 rpm, the required P_d for P_c = 0.9 in 20 and 60 seconds is 0.683 and 0.318, respectively, with the corresponding $(\bar{S}_0/N)$ requirement of 16.4 dB and 11.4 dB. The SNR margin in each case is 12.2-16.4=-4.2 dB and 12.2-11.4=0.8 dB. By comparing these margins to the margins under 3 NCI with frequency agility at an antenna scan rate of 3 rpm, the improvement is seen to be 5.3 dB and 4.2 dB, respectively, for P_c = 0.9 in 20 and 60 seconds.

Performance improvements obtained in this manner for several signal processing options considered for a Swerling case 1 target are summarized in Table 5.4-3. The options include with and without frequency agility and with and without back-to-back antennas. Note that the degree of improvement depends on the performance criterion adopted.

Table 5.4-3

Summary of Performance Improvement with the Antenna Scan Rate of 3 rpm for a Swerling Case 1 Target

---

a. antenna scan rate of 3 rpm (360° coverage in azimuth)

req'd P_d	P_c in 60 sec. 0.535			P_c in 20 sec. 0.90		
	SNR(dB)	margin	gain*	SNR(dB)	margin	gain*
(w/o frequency agility)						
3 NCI	13.4	3.7	2.9	21.2	-4.1	0.1
3 of 3	14.3	2.8	2.0	22.1	-5.0	-0.8
3 of 6	11.4	0.8	0.0	19.2	-7.0	-2.8
6 NCI	10.5	1.7	0.9	18.4	-6.2	-2.0
(w/ frequency agility)						
3 NCI	12.1	5.0	4.2	16.0	1.1	5.3
3 of 3	17.4	-0.3	-1.1	25.4	-8.3	-4.1
3 of 6	10.5	1.7	0.9	13.8	-1.6	2.6
6 NCI	8.9	3.3	2.5	11.6	0.6	4.8

b. antenna scan rate of 3 rpm with a back-to-back antenna (180° coverage in azimuth)

req'd P_d	P_c in 60 sec. 0.535			P_c in 20 sec. 0.683		
	SNR(dB)	margin	gain*	SNR(dB)	margin	gain*
(w/o frequency agilility)						
3 NCI	10.8	6.3	5.5	15.5	1.6	5.8
3 of 3	11.5	5.6	4.8	16.4	0.7	4.9
3 of 6	8.6	3.6	2.8	13.5	-1.5	2.7
6 NCI	8.0	4.2	3.4	12.7	-0.5	3.7
(w/ frequency agilility)						
3 NCI	10.6	6.5	5.7	13.3	3.8	8.0
3 of 3	14.7	2.4	1.6	19.6	-2.5	1.7
3 of 6	9.0	3.2	2.4	11.5	0.7	4.9
6 NCI	7.8	4.4	3.6	9.7	2.5	6.7

c. antenna scan rate at 6 rpm

req'd P_d	P_c in 60 sec. 0.318			P_c in 20 sec. 0.683		
	SNR(dB)	margin	gain	SNR(dB)	margin	gain
3 of 3	11.4	0.8	ref	16.4	-4.2	ref

---

*compared to the corresponding SNR margin with 3 of 3 processing @ antenna scan rate of 6 rpm

If the criterion is the track update rate instead, which is defined as the blip scan ratio multiplied by the number of scans in a specified time interval, improvement figures different from those shown in Table 5.4-3 result. For example, at the range where $P_c = 0.9$ is reached, the average number of track updates (hits) in 5 minutes for P_c intervals of 20 and 60 seconds at the antenna scan rate of 3 rpm are 13.5 and 8, respectively. The corresponding average numbers of track updates at the antenna scan rate of 6 rpm are 20.5 and 9.5.

To yield the same level of track update rate at 6 rpm, a P_d level of only 0.45 and 0.27 is required for P_c intervals of 20 and 60 seconds, respectively. Corresponding values of the required $(\tilde{S}_0/N)$ are 13.1 dB and 10.8 dB. Again, by comparing SNR margins, the improvement figure is determined to be 2.0 dB and 3.6 dB for P_c intervals of 20 and 60 seconds, respectively. Even though the improvement figures are smaller, it is significant that the track update rate is improved at this range by slowing down the scan rate. This improvement increases at ranges further out and decreases at ranges closer in. This subject is further discussed at the end of the Chapter.

Now assume that the azimuth coverage is reduced from 360 to 180 degrees. With a back-to-back antenna configuration where the receiver/transmitter set is switched to one or the other antenna every 180 degrees of the rotodome rotation sr that the same 180 degree azimuth sector is covered by both antennas, the revisit rate at 3 rpm for the covered sector is the same as that provided by a single antenna at a scan rate of 6 rpm. Therefore, the performance improvement measure based on P_c is the same as that based on the average number of hits. Following the same procedures as above, the equivalent dB improvement figures with frequency agility and 3 NCI with the back-to-back antenna are 8.0 dB and 5.7 dB based on 0.9 P_c in 20 and 60 seconds, respectively.

These results demonstrate the efficiency of NCI in the region of high SNR or high probability of detection rendered by the slower scan rate when used in conjunction with frequency agility. The improvement would be even greater had the highly desirable track update rate of once every 10 seconds been required. This would require a single scan P_d of 0.9. With two back-to-back antennas rotating at 3 rpm and slant-to-slant frequency agility, this level of performance is achievable at a range equal to 1.06(R_0) for a 3 NCI and at 0.96(R_0) for a 6-NCI where (R_0) denotes the reference

range. This results from the the direct conversion of one-fourth power of the SNR margin available at (R_0), which are 1.1 dB and -0.6 dB, respectively, for 3 NCI and 6 NCI. In che baseline 3 of 3 post detection integration, $P_d = 0.9$ is rarely reached due to range eclipsing even when a target is at a close range. Ignoring range eclipsing for ease of comparison of other effects on detection performance, the SNR margin for 0.9 P_d at the reference range is -9.9 dB. Thus, the equivalent dB improvement is 11.0 dB and 9.3 dB for 3 NCI and 6 NCI, respectively.

To facilitate the performance comparison, P_c values for 20 and 60 seconds are plotted in Figures 5.4-5 and 5.4-6, respectively, as a function of the mean normalized SNR, x, defined as $(\bar{S}_0/N)$ divided by the respective $(\bar{S}_0/N)_0$. This eliminates the need for computing SNR margins. Comparison on the basis of track update rate can be generated similarly. Let u denote the average number of hits in a specified time interval, say 5 minutes. Since there are 15 and 3c antenna scans in a 5 minute interval for 3 and 6 rpm antenna scan rates, respectively, u as a function of the normalized SNR, x, is given by

$$u(x) = \begin{cases} (15)\,[P_d(x)\,(\bar{S}_o/N)_o]: & \text{antenna scan rate at 3 rpm} \\ (30)\,[P_d(x)\,(\bar{S}_o/N)_o]: & \text{antenna scan rate at 6 rpm.} \end{cases}$$
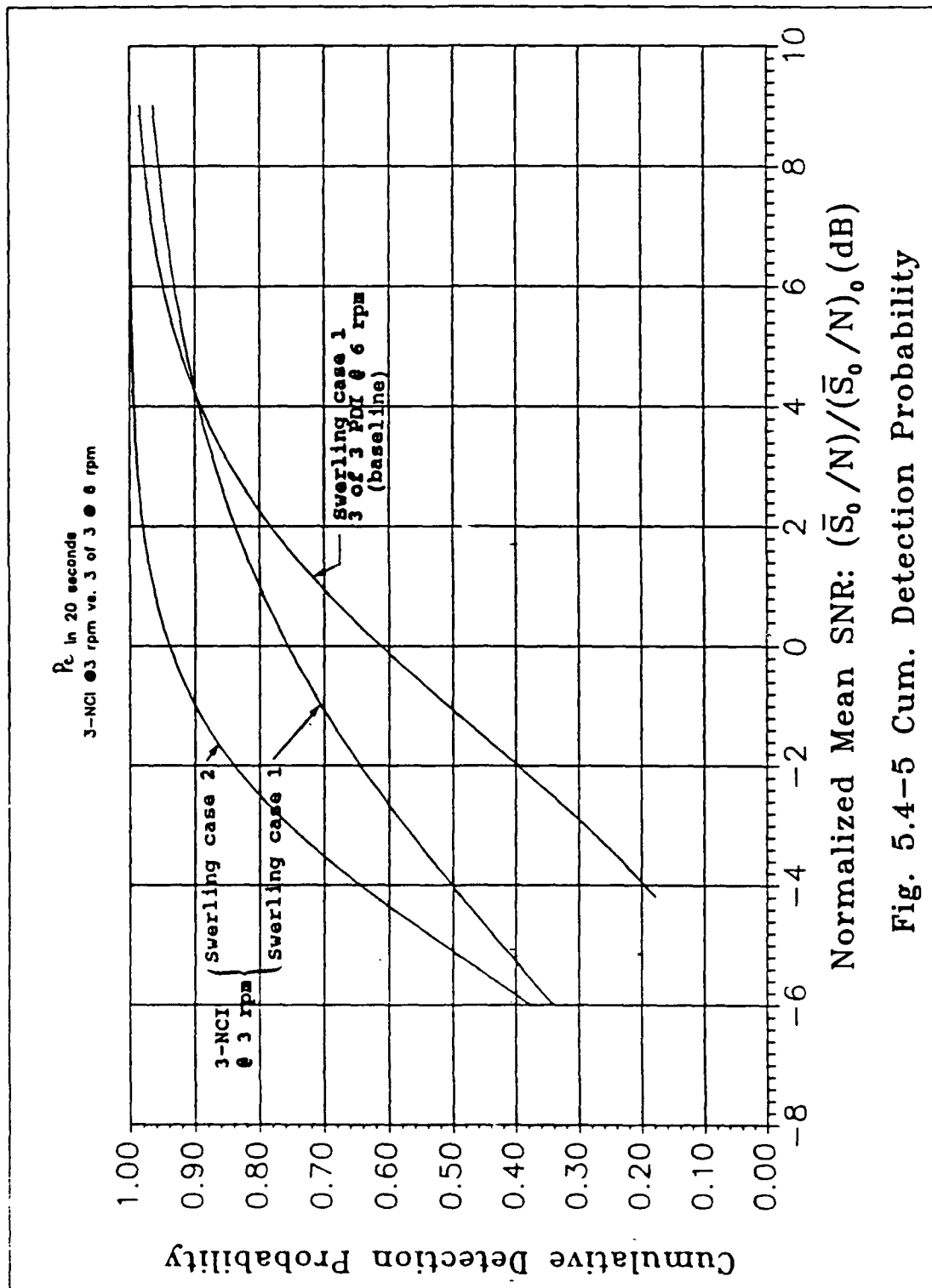
Fig. 5.4-5 Cum. Detection Probability

3-NCI @ 3 rpm vs. 3 of 3 @ 6 rpm

Swerling case 1
3 of 3 PDI @ 6 rpm
(baseline)

3-NCI
@ 3 rpm

Swerling case 2

Swerling case 2

Cumulative Detection Probability
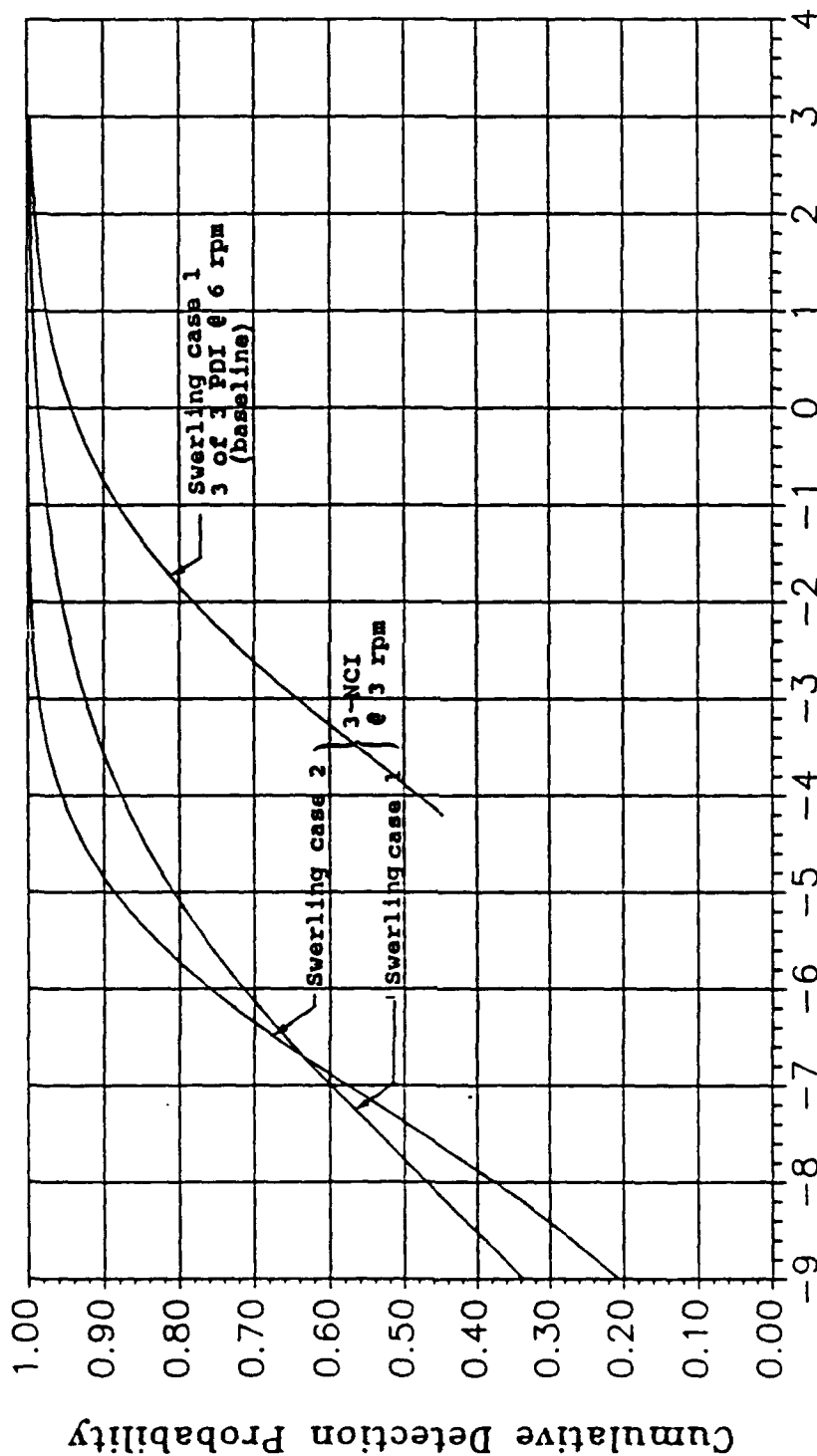
Normalized Mean SNR:, $(\bar{S}_o/N)/(\bar{S}_o/N)_o$ (dB)

Fig. 5.4-6 Cum. Detection Probability

In 60 seconds

The plots of the average number of track updates in a 5 minute interval with 3-NCI at 3 rpm for Swerling case 1 and 2 targets together with the same in the baseline 3 of 3 processing at 6 rpm for Swerling case 1 targets are shown in Figure 5.4-7. These figures clearly demonstrate that not only is the P_c range extended with a slower scan rate but the track update rate is also improved in the outer range.

Normalized Mean SNR: $(\bar{S}_o/N)/(\bar{S}_o/N)_o$ (dB)
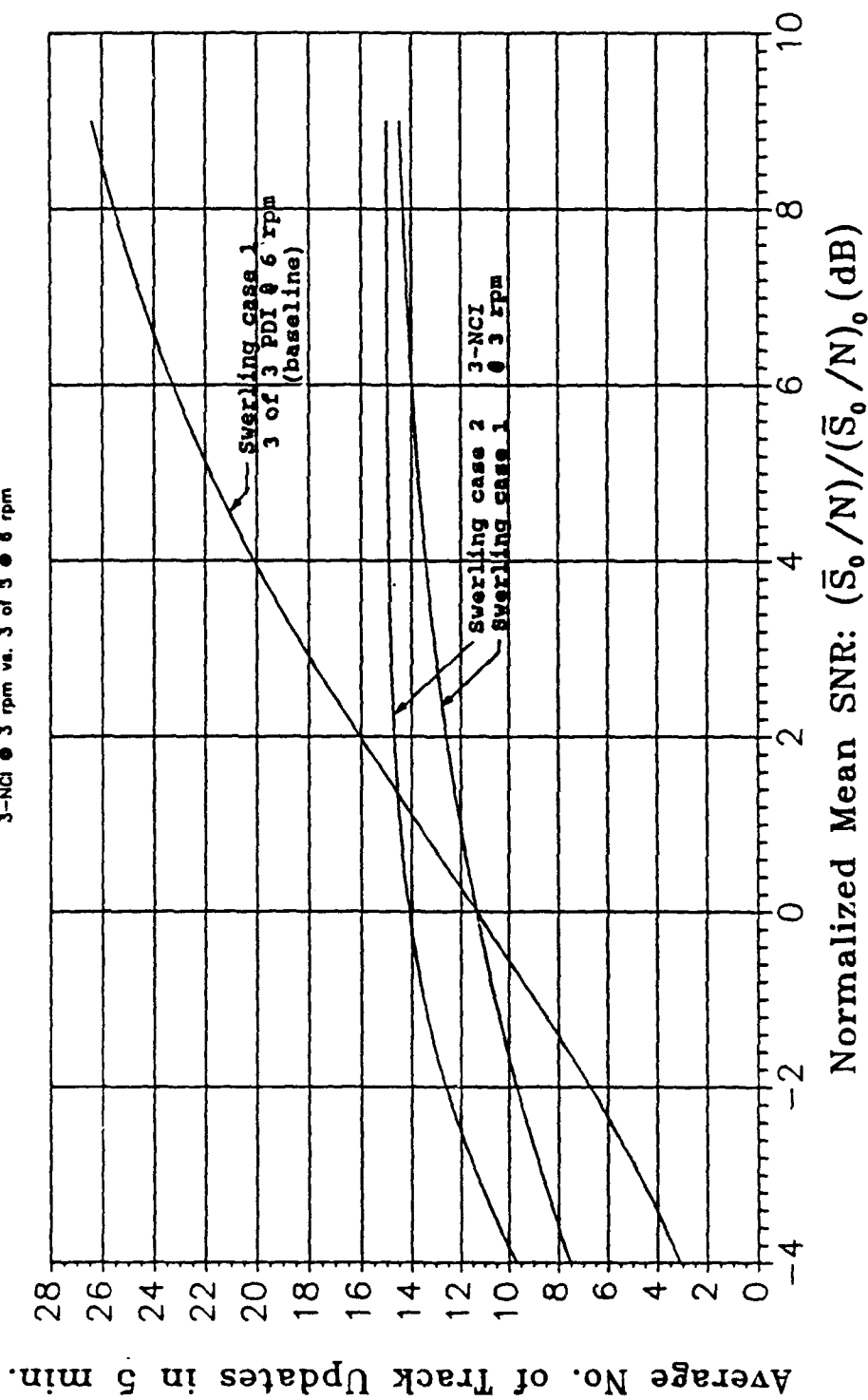
Fig. 5.4-7 Average No. of Track Updates
in 5 minutes

Average No. of Track Updates in 5 min.

Swerling case 1
3 of 3 PDI @ 6 rpm
(baseline)

3-NCI
@ 3 rpm

Swerling case 2
Swerling case 1

CHAPTER 6

SUMMARY AND RECOMMENDATIONS FOR FUTURE WORK

6.1 Summary

This report presents results of an investigation into the effectiveness of (a) scan-to-scan processing and (b) scan rate reduction in improving the detection performance of an existing airborne surveillance radar subjected to power-aperture product and system false alarm constraints. As background, considerations involved in a performance comparison of the baseline and modified radar configurations were clearly explained where the primary performance criterion was the cumulative detection probability. Following an introduction in Chapter 1 of the radar system under investigation together with basic concepts associated with the detection problem in a long range airborne surveillance radar, those parameters which go through changes with the system modification were identified and methods for quantifying those parameters were developed in Chapter 2. These included the number of coherent processing intervals in a beam dwell given the search frame time, the number of available pulses in a coherent processing interval, beam shape loss, false alarm probability allocation, and target models. It was shown how two different approaches to false alarm calculations, one proposed by Marcum and the other by Barton and Skolnik, could be used to relate cell

false alarm to system false alarm in a complex high PRF radar.

The baseline radar configuration was then analyzed in Chapter 3. Probability density functions for the sufficient statistic appearing in the likelihood ratio test were developed. Expressions for the detection probabilities after M of N post detection binary integration were derived. These results were then averaged with respect to the assumed target radar cross section fluctuations to obtain the expected detection probabilities for five different target models. Graphs of detection probability versus signal-to-noise ratio were generated and presented for the five target models.

The scan-to-scan processing (SSP) was dealt with on a theoretical basis (as opposed to simulation) in Chapter 4. The baseline radar configuration was modified by incorporating two different versions of scan-to-scan processing: One was a conventional J of K SSP while the other was a modified J of K SSP. The philosophy is to lower the threshold to enable detection of extremely weak targets or extend the detection range for conventional targets. This results in a drastic increase of false alarms. These are suppressed by requiring J detections in a K scan wide correlation window associated with L total scans. The size of the correlation window was determined by imposing limits consistent with realistic target maneuvers. An analysis was carried out to

relate cell false alarm probability to system false alarm rate when scan-to-scan processing is incorporated. The corresponding cumulative detection probabilities are derived. It is shown, contrary to widely held optimistic projections, that only a very marginal improvement results over the cumulative detection probability of the baseline radar.

With a power-aperture product constraint, the only adjustable system parameter available for improving performance is the scan rate over the surveillance volume. In Chapter 5 previous work on scan rate optimization for a low PRF radar is reviewed. The results suggested that improvement could be achieved by slowing down the scan rate for a given surveillance volume. An example was worked out in the investigation to show that slowing down the scan rate in the baseline radar could result in significant improvement. As a result, the previous scan rate optimization for the low PRF radar was extended to the high PRF case. Because of track update requirements, scan rate reduction was limited to a factor of two compared to what was specified for the baseline radar. Both binary M of N and noncoherent post detection integration were compared in conjunction with the reduced scan rate in the analysis. Noncoherent post detection integration combined with a reduced scan rate was shown to give rise to significant detection performance improvement.

6.2 Recommendations for Future Work

The main body of this investigation dealt with detection of Swerling and Marcum target models embedded in white Gaussian noise. This is a problem encountered in a well designed high PRF radar where the majority of targets of interest fall in the clutter free doppler zone. The solution to this problem is generally assumed in the literature to be well known. However, the problems posed and the concepts and methodology developed in this investigation while critical in addressing the issues facing modern surveillance radar problems today, cannot be readily found in the literature.

One of the major areas of radar research activity over the past decade appears to center on optimum detection in non-Gaussian interference, the principal source of the non-Gaussian interference being clutter. Frequently, the instantaneous power of radar returns from land clutter is characterized as lognormal [10] or Weibull distributed [16], while that from sea clutter is K-distributed [17]. This led to a flurry of research activity into detection schemes based on stochastic estimation, which is an extension of the optimum detection theory [18], or Locally Optimum Detector (LOD) [19] or Asymptotically Optimum Detector [20] on the one hand, and adaptive clutter cancelling techniques on the other [21, 22].

While these topics are interesting, detection approaches under non-Gaussian clutter may be irrelevant to a majority of the detection problems in clutter. It is indeed true that the aggregate of returned clutter power observed over the entire surveillance volume can assume lognormal, Weibull, or K-distributed density. However, the conditional density given the local mean of the clutter power taken from one radar resolution cell over the time period during which each detection decision is made within a radar scan is likely to be either exponential or Rician. The assumption of exponential or Rician density in turn depends on whether or not the entire sequence of radar pulses is transmitted at the same carrier frequency [23].

Describing the probability density of the entire set of returned clutter power in a surveillance sector as an integral of the conditional probability density of the clutter given its local mean multiplied by the probability density of the mean using the mean as the variable of integration (see Eqn. 6.2-1, p276) is based on the point of view arising from the nonstationary characterization of clutter [24, 25, 26, 27]. Not only does this approach provide a means to explain a more complex form of clutter distribution, but more importantly it allows the correlation property of the clutter to be correctly modeled. Stating it differently, the voltages associated with the in-phase and quadrature components of the clutter returns during a beam dwell from a

given range-azimuth resolution cell is likely to be Gaussian, albeit nonzero mean, when the radar resolution cell intersects the ground patch which contains many elemental clutter cells. An elemental clutter cell is that clutter patch bounded by its spatial correlation distance. Returns from elemental cells of a ground patch may be also Weibull [23] or Lognormal distributed [28]. However, when the radar resolution cell encompasses many elemental cells, the central limit theorem evidently is at work to render the distribution of the received clutter power to be exponential or Rician conditioned on its mean taking a certain value. The assumption of multiple elemental cells will fail to hold eventually as the radar resolution cell is made sufficiently small as in a synthetic aperture radar (SAR) used for ground imaging. Some authors report that the Gaussian assumption also fails to hold at very low grazing angles.

Thus, for the majority of practical situations the detection problems in Weibull, lognormal, or K-distributed clutter usually break down to problems of detection in Rayleigh or Rician clutter (for the envelope voltage after combining the in-phase and quadrature components) during each decision interval [25]. The detection decision is made with an adaptive threshold that yields the desired constant false alarm rate throughout the surveillance volume. The expected detection probability over the entire surveillance volume is obtained by averaging the local detection results over the

variation of the clutter mean. Note that this process is exactly the same as the procedure for obtaining the expected detection probability after post detection integration of Swerling case 1 and 3 targets (slowly varying with respect to a CPI) in white Gaussian noise. This process was explained in Chapter 3. Totally irrelevant detection predictions would result for Swerling case 1 and 3 target models when a method appropriate for Swerling case 2 and 4 were applied to these models. Similarly, an optimum detector under non-Gaussian interference produces an incorrect result when the local interference over the detection decision interval is Gaussian.

A preliminary analysis of clutter samples collected with a high PRF radar is presented in Section 6.2.1. The result tends to support the nonstationary characterization approach to clutter. In particular, the mean and variance of the clutter samples are found to vary significantly from one range cell to the next.

As for the adaptive clutter canceller, which is an adaptive implementation of an optimum filter in the sense that it maximizes the output signal-to-clutter-plus-noise ratio, its predicted performance in comparison to that of a conventional processor (MTI followed by a windowed FFT) is usually based on artificially simple assumptions which may be irrelevant to the real situation encountered. Much of the

recent adaptive clutter canceller work which is of significance is contained in MTI RADAR edited by Schleher [21] and Optimized RADAR PROCESSORS by Farina [22]. Simplistic assumptions typically made are:

1. The interference is a zero mean Gaussian random process.

2. The interference has an exponential autocorrelation function and the covariance matrix can be normalized such that it is a positive definite hermitian matrix with unity diagonal elements.

3. The number of pulses used for processing is small (usually 8 or 16 pulses).

4. Adjacent range gate samples are independent and identically distributed so that the signal free sample covariance matrix can be obtained by averaging a number of adjacent range gate samples.

While assumptions 1 and 2 are reasonable for an adaptive array design in the presence of sidelobe clutter interference [29], the mean of mainbeam clutter samples over a CPI is hardly ever zero, and the sample correlation matrix does not have identical diagonal elements (i.e., nonstationary). Assumption 3 is valid for a very simple low PRF radar. In a medium or high PRF radar the number of pulses integrated is much larger which, when coupled with the fact that the

clutter correlation matrix is almost singular (i.e., clutter returns are highly correlated between pulse-to-pulse), makes it difficult to invert or decompose the correlation matrix of a large dimension. As for assumption 4, the clutter returns in adjacent range cell samples taken with a high PRF radar show that they are not identically distributed. In fact, the mean and variance of the clutter samples exhibit significant variations from one range cell to the next so that they cannot be used to form a sample correlation matrix. This is also reported to be true for a low PRF radar. the sample correlation matrix can be formed from temporal samples in the same range cell. The signal free correlation matrix would be difficult to obtain by this means, however.

A performance comparison of different clutter cancellers is given in Secton 6.2.2. An infinite impulse response (IIR) filter giving shaped velocity response, a finite impulse response (FIR) filter using binomial coefficients as its weights and and an FIR filter that derives its weights from the eigen vector corresponding to the minimum eigen value of the clutter correlation matrix are compared using actual high PRF clutter data as inputs. No one approach was found to be superior to the others tried.

In view of the lack of noticeable improvement in performance of the optimum linear clutter canceller with real clutter data, it seems reasonable to consider an option alternate

to the classical approach examined. This alternate approach views the clutter as an a priori unknown, but deterministic, process. Observation of a time sequence of clutter returns reveals a slow monotonic variation of clutter amplitude over a CPI. There is no random jump in amplitude or phase from pulse to pulse. One possible explanation for this phenomenon can be that the mainbeam clutter is dominated by a few discrete scatterers whose signal amplitudes are slowly modulated by the antenna scanning and platform motion. A smooth curve fit to, or a low pass replica of, the clutter amplitude and phase variation over a CPI can be made after reception of the data and subtracted from the original data, which in effect adaptively takes out a majority of the undesirable clutter returns leaving uncancelled target signals separated from the clutter doppler. Limited trials with collected clutter data show good results when the smooth curve chosen for curve fit is a third or fourth degree polynomial. The topics discussed briefly in this section require further studies.

6.2.1 Clutter Model

The result of a preliminary investigation of the distribution of clutter power received through a high PRF airborne pulse doppler radar is presented in this section. The characteristics of the radar used to collect the data and the sample size are described in Table 6.2-1.

274

Table 6.2-1   Radar Characteristics and Clutter Sample Size

no. of pulses per range cell	175
no. of range cells per azimuth sample	40^+
no. of azimuth samples	4
size of terrain covered	
range	50-210 nmi
cross range	7.6 nmi at 210 nmi range
waveform	high PRF
receiver bandwidth	1.25 MHz
carrier frequency	S-band

Since the radar employs a high PRF wavaeform, the clutter returns from over 200 nautical mile range swath are folded into one approximately 3 nautical mile range interval which is divided into some 40 or so range cells on the average. In addition, these returns are modulated by the antenna beam shape and the two way range attenuation on the one hand, and by the antenna scanning and the platform motion on the other. The platform is assumed to move at a speed of 360 knots at the altitude of 30,000 feet. Of the range cells available, only samples from every other range cell are used for analysis.

The objective of the investigation is to determine how

well the actual received clutter sample can be fit to the nonstationary clutter model. The conventional view giving rise to Weibull or lognormal distribution for clutter is based on representing the clutter process as a wide sense stationary random process. An alternate view, which is the nonstationary characterization adopted in this investigation, is modeling the clutter process as a time varying process whose parameters are stationary within a radar detection decision interval within a beam dwell.

This nonstationary characterization is described mathematically as follows: Let the instantaneous scattered clutter power, which is proportional to the mean radar cross section of the clutter patch or the clutter reflectivity, be denoted by a random variable z, and the local mean of z be denoted by another random variable u. Let $p_1(z|u)$ and $p_2(u)$ denote the conditional density of z given u and the probability density of u, respectively. The probability density $p_1(\ )$ corresponds to the short term or a local density for a scattered clutter power while $p_2(\ )$ corresponds to the variation of u over time or space (entire terrain in the surveillance volume).

The unconditioned density of z is given by

$$p(z) = \int p_1(z|u)p_2(u)\,du. \tag{6.2-1}$$

Lewinski [24] has proposed gamma densities for the density functions of both z and u which are expressed as

$$p_1(z|u) = \frac{(k)^k z^{k-1} \exp(-kz/u)}{\Gamma(k)(u)^k} \qquad (6.2\text{-}2)$$

and

$$p_2(u) = \frac{(m)^m u^{m-1} \exp(-mu/u)}{\Gamma(m)(\bar{u})^m} \qquad (6.2\text{-}3)$$

where overbar signifies the expected value, ( ) is the gamma function, and k and m are the inverse of the normalized variance of z and u (the square of the mean divided by the variance), respectively. The parameter k is also known as the shape factor while u is known as the scale factor. Substituting the above expressions into Eqn. (6.2-1) yields

$$p(z) = \frac{2(km)^{(k+m)/2}(z)^{(k+m-2)/2}}{\Gamma(k)\Gamma(m)(u)^{(k+m)/2}} K_{m-k}((4mkz/u)^{1/2}) \qquad (6.2\text{-}4)$$

where $K_p(\cdot)$ is the modified Bessel function of second kind of order p. When k = 1, p(z) becomes the density of the K-distribution and when k = 1 and m = 1/2, p(z) becomes a Weibull density with Weibull parameter equal to 1/2 [24].

The gamma density encompasses a large class of density functions. When k = 1, it represent the exponential density used in the Swerling case 1 and 2 models (see Section 2.6).

277

When k > 1, it represents the Rician density [29]. Actually, it is slightly different from the Rician density commonly used in the literature [10, 21, 23] for representing the reflected clutter power which is given as

$$p(z) = [(1+a)/u] \exp[-a-(1+a)z/u] \, I_o(2[a(1+a)z/u]^{1/2}) \tag{6.2-5}$$

where a is the DC to AC power ratio and $I_o(\cdot)$ is the modified Bessel function of the first kind of order zero.

The random variable u, the mean of z, is best obtained by taking the mean of the sample values taken from multiple carrier frequencies with the frequency spacing equal to or larger than the waveform bandwidth. Since a single frequency is used in the sample at hand, the average value of 175 pulses for each range cell is taken as the mean for that range cell. It is assumed that a sufficient platform motion and antenna scan occurred during the duration of the pulse group to give a representative estimate of the mean.

The approximate density function for $p_2(u)$ is obtained by finding the value of m that gives a good fit between the plot of Eqn. (6.2-3) (after multiplication by a number equal to the area under the histogram) and the histogram of the mean of each range cell in the test set. The approximate density function for p(z) is similarly obtained by finding the value of k that gives a good fit between the plot of

Eqn. (6.2-4) and the histogram of individual pulse returns from all range-azimuth samples in the test set treated as a single population. Note that knowing the value of k also gives the conditional probability density function $p_1(z|u)$.

It is convenient for plotting purposes to use the normalized gamma density according to the variable transformation, $u \rightarrow u/\bar{u} = y$. Then, $p(y)$ is given by

$$p(y) = \frac{m^m \, y^{m-1} \, \exp(-my)}{\Gamma(m)} .$$

(6.2-6)

The histogram of the normalized mean value of the clutter, $u/\bar{u}$, is shown in figure 6.2-1. The plots of Eqn. (6.2-6) versus $y = u/\bar{u}$ for $m = 1$, and 2 are shown in Figure 6.2-2. It can be seen that the gamma density with $m = 2$ is a good fit to the histogram although the computed m is close to 1. The histogram of individual pulse returns from all range-azimuth samples in the test set, when matched to the plot of a scaled version of Eqn. (6.2-4) represeenting $p(z)$ would allow the determination of k and $p_1(z/u)$. Unfortunately, a way of plotting Eqn. (6.2-4) for a non-integer order of the modified Bessel function of the second kind was not found within the time constraint of this investigation and the k value needed for $p_1(z|u)$ was not established by this means.

An alternate approach was taken based on the assumption

279
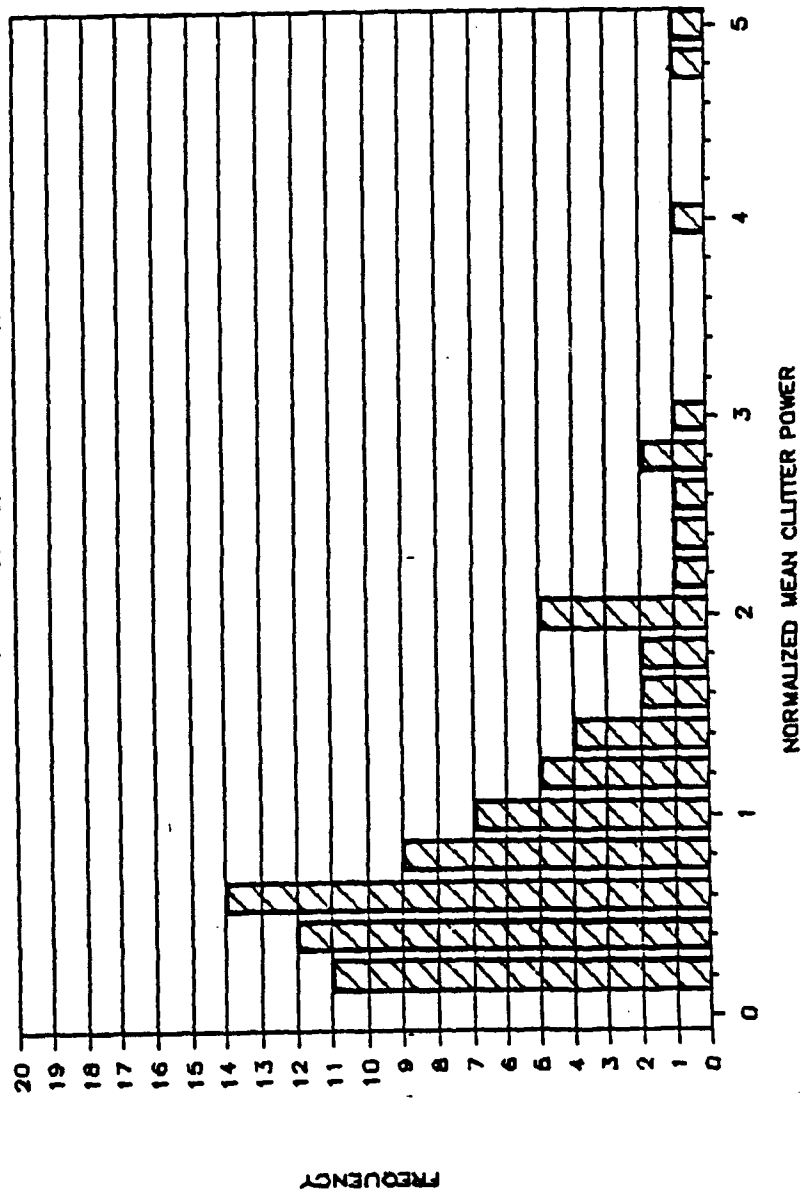
Figure 6.2-1

Histogram of the Normalized Mean Values of Clutter Returns

280
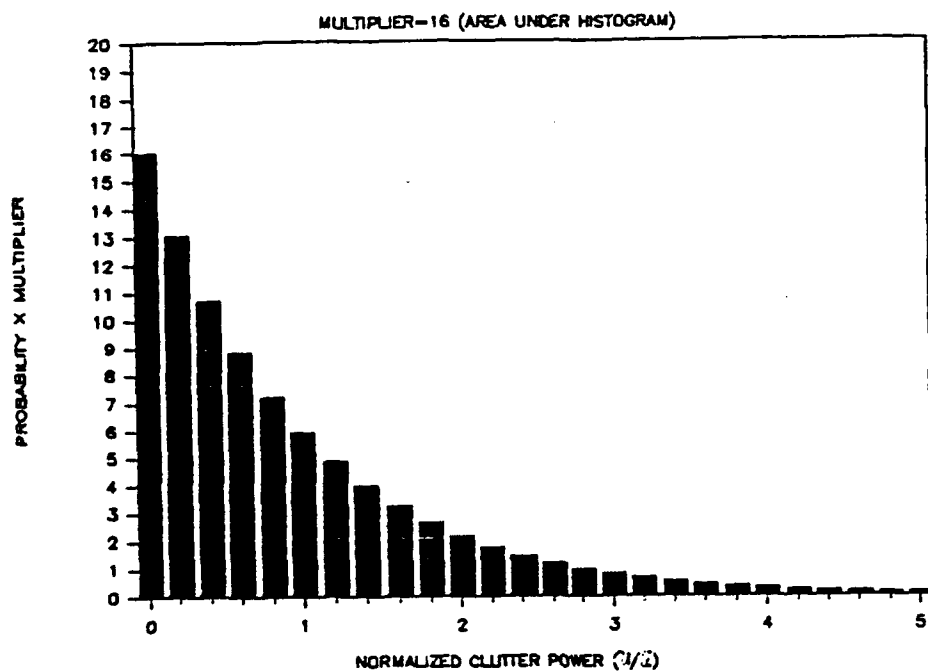
(a) GAMMA DENSITY (SHAPE FACTOR(K)=1.0)
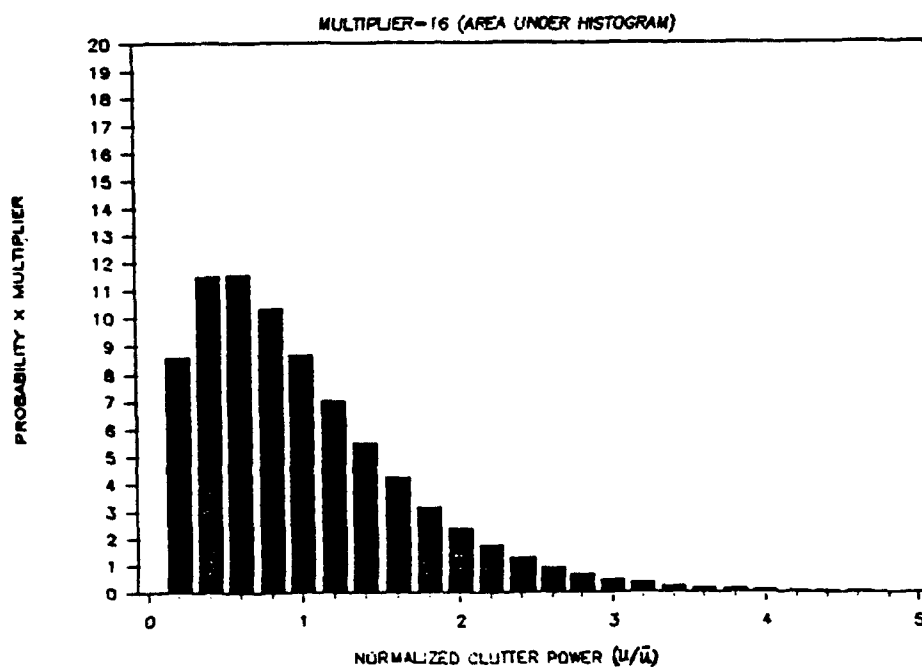
(b) GAMMA DENSITY (SHAPE FACTOR(K)=2.0)

Figure 6.2-2
Scaled Gamma Density Function with Shape Factor of 1 and 2

281

that the distribution of returns in each range cell all be-
long to a gamma density. The distribution of clutter returns
in individual range cells should reflect the conditional
density. Histograms of the normalized values of clutter re-
turns for a few range cells are shown in Figures 6.2-3 (a)
through (d). It is obvious that additional samples are
needed to give them a recognizable form. With the assump-
tion that returns in all range cells belong to a family of
gamma density, it can be conjectured that the histogram of
normalized clutter returns for a single range cell can be
approximated by averaging the same from all range cells.
The normalization is accomplished by dividing the variable
by its local mean (i.e., z/u) for each range cell. This is
done and the result is plotted in Figure 6.2-4. The result
reasonably matches with a Rician density of DC/AC ratio
equal to 40 which is plotted in Figure 6.2-5. The gamma den-
sity with the shape factor k equal to that computed from the
samples used ($k = 27.5$) is also plotted in Figure 6.2-5.
Based on visual inspection, it can be seen that a better
match is possible if a shape factor somewhat less than that
computed is used.

The most significant findings are that the mean and vari-
ance of the clutter returns vary significantly from one
range cell to the next. This contrasts with the frequently
used conventional assumption. The values for samples from
one azimuth look are listed in Table 6.2-2 for illustration.

282

SAMLE SIZE=175, MEAN=175.872.

(a) HISTOGRAM OF CLUTTER RETURN *(RG=05)*

SAMLE SIZE=175, MEAN=1363.9%.
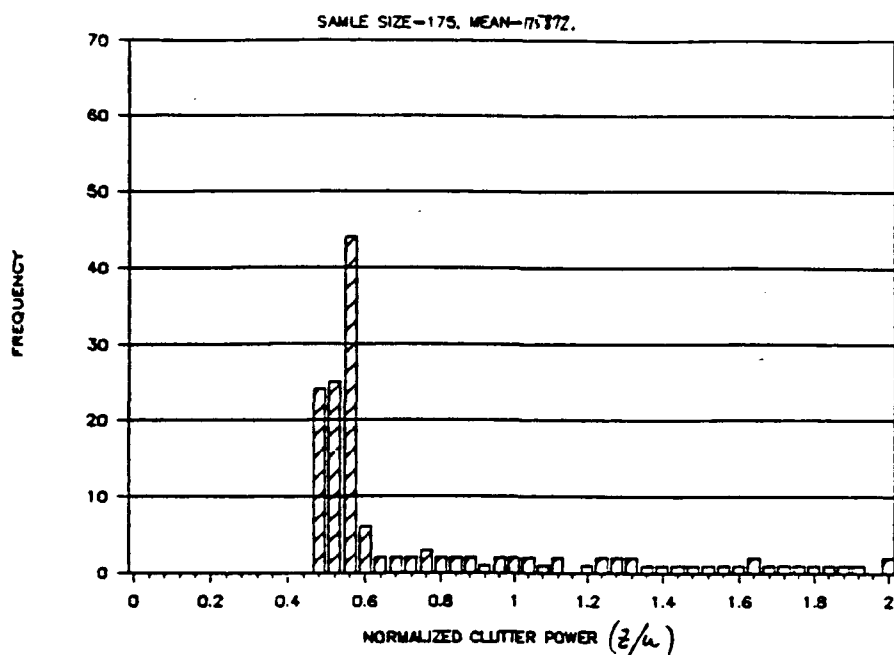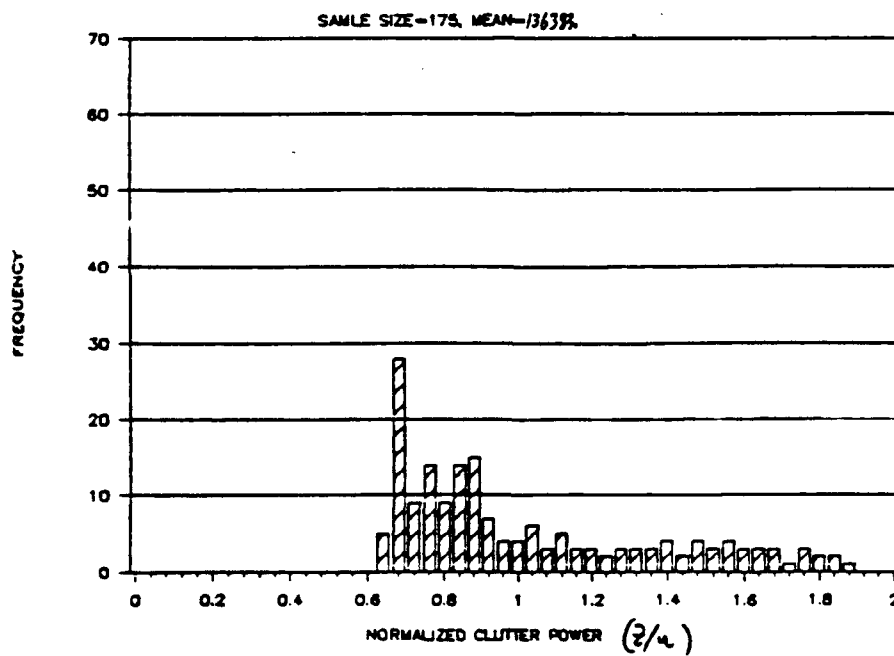
(b) HISTOGRAM OF CLUTTER RETURN *(RG=07)*

Figure 6.2-3

Histograms of Normalized Clutter Returns
for Individual Range Cells
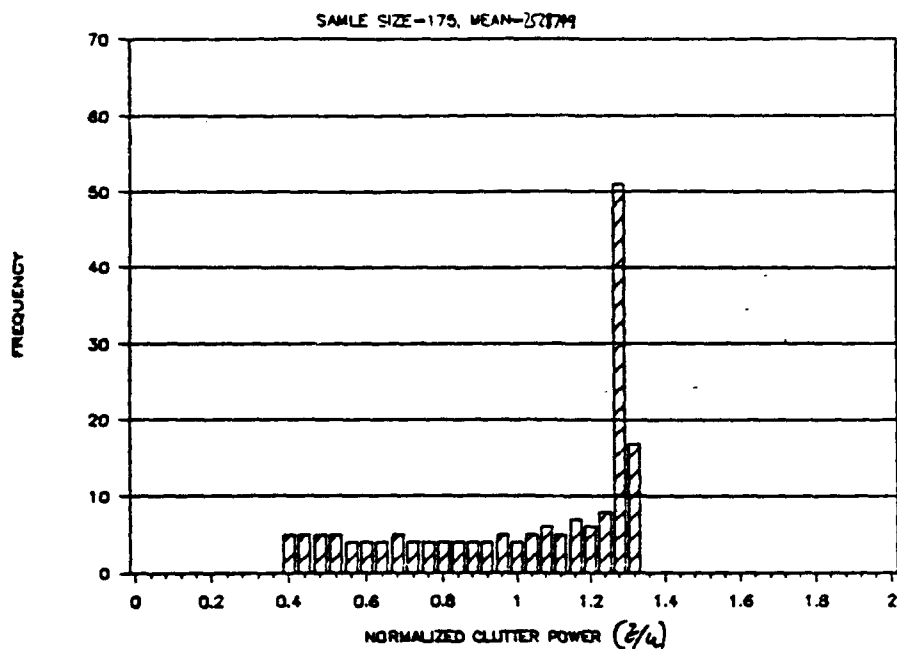
(c) HISTOGRAM OF CLUTTER RETURN *(RG=09)*
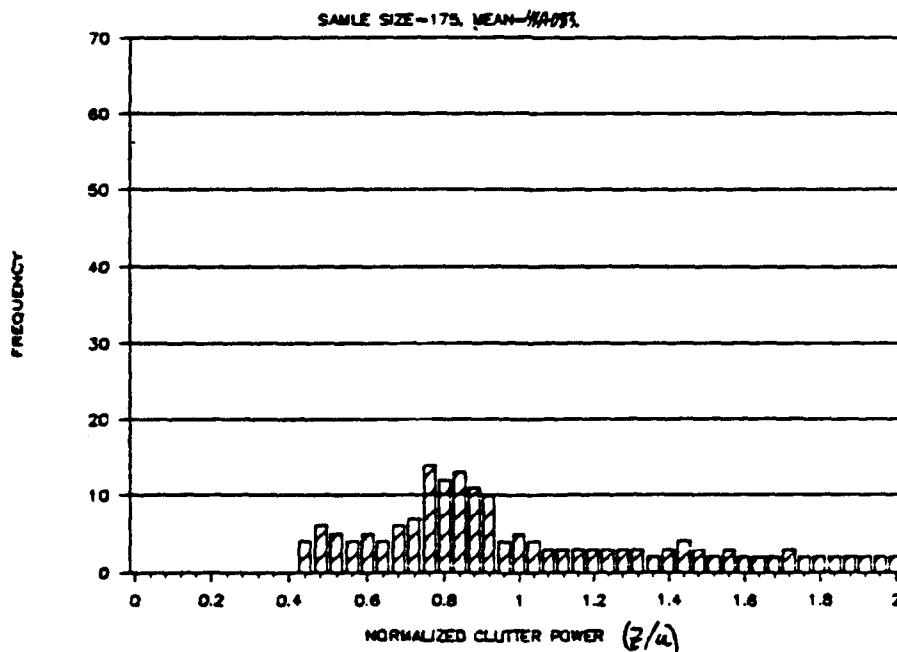
(d) HISTOGRAM OF CLUTTER RETURN *(RG=11)*

Figure 6.2-3

Histograms of Normalized Clutter Returns
for Individual Range Cells (cont'd)

284
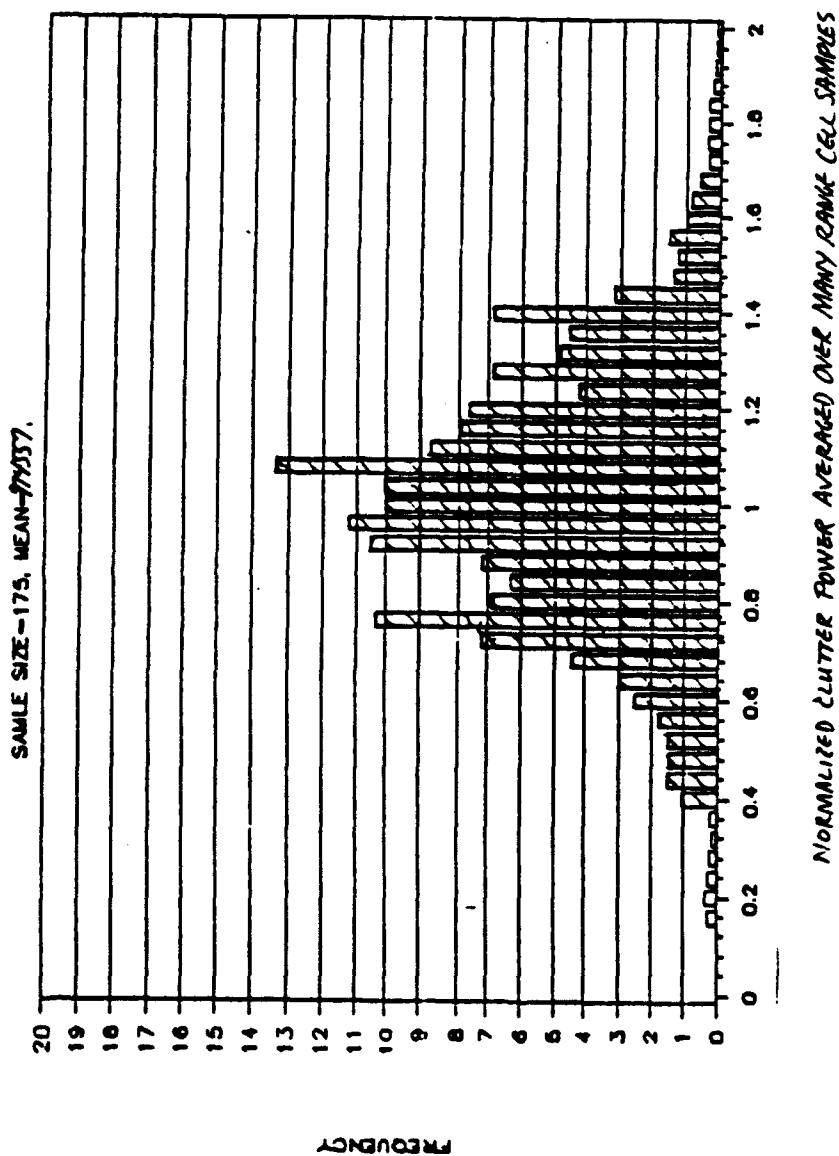
Figure 6.2-4

Averaged Histogram of Normalized Clutter Returns
of a Range Cell

285

(a) RICIAN DENSITY (DC/AC=40)

(b) GAMMA DENSITY (SHAPE FACTOR(K)=27.5)
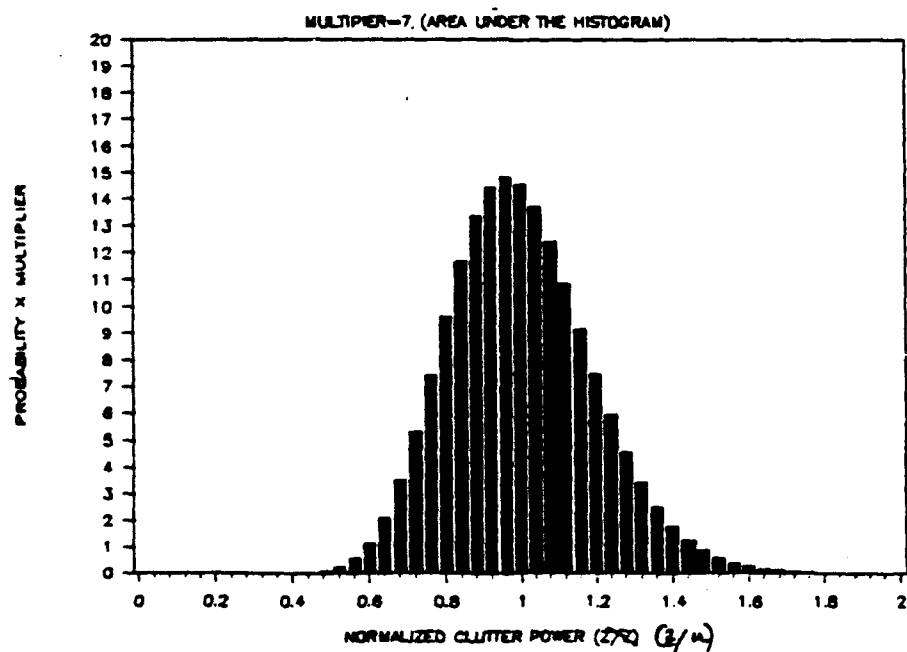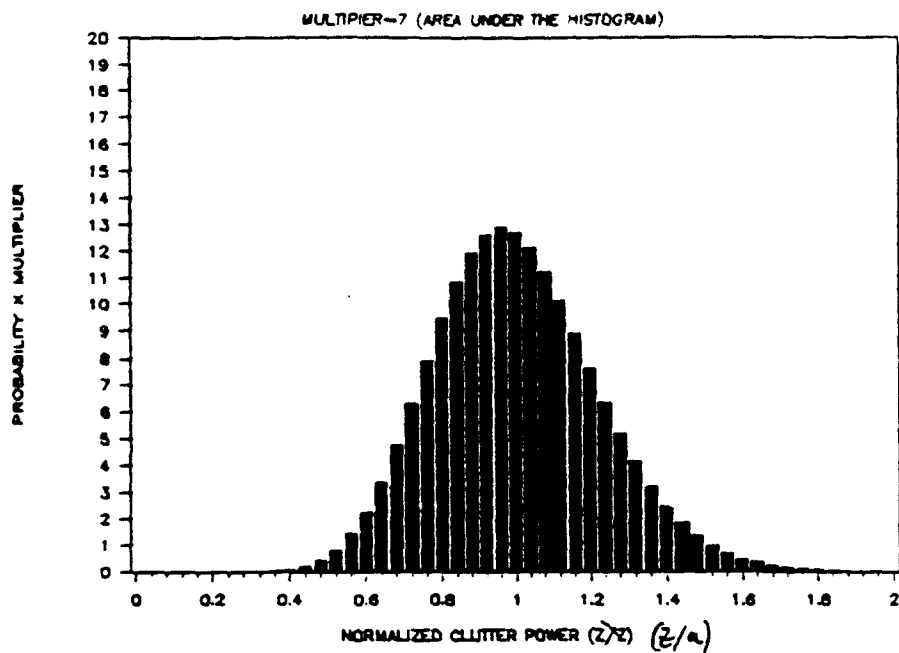
Figure 6.2-5

Candidate Rician and Gamma density
for the Conditional Density for the Clutter

Table 6.2-2

Range Cell to Range Cell Variation of Clutter Statistics

clutter power statistics

range cell #	mean	variance	max. value	min. value
7	136,383	$2.2\text{x}10^{09}$	254,530	86,725
9	2,528,749	$5.8\text{x}10^{11}$	3,257,461	939,497
11	464,083	$3.5\text{x}10^{10}$	914,689	197,640
15	382,682	$6.9\text{x}10^{09}$	517,985	153,493
17	90,185	$1.7\text{x}10^{09}$	141,520	13,253
19	1,706,289	$1.6\text{x}10^{10}$	1,946,404	1,566,850
21	338,809	$1.3\text{x}10^{10}$	472,066	122,509
23	1,225,326	$7.7\text{x}10^{09}$	1,376,500	1,116,757
25	1,677,916	$9.0\text{x}10^{10}$	2,002,568	1,081,825
27	229,145	$4.0\text{x}10^{09}$	322,592	117,625
29	581,995	$2.8\text{x}10^{10}$	941,845	411,956
33	458,439	$2.2\text{x}10^{10}$	862,948	332,100
35	2,431,334	$1.8\text{x}10^{11}$	3,075,201	1,667,818
37	3,427,057	$6.2\text{x}10^{10}$	3,686,800	2,877,200
39	668,303	$5.1\text{x}10^{10}$	1,118,617	388,145
43	751,256	$5.8\text{x}10^{10}$	1,039,725	273,320
45	277,727	$7.2\text{x}10^{08}$	327,625	242,045
47	166,344	$2.2\text{x}10^{09}$	238,954	113,074

6.2.2 Clutter Cancellation Techniques

In this section a performance comparison of three types of clutter cancellers is made using live data collected from a high PRF airborne pulse doppler radar. The three types of clutter cancellers compared are

   a. Velocity shaped IIR filter.
   b. Delay line canceller with binomial coefficients as its weight.
   c. Optimum linear filter whose weights are derived from the eigen vector corresponding to the minimum eigen value of the clutter correlation matrix.

The velocity shaped IIR filter consists of two sections of 2-pole, 2-zero recursive digital filters in cascade whose coefficients are chosen so as to give a flat magnitude response above its cutoff frequency which can be selected for either 70 or 90 knots.

The filters of (b) and (c) above are known also as transversal filters whose outputs are a weighted sum on a sliding window of the input sequence or the input vector. The output sequences of these filters are weighted and summed again to produce a specific doppler filter output. A representation of the above processes in terms of matrix multiplications is given by Andrews [30].

288

According to linear optimum filter theory, the above process can be performed by one operation. This is expressed mathematically as

$$x = W^* Y \qquad\qquad (6.2\text{-}7)$$

where x is the scalar output, $Y = Z+S$ is the input column vector consisting of the clutter plus thermal noise interference vector Z and the signal vector S, and W^* is the transpose of the complex conjugate of the weight vector W defined as

$$W = M^{-1} S \qquad\qquad (6.2\text{-}8)$$

and M is the correlation matrix of the interference process assumed to be zero mean [31].

One difficulty with this approach is that the signal vector is a priori unknown. In this case the signal vector, in particular its doppler frequency, is assumed to be equally likely to be anywhere within frequency interval corresponding to one PRF. Then, the optimum weight is given by the eigen vector corresponding to the minimum eigen value of the interference correlation matrix [32, 33].

The real difficulty with this optimum filter is that the interference correlation matrix is also unknown and cannot

be approximated from the adjacent range gate samples as assumed by others [31, 34, 35]. This is because the clutter statistics are different from one range cell to the next as shown in the previous section. Furthermore, in a high PRF radar the dimension of the correlation matrix is large typically on the order of 128 or larger; and the operation indicated by Eqn. (6.2-7) and (6.2-8) is extremely difficult, if not impossible, to carry out. While M is a positive definite Hermitian matrix in theory, an examination of real clutter data shows that it is highly ill conditioned. The difficulty arises due to the high degree of clutter correlation from pulse to pulse. At the same time, the correlation is not perfect enough with the result, when binomial coefficients are used as the weight, that the performance of the delay line canceller deteriorates rather than improves as the number of canceller stages increases beyond two. In addition Hsiao [37] shows, even under ideal assumptions such as a known exponential auto-correlation function for the clutter, that the increase in the clutter canceller improvement factor diminishes rapidly as the number of stages is increased beyond 7 or 8. These considerations limited the number of stages for transversal filters examined in the performance comparison to 7 making it an 8 pulse canceller at the maximum.

In the data sample examined, there are approximately 175 pulses available for processing after the multiple time

290

around echoes settle down in each CPI (see Figure 2.1-2). With the velocity shaped IIR filter, a 128-point FFT follows the clutter canceller after those pulses in the early portion of the filter output are discarded during which the filter goes through a transient period (see Figure 2.1-3). For the transversal filters, there are no transient periods. Thus, (175-N) output pulses are zero padded for a 256-point FFT where N is the number of canceller stages.

The frequency span equal to one PRF of the data set corresponds approximately to a velocity span of 0 to 2,454 knots. In each trial, a synthetic target is injected with varying amplitude at a doppler frequency corresponding to a specific target velocity. The results with the velocity shaped IIR filter are shown in Figures 6.2-6 (a) through (d) together with those for a 2-stage delay line canceller with binomial coefficients as its weights for comparison. The two humps appearing near the right edge in the figure correspond to (from left to right) the altitudeline clutter and the first sideobe clutter, repectively. Different adaptive constant false alarm rate (CFAR) thresholds are used in these range-doppler zones in the actual radar implementation. The results obtained using delay line cancellers with binomial coefficient weights for canceller stages of 2, 3, and 4 are shown in Figure 6.2-7. The canceller transfer function (gain as a function of frequency) is superimposed on the figure for visual aid. Increasing the number of
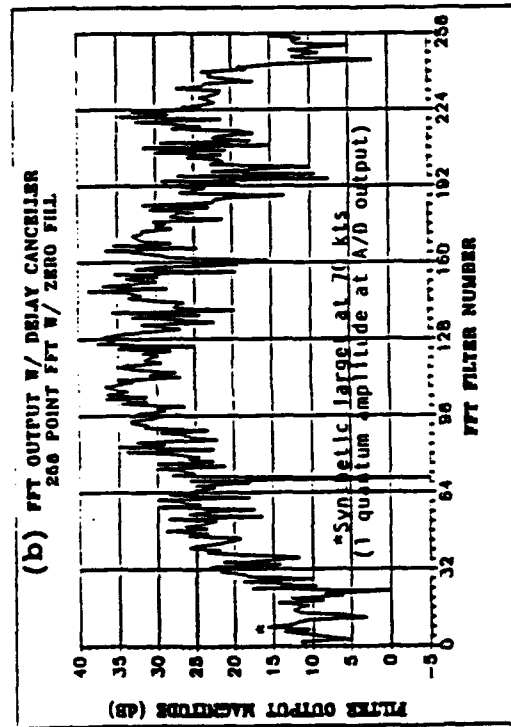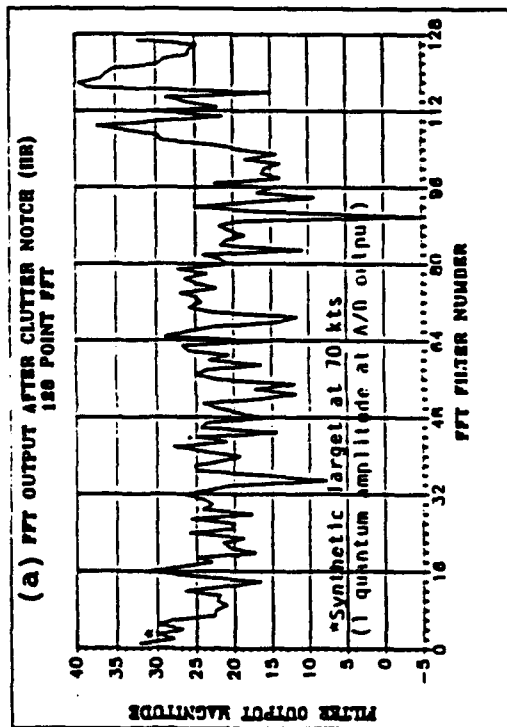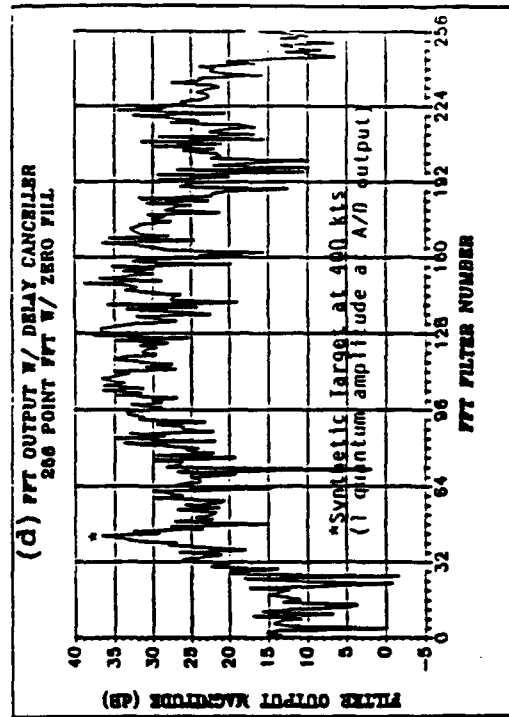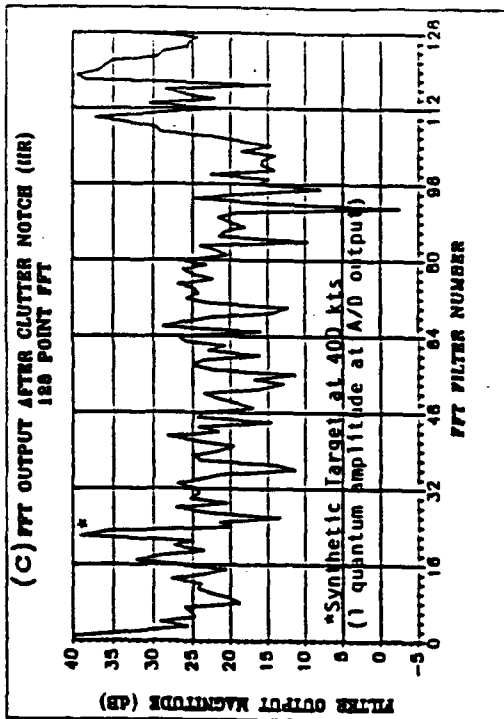
291

Figure 6.2-6 Performance Comparison of Clutter Cancellers:
IIR vs. FIR with Binomial Coefficients as Weights

292
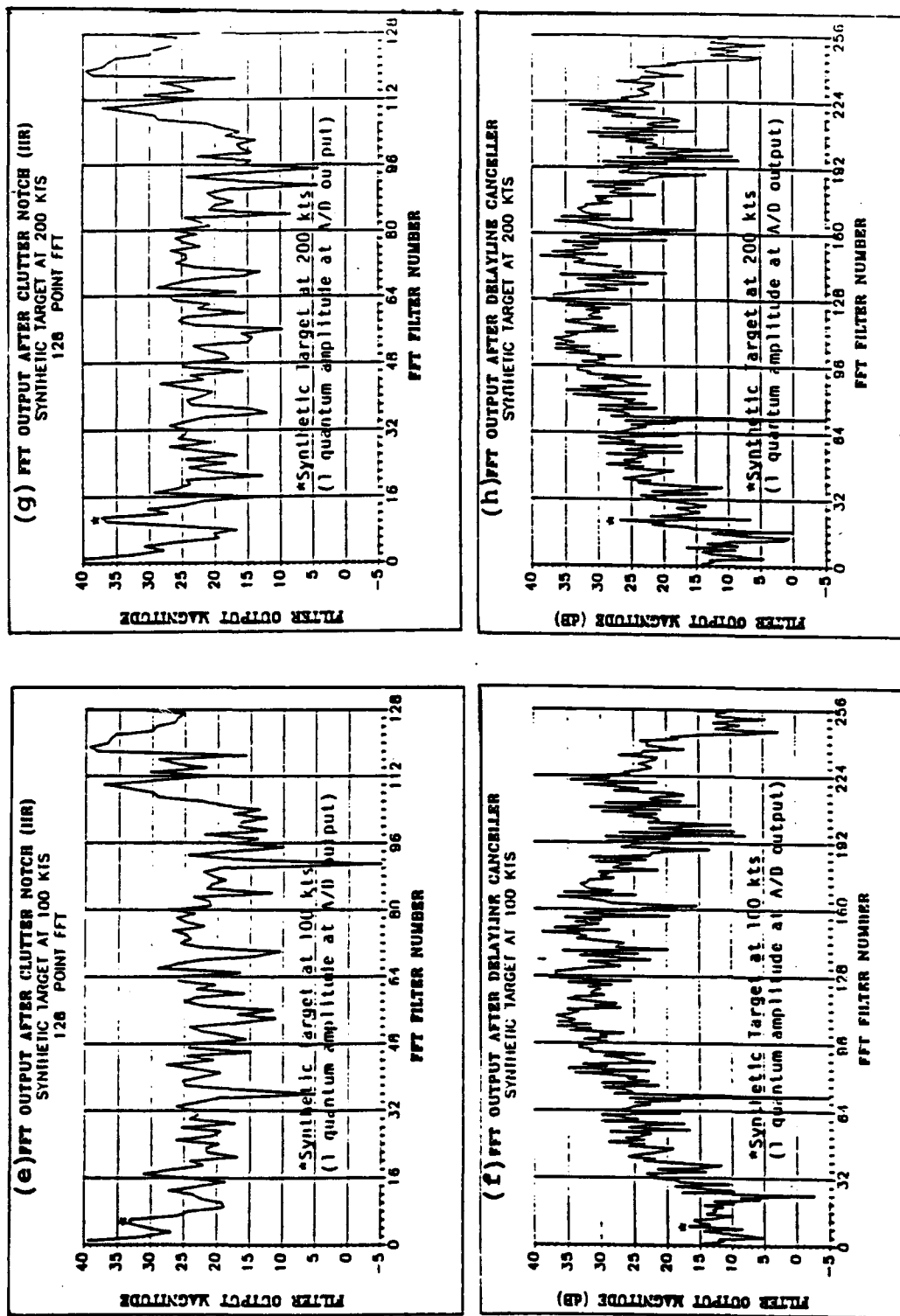
Figure 6.2-6 Performance Comparison of Clutter Cancellers: IIR vs. FIR with Binomial Coefficients as Weights(cont'd)
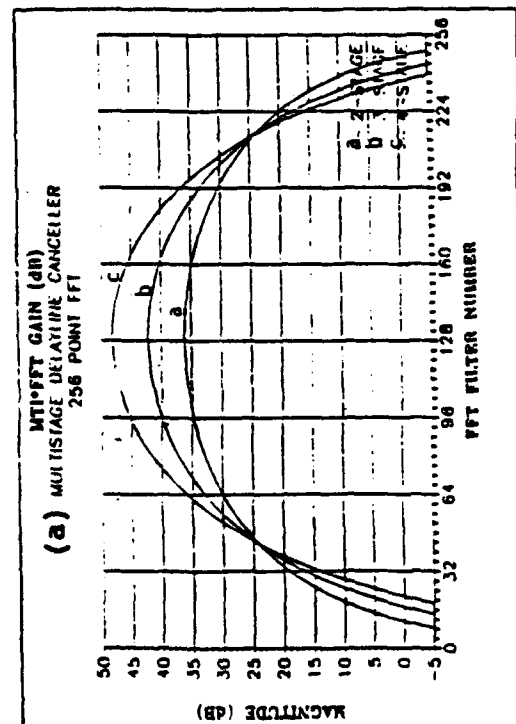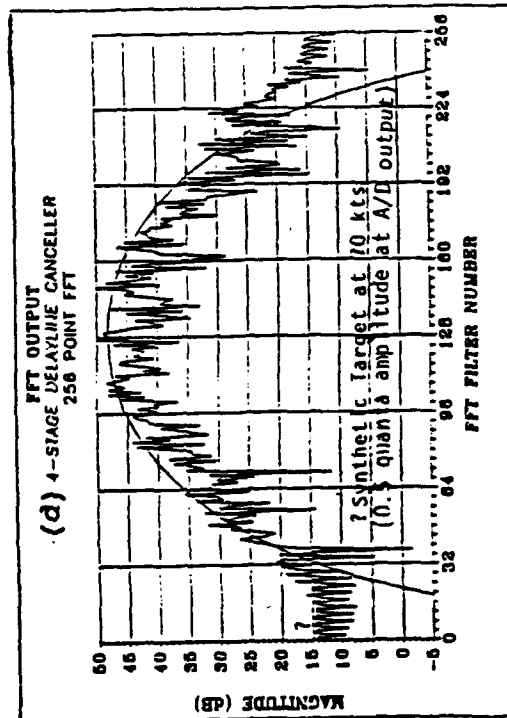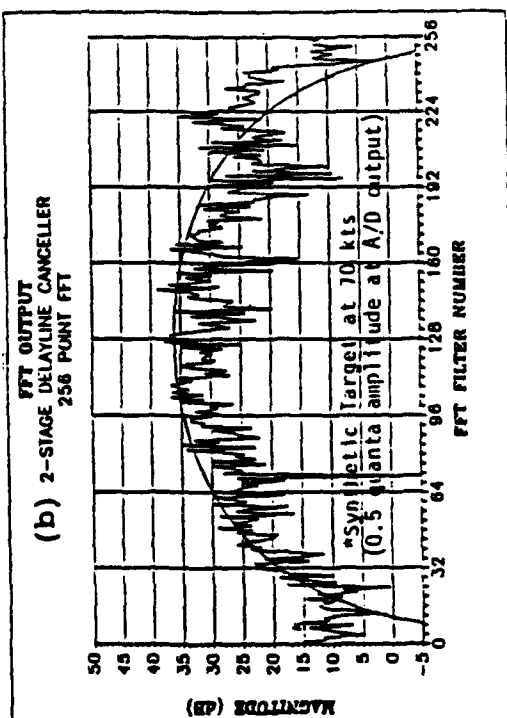
293
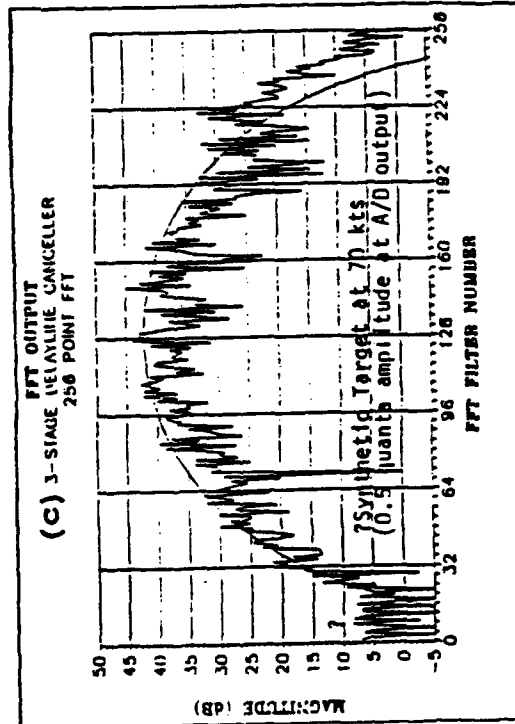
Figure 6.2-7 Performance of Delay Line Cancellers with Binomial Coefficients as Weghts: 2, 3, and 4 Stages

stages beyond two resulted in performance degradation. This is due to imperfect pulse-to-pulse clutter correlation. A comparison of 2-stage and 7-stage cancellers is shown in Figure 6.2-8. The performance deterioration is even more evident.

The above results are for samples from range cell 33 at a particular azimuthal direction. The results for different range cells in the same azimuth set with the eigen vector obtained from the estimated clutter correlation matrix as filter weight are shown in Figures 6.2-9. Also shown in the figure in parallel is the corresponding results with the IIR filter. The transfer function for the transversal filter is shown in Figure 6.2-10 for each of the range cells examined. In computing the eigen vector, a sample correlation matrix, which is an average of a set of 8x8 correlation matrices each formed by the outer product of 8 pulses taken at 16 or 32 pulse interval from the received pulse train for the test cell, is first obtained. The eigen values and eigen vectors for the sample correlation matrix for each range cell sample are then computed using the EISPACK computer program developed by Argonne National Laboratory on a mini VAX computer. Without exception, in all trials some eigen values turned out to be negative. The eigen vector corresponding to the minimum positive eigen value was used to provide filter weights for each range cell sample.
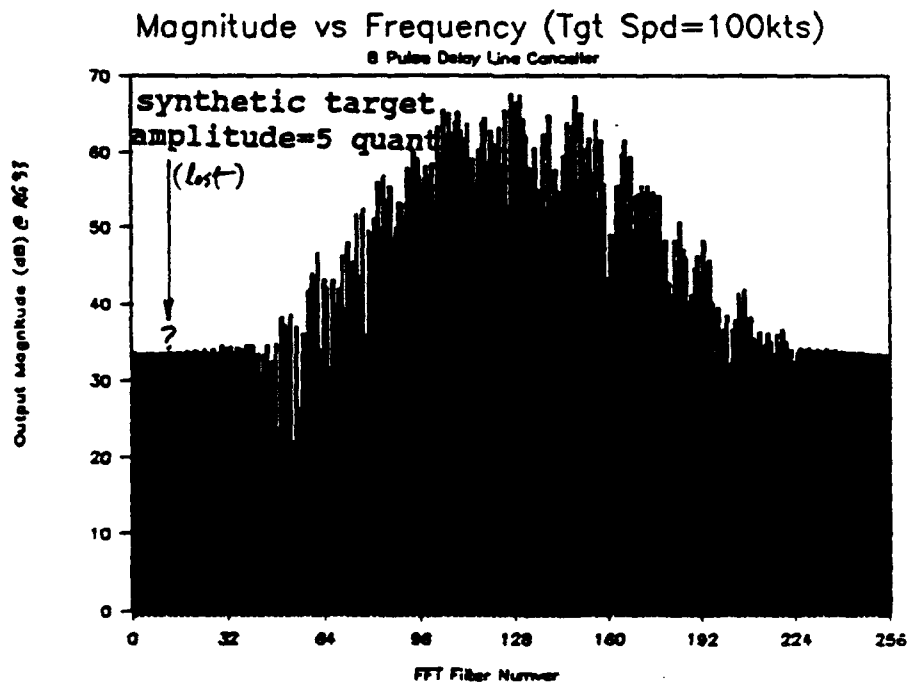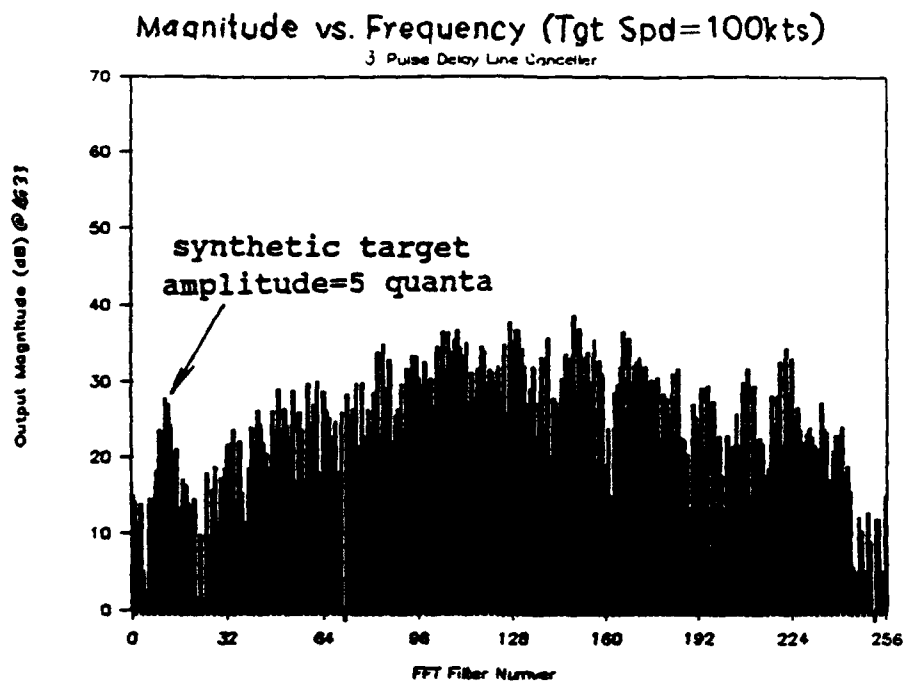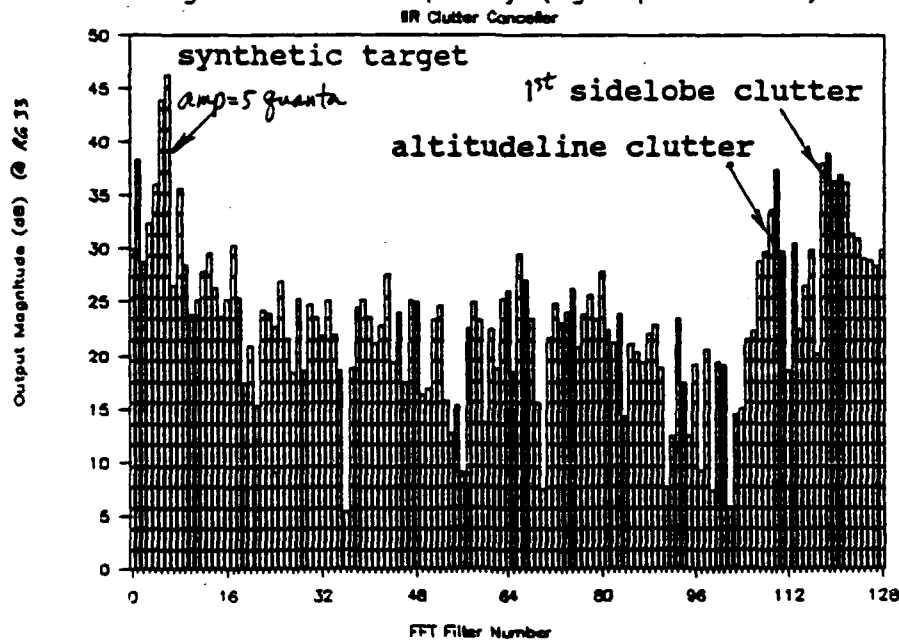
Magnitude vs. Frequency (Tgt Spd=100kts)

3 Pulse Delay Line Canceller

synthetic target
amplitude=5 quanta

Magnitude vs Frequency (Tgt Spd=100kts)

8 Pulse Delay Line Canceller

synthetic target
amplitude=5 quanta
|(lost)
?

Figure 6.2-8.

Performance of Delay Line Cancellers with Binomial
Coefficients as Weghts:

296

(a) Magnitude vs Frequency (Tgt Spd=100kts)

IIR Clutter Canceller

(b) Magnitude vs Frequency (Tgt Spd=100kts)
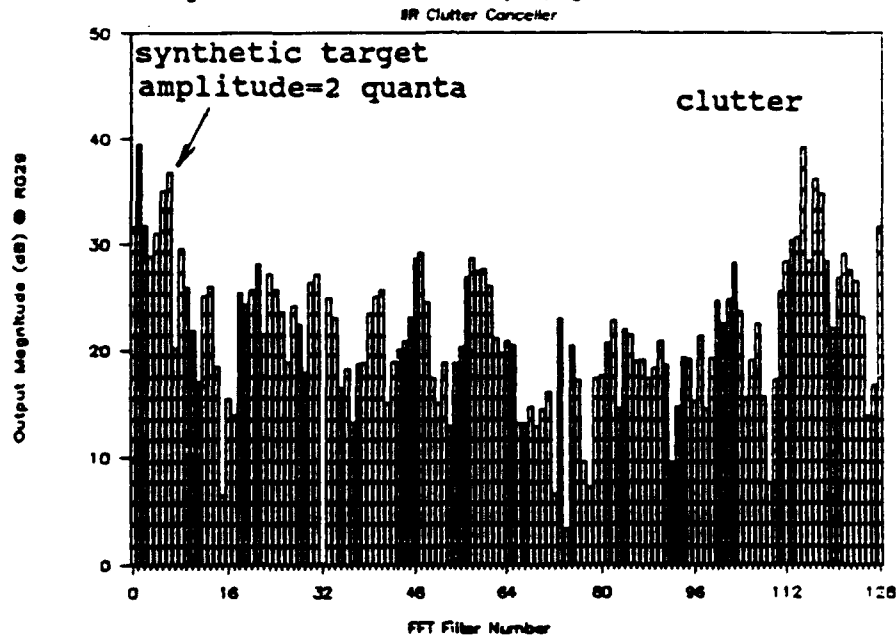
Eigenvector of Length 8 Used as Weights

Figure 6.2-9.

**Performance Comparison of Clutter Canceller:
IIR vs. FIR with Eigen Vector as Weights**

297

(c) Magnitude vs Frequency (Tgt Spd=100kts)

IIR Clutter Canceller

(d) Magnitude vs Frequency (Tgt Spd=100kts)

Eigenvector of Length 8 Used as Weights
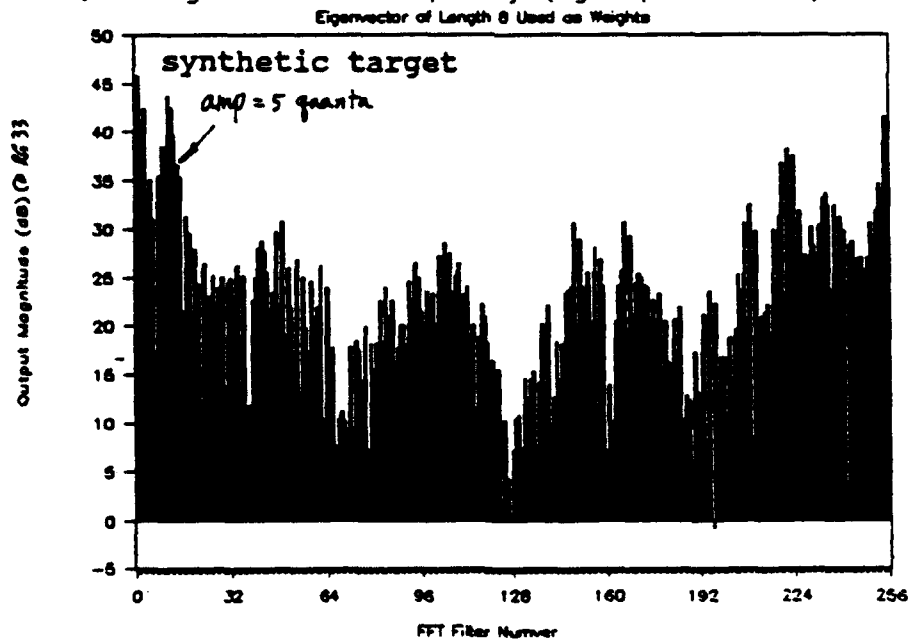
Figure 6.2-9

**Performance Comparison of Clutter Canceller:
IIR vs. FIR with Eigen Vector as Weights (cont'd)**

(e) Magnitude vs Frequency (Tgt Spd=100kts)
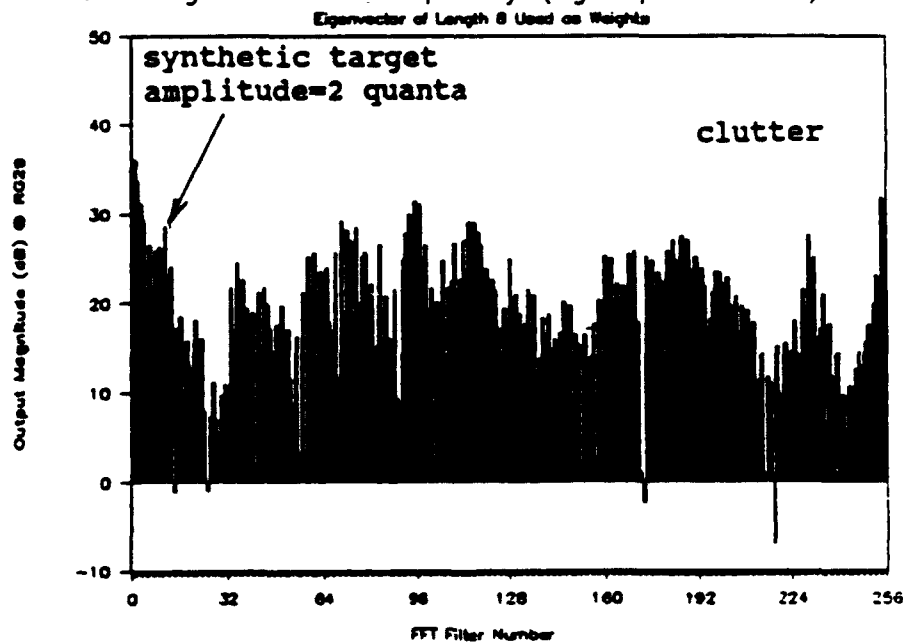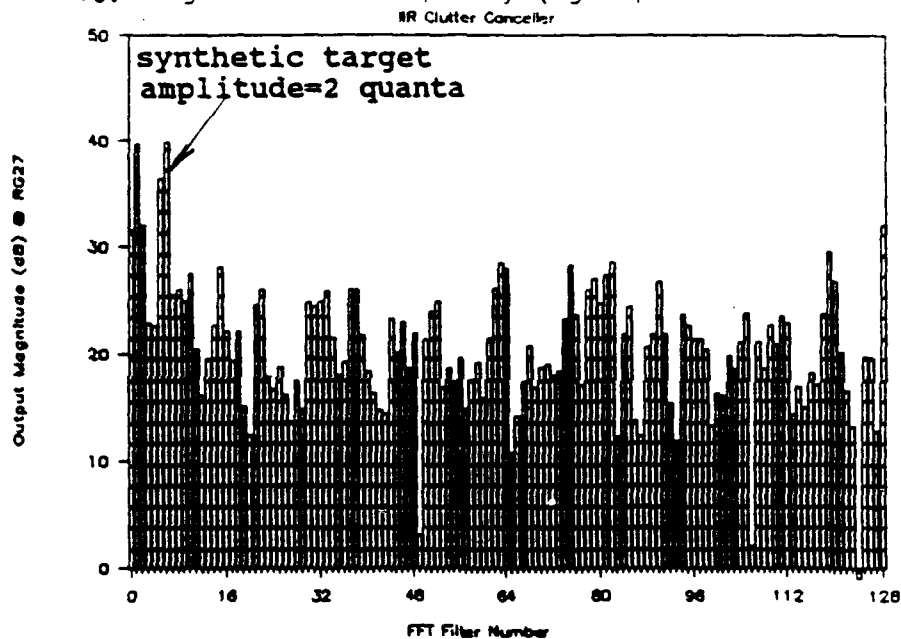

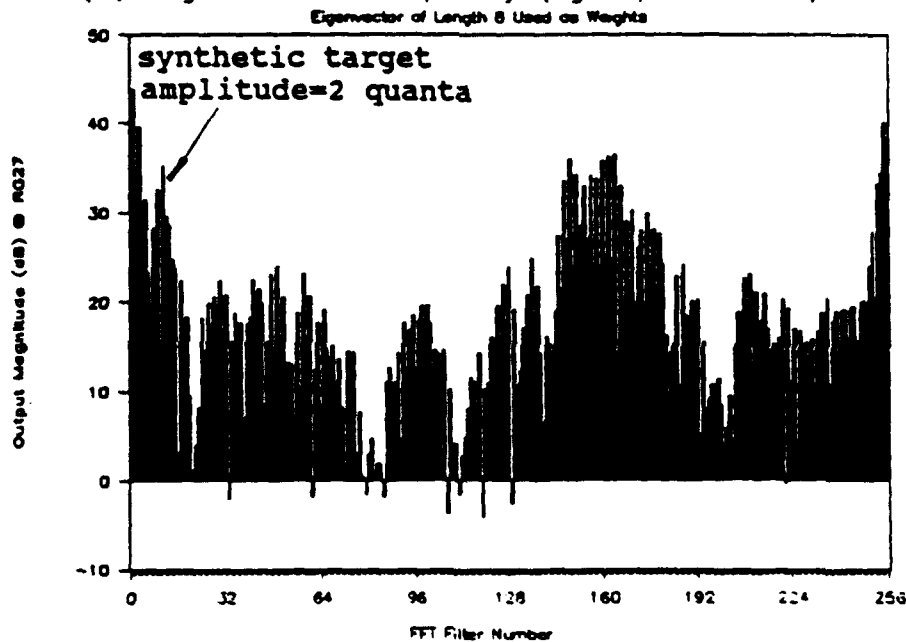**(f)** Magnitude vs Frequency (Tgt Spd=100kts)

Figure 6.2-9

Performance Comparison of Clutter Canceller:
IIR vs. FIR with Eigen Vector as Weights (cont'd)

(g) Magnitude vs Frequency (Tgt Spd=100 ts)

IIR Clutter Canceller

(h) Magnitude vs Frequency (Tgt Spd=100kts)
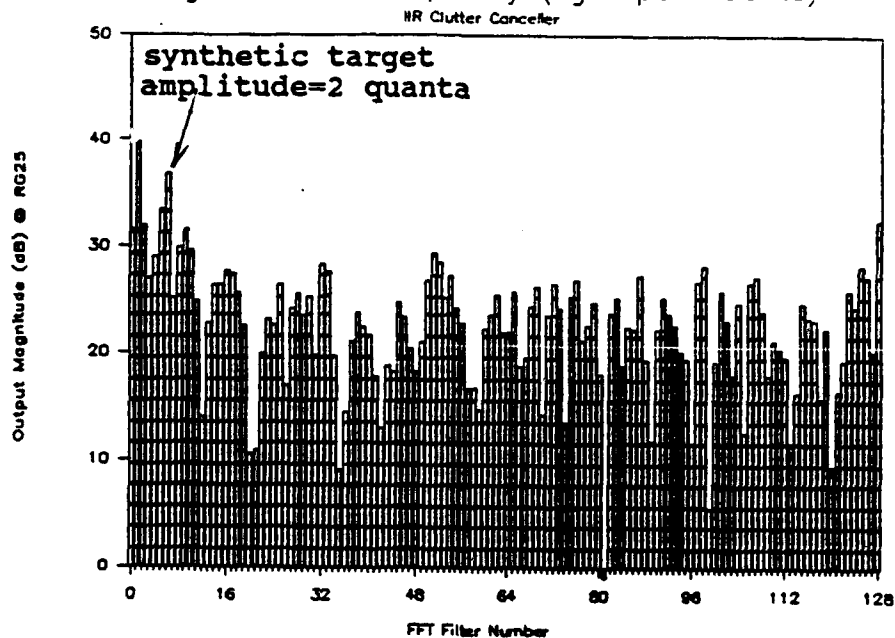
Eigenvector of Length 8 Used as Weights

Figure 6.2-9

Performance Comparison of Clutter Canceller:
IIR vs. FIR with Eigen Vector as Weights (cont'd)

(i) Magnitude vs Frequency (Tgt Spd=100 ts)

IIR Clutter Canceller

(j) Magnitude vs Frequency (Tgt Spd=100kts)
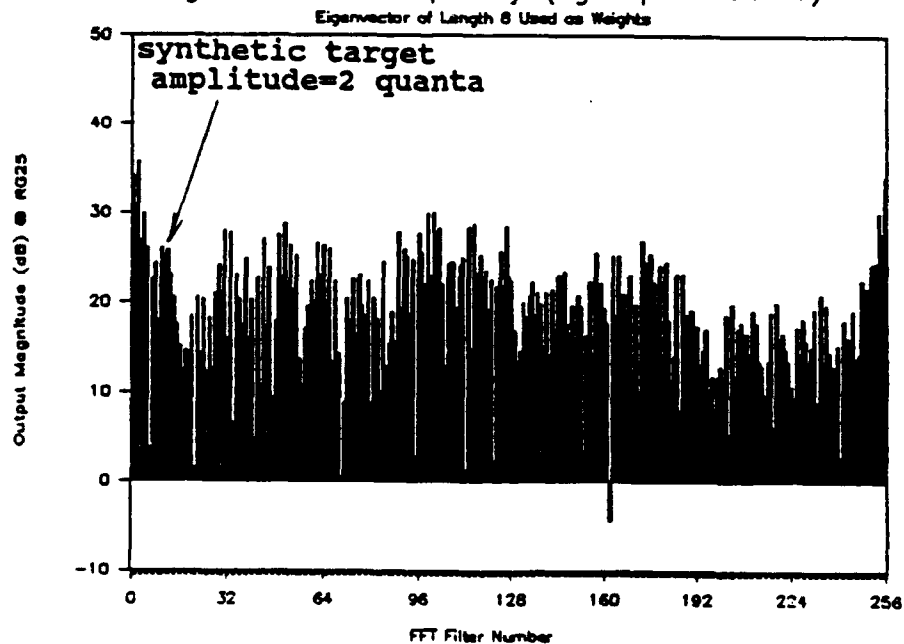
Eigenvector of Length 8 Used as Weights

Figure 6.2-9

Performance Comparison of Clutter Canceller:
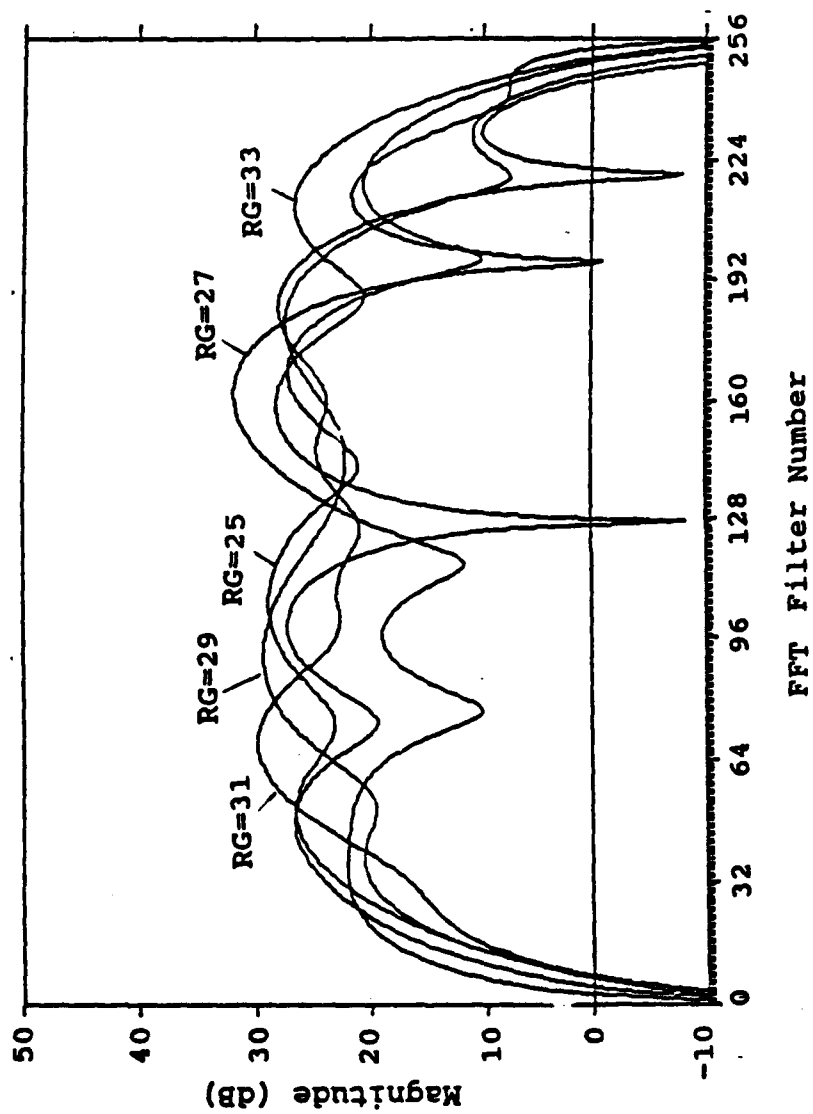IIR vs. FIR with Eigen Vector as Weights (cont'd)

301

Figure 6.2-10

Gain vs. Frequency of the FIR Filter
with Eigen Vector as Weights

302

These results can be compared by visual inspection (the best knowledge based detector). While subjective, it is apparent that no one technique is noticeably superior to the other for discriminating the injected synthetic target from the clutter. As a matter of fact, performance of the optimum filter (filter with the eigen vector as its weight) seems inferior to that of conventional filters used almost exclusively in radar systems operating today. However, a higher degree of reduction in amplitude of the altitudeline and the first sidelobe clutter away from the mainbeam clutter is quite evident when the optimum filter is employed.

Bibliography

1. E. Brookner, <u>Radar Technology</u>, Artech House, Inc. 1977.

2. DiFranco and Rubin, <u>Radar detection</u>, Artech House, Inc. 1980.

3. M. Skolnik, <u>Radar Handbook</u>, McGraw-Hill Company, 1970.

4. D. K. Barton, <u>Radar System Analysis</u>, Artech House, Inc. 1976.

5. A. Popoulis, <u>Probability, Random Variables and Stochastic Processes</u>, McGraw-Hill Company, 1965.

6. J. D. Mallet and L. E. Brennan, "Cumulative Probability of Detection for Targets Approaching a Uniformly Scanning Search Radar'" Proceedings of the IEEE, vol.,51, No. 4, pp. 596-601, April, 1963.

7. L. Blake, "The Effective Number of Pulses per Beamwidth for a Scanning Radar," Proc. IRE, 41, No. 6 pp. 770-774, June, 1953.

8. M. Schwartz, "A Coincidence Procedure for Signal Detection," Trans. IRE, vol. IT-2, No. 4, pp. 135-139, Dec. 1956.

9. M. Skolnik, <u>Introduction to Radar Systems</u>, McGrow Hill Book Company, New York, 1962.

10. F. E. Nathanson, <u>Radar Design Principles</u>, McGraw Hill Book Co., New York, 1969.

11. V. C. Vannicola and J. A. Mineo, "Application of Knowledge Based Systems to Surveillance," 88 CH 2572-6/88/0000-0157 $01.00, 1988 IEEE.

*12. A. Corbeil, et al., <u>Track Before Detect Development and Demonstration Program</u>, Phase II, RADC-TR-86-68, May, 1986.

13. I. S. Reed and R. M. Gargliardi, "A Recursive Moving-Target-Indication Algorithm for Optimum Image Sequences," IEEE Trans. on Aerospace and Electronic Systems, Vol. 26, NO. 3, May 1990.

14. S. Haykin, <u>Communication Systems</u>, 2nd edition, John Wiley & Sons, New York, 1983.

15. P. Swerling, "Probability of Detection for Fluctuating Targets, Special Monograph," Trans. IRE on Information Theory, IT-6: (2). PP269-308, April, 1960.

16. R. R. Booth, "The Weibull Distribution Applied to the Ground Clutter Backscatter Coefficient," U.S. Army Missile command, Redstone Arsenal, AL, Report RE-TR-69-15, June, 1969.

17. R. L. Fante, "Detection of Multiscatter Targets in K-Distributed Clutter," IEEE Trans. on Antennas and Propagations, AP-32, 12, pp. 1358-1363, 1984.

18. A. Farina, A. Russo, and F. Scannapieco, "Radar Detection of Target Signals in Non-Gaussian Clutter: theory and Applications," Chinese Intl. Radar Conference, Nnanjing, pp. 442-449, November 1986.

19. G. Fedele, L. Izzo, and L. Paura, "Optimum and Suboptimum Space Diversity Detection of Weak Siganls in Non-Gaussian Noise," IEEE Trans. Comm., vol. COM-32, pp. 990-997, Sept. 1984.

*Although this report references limited document (item 12), no limited information has been extracted. Dist Statement - DOD & DOD contractors only; critical technology; May 86.

20. Conte, Izzo, Longo, and Paura, "Asymtotically Optimum Radar Detection in Sea Clutter," MELECON 85, Madrid, Oct. 1985.

21. MTI RADAR, edited by D. C. Schleher, Artech House, 1980.

22. Optimized RADAR PROCESSORS, edited by A. Farina, IEE RADAR, SONAR, NAVIGATION and AVIONICS Series 1, Peter Peregrinus Ltd., 1987.

23. FAA-E-2763, Federal Aviation Administration Specification, "ARSR-4 RADAR SYSTEM, APPENDIX A: Radar Clutter Model," U.S. Dept. of transportation, Oct. 1986.

24. D. J. Lewinski, "Nonstationary Probabilitic Target and Clutter Scattering Models," IEEE Trans., vol. AP-31, No. 3, May, 1983.

25. S. Watts, "Radar Detection Prediction in K-Distributed Sea Clutter and Thermal Noise," IEEE Trans., vol AES-23, No. 1, pp. 40-45, Jan. 1987.

26. E. Jakeman and P. Pusey, "A Model for Non-Rayleigh Sea Echo," IEEE Trans., vol. AP-24, PP 806-814, Nov. 1976.

27. R. J. Miller, "A Coherent Model of Radar Clutter," Proc. of the 1988 IEEE National Radar Conference, pp. 246-248.

28. Greenstein, Brindley, and Carlson, "A Comprehensive Ground Clutter Model for Airborne radars," IIT Research Institute, Sept. 1969.

29. M. Nakagami, "The M Distribution – A General Formula of Intensity Distribution of Rapid Fading," in Statistical Methods in Radio Wave Propagation, W. C. Hoffman, Ed., Pergamon, NY 1960.

30. G. A. Andrews, Jr., "Performance of Cascaded MTI and Co-
    herent Integration Filters in a Clutter Environment,"
    Naval Research Lab., Washington, D.C., March 27, 1973

31. I. Reed, J. Mallett, and L. Brennan, "Rapid Convergence
    in Adaptive Arrays," IEEE Trans., vol. AES-10, No. 6,
    pp. 853-863, Nov. 1974.

32. R. C. Emerson, "Some Pulsed Doppler MTI and MTI
    Tehniques," Rand Corp., Report R-274, pp. 1-124, March,
    1954.

33. B. Noble and J. Daniel, <u>Applied Linear Algebra</u>,
    Prentice-Hall, Inc. New Jersey, 1977.

34. E. J. Kelly, "Adaptive Detection in Nonstationary Inter-
    ference, Part I and Part II," MIT Lincln Lab. Tech. Re-
    port 724, June, 1985.

35. E. D'Addio, A. Farina, and E. Studer, "Performance Com-
    parison of Optimum and Conventional MTI and Doppler Pro-
    cessors," IEEE Trans. on Aerospace and Electronic Sys-
    tems, Vol. AES-20, NO. 6, pp. 707-715, November 1984.

36. J. K. Hsiao, "On The Optimization of Clutter Rejection,"
    IEEE Trans., vol. AES-10, No. 5, pp. 622-629, Sept.
    1974.

MISSION

OF

ROME LABORATORY

Rome Laboratory plans and executes an interdisciplinary program in research, development, test, and technology transition in support of Air Force Command, Control, Communications and Intelligence (C^3I) activities for all Air Force platforms. It also executes selected acquisition programs in several areas of expertise. Technical and engineering support within areas of competence is provided to ESD Program Offices (POs) and other ESD elements to perform effective acquisition of C^3I systems. In addition, Rome Laboratory's technology supports other AFSC Product Divisions, the Air Force user community, and other DOD and non-DOD agencies. Rome Laboratory maintains technical competence and research programs in areas including, but not limited to, communications, command and control, battle management, intelligence information processing, computational sciences and software producibility, wide area surveillance/sensors, signal processing, solid state sciences, photonics, electromagnetic technology, superconductivity, and electronic reliability/maintainability and testability.